Table of contents

1 INTRODUCTION

1.1 The political scene in the field of magnetic fusion in 2002

In 2002, the future of the International Tokamak Experimental Reactor (ITER) dominated the political scene in magnetic fusion. Many important and positive steps were taken towards the decision to build this large international fusion project. Progress was made in the international negotiations to determine the legal frame between the four Parties (Canada, the European Union, Japan and Russia). Four sites have now been proposed, namely Clarington in Canada, Rokkasho Mura in Japan, Cadarache in France and Vandellós in Spain. Their technical assessment will be completed at the end of 2002 to be reported early in 2003.

Several other countries are considering joining ITER. The US, one of the founding fathers of the original ITER project, organised a meeting of the whole US fusion community in Snowmass during the summer of 2002. After a thorough analysis of the different routes towards a fusion reactor, it was concluded by an overwhelming majority that ITER should be the first priority and that the US should re-join the ITER process as a full partner. This "grass roots" opinion was subsequently confirmed by science policy bodies at a high level in the US government, and a final government decision is expected for the beginning of 2003. The Republic of China and Korea have also expressed an interest in becoming partners of ITER.

In summary, the international commitment to ITER is now very strong, due to the recognition by governments that fusion is an important energy option in a sustainable development policy, that ITER is the right next step to take and that now is the right time to take it.

In the European Union, the fusion programme under the Euratom treaty was approved by the Council of Ministers. The reactor orientation of the 5th Framework Programme (FP) was confirmed in the 6th FP (2003-2006). Within the total community budget for fusion of 750 million Euros, up to 200 million Euros are earmarked for ITER from 2003 to 2006.

1.2 The CRPP in 2002

In 2002, the new structure of the Ecole Polytechnique Fédérale de Lausanne (EPFL) was implemented. The CRPP became a Centre of the Faculty of Basic Sciences (FSB). Its mission, its internal structure and its role as an Association within the Euratom programme have remained unchanged. This first year integrating into the new structure of the EPFL and the FSB went smoothly, with strong support provided to the CRPP by the Directorates of both the EPFL and the FSB.

The formal collaboration between the EPFL and the Paul-Scherrer-Institute in the field of fusion has been redefined and a new contract was signed at the end of 2002, defining the financial contribution of each party.

On the research front, 2002 has yielded important scientific results in all the fields of activities of the CRPP, including:

- Record electron temperature of 18keV, quasi-stationary enhanced confinement regime (electron Internal Transport Barrier) and demonstration of 3rd harmonic plasma heating, all in the TCV tokamak;
- Technical breakthroughs in non-linear gyrokinetic simulations, permitting the study of the saturation mechanism of unstable drift waves;
- Significant results leading to better understanding and control of MHD and fast particle instabilities, and in the field of edge physics, obtained on the large European JET tokamak in the UK;
- An ever increasing interest from industry for the original applications of our plasma science in the field of plasma processing;
- Significant contributions to the evolution of the superconducting magnets for ITER, especially new and detailed studies of the inter-strand resistance;
- Continued progress in the understanding of basic properties of fusion neutron resistant alloys.

This wealth of results is reflected in an increasing number of overview, invited and contributed papers in international conferences on physics and technology, and in numerous papers appearing in refereed journals. The 29th EPS Conference was organised by the CRPP in Montreux and was attended by more the 630 delegates from all over the world.

The construction of the TORPEX device for basic plasma research has almost been completed. Full scientific operation is foreseen for early in 2003. This new device will renew a long tradition in basic plasma physics at CRPP. TORPEX will investigate fundamental plasma physics issues of interest for magnetic fusion in a well diagnosed laboratory plasma device and at the same time train graduate students.

A detailed description of all our results and activities, can be found in the following pages. Some of these activities are carried out within the frame of the Euratom Contract of Association and others are funded outside this contract. Our special thanks go to all the funding bodies that support our long-term research goals.

1 INTRODUCTION

1.1 La scène politique dans le domaine de la "fusion magnétique" en 2002

En 2002, le futur d'ITER (International Thermonuclear Experimental Reactor ou encore Réacteur Expérimental Thermonucléaire International de type Tokamak) a dominé la scène politique dans le domaine de la "fusion magnétique". De nombreuses étapes importantes ont marqué positivement le processus décisionnel concernant la construction de ce grand projet international. Les négociations internationales ont permis de progresser dans l'établissement d'un cadre légal liant les quatre partenaires (Canada, Union Européenne, Japon et Russie). Quatre sites ont été proposés, Clarington (Canada), Rokkasho Mura (Japon), Cadarache (France) et Vandellos (Espagne). Leurs évaluations techniques respectives étaient terminées à la fin 2002 et feront l'objet d'un rapport final début 2003.

Plusieurs autres pays considèrent se joindre à ce projet. Les Etats-Unis, un des pères fondateurs du projet original ITER, ont organisé à Snowmass, pendant l'été 2002, un atelier réunissant l'entière communauté américaine de fusion. Après une soigneuse analyse des différentes voies débouchant au réacteur à fusion, une large majorité des participants s'est dégagée : elle a conclu qu'ITER devait être la première priorité et que les Etats-Unis se devaient de revenir dans le programme ITER, en tant que partenaire à part entière. Cette opinion de la base a été confirmée par les plus hautes instances de la politique de la science au sein du gouvernement américain. Finalement une décision gouvernementale américaine est attendue pour le début 2003. Par ailleurs la République Populaire de Chine et la Corée du Sud ont exprimé clairement leur intérêt à devenir partenaires dans le projet ITER.

En résumé, l'engagement international pour ITER est actuellement très fort, dû notamment au fait que les gouvernements reconnaissent en la fusion une option énergétique importante s'intégrant dans la politique du développement durable, qu'ITER est la prochaine étape à réaliser et que la communauté est prête à ce défi du point de vue scientifique et technique.

Dans l'Union Européenne, le programme «Fusion » dans le cadre du traité de l'Euratom, a été approuvé par le Conseil des Ministres. L'orientation « Réacteur » du cinquième programme cadre a été également confirmée dans le sixième programme cadre. C'est ainsi que 200 millions d'euros des 750 millions du budget de la fusion pour la période 2003-2006 ont été prévus pour la construction d' ITER.

1.2 Le CRPP en 2002

En 2002, la nouvelle structure de l'Ecole Polytechnique Fédérale de Lausanne (EPFL) a été introduite. Le CRPP est devenu un Centre de la Faculté de Sciences de Base (FSB). Sa mission, sa structure interne et son rôle en tant qu 'Association du programme Euratom restent inchangés. Cette première année d'intégration, dans cette nouvelle structure, s'est bien déroulée et a été marquée par le support total de la Direction de l'EPFL et de celle de la FSB.

La collaboration formelle entre l'EPFL et l'Institut Paul Scherrer, dans le domaine de la fusion, a été redéfinie et un nouveau contrat, signé fin 2002, définit la contribution financière de chaque parti.

Sur le front de la recherche, les activités du CRPP en 2002 ont permis de récolter d'importants résultats scientifiques dans la plupart des domaines de recherches. Citons par exemple:

- Dans le tokamak TCV: record de la température électronique de 18 keV, en régime de confinement amélioré quasi stationnaire (barrière de transport électronique interne) et démonstration du chauffage du plasma à la 3ème harmonique de l'onde cyclotron électronique;
- Percée dans les techniques de simulation de la gyrocinétique non-linéaire, permettant l'étude des mécanismes de saturation des ondes de dérive instables;
- Résultats significatifs obtenus sur le tokamak européen JET (en G.-B.) conduisant à une meilleure compréhension et un meilleur contrôle d'une part des instabilités MHD et dues aux particules rapides, et d'autre part de la physique du plasma de périphérie;
- Un intérêt toujours croissant de la part des industries pour les applications originales des procédés par plasmas développés dans notre laboratoire;
- Contribution significative aux travaux de R&D concernant les aimants supraconducteurs pour ITER, spécialement par de nouvelles études poussées de la résistance entre les brins;
- Progrès continus dans la connaissance des propriétés fondamentales des alliages résistants aux neutrons de fusion.

Cette richesse de résultats se reflète dans le nombre croissant des contributions et des interventions aux conférences internationales de physique et de technologie, ainsi que dans de nombreuses publications soumises à arbitres dans des revues spécialisées. La 29ème Conférence Européenne de Physique, Division Fusion et Physique des Plasmas, était organisée par le CRPP à Montreux en juin 2002; plus de 630 délégués du monde entier y ont participé!

La construction de l'expérience TORPEX destinée à la recherche de physique fondamentale du plasma a été presque terminée. L'exploitation scientifique est prévue pour le début 2003. Cette nouvelle installation renoue avec la longue tradition de la recherche de physique fondamentale du plasma au CRPP. TORPEX permettra tout à la fois d'étudier des problèmes essentiels de la physique des plasmas ayant un intérêt direct avec la fusion magnétique sur une installation de laboratoire pourvue de nombreuses méthodes de diagnostic et d'offrir une expérience pour former les étudiants.

Une description détaillée de nos activités et de nos résultats peut être consultée dans les pages suivantes. Les activités touchant la fusion sont effectuées dans le cadre du Contrat d'Association avec l'Euratom. Le succès scientifique n'a été possible que grâce au financement de nombreux institutions tant publiques que privées : nous tenons à les remercier pour leur soutien, sans lequel les travaux décrits ici n'auront pas pu être accomplis avec un si grand succès.

1 EINLEITUNG

1.1 Die politische Szene auf dem Gebiet der magnetischen Fusion im Jahr 2002

Im Jahr 2002 dominierte der Internationale Experimentelle Tokamak Reaktor (ITER) die politische Szene in der magnetischen Fusion. Es wurden verschiedene wichtige und positive Schritte in Richtung einer Entscheidung für die Konstruktion dieses grossen, internationalen Fusionsprojekts gemacht. Insbesondere wurden Fortschritte in den internationalen Verhandlungen zwischen den vier Partnern (Kanada, Europäische Union, Japan und Russland) in Bezug auf die rechtliche Grundlage erzielt. Vier mögliche Standorte wurden vorgeschlagen, nämlich Clarington in Kanada, Rokkasho Mura in Japan, Cadarache in Frankreich, und Vandellós in Spanien. Die technischen Bewertungen werden bis Ende 2002 abgeschlossen und die Berichterstattung wird zu Beginn des Jahres 2003 erwartet.

Verschiedene andere Länder ziehen in Betracht, dem ITER Projekt beizutreten. Die Vereinigten Staaten, als Mitbegründer des urpsrünglichen ITER Projekts, organisierten im Sommer 2002 ein Meeting der ganzen amerikanischen Fusionsgemeinschaft in Snowmass. Nach einer gründlichen Analyse der möglichen Wege zu einem Fusionsreaktor, wurde mit überwältigender Mehrheit beschlossen, dass ITER erste Priorität erhalten und dass die Vereinigten Staaten dem ITER Projekt wiederum als voller Partner beitreten sollten. Diese “Volksmeinung” wurde schliesslich durch der amerikanischen Regierung nahestehende wissenschaftliche Gremien bestätigt und eine endgültige Regierungsentscheidung wird zu Beginn des Jahres 2003 erwartet. Auch die Republiken von China und Korea bezeugten ein Interesse daran, ITER Partner zu werden.

Zusammenfassend kann festgehalten werden, dass das internationale Engagement für ITER jetzt sehr stark ist. Die Gründe sind einerseits die Erkenntnis der Regierungen, dass die Fusion eine wichtige Rolle in der nachhaltigen Energie-Entwicklungsstrategie zu spielen hat, dass andererseits ITER der richtige nächste Schritt und die Zeit nun reif für eine Entscheidung ist.

In der Europäischen Union wurde das Fusionsprogramm im Rahmen des Euratom Vertrages vom Ministerrat genehmigt. Die Reaktorausrichtung des fünften Rahmenprogramms (FP) wurde im sechsten (2003-2006) bestätigt. Ueber 200 Millionen Euros des totalen Gemeinschafts-Budgets für Fusion von 750 Millionen Euros sind während der Periode 2003-2006 für ITER vorgesehen.

1.2 Das CRPP im Jahr 2002

Im Jahr 2002 wurde die neue Struktur der Ecole Polytechnique Fédérale de Lausanne (EPFL) eingeführt. Das CRPP wurde ein Forschungszentrum innerhalb der Fakultät für Grundwissenschaften (FSB = faculté des sciences de base). Seine Mission, interne Struktur und Rolle als Assoziationsmitglied des Euratom Programms blieben unverändert. Das erste Jahr der Integration in die EPFL und

FSB verlief dank der starken Unterstützung des CRPPs durch die Direktionen von EPFL und FSB problemlos.

Die formelle Zusammenarbeit zwischen EPFL und Paul Scherrer Institut auf dem Gebiet der Fusion wurde neu definiert und ein neuer Vertrag, der die Verteilung der Finanzbeiträge regelt, wurde am Ende von 2002 unterzeichnet.

Auf der Forschungsebene wurden im Jahr 2002 wichtige wissenschaftliche Resultate erzielt, und zwar auf allen Aktivitätsgebieten des CRPP, insbesondere:

- Rekord Elektronentemperaturen von 18keV, quasi-stationäre erhöhte Einschluss-Regime (interne Elektronen Transport Barrieren) und Demonstration von Plasmaheizung bei der dritten harmonischen Frequenz, all dies im TCV Tokamak;
- Technische Durchbrüche in den nichtlinearen gyrokinetischen Simulationen, die Untersuchungen der Sättigungsmechanismen von instabilen Driftwellen erlaubten;
- Wichtige Resultate, die zu besserem Verständnis und Kontrolle von MHD und Instabilitäten von schnellen Teilchen führte und die, was die Randphysik anbetrifft, auf dem JET Tokamak in Grossbritannien durchgeführt wurden;
- Ein ständig zunehmendes Interesse der Industrie für unsere Originalerkenntnisse auf dem Gebiet der Plasmaverarbeitung;
- Beträchtliche Beiträge zur Weiterentwicklung von supraleitfähigen Magneten für ITER, insbesondere neue und detaillierte Erkenntnisse des Widerstands zwischen Strängen;
- Kontinuierliche Fortschritte im Verständnis der grundlegenden Eigenschaften von Fusionsneutronen-resistenten Legierungen.

Dieser Reichtum an Resultaten widerspiegelt sich in der zunehmenden Zahl von Uebersichtsvorträgen, eingeladenen und eingereichten Papers an internationalen Konferenzen über Physik und Technologie und in zahlreichen Papers in begutachteten wissenschaftlichen Journalen. Die 29. EPS Konferenz in Montreux wurde vom CRPP organisiert und von über 630 Delegierten aus aller Welt besucht.

Die Konstruktion der TORPEX Maschine für Plasma Grundlagenphysik ist fast vollendet. Es wird erwartet, dass sie zu Beginn des Jahres 2003 für Experimente voll einsatzbereit sein wird. Mit diesem neuen Gerät wird die alte Tradition der Plasma Grundlagenphysik am CRPP erneuert. Mit TORPEX werden fundamentale plasmaphysikalische Probleme, die für die magnetische Fusion von Interesse sind, in einem gut diagostizierten Laborplasma untersucht. Gleichzeitig dient das Gerät zur Ausbildung von Doktoranden.

Auf den folgenden Seiten ist eine detaillierte Beschreibung aller Resultate und Aktivitäten wiedergegeben. Einige dieser Aktivitäten werden im Rahmen des Euratom Assoziationsvertrags durchgeführt und andere wiederum werden ausserhalb dieses Vertrags finanziert. Unser spezieller Dank richtet sich an alle Geldgeber, die unsere langjährigen Forschungsziele unterstützen.

1 INTRODUZIONE

1.1 Avvenimenti principali nel campo della fusione magnetica durante 2002

Nel 2002, il futuro di ITER (*International Tokamak Experimental Reactor*) ha dominato la scena politica nel campo della fusione magnetica. Diversi passi positivi importanti sono stati intrapresi verso la decisione di costruire il piu' grande progetto internazionale mai concepito in fusione. Progressi significativi sono stati compiuti durante le negoziazioni che definiscono la struttura legale per la collaborazione dei quattro partners (il Canada, l'Unione Europea, il Giappone e la Russia). Quattro siti sono stati proposti, Clarington in Canada, Rokkasho Mura in Giappone, Cadarache in Francia, e Vandellos in Spagna. La valutazione tecnica dei siti sarà completata alla fine del 2002 e pubblicata nella prima parte del 2003.

Diversi altri paesi stanno considerando di participare a ITER. Gli Stati Uniti d'America, co-fondatori del progetto originale di ITER, hanno riunito tutta la comunità di fusione americana a Snowmass in Colorado nell'estate del 2002. Dopo un'analisi completa delle diverse strade possibili per lo sviluppo di un reattore a fusione, la grande maggioranza dei presenti ha concluso che ITER deve costituire la priorità per la ricerca e sviluppo in questa direzione, e che gli Stati Uniti devono tornare a far parte del processo ITER allo stesso livello degli altri paesi membri. L'opinione della comunità scientifica della fusione americana è stata in seguito confermata da rappresentati del governo americano per la politica della scienza. Una decisione finale è attesa per l'inizio del 2003. Le repubbliche di Cina e Corea hanno anch'esse espresso un forte interesse per partecipare alla collaborazione ITER.

L'impegno della comunità internazionale per ITER è in questo momento molto forte. Tale impegno è basato sulla convinzione dei governi che la fusione rappresenta un'importante opzione per il futuro dell'energia nell'ambito di una politica di sviluppo sostenibile, che ITER è il prossimo passo da intraprendere, e che il momento è maturo per intraprendere tale passo.

Nell'Unione Europea, il programma di fusione all'interno del trattato Euratom è stato ratificato dal Consiglio dei Ministri. L'orientamento verso uno sviluppo di un reattore a fusione, già proposto per il 5^0 Programma Quadro, è stato confermato per il 6^0 Programma Quadro (2003-2006). Una frazione importante del budget per la fusione, fino a 200 milioni di Euro, su un totale di 750 milioni, è stata attribuita a ITER per il periodo 2003-2006.

1.2 Il CRPP nel 2002

Nel 2002 è stata introdotta la nuova struttura del Politecnico Federale di Losanna (EPFL). Il CRPP è diventato un Centro della Facoltà delle Scienze di Base (FSB). La sua missione, la sua struttura interna ed il suo ruolo di Associazione nell'ambito del programma Euratom sono rimasti inalterati. L'integrazione nella nuova

struttura durante il 2002 si è svolta senza problemi maggiori, grazie anche all'importante supporto fornito dalle direzioni della FSB e di tutta l'EPFL.

La collaborazione formale del CRPP con l'Istituto Paul-Scherrer nel campo della fusione è stata ridefinita, ed un nuovo contratto che stabilisce la contribuzione finanziaria di entrambe le parti è stato firmato alla fine del 2002.
Sul fronte della ricerca, il 2002 ha portato risultati scientifici importanti in tutti i campi di attività del CRPP. Fra questi citiamo:

- Record di temperatura elettronica di 18 keV nel tokamak TCV, un regime quasi-stazionario di confinamento migliorato con una barriera di trasporto interna per gli elettroni, e la dimostrazione di riscaldamento del plasma tramite la terza armonica della frequenza di ciclotrone elettronica.
- Progressi nei codici numerici di simulazione del plasma basati sul modello giro-cinetico, che hanno permesso lo studio dei meccanismi di saturazione delle onde di deriva in un tokamak
- Risultati sperimentali ottenuti presso il tokamak europeo JET, nel Regno Unito, che portano ad una miglior comprensione e controllo di instabilità MHD e legate a particelle energetiche, e per la fisica del bordo del plasma.
- Risultati nell'ambito di applicazioni industriali dei plasmi, che hanno ulteriormente motivato un interesse per la scienza dei plasmi da parte dell'industria
- Contributi significativi all'evoluzione dei magneti superconduttori per ITER, in particolare tramite studi innovativi della resistenza fra conduttori individuali.
- Progressi nella comprensione della proprietà fondamentali di leghe metalliche resistenti ai neutroni prodotti dalle reazioni di fusione

Questa grande quantità di risultati è stata presentata in un numero sempre maggiore di presentazioni invitate e contributi a conferenze internazionali di fisica e tecnologia, e in numerosi articoli apparsi su riviste scientifiche internazionali. La 29ª conferenza della divisione di fisica del plasma della Società Europea di Fisica è stata organizzata dal CRPP a Montreux. Più di 630 delegati provenienti da tutto il mondo vi hanno partecipato.

La costruzione di nuovo esperimento per la fisica del plasma di base, TORPEX, che rinnoverà una lunga tradizione al CRPP in questo ambito, è stata intrapresa e quasi completata. L'inizio degli esperimenti è previsto per la prima parte del 2003. TORPEX sarà utilizzato per studiare fenomeni fondamentali di fisica del plasma che hanno un'applicazione nella fusione magnetica in condizioni che permettono l'utilizzo di una grande varietà di tecniche di misura, e per contribuire alla formazioni di studenti universitari e di dottorato.

Una descrizione dettagliata di tutte le attività del CRPP ed i risultati ottenuti nel corso del 2002 è riportata nel seguito. Una parte di queste attività sono state condotte nell'ambito del contratto di Associazione con l'Euratom, altre sono state finanziate indipendentemente dall'Euratom. I nostro ringraziamenti vanno a tutte le sorgenti di finanziamento che ci hanno permesso, e ci permetteranno di perseguire i nostri scopi di ricerca a breve ed a lungo termine.

2 RESEARCH ACHIEVEMENTS OF THE CRPP IN 2002

2.1 The TCV tokamak

2.1.1 The TCV tokamak: recent advances

The *Tokamak à Configuration Variable*, TCV (major radius R=0.88m, minor radius a<0.255m, toroidal magnetic field B_T<1.54T, vessel elongation of three), continues to concentrate the efforts of the CRPP in the field of magnetic fusion physics. The worldwide fusion community is now focusing on ITER, the large next step device aimed at technology and physics issues in plasma environments of direct relevance to fusion reactors. The role of small and medium sized experiments in Europe is therefore concentrating on scientific and technical support for ITER, and on providing facilities for the training of next generation researchers. On one hand, these must address the scientific questions that have been recognised as limiting our understanding of magnetically confined plasmas and our ability to control them in ITER relevant scenarios. On the other hand, experiments of the TCV class are best able to explore new avenues to improve the performance of tokamak plasmas on the way to a conceptual fusion power plant that cannot necessarily be covered by ITER.

The success of ITER and future fusion reactors based on the tokamak concept relies heavily on the achievement of high performance regimes, i.e. large core plasma pressures without macroscopic plasma instabilities and good energy and particle confinement. Optimising the performance and limits of operation of these scenarios is one of the major tasks that the fusion community faces at present. Such improvements require appropriate choices of plasma geometry and the ability to control the profile of a number of plasma parameters such as the plasma pressure and the electrical current.

The flexibility of its configuration and control systems makes TCV a unique tool worldwide to contribute to research in this direction, in particular to investigate the effects of plasma shape on a number of features of tokamak plasmas, including stability and confinement. Such versatility is matched by that of the main heating system, Electron Cyclotron Heating, ECH. Timing and geometrical flexibility, ease of controlling the deposition location and the ability to be absorbed in a very narrow region are unique properties of ECH systems. The TCV ECH system has progressed dramatically during the past few years. The second cluster of three second-harmonic (X2) 82.7GHz gyrotrons came on line in 1999. The first of three third harmonic (X3) 118GHz gyrotrons became available in 2000 and was used in an initial set of experiments with lateral heating through one of the X2 launchers. Finally, the full three-gyrotron X3 system was available in 2001 and full power heating through a combination of its dedicated top launcher and a lateral launcher has been demonstrated in 2002. Nearly all of the TCV ECH design goals have now been met, with a total power of 4.5MW, of which up to 3.5MW have been injected into the plasma.

The installation of a third harmonic ECH system is expected to extend the range of densities achievable on TCV, improving the electron-ion collisional coupling and increasing the value of plasma β, advancing the reactor relevance of TCV plasmas.

In addition to providing a tool to improve the TCV performance and approach the β limits, these systems can be used to drive plasma current non-inductively, and investigate a number of questions related to profile modifications, advanced tokamak scenarios, as well as the physics of energetic electrons.

This overview highlights the most salient progress made on TCV during 2002, while the details are discussed in the individual sections of this chapter. Investigations followed five main avenues, namely focusing on effects of plasma shape on operational and stability limits (Section 2.1.2), H-modes and the associated edge localised mode dynamics (Section 2.1.3), edge and divertor physics (Section 2.1.4), the physics of ECH and EC Current Drive (ECCD) (Section 2.1.5), and the use of ECH and ECCD as tools for advanced tokamak physics of relevance for next step developments (Section 2.1.6).

The TCV operational domain has been extended by applying off-axis ECH. This leads to a broadening of the current profile, which allows us to obtain highly elongated discharges at relatively low plasma currents. Such a technique is particularly promising to heat overdense plasmas off-axis using second harmonic ECH and in the core using third harmonic ECH. The latter method will be used to approach the β limit at intermediate values of normalised current.

A common operational limit observed on all tokamaks is related to the density. In the highly elongated TCV plasmas neither Hugill nor Greenwald empirical expressions for the maximum achievable density seems to apply, as the density limit depends not only on the elongation, but also on the divertor geometry and the power flux through the separatrix.

The dependence of the lifetime of impurities on plasma shape and other parameters has been investigated by injecting Si traces. While for triangularity and plasma current there seems to be little dependence above a certain value, the impurity lifetime is observed to decrease with increasing toroidal field and elongation, even if the energy confinement time remains essentially unchanged.

The role of the plasma shape is important in limiting the deleterious effects of MHD activity during the current ramp-up phase. Small degrees of plasma shaping are shown to be sufficient to avoid modes that lead to disruptions. A reduction of sawtooth activity was found for sufficiently large values of plasma elongation. The possibility of controlling sawtooth stability by using a combination of injection angles for the second harmonic ECH was demonstrated. These results illustrate methods to avoid potentially deleterious instabilities that are triggered by large sawteeth, such as neoclassical tearing modes.

The ELMy H-mode regime, the reference scenario for ITER operation, has been studied in TCV ohmic plasmas in terms of LH transition and ELM physics. Although Ohmic H-modes are easy to obtain in TCV, even with the ion ∇B drift direction away from the X-point, transitions to steady-state ELMy H-modes are only obtained in a narrow region of the operational domain.

A number of experiments were conducted on the ELM dynamics in H-modes, leading to results such as the discovery of the chaotic but deterministic nature of the ELM process, the observation of synchronisation between sawteeth and ELMs and the first experimental evidence that the ELM frequency can be affected by externally applied perturbations.

The shaping capabilities of TCV can also be applied to vary the geometry of the divertor. Understanding Ohmic divertor detachment for different geometries has continued to be a central theme of the edge physics studies on TCV. A common feature of detached plasmas is the very low divertor target electron temperatures required for the detachment to occur. It has recently become clear that target embedded Langmuir probes yield temperatures considerably in excess of expected values. One possible explanation for this, the presence of fast electrons in the scrape-off layer, has been extensively studied. Arrays of divertor target probes and a new fast reciprocating probe have been used to study the effects of Type III ELMs on the TCV scrape-off layer and divertor. A fast electron Type III ELM precursor, synchronous with upstream MHD activity, has clearly been observed.

Pure helium plasmas have been produced on TCV with the aim of comparing edge and divertor physics in deuterium and helium plasmas on a compact, open divertor tokamak with observations in JET, a much larger device with a more closed divertor.

The range and potential impact of ECH and ECCD physics studies on TCV have been significantly extended by enhancing the relevant diagnostic and modelling tools. The reliability of modulated EC power deposition measurements with soft X-ray signals has been enhanced through the development of a system identification method based on singular value decomposition. Continuing use has been made of our high field side electron cyclotron emission (ECE) radiometer and hard X-ray (HXR) camera to diagnose the suprathermal electron population created by ECCD. The quasi-linear Fokker-Planck code CQL3D has been equipped with a radial electron transport model and a module to calculate the HXR emissivity, leading to novel comparisons with experimental results.

This powerful set of tools has led to a number of detailed investigations of the physics of ECH and ECCD, including wave-particle interaction and suprathermal electron dynamics, in new regimes characterised by the highest EC power density achieved on any tokamak.

The stabilisation and destabilisation of sawteeth with ECH and ECCD in different heating geometries has been successfully reproduced with first principles-based numerical simulations. The effect of ECH on sawteeth is indeed so reproducible that it has become the standard tool for ECH launcher alignment.

High-density discharges, inaccessible to the X2 system, have been heated with 1.5MW X3 ECH, resulting in a significant extension of the operational regimes of interest in TCV. By steering the top launcher, the X3 waves can be selectively coupled to different electron energies, providing an additional powerful tool for studies of suprathermal electron dynamics, to extend the investigations already performed with the HXR and ECE systems.

In the course of the past few years TCV has become a unique test bed for studying the fundamental properties of ECCD. The exceptional flexibility provided by the six independently steerable X2 launchers has been used in a series of experiments aimed at elucidating both the global properties of ECCD and the dynamics of the current-carrying suprathermal electrons. HXR and ECE measurements, combined with Fokker-Planck modelling, have already allowed us to establish the importance of cross-field transport of the current carriers in the physics of ECCD: with a diffusivity in excess of $1.5 m^2/s$, nonlinear enhancement of the ECCD efficiency is inhibited and centrally peaked ECCD profiles are obtained even with purely off-axis

heating. Further insight in the physics of ECCD has been provided by our ability to run fully non-inductively driven discharges in steady state, without the complicating effects of a toroidal electric field.

TCV is at the forefront of this field of research, benefiting in particular from the high quality and flexibility of its EC system and the highest power density available. In addition, in the low collisionality TCV plasmas, the heating power that is directly coupled to the electrons cannot be transferred to the ions, making it possible to isolate the transport mechanisms affecting the only electrons.

ECH and ECCD have proven to be powerful tools for current profile modification for establishing and controlling improved core electron confinement modes. Reversed or weak central shear discharges at moderate elongation, produced by central counter-current drive in combination with pure ECH deposited off-axis for improving MHD stability, lead to stable electron confinement enhancements of a factor up to 4.5 over Rebut-Lallia-Watkins scaling, and new record electron temperatures of 18keV.

A steady-state fully non-inductively driven reverse shear scenario with 80% bootstrap fraction and a clear electron Internal Transport Barrier (eITB) has been obtained, showing that it is possible to align the maximum of the bootstrap current density, dependent on the maximum of the pressure gradient and thus on the ITB location, with the position of the minimum of the q profile, which determines the confinement properties and therefore the ITB position. This remarkable experimental achievement indicates the way towards the development of advanced scenarios based on steady-state discharges with a large bootstrap fraction.

2.1.2 The effects of plasma shape on tokamak operational space and performance

One of the original goals of TCV was the exploration of the plasma shapes that can be produced and stably maintained in a tokamak. In the past few years that systematic investigation has been completed.

The operational domain that can be achieved in the Ohmic regime has been extensively investigated, including extremely elongated plasmas (κ=2.8) and unconventional plasma shapes. Extension of the Ohmic operational domain requires control of the current profile to sustain the different shapes in a reactor relevant range of performance parameters.

On TCV this is possible by applying off-axis ECH, leading to a broadening of the current profile, which generates more elongated discharges at relatively low plasma currents. Such a technique is particularly promising to heat overdense plasmas in the core using third harmonic (X3) ECH and off-axis using second harmonic (X2) ECH.

As the database of TCV discharges becomes more and more complete, statistical analyses assume deeper and deeper meaning. Among these, we performed comparisons between the measured properties of TCV Ohmic discharges in L-mode and those predicted by first principles turbulent equipartition theory.

A serious limitation for next step devices such as ITER is the existence of a limit value for the plasma density above which stable operation is prevented. TCV

contributes to the understanding the physics behind this limit by exploring its dependence on the plasma shape.

The confinement is also shown to depend on the plasma shape, for both the bulk plasma and the impurities. The electron and bulk ion transport is characterised by a similar improvement in the energy confinement time with plasma elongation, up to about two, as expected from geometrical effects. The dependence of the lifetime of impurities on plasma shape and parameters has been investigated by injecting traces of Silicon. While for triangularity and plasma current there seems to be little dependence, the impurity lifetime is observed to decrease with increasing toroidal field and elongation.

With its variable plasma shape and localised EC heating system, TCV also provides a unique environment for investigating the basic properties of MHD modes and their effect on the tokamak operational limits. The role of the different plasma shape parqameters in limiting the deleterious effects of MHD activity during the current ramp-up phase was investigated. Modest plasma shaping is shown to be sufficient to avoid locked modes that lead to disruptions. A reduction of sawtooth activity was also found for sufficiently large values of the plasma elongation. The possibility of controlling sawtooth stability, and consequently the occurrence of the potentially deleterious Neoclassical Tearing Modes (NTMs), by using X2 ECH has been demonstrated.

Extension of TCV operational space towards high elongation and high normalised plasma current

Elongated discharges are vertically unstable and can only be stabilised if the current profile is broad by providing sufficient current density close to the plasma edge. For Ohmic discharges, this is achieved by operating at a low edge safety factor, q_{edge}. Discharges with elongation in the range $2.2<\kappa<2.8$ have been stabilised at high values of the normalised plasma current $I_N=I_p/aB\sim2.8$-3.5MA/mT. However, for highly elongated plasmas, the β-limit predicted by ideal MHD can only be approached at intermediate I_N values, $I_N\sim2$MA/mT. For these values Ohmic discharges are too vertically unstable to be controlled, but TCV plasmas have been rendered controllable by current profile broadening using far off-axis second harmonic electron cyclotron heating (X2 ECH), up to $\kappa\sim2.48$, with $I_N\sim1.05$MA/mT and $q_{edge}\sim10$. Such discharges also provide information on the confinement properties of highly elongated plasmas, leading in particular to a decoupling of κ and I_p, important in establishing confinement scaling laws.

Typical time traces for a highly elongated plasma produced with off-axis ECH are shown in Fig. 2.1.1. ECH is launched into an intermediate elongation plasma, keeping the pre-programmed quadrupole and hexapole fields constant. The X2 power is deposited far off-axis ($\rho_{dep}>0.5$), using upper lateral launchers with a short beam path in the plasma to minimize refraction effects. The local EC power deposition leads to a local increase in temperature and conductivity, hence to a broadening of the inductively driven current profile (ECCD and bootstrap currents are negligible in this case). As a result, the plasma elongation increases over a current redistribution time. The internal inductance l_i decreases when the current profile is broadened or when the elongation is increased. To separate the direct plasma shape influence, a normalised inductance is defined: $l_i^* \sim l_i\,(l^2/4\pi S)$. Here S is

the plasma cross-section area, and l is a parameter depending on the perimeter of the plasma cross-section and the poloidal magnetic field.

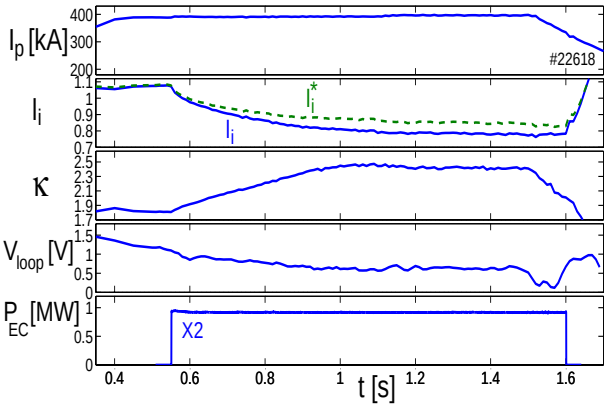

Fig. 2.1.1 *Decrease of l_i and increase of κ with far off-axis ECH applied during the current flattop*

The experimental results are compared to those of the fixed boundary transport code PRETOR based on the Rebut-Lallia-Watkins (RLW) model. Both the experiment and the PRETOR simulation show that the optimal location of the EC power deposition for broadening the current profile is restricted to the region $0.55<\rho_{dep}<0.7$ (Fig. 2.1.2). For $\rho_{dep}<0.55$, the current profile broadening effect is reduced, and for $\rho_{dep}<0.4$ the ECH power makes the profile even more peaked. For $\rho_{dep}>0.75$, the ECH power is not well confined and its effect on the current profile is substantially reduced.

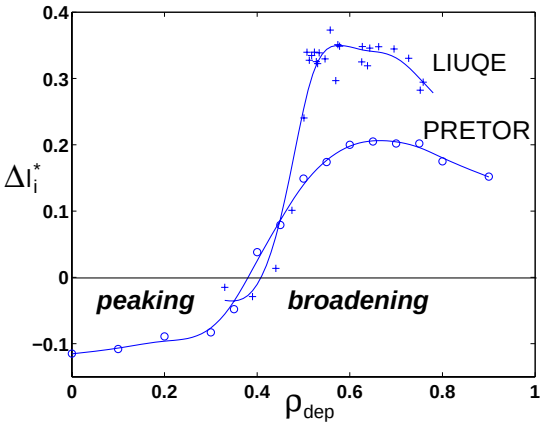

Fig. 2.1.2 *Current profile change for different radial deposition location; I_p=300kA, P_{EC}=1MW.*

The rate at which l_i^* grows during the initial part of the plasma discharge increases with the EC power, but this increase is observed to saturate above a certain EC power level. This observation suggests an increase of the thermal diffusivity χ_e with absorbed power faster than linear and is qualitatively confirmed by the PRETOR simulations. The experimental χ_e profiles for an EC power scan are shown in Fig. 2.1.3, indicating an increase of χ_e with power just outside the deposition radius, corresponding to a decrease of the global electron confinement time from 6.5 to 3.5ms. Direct heat wave information using local power modulation techniques will help clarifying the relation between energy transport and the current profile.

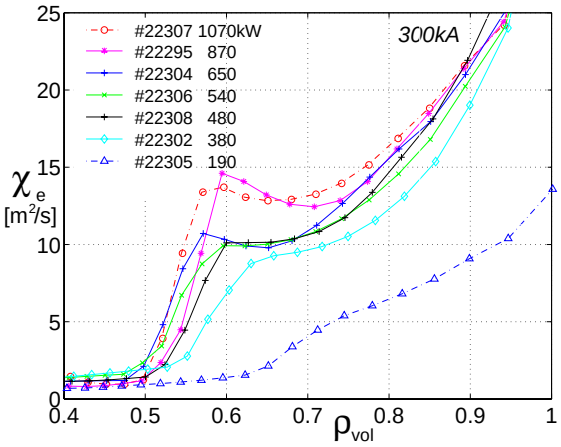

Fig. 2.1.3 *Profiles of electron thermal diffusivity χ_e for different absorbed powers (ρ_{dep}~0.6).*

Operation at high plasma density, even overdense in the core, is observed to improve the efficiency of off-axis deposition to increase plasma elongation (Fig. 2.1.4). For constant injected power, higher elongation is obtained at higher density. This is due to the usual increase of confinement with density, corresponding to a decrease of the electron thermal diffusivity (Fig. 2.1.5), and to an increased electron to ion coupling, corresponding to a flattening of the current profile. In the absence of a direct measurement of the current profile, two pieces of evidence confirm this hypothesis. First, the temperature profile, related to the conductivity profile, proportional to $T_e^{3/2}(\rho)$, is flattened. The second piece of evidence comes from MHD activity. At low density, with off-axis heating at low current, 300kA, sawteeth are lost during the elongation ramp-up when $q_o>1$, without noticeable mode activity. Above a threshold density, internal mode activity occurs at the q_o~1 crossing. At higher current, this activity can persist during the whole discharge without a significant change of the q=1 radius (Fig. 2.1.6). Such mode activity is analysed using a 64-channel multi-wire proportional soft X-ray diagnostic. An m=1,2,3 mode structure inside the inversion radius (Fig. 2.1.7) is found where the m=2 and 3 mode amplitudes are respectively 70% and 20% of the m=1 amplitude, a typical signature of a flat current profile in the core.

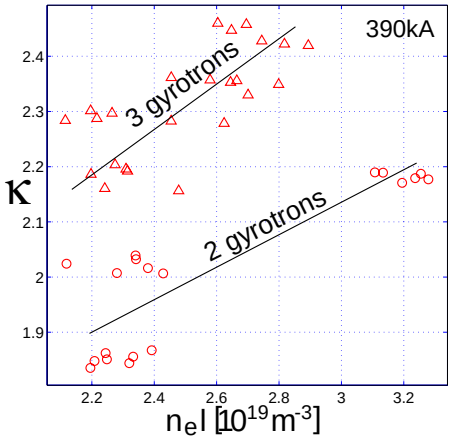

Fig. 2.1.4 *Increase of elongation κ at high density with constant EC power against the line integrated electron density.*

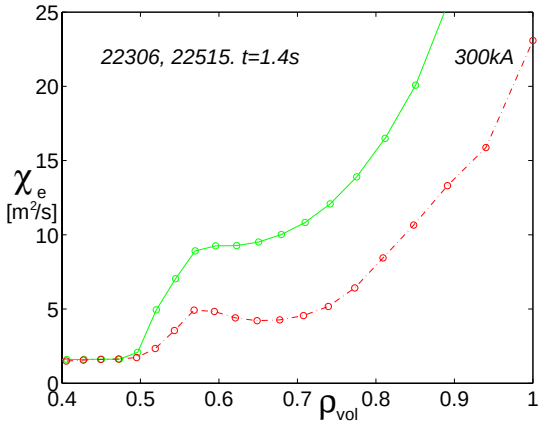

Fig. 2.1.5 *Reduction of χ_e with density (green: n_{eo}~3.7 $10^{19}m^{-3}$, red: n_{eo}~2 $10^{19}m^{-3}$).*

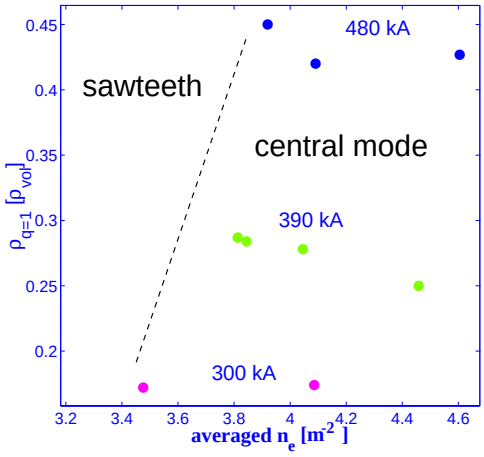

Fig. 2.1.6 *Above a threshold density, sawteeth are replaced by a continuous rotating mode, without significant change in the q=1 radius.*

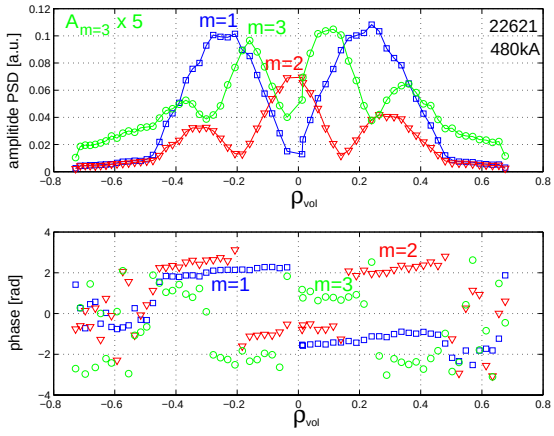

Fig. 2.1.7 *m=1,2,3 mode activity inside the inversion radius ρ_{inv}=0.4, from the 64 channel soft X–ray multiwire proportional chamber diagnostic.*

In summary, the use of far off-axis X2 ECH in high-density discharges has allowed us to extend the range of elongated equilibria at intermediate currents substantially, Fig. 2.1.8.

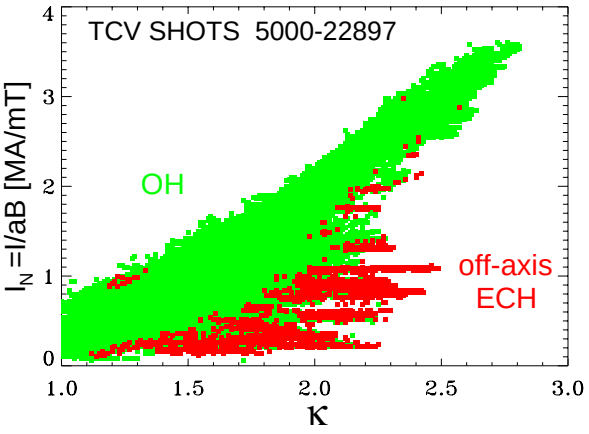

Fig. 2.1.8 *Extension of TCV operation: Ohmic discharges (green) and ECH (red).*

High-elongation, high-density discharges, overdense to X2 in the core, are being developed with the long-term goal of approaching β-limits. At present, these discharges provide the target plasma for initial X3 heating and deposition studies, in which X3 absorption is high due both to high n_eT_e and to high κ, the latter enhancing the absorption by the shallow incidence on the resonance.

A typical scenario for these studies consists of a first X2 heated phase, which reaches an elongation limited by vertical stability. Subsequent X3 heating with central deposition peaks the current profile. The resulting increase of l_i and decrease of κ can only be partly compensated by the shaping coils: keeping the elongation constant, while X3 peaks the current profile, leads to an increase of the vertical instability growth rate, limiting the maximum stable elongation.

With the help of far off-axis X2 power deposition to broaden the current profile, discharges with high elongation, κ~2.5, I_N~1.05, and centrally overdense to X2, have been created and sustained. Higher values of κ and I_N will be achievable with the full X2 power (4 beams) from the upper lateral ports. In these plasmas, X3 power absorption close to 100% has already been reached, with typically 60-70% deposited centrally on the bulk electrons, and the rest on suprathermals with a broader and sometimes hollow radial distribution in the presence of suprathermal electrons (see Section 2.1.5).

Modelling of density profile peaking

Previous investigations in TCV have established that temperature, pressure and density profile peaking factors follow a scaling with the parameter $\langle j \rangle / (q_0 j_0)$ irrespective of plasma shape and nearly independent of ECH heating, when power is centrally deposited and no ITB is formed. Moderately peaked density profiles are observed in steady-state discharges, both in small and in large devices (such as JET), in L-mode as well as in H-mode confinement. The phenomenon is interesting due to its effect on fusion performance, but also because it may provide information on the underlying transport processes. The physical mechanisms leading to peaked density profiles are a topic of active research and controversy. The large variety of discharge conditions in the TCV confinement and profile database, including an unequalled set of different plasma shapes, provides some indications on the relative importance of the mechanisms proposed in the literature, Turbulent Equipartition

(TEP, sometimes also dubbed 'q-pinch'), anomalous thermodiffusion and the Ware pinch (or the related, albeit controversial Varma pinch).

The steady-state density gradients resulting from a balance of diffusive and convective fluxes in the source-free plasma interior can be written as

$$\nabla n/n=-\alpha_q \nabla q/q+\alpha_{Tj}\nabla T_j+v_{Ware}/D$$

where n is the density of the species under consideration, α_q and α_{Tj} refer to normalised off-diagonal fluxes and v_{Ware} is the Ware pinch and D the particle diffusion coefficient.

A magnetic shear dependent term, as above, is born out of both fluid model simulations (with $\alpha_q<0.4$ typically) and from TEP based on kinetic theory (with $0.3<\alpha_q<1$). The coefficient of the thermodiffusive fluid term is $\alpha_{Tj}<0.5$. In the presence of a Ware pinch, the absolute magnitude of the particle diffusion coefficient must be given to evaluate density profile peaking from the above equation. Since this is generally not available, we attempt to infer it from the heat diffusivity obtained from the power balance, using the ansatz $D\propto\chi_{eff}$. From purely convective turbulent heat transport one would expect $D\approx 2\chi_{eff}/3$.

Density profiles and the scaling of peaking factors with $\langle j\rangle/(q_0 j_0)$ can be satisfactorily modelled, assuming TEP with $\alpha_q\approx 1$ in Ohmic L-mode and H-mode discharges and $\alpha_q\approx 0.8$ in ECH discharges. Pure thermodiffusion is somewhat less satisfactory, since at low values of $\langle j\rangle/(q_0 j_0)$, $\alpha_{Te}>0.5$ would be required. TCV data are not consistent with particle diffusivities as low as sometimes quoted in the literature ($0.01<D/\chi_{eff}<0.25$). Density peaking in Ohmic plasmas can only be modelled satisfactorily by the Ware pinch, assuming D/χ_{eff} in the range 0.2-0.3. However, consideration of ECH heated discharges, in which heat diffusivities are significantly increased, excludes such low values of D/χ_{eff}, because they would lead to much flatter density profiles than those actually observed. The modest amount of flattening observed in ECH discharges is however consistent with $D\approx 2\chi_{eff}/3$, when combined with TEP and/or thermodiffusion. As an example, Fig. 2.1.9 shows how TCV Ohmic peaking is modelled assuming $\alpha_q=0.7$, $\alpha_{Te}=0$ and $D=2\chi_{eff}/3$. Figure 2.1.10 shows the prediction for the diminishing effect of the Ware pinch, as ECH power (hence D) is increased, together with the experimental data.

In conclusion, the main cause of density peaking must be an anomalous pinch effect, such as produced by TEP or thermodiffusion, with the Ware pinch playing a smaller role. Plasma shaping is not in itself responsible for the peaking effects, although proper scaling of the effect across different plasma shapes requires the use of an appropriate shape dependent scaling parameter

$$\frac{\langle j\rangle}{q_0 j_0}=\frac{\kappa_0}{1+\kappa_0^2}\times\frac{\mu_0 I_p}{B_0 A_p}$$

where κ_0 and B_0 are the axial elongation and toroidal field, I_p the plasma current and A_p the plasma cross-sectional area. Future research will be directed at comparing TCV experimental results directly with predictions from anomalous transport theories.

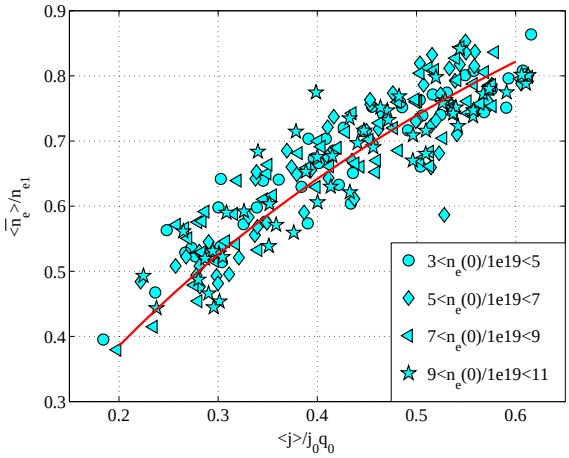

Fig. 2.1.9 *Modeling of Ohmic density profile peaking with α_q=0.7, α_{Te}=0 and D=2χ_{eff}/3 (red line). Symbols are experimental values and distinguish between classes of central density. A wide range of plasma shapes are represented (1<κ<2.5, –0.4<δ<0.7).*

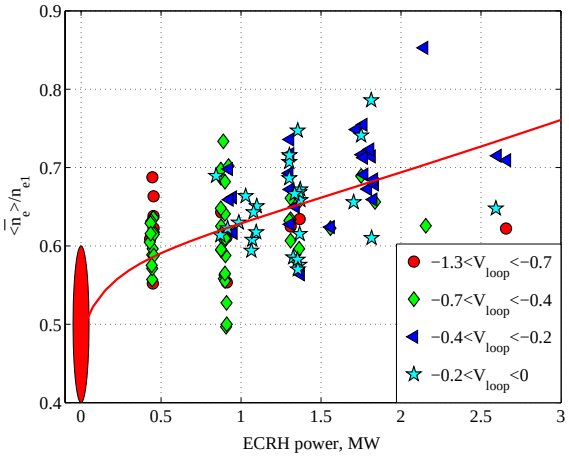

Fig. 2.1.10 *Dependence of density peaking on ECH power (symbols) and average prediction (red line) assuming a contribution from the Ware pinch with D=2χ_{eff}/3.*

Density limits

Experimentally, it is observed that the density in tokamaks can only be increased up to a limit at which the plasma disrupts. The analysis of different experiments has led to a number of empirical expressions for this density limit, among which the most commonly used are the Hugill and Greenwald formulas. The two empirical limits agree for circular plasmas but diverge for elongated plasmas. Data from TCV discharges is used to assess the range of applicability of both empirical expressions and, more generally, to study the influence of the plasma shape on the density limit.

This phenomenological approach is based first on the creation of a database of high-density discharges terminated by a disruption that is not caused for any obvious reasons other than the density limit. For the different classes of plasma geometries, such as limited and diverted configurations, the maximum density did not appear to correspond to either empirical density limit. However, the discharges in the database differed in many other parameters, making the extraction of a dependence of the density limit on the plasma shape difficult.

Dedicated experiments were therefore performed in 2002. In a single null discharge the plasma density was ramped up to the disruption and the density prior to the disruption recorded. The plasma elongation was scanned from pulse to pulse. In

order to decouple the effect of plasma current or safety factor from the elongation scans, different plasma currents were chosen for each plasma elongation. The divertor geometry was found to play an important role in the maximum density obtained in these discharges. The combined scans in plasma current and plasma elongation were therefore performed in two divertor geometries, first with both separatrix legs against the central column and second with one separatrix leg extended down to the floor of the vacuum vessel.

Together with the density, all plasma parameters entering in the expressions for the density limit were measured prior to the disruption, allowing us to estimate at what fraction of the predicted density limit the disruption occurred. This ratio is plotted against the plasma elongation in Fig. 2.1.11 for the Hugill expression. At low plasma elongation the ratio remains below one indicating a real density limit below the Hugill estimation. At high elongation, some scatter of the data is observed. Generally, when the plasma separatrix leg is in contact with the floor of the vacuum vessel the density limit may reach values over the Hugill density limit. In the other case, the density limit remains below the Hugill limit. A cluster of points lies at intermediate values. No explanation has been found so far for these intermediate cases.

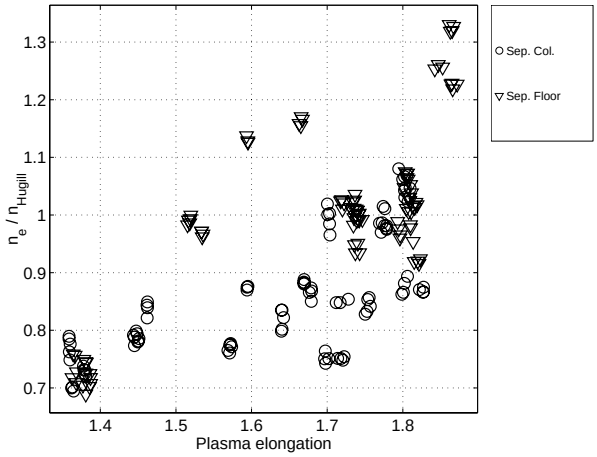

Fig. 2.1.11 *Hugill-normalised density just prior to the density limit disruption as a function of the plasma elongation for two different divertor configurations*

The analogous plot using the Greenwald expression (Fig. 2.1.12) shows a more constant value of the ratio, at least in the long separatrix leg case. Contrary to the previous figure, a decrease of the fraction appears here in the case with the small separatrix leg. In both cases, the value is too low by a factor of two.

In conclusion, the Greenwald density limit accounts more precisely for the dependence on plasma elongation, which was the reason for its proposal, but the predicted limit is too high by about a factor of two for TCV. In addition, the scatter in the data shows that the physics behind the empirical density limit is more complex than that described by the simple Hugill or Greenwald expressions.

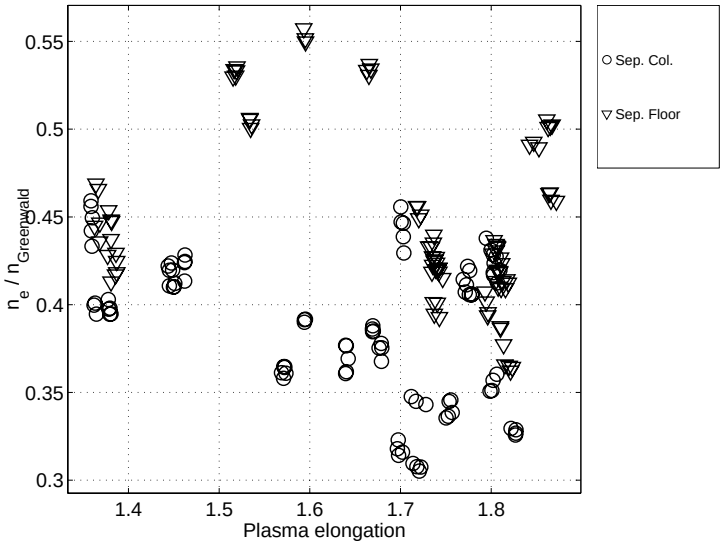

Fig. 2.1.12 *Greenwald-normalised density just prior to the density limit disruption as a function of the plasma elongation for two different divertor configurations*

Triangularity and elongation dependence of impurity transport

To avoid excessive impurity and He ash accumulation in fusion reactors, impurity particle residence times must be sufficiently short with respect to the global energy confinement time. This requirement motivates systematic experimental investigations of laser-ablated trace impurity transport on TCV, focusing in particular on the effects of plasma shape. Experimental data obtained over a wide range of plasma conditions have then been modelled using the STRAHL code.

Impurity residence times were inferred from the exponential decay phase of soft X-ray signals of the transient pulse produced after ablation of Silicon, a non-recycling element. These signals originate essentially from the hotter parts of the plasma, typically $r/a<0.8$, and are mostly due to SiXIII and SiXIV lines, which all decay with the same time constant. Recent measurements using the newly commissioned SPRED VUV spectrometer have shown that SiXII signals, originating from nearer the edge ($r/a\approx0.9$) also decay at the same rate.

The dependence on parameters such as the plasma current, density, toroidal field, triangularity and elongation were obtained in Ohmic L-mode discharges. The triangularity and elongation dependencies of the impurity residence time are shown in Figs 2.1.13 and 2.1.14. The triangularity dependence qualitatively reproduces the dependence of the energy confinement time with $\tau_{imp}/\tau_{Ee}\approx2$, except at the lowest (negative) triangularity discharge. The results from an elongation scan at constant q_{eng} (I_p proportional to elongation) were more surprising. The impurity residence time was seen to drop by a factor of 2.5 as the elongation was increased from 1.6 to 2.3. More importantly, the ratio of impurity to electron energy confinement time, $\tau_{imp}/\tau_{Ee,}$ decreased from near 3 to near 1.2 during the scan.

The STRAHL code uses measured electron density and temperature profiles, the plasma magnetic geometry from an equilibrium reconstruction, and user supplied profiles of impurity diffusivity and radial convective velocity as inputs. It also includes a simulation of the effect of sawtooth relaxations, by periodically mixing

the impurities within the mixing radius. It computes the expected behaviour of line integrated soft X-ray emission, as measured using the 200 channel soft X-ray system on TCV. The simulations are most sensitive to transport parameters in the peripheral region outside the mixing radius. A set of best fitting transport parameter profiles is obtained iteratively by means of scans over a class of predefined parameterised profiles. The impurity diffusion coefficient was assumed to have the form $D(\rho)=D_0+(D_{edge}-D_0)\rho^2$, where $D_0=0.05m^2/s$, $\rho=r/a$ and the convective velocity was assumed to increase linearly with the radius, $v(r)=v_{edge}\rho$.

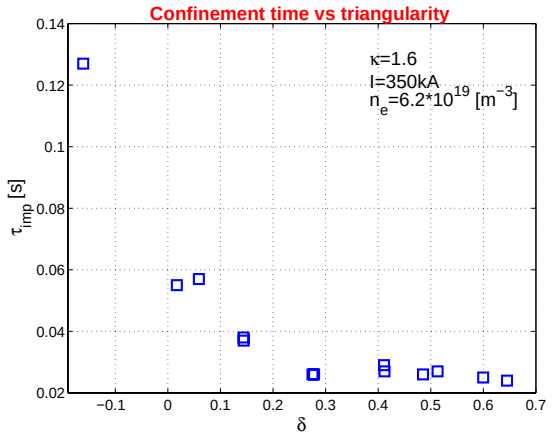

Fig. 2.1.13 *Impurity residence time vs triangularity at nominal toroidal field (B_T=1.43T)*

The convective velocities are always directed outward, with magnitudes up to v_{edge}=5m/s in limiter L-modes, while diverted L-modes appear to be characterized by zero convective velocity. Fig. 2.1.15 shows the simulation for the triangularity scan. It exhibits a moderate drop of the impurity diffusion coefficient with triangularity and a marked increase of the convective velocity. The changes in impurity residence time in the elongation scan are entirely due to a four-fold increase in D_{edge}, with no systematic dependence of the convective velocity as seen in Fig. 2.1.16. A fourfold increase in diffusivity does not lead to a fourfold decrease in residence time because it is partly offset by the reduced average gradients at high elongation. This geometrical effect (named shape enhancement factor) has previously been invoked to model the shape dependence of the energy confinement, where it was found that effective heat diffusivities exhibit no significant dependence on plasma shape.

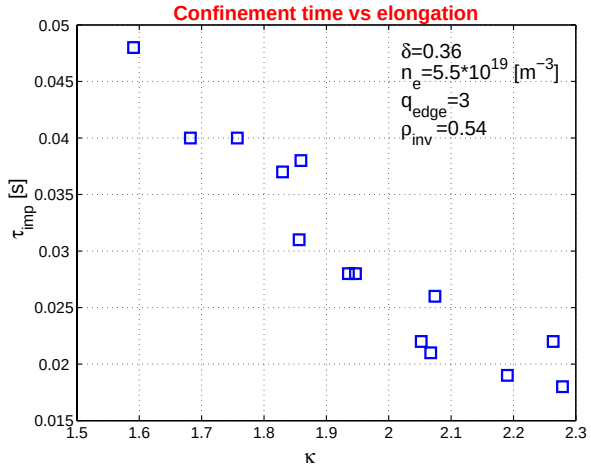

Fig. 2.1.14 *Impurity residence time vs. elongation at B_T=0.9T and fixed inversion radius $\rho_{inv}\approx 0.5$.*

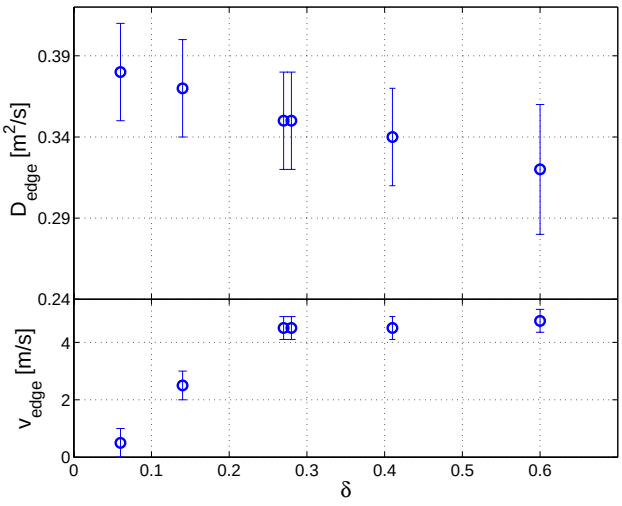

Fig. 2.1.15 *Dependence of impurity diffusivity and convective velocity on triangularity.*

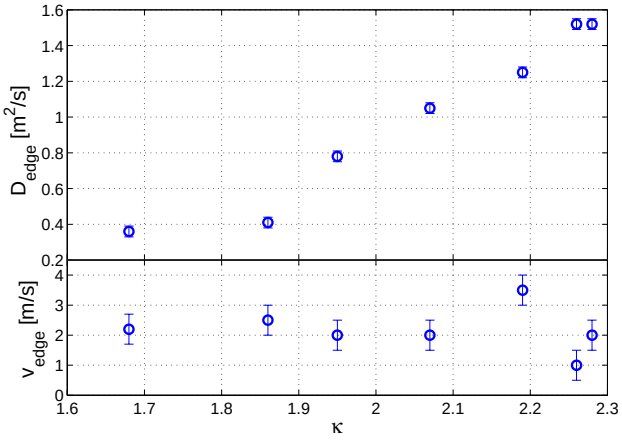

Fig. 2.1.16 *Dependence of impurity diffusivity and convective velocity on elongation.*

MHD activity in shaped plasmas

With its widely variable plasma shape and localised EC heating system, TCV provides a unique environment for investigating the basic properties of plasma MHD modes and the related tokamak operational limits. The control, through plasma shape, of the sawtooth amplitude or of the MHD activity at the q=3 crossing during the current ramp helps avoiding deleterious modes, such as NTMs or modes leading to disruptions.

The beneficial effect of plasma shaping during the initial current ramp-up was noticed early in TCV operation as an effective way to reduce or suppress MHD activity and disruptions. A statistical analysis led to the determination of the region of the parameter space (in q, n_e, κ, δ) where the crossing of q=3 is associated with the generation of locked modes and subsequent disruptions, quantifying the beneficial effect as a function of plasma shape, triangularity and elongation. We have now investigated the evolution of the mode structure in detail together with the coupling between modes arising on the different rational surfaces to describe the dynamics of the MHD modes leading to disruption.

With reduced plasma shaping, bursts of low (m,n) MHD modes are observed when flux surfaces with integer q_{edge} value (q_{edge}=3,4 and 5) approach and cross the plasma boundary. While the modes excited when crossing q=4 and 5 remain at low

amplitude and quickly vanish with no harm, crossing q=3 can cause the termination of the plasma. During the current rise, the MHD activity starts when the q=3 flux surface reaches the plasma edge, with $q_{95\%}<3<q_{edge}$, as shown in Fig. 2.1.17. The dominant toroidal mode number is n=1, while the dominant poloidal number shows a slow transition from m=3 to m=2. These two components have the same frequency implying that the perturbations, resonant at different surfaces, rotate at the same speed, as a result of strong interaction. Moreover, a destabilising influence of the 3/1 external kink on the internal 2/1 mode is suggested. The modes then grow in amplitude while slowing down in frequency and eventually lock to the wall. Prior to the disruption, the 3/2 mode is destabilised, again rotating with the same toroidal speed of the n=1 component. The 2/1 and 3/2 modes are identified as tearing modes.

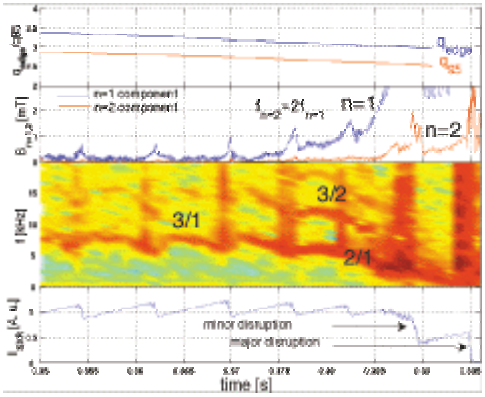

Fig. 2.1.17 *Mode activity in discharge #21400*

When they reach large enough amplitudes (≥1mT), these instabilities can lead to a disruptive termination of the discharge. The outer driving mode couples with the sawtooth precursor, which also rotates at the same frequency during the slowing down phase. Both elongation and triangularity reduce the amplitude of the global n=1 mode to a level such that the 3/2 mode is not induced. A small amount of plasma shaping ($\kappa>1.3$, $\delta>0.25$) is sufficient to avoid disruptions. According to theoretical calculations in the cylindrical approximation, the changes in the current profile due to the plasma shaping are not sufficient to explain this behaviour. On the other hand, toroidal resistive stability calculations suggest that the 3/1 external kink mode can strongly destabilise the 2/1 tearing through mode coupling. As the strength of the coupling between the different resonant surfaces depends on the plasma shape, this explains why, by acting on the shape of the plasma equilibrium, one can completely stabilise the 2/1 tearing mode.

2.1.3 H-mode and ELM dynamics

The accessibility of enhanced confinement modes (H-modes) and the characterisation of the dynamics of the Edge Localised Modes (ELMs) that tend to be present in these plasma scenarios constitute an important problem of tokamak physics. Ohmic H-mode plasmas have been regularly obtained in TCV since 1994. However, most of the H-mode phases were ELM free, with the plasma density rising uncontrollably until the plasma disrupts. These last few years, an extensive search of the operational limits of the Ohmic H-mode ELMy regime was undertaken for diverted single null plasmas with the ion grad B drift directed away from the X–

point. In 2002, the access to the ELMy H-mode, in the configuration with the ion grad B drift directed towards the X–point, was addressed. This allowed us to start investigating the effect of ECH on ELMy plasmas. Control of the ELMy regime using the fast internal coils was developed. The different analysis techniques developed over the previous years were improved and applied to new ELMy discharges.

H-mode operational limits

The operational limits of the ohmic ELMy regime were already well established in the case of a single null diverted configuration with the ion grad B drift directed away from the X-point (Single Null Down, SND). In the opposite configuration (SNU), the ELMy regime was rarely obtained. Almost all discharges that underwent an LH transition entered an ELM free regime and terminated in a plasma disruption, after an uncontrollable density rise.

The strategy used for this configuration consisted first in finding the threshold values of plasma current and density for which the plasma presents an L-mode to H-mode transition. Then, the plasma configuration was smoothly changed, from discharge to discharge, while keeping the plasma current and density just above the threshold value. LH transitions directly leading to the ELMy regime were found close to the threshold values.

The accessibility of the ELMy regime in this configuration was not studied as extensively as in the other configuration. Therefore, the values shown in the Table 2.1.1 indicate a point in the operational place where L-mode to ELMy H-mode transitions were obtained but cannot be considered as limits of the operational domain. The table also shows the operational domain for the other configuration.

	I_p [kA]	n_e [$10^{19}m^{-3}$]	κ	δ	Plasma wall distance [m]
Operating point of L-mode to ELMy H-mode (SNU - ion gradB drift to Xpt)	350	4.8	1.58	0.55	>0.005
Operational domain of L-mode to ELMy H-mode (SND - opposite ion grad B drift)	380 : 420	4.5 : 7.5	1.6 : 1.7	0.5 : 0.6	>0.015

Table 2.1.1 *Boundaries of the operational domain to the ELMy regime and of the ELMy regime in terms of operational parameters*

Since the operational domain of the L-mode to the ELMy H-mode transition lies along the border between L-mode and H-mode, Table 2.1.1 also shows that the threshold values to access the H-mode are lower in the case with the ion grad B drift directed towards the X-point than in the opposite case. This result is in

accordance with the widely recognised effect of the ion grad B drift direction on the power threshold.

ELMy H-modes are now achievable either at the top of TCV in the single null down configuration or at the bottom of TCV in the single null upper configuration, even if the ion grad B drift is directed away or towards the X-point, respectively. For some experiments, ELMy H-mode plasmas at the mid-plane of TCV are desirable. Attempts to create a stationary ELMy discharge at that position in the vacuum vessel did not have the expected success. The bad conditioning of parts of the vacuum vessel walls, where the separatrix legs strike, are thought to be responsible for this, since all controllable plasma parameters such as current, density, configuration and shape are similar to the successful case obtained at the top of the vessel.

Attempts to obtain H-mode in He plasmas were also performed. The single null down configuration was chosen since it has the most reliable discharge breakdown. The plasma current was increased from discharge to discharge up to its maximum possible value for this configuration without achieving any L- to H-mode transition.

H-mode and ECH

ELMy H-modes have been heated using EC waves. Because of the relatively low cut-off density, X2 ECH can only be applied to the edge of an H-mode plasma. Therefore, SNU plasmas were used in these experiments to present a perpendicular edge surface to the waves incident from the X2 launcher. Even with this optimised geometry, only a part of the beam power was deposited in the edge of the plasma because of wave refraction. Pulse length was therefore kept short to avoid excessive power deposition in unwanted places in the vacuum vessel. Nevertheless, the effect of the additional power on the ELM characteristics was clearly observed, as shown in Fig. 2.1.18.

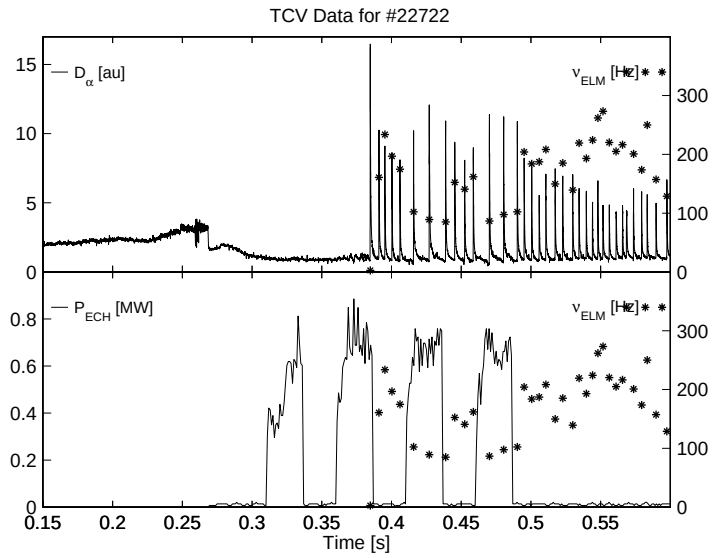

Fig. 2.1.18 *Effect of the ECH X2 on an ELMy H-mode plasma*

According to the widely recognised rule on the ELM type determination, the decrease in the ELM frequency when additional power is injected would indicate

that the ELMs are of type III. However, these ELMs also behave like type I ELMs. Therefore, the classification of TCV ELMs still remains unclear.

X3 ECH waves were also injected in ELMy H-mode plasmas. In this case, a SND more elongated configuration was chosen since the absorption of the third harmonic wave is lower than the second one and the absorption depends critically on the launching angle. In the preliminary experiments reported here, the launch mirror was tilted during the discharge in order to determine the angle of maximum absorption, where a clear decrease in the ELM frequency is observed. The minimum in ELM frequency corresponds to the maximum power coupled to the plasma, as discussed in detail in Section 2.1.5. The decrease of the ELM frequency with the additional power would also indicate type III ELMs. The search for type I ELMs is ongoing.

ELM dynamics

The ELM dynamics have been investigated on TCV with the aim of finding domains in which the ELM behaviour is deterministic and of assessing the coupling between ELMs and sawteeth. The timing relationship between sawteeth and ELMs was studied for all plasmas with a stationary ELMy regime. The ELM frequency is often half, equal, double or even triple the sawtooth frequency. In most cases, the phase relationship between the ELMs and the sawteeth is constant, strongly indicating a link between the ELM and sawtooth dynamics. The extent of synchronisation depends particularly on the size of the preceding sawtooth crash as well as on plasma elongation, triangularity and safety factor.

Investigating the hierarchical structure of Unstable Periodic Orbits (UPOs) using a new topological analysis method may provide a crucial tool for identifying the correct physical model for ELMs, and is being implemented on TCV data. Initial analysis has indeed revealed a hierarchy of period 1, 2 and 3 orbits in soft X-ray emissivity data taken from a chord that passes through the plasma edge (sampling both ELM and sawtooth events). New methods for detecting UPOs have also been implemented on TCV D_α emission data, and the database of UPOs has been extended to include discharges from the 2002 campaign.

ELM triggering

New attempts at triggering ELMs by magnetic perturbations provided by the fast internal control coils have been performed in the SNU and SND configuration. The locking of the ELM frequency on the perturbation was less clear than in the first experiments performed in 2001. The most significant difference between these attempts appears to be the plasma vertical speed produced by the perturbation.

The observed synchronisation of ELMs with the applied perturbation may be interpreted in terms of peeling and ballooning mode model for ELMs as follows. The applied magnetic perturbation gives rise to a plasma vertical motion, which produces a net surface voltage due to the vertical gradient of the vcuum flux. This in turn perturbs the edge current density. This changes the edge shear and either delays or advances the crossing of the peeling mode stability boundary, effectively synchronising the ELMs with the perturbation. A simple dynamical model representing the ELM cycle was built, including a mode stability threshold and simulating the trajectory of the ELMy cycle. The edge current perturbation was

included in the model and qualitatively reproduced the observed synchronising effect. Work is ongoing to refine this model.

2.1.4 Edge and Divertor Physics

In comparison with previous years, edge and divertor physics during 2002 has consumed a lower fraction of TCV operational time, due largely to commitments of appropriate personnel to the JET programme (see Section 4.1.1). Preparations have also been underway for experiments in 2003 dedicated to the measurement of edge turbulence and the characterisation of helium plasma operation in an all-graphite machine. Further effort has also been devoted to edge plasma modelling using the SOLPS5 (B2.5-Eirene package), with emphasis on the extension of this modelling to the inclusion of molecular reactions.

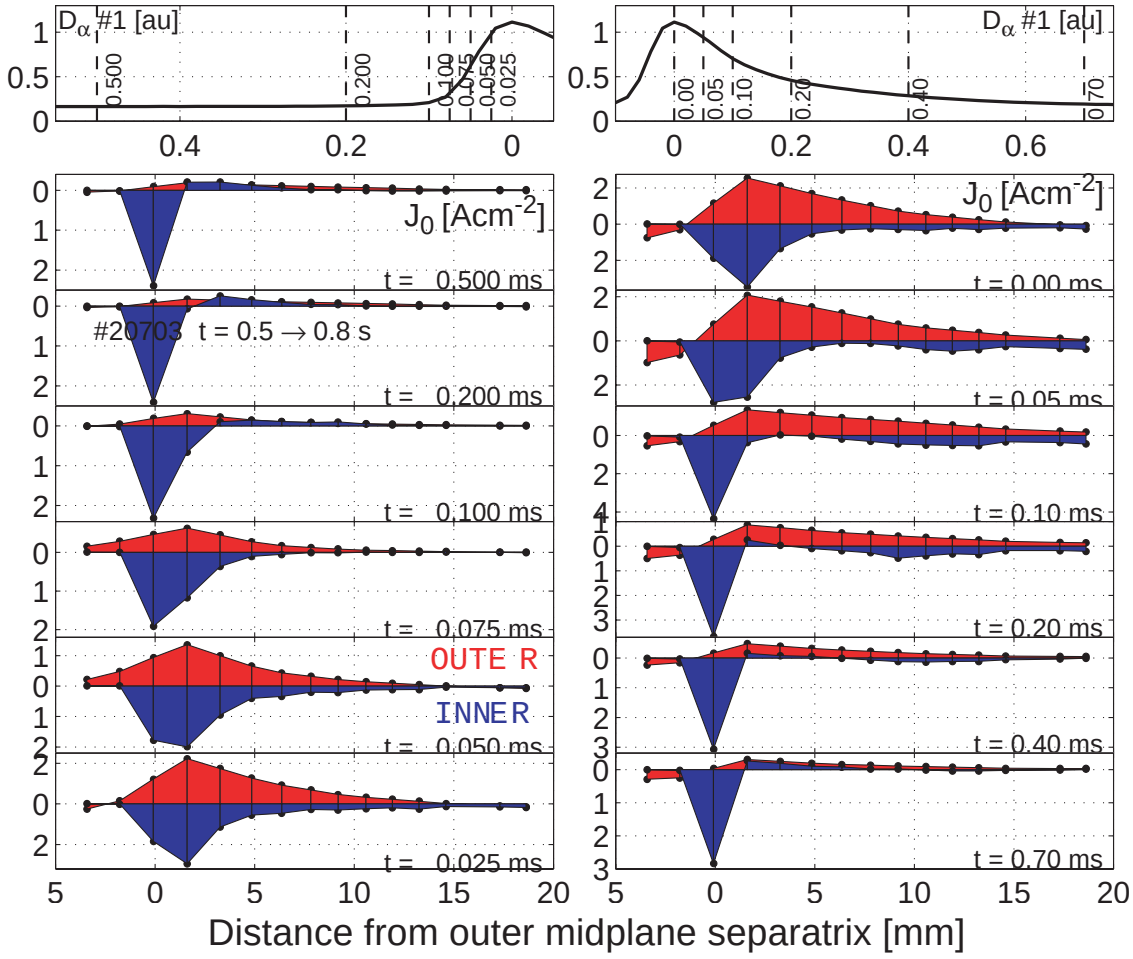

Fig. 2.1.19 *Profiles, mapped to the outside magnetic midplane, of currents perpendicular to the divertor targets measured during an ELM event. The data are obtained by coherent averaging of many ELMs. The coherently averaged D_α event at the top of the figure indicates the instant, during the ELM, at which each current profile is plotted.*

Analysis of ELM currents featured in the previous report has continued, using the technique of coherent averaging to yield profiles of ELM driven currents across the divertor targets. Figure 2.1.19 illustrates how during the ELM peak (defined as the

peak intensity on a vertically viewing, wide-angle D_α photodiode), the current flowing to the targets (measured by embedded Langmuir probe arrays held at target potential) also peaks, is positive at the outer target and negative at the inner. Integral current balance to the targets is satisfied to within a factor of two. Given the known discrepancies between current measurements obtained from probes and the more accurate technique of target tile shunts, this indicates reasonably good current balance and shows that a strong parallel current flows during the ELM in these TCV single null lower ohmic H-modes (BxVB drift away from the X-point).

Such currents in TCV are almost certainly thermoelectric in origin, driven by differences in T_e between the inner and outer divertor plasmas. Such asymmetry is regularly observed in TCV in L-mode plasmas (as are thermoelectric currents), but T_e cannot be measured sufficiently rapidly in TCV during the ELM to confirm the thermoelectric current hypothesis. Integral currents of order 3kA flow at the ELM peak, equivalent to 0.7% of the plasma current for the discharge from which the data of Fig. 2.1.19 are obtained. Should the phenomena also be present in ITER, currents of order several 100 kA would flow in the scrape-off layer during ELMs.

Previously reported studies on TCV have clearly indicated that an alternative recombination pathway must be sought to explain the observed level of divertor detachment. One serious candidate is molecular assisted recombination (MAR), which occurs if significant molecular hydrogen densities are present in the divertor plasma. This is indeed possible in TCV owing in large part to the extensive open volume adjacent to the divertor plasma (in comparison to larger tokamaks) and the rather low electron density that appears to characterise the detachment threshold. This possibility is now being studied theoretically using the SOLPS5 code package, now fully installed at CRPP, though inclusion of molecular reactions in the code requires considerable departures from the standard mode of operation.

The first of these is the extension of the B2.5 plasma grid to a discretisation of the entire TCV vacuum vessel volume outside the separatrix (using a finite element mesh generator) and the inclusion of proper accounting for the toroidal curvature of the vessel (in place of the usual cylindrical assumption). The latter is important for molecular species that travel almost collisionless in the region between the divertor plasma and the vessel walls. Figure 2.1.20 illustrates the result of including these modifications, which are the starting point for the study of the potential for dissociative attachment and ion conversion reaction chains as the driving mechanisms behind the anomalous detachment observed in TCV.

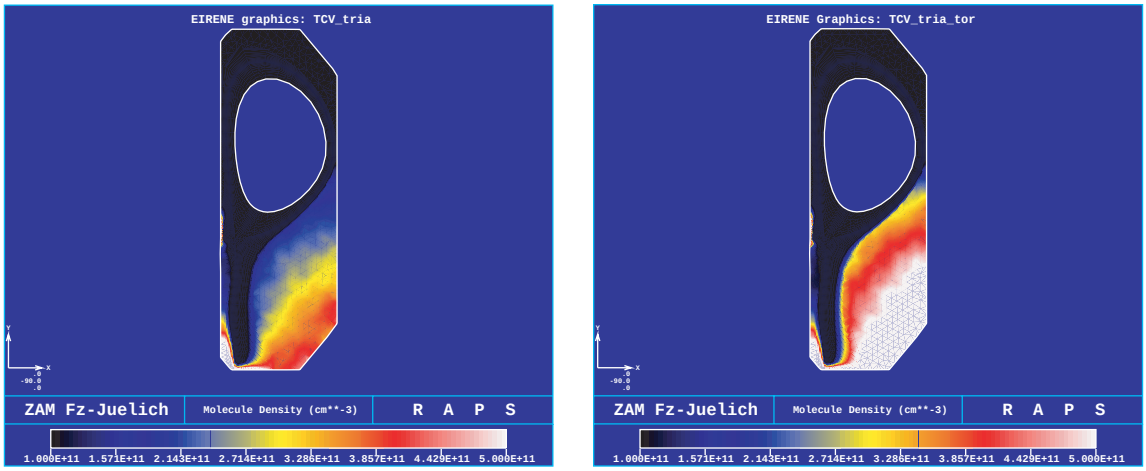

Fig. 2.1.20 *Eirene calculated distribution of D_2 molecular density on an extended finite element mesh for a standard B2-Eirene TCV model result. On the left, molecular density profile for the conventional cylindrical approximation. On the right, when the true toroidal configuration is accounted for.*

In support of an extensive campaign of pure helium plasmas at JET in March 2001, a limited campaign of preparatory experiments were performed on TCV during 2002. These experiments, which are likely to be extended in 2003, study the differences between deuterium and helium operation, both from the point of view of the very different impurity production and atomic physics characteristics of He and D and in view of the considerable differences in size and first wall armour between JET and TCV. Replacing D with He largely eliminates carbon-deuterium chemistry and hence one of the principal impurity production mechanisms. This is of particular interest in a machine like TCV with its nearly 100% first wall graphite coverage.

Unfortunately, the large image currents in the conducting vacuum vessel wall of TCV precludes breakdown in pure He. Discharges are thus established with a D_2 pre-fill followed by He gas puff, but analysis of the D neutral particle outflux in any given He discharge shows that the D pre-fill has been effectively pumped by the first wall within ~250ms of discharge initiation. A more complete campaign awaits the imminent installation of new diagnostics, but first results from 2002 already indicate that in the areas of impurity production, density limits and divertor detachment, comparison with JET data should provide interesting insights. Stable H-mode plasmas with X3 heating have not been achieved within the period covered by this report and so only a brief study of H-mode accessibility in He with ohmic heating has been possible. As in JET, the L-H transition power in He is higher than in D in TCV, although with ohmic heating alone, the precise difference in He compared with D cannot be quantified. These preliminary experiments indicate that the threshold is at least 30% higher in He than D for TCV. In JET, the transition power has been measured to be 50% higher in He than in closely matched D discharges.

2.1.5 ECH and ECCD Physics

X2 launcher alignment

The ECH deposition location is routinely varied by several methods. Some involve varying the plasma magnetic equilibrium by external field coils, e.g. by moving the magnetic axis vertically, or by moving the resonance location by varying the toroidal field. However, moving the launcher mirror is the method most often employed on TCV, because it is relevant to future burning plasmas in ITER.

TCV data shows that the variation of the sawtooth period as the ECH deposition is swept across the q=1 region of the plasma is reproducible. Each of the six X2 launchers is used separately in six identical discharges and the sawtooth period variation is analysed as a function of the pre-calibrated launcher angle. This method allows a relative alignment between upper lateral X2 launchers to within ±3mm, whereas the precision in the determination of the absolute plasma axis height relative to the vacuum chamber (and therefore the launching mirrors) was

~2cm. This led to an improvement in the use of the LIUQE code used to reconstruct the magnetic equilibria.

In order to align the equatorial launchers with respect to each other, the same method is used. However, to align them with respect to the upper lateral launchers we rely on the knowledge of the plasma axis position and symmetry of the sawtooth response. Using one equatorial launcher with the plasma placed very near the equator, it was shown that the plasma axis determined by LIUQE was incorrect by 5mm. Therefore the remaining uncertainty in the relative alignments of equatorial to upper later launchers was removed, and an error of 1.65° in the pre-calibration of one of the launchers could be corrected.

A novel alternative method of alignment also confirmed the 1.65° error. The plasma was placed directly in front of the equatorial launchers and each beam was swept in the toroidal direction. The Doppler shifted absorption location thus swept across the q=1 location and the sawtooth peaking was measured. This provided the first example of Doppler-shifted sweeping in which the Doppler shifted deposition location can be clearly measured using the sawtooth period.

The ultimate test of the alignment is the ability to increase the local power density by overlapping the power deposition profiles of several beams. This has been done in the past only for two upper launchers: when a second swept beam is added, the sawtooth period increases. Nevertheless, only when the two beams were swept in opposition to each other were the longest sawtooth periods found.

Sawtooth control

In burning plasmas, sawteeth should prevent the accumulation of helium ash. On the other hand, the PRETOR-ST code predicts that energetic alpha particles will also stabilise sawteeth. Long-period sawtooth crashes are expected to provide seed islands of sufficient size to trigger neoclassical tearing modes, leading in turn to a strong reduction of the neutron yield. It therefore is of great importance to understand how to control the sawtooth period. PRETOR-ST has been used to determine the optimum location for destabilising sawteeth, i.e. for shortening their period. Three main features are considered in the comparison with experiments: the influence of ECCD, the location of optimum stabilisation and destabilisation and the 1D nature of the code versus the 2D nature of the experiments.

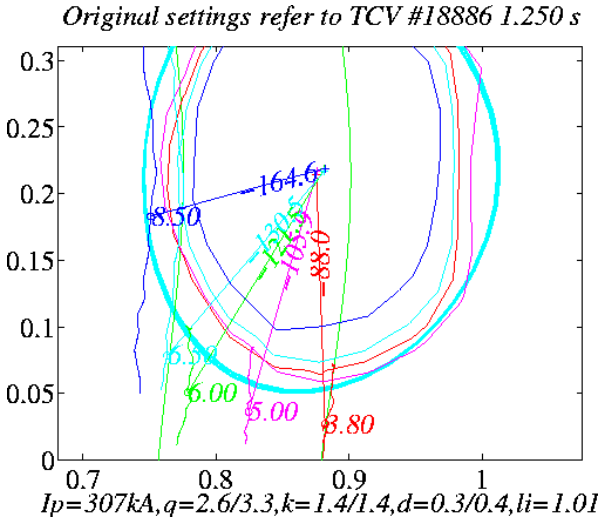

Fig. 2.1.21 *Poloidal view of the LIUQE q=1 surface (thick, solid, cyan oval) and sawtooth inversion surfaces from X-ray tomography for 5 different discharges at the time of maximum sawtooth period (thin ovals inside the q=1 surface). The X2 resonance curves for two of the discharges (smooth, thin, green, vertical curves) and X2 deposition locations during the five sweeps (thin, coloured, vertical curves) as well as the location of the maximum sawtooth period (o's connected to the magnetic axis by solid lines) is shown. The poloidal angles and maximum sawtooth periods are indicated. The maximum sawtooth period occurs with deposition outside both the inversion radius and q=1 radius in nearly all shots.*

In earlier TCV experiments it was not possible to discern whether the peaking of the sawtooth period occurred when the ECH deposition was slightly inside, outside or directly on the q=1 surface. To improve the precision in locating the q=1 surface, the elongation and plasma current were increased, resulting in a larger q=1 surface. These plasmas were used for testing the current drive efficiency as a function of poloidal angle (Fig. 2.1.21) and for the alignment described above. Figure 2.1.22 clearly shows that the maximum in the sawtooth period increases as the deposition moves to the high field side. This is evidence that the current drive increases due to reduced trapping. It is also clear that the peak sawtooth period occurs outside the sawtooth inversion radius. It is not certain, however, that the peak is outside the q=1 surface, since the q=1 radius is not directly measured.

The dependence of the sawtooth period on the ECH power density, current drive and sweep direction near the q=1 surface has been successfully reproduced using the PRETOR-ST 1D transport code that includes a sawtooth crash model. The ECH deposition location which corresponds to the peak in the sawtooth period is shown by PRETOR-ST to occur outside the q=1 surface. The good match of the modelled sawtooth period to the measured sawtooth period indicates that the sawtooth model is valid for TCV conditions and that the q profile determined by PRETOR-ST is more accurate than that determined by LIUQE.

The full value of PRETOR-ST is realised when the code is run in predictive mode. The simulations allow the influence of current drive to be separated from that of the accompanying heating. Naturally, both current drive and heating occur simultaneously in experiments and heating on its own has a strong effect on the sawtooth period. The predictive simulations were stimulated by failed alignment experiments in which the number of swept beams was increased from one to four. The fourth beam failed to sweep, and eliminated the stabilising effect of the other three when it provided constant deposition just inside the q=1 surface. A predictive simulation was therefore carried out in which three beams were fixed on the optimum stabilising location just outside the q=1 and a 4^{th} beam was swept from inside to outside the q=1 location. The results of the simulation are shown in Fig. 2.1.22.

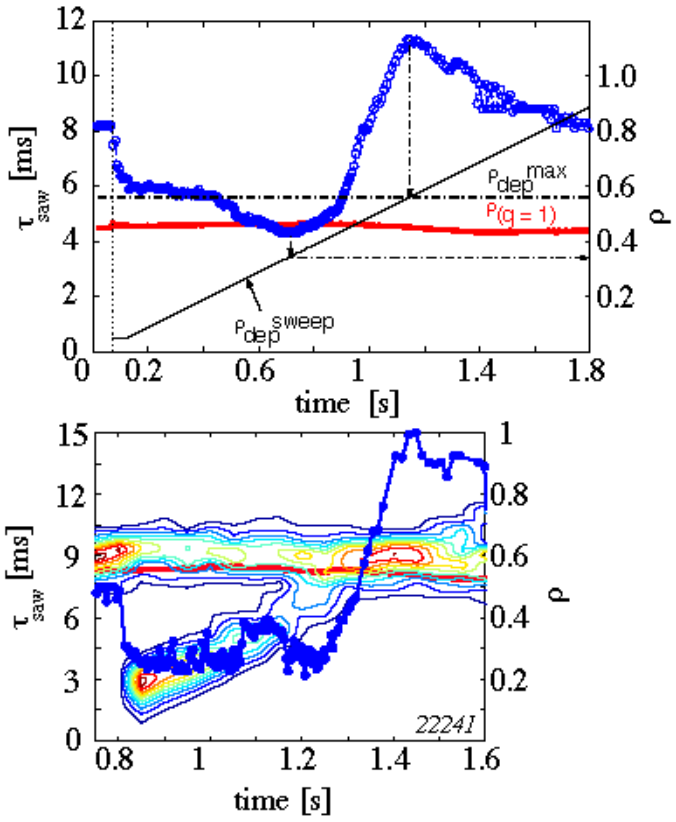

Fig. 2.1.22 *Top: Simulation: 1.3MW ECH fixed for optimum stabilization; 0.45MW of swept ECH. Sawtooth period, q=1 and ρdep are shown. Bottom: Experimental sawtooth period, LIUQE q=1 (red line) and TORAY ECH power density contours: 0.9MW ECH (slight co-ECCD) fixed for optimal stabilisation; 0.45MW of swept ECH (slight co-ECCD). ECH destabilises sawteeth, inside q=1.*

Subsequently, the effect of current drive alone was simulated for the 4th beam. The sawtooth period was predicted to decrease (increase) with co-ECCD (counter-ECCD) when the deposition was just inside the q=1 surface. In experiments with zero toroidal injection angle of the beams a slight co-ECCD component exists when the upper lateral beams are swept. This must be taken into account when comparing the simulation and the experiment.

The reduction of the sawtooth period by the ECH beams was demonstrated experimentally using a combination of three beams. Two beams were placed at the optimum location for increasing the sawtooth period, creating sawtooth periods of ~7ms, then a third beam was turned on with near central deposition and swept across the q=1 surface. When the third beam deposition was inside the q=1 surface, the sawtooth period decreased to ~4ms (with near on axis and just inside the q=1 surface) before increasing to ~15ms outside the q=1 surface. The general features of the simulation are confirmed by the experiment, with a small peak present when heating inside the q=1 location (~1.1s). These sawteeth also show 2D feature, which cannot be reproduced by the 1D model.

Vertically injected third harmonic ECH in X-mode

During 2002, experiments with the newly installed vertically injected X3 system operating at 118GHz were devoted to studying the heating capabilities of this novel launching scheme. The main feature of X3 ECH on TCV is its ability to heat higher density plasmas, since the cut-off density is 1.1 $10^{20}m^{-3}$, a factor of three higher than for X2. Access to these higher densities with additional heating considerably extends the operational regime of TCV.

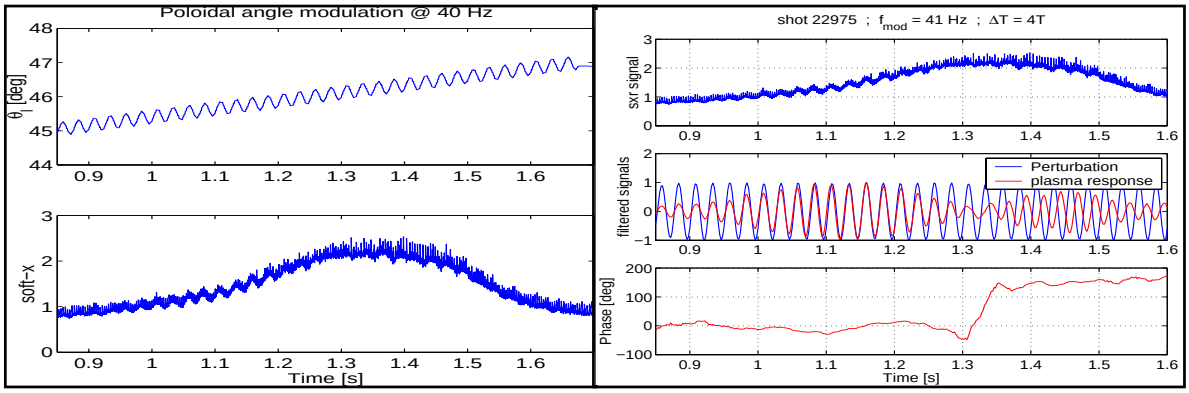

Fig. 2.1.23 *Left: (top) shows the mirror sweep with the sinusoidal perturbation and (bottom) shows the plasma response measured using a centrally viewing SXR camera. By post processing the SXR signal it is possible to extract the amplitude and phase of the plasma response to the imposed perturbation. The phase response is shown on the right along with the SXR signal and the digitally filtered signals. The deduced phase jump of 180° shows where the maximum plasma response is located.*

The first investigations were dedicated to the commissioning of the X3 system and in particular to the steering of the top launcher, together with a study of the sensitivity of the plasma response to the launcher injection angle. For steady-state plasmas good agreement was found between the experimentally optimal launching angle and the angle predicted by the TORAY-GA code. However, with vertical injection and the corresponding long resonance layer, the sensitivity of the optimal injection angle with plasma parameters variations is much stronger than for low-field side launch. Experiments were performed to test real time data analysis methods and to determine the best signal for use for real time feedback control of the launching mirror angle. In these experiments the launcher mirror angle was swept linearly in time through the resonance layer with low amplitude sinusoidal oscillations superimposed on it. The oscillations allowed us to determine the maximum response by examining the phase and amplitude of the perturbations measured on soft X-ray camera with a line of sight through the plasma centre. Figure 2.1.23 shows the applied perturbation and the plasma response, as well as the amplitude and phase of the analysed signals. Using the phase response as a feedback signal it will be possible to adjust the launcher angle in real time to maintain maximum absorption throughout the discharge. Algorithms that can be implemented in a digital signal processing system are being developed.

A quantitative study of single-pass absorption in a variety of plasma conditions with central densities higher than the X2 cut-off has been performed. In these experiments, L-mode plasmas with purely X3 heating and/or both off-axis X2 heating together with X3 core heating have shown single pass-absorption of the X3 wave as high as 100%. X3 heating experiments of ELMy H-mode plasmas have been performed to establish quasi-stationary additionally heated ELMy H-modes and to study the effect of the additional heating on the ELMs.

An example of X3 heating experiments of ohmic L-mode target plasmas is shown in Fig. 2.1.24. For this discharge, the central electron density, 4.5-5·$10^{19}$$m^{-3}$, is above the cut-off density for the X2 system (4·$10^{19}$$m^{-3}$) and the injection of the top launcher mirror is kept fixed at an optimised angle of 46.2°. At 4.5·$10^{19}$$m^{-3}$ the ECE–HFS radiometer channel is in cut-off and the observed deviation of the signal (0.9s–1.3s) from its base level must be attributed to the presence of suprathermal electrons generated by the X3 wave. The fast electrons are spatially located outside the normalised radius r/a>0.2. The q=1 radius is located at r/a=0.3. The absorption measurement with the DML is made during RF power modulation of only one gyrotron (square wave at 237Hz) between t=1.2s and 1.4s.

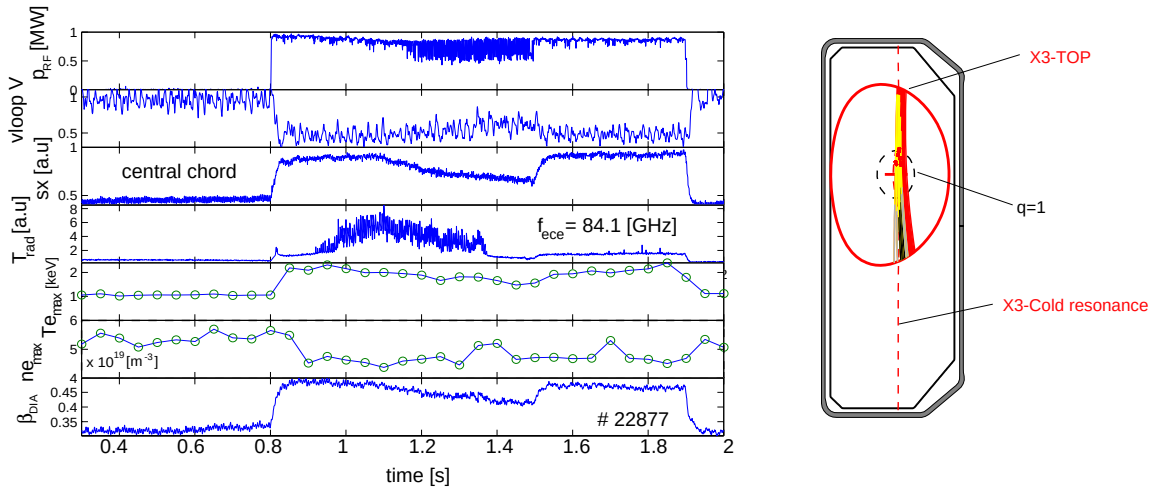

Fig. 2.1.24 *From top to bottom: X3 power corresponding to 0.9MW of injected power, loop voltage, soft X-ray signal (central chord), non-calibrated radiation temperature from one channel of the ECE-HFS radiometer, peak temperature and density from Thompson scattering (every 50ms) and diamagnetic β. Plasma current: Ip = 230kA. On the right, the plasma cross-section with the ray tracing calculated with the TORAY code.*

With this launching geometry the deposition profile calculated by the TORAY-GA code indicates that the power is deposited inside a normalised radius of r/a=0.45 and the absorbed fraction is 66%. A discrepancy between the measured and the predicted launching angle of 0.4° was found. As the mechanical accuracy of the top launch mirror setting is better than 0.1°, we believe that the discrepancy originates in the limited accuracy of the ray-tracing calculation using the reconstructed equilibrium. This is being investigated together with other possibilities, such as beam diffraction or hot plasma effects on the refraction. In order to cope with the high sensitivity of the absorption on the launcher injection angle, plans to implement a real time feedback on the top launcher mirror are underway.

In a second set of experiments with X3 core heating of L-mode plasmas with combined X2 far off-axis heating, nearly full single pass absorption has been obtained. In this experiments the X2 far off-axis ECH/ECCD is used to reduce the vertical instability at high elongation by broadening the current profile in stationary conditions. In these discharges, which are overdense to X2 in the centre, the X3 wave is injected from the top launcher to deposit power in the centre and increase the central pressure. The launching geometry and the main plasma parameters for a typical shot in this set of experiments are shown on Fig. 2.1.25.

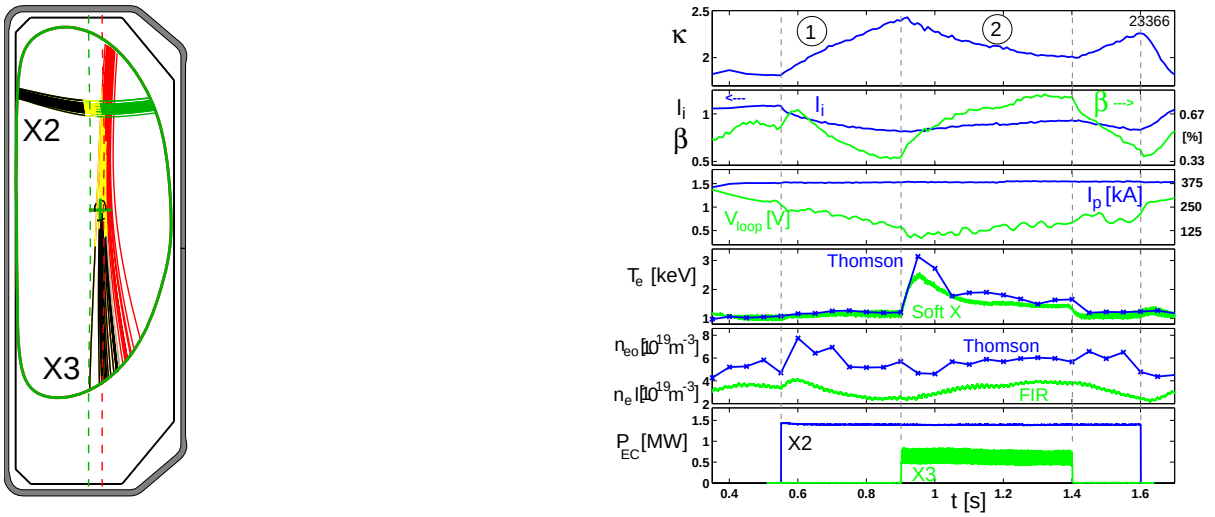

Fig. 2.1.25 *Left: launching geometry of the X2 and X3 waves. Right: from top to bottom: elongation, internal inductance and β, loop voltage and plasma current, central electron temperature (Thompson and soft X-ray), central and line integrated density, X2 and X3 RF power.*

The time evolution of the measured and predicted X3 absorbed power (by DML (P_{DML}) and TORAY-GA (P_{TORAY}), respectively), the central electron temperature (by Thomson and soft X-ray), and the emissivity profile measured with a 64 channel soft X-ray wire chamber (MPX) are shown in Fig. 2.1.26. The optimal X3 power modulation frequency (337Hz) yields reliable results for both the DML and MPX and gives a response phase close to 90°. The power deduced from the DML is identical to that from ray tracing for most of the time slices, which implies a fully thermal plasma. For these times the deposition profile, similar to the one deduced from ray tracing, is monotonic and peaked on axis. The fact that $P_{DML}>P_{TORAY}$ indicates absorption on suprathermal electrons. The presence of suprathermal electrons is confirmed by $T_{ECE}/T_{THOMSON}>1$, were T_{ECE} is the radiation temperature measured with a high-field side radiometer. These suprathermal electrons already exist during the X2 phase, and extend over most of the X3 heating period. At the beginning of X3, full absorption is measured by the DML which is correlated with an increase of the T_{ECE} profile.

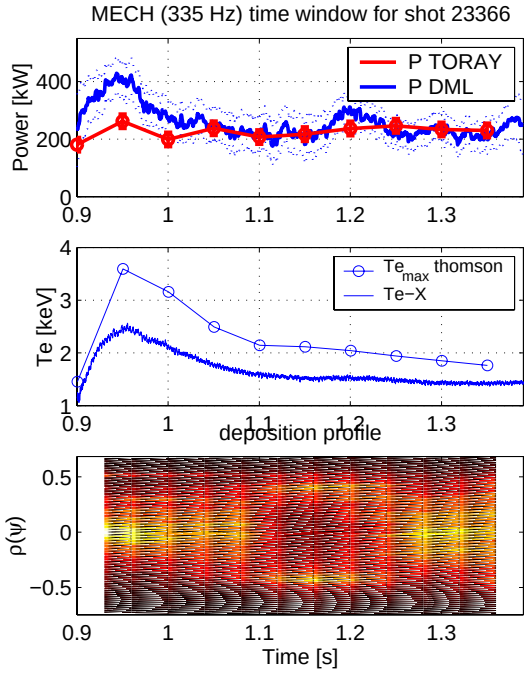

Fig. 2.1.26 *From top to bottom, X3 absorbed power from DML and ray-tracing, electron central temperature from Thomson and soft X-ray, Power deposition profile from MPX, showing different deposition profile widths, from peaked to hollow.*

These experiments confirm that the absorption is very sensitive to the X3 launcher angle. Differences of the order of 0.2º in the mirror angle and variations of the plasma parameters modify the absorbed power significantly, which again justifies the development of a feedback system to maximise absorption throughout the discharge.

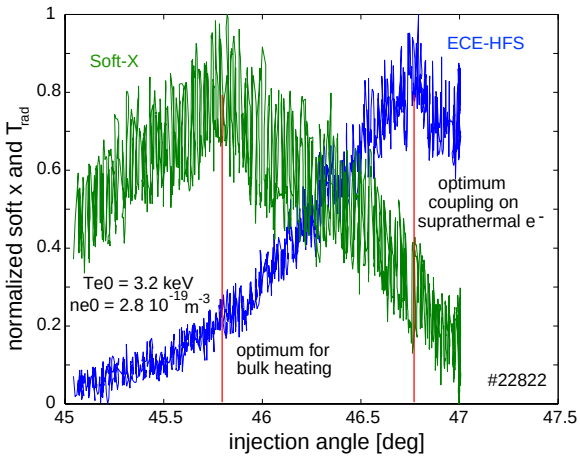

Fig. 2.1.27 *SXR (green) and ECE (blue) signals, as a function of launcher angle for a discharge with X2 preheating. The SXR signal reflects heating on the bulk while the ECE signal reflects heating on the fast electron tail. As the mirror is scanned from the cold resonance to the high field side the X3 power is selectively coupled to the bulk (SXR signal peak) and subsequently to the suprathermal electrons (ECE signal peak).*

Preliminary experiments on the capability of the X3 vertical launch to selectively couple to different electron energies have been performed on an L-mode plasma with combined X2 and X3 heating. When the mirror was swept during the

discharge, with the absorption location moved from the X3 cold resonance towards the high field side, we observe that the top X3 launch selectively couples to different electron energies. This can be extremely useful for studying the dynamics of suprathermal electrons. This observation is illustrated in Fig. 2.1.27, where the soft X-ray signal, which is sensitive to the bulk, and one channel of the ECE-HFS radiometer are plotted against the top launch angle.

For X3 heating of ELMy H-mode plasmas experiments were carried out to establish quasi stationary additionally heated ELMy H-modes and study the effect of heating on the ELMs. Quasi stationary ELMy and non-stationary ELM-free H-modes have been established at densities far exceeding the X2 cut-off using X3 pulse lengths of several hundred milliseconds. In these experiments it was impossible to measure the absorbed power with the DML and modulated injected power because the ELMs significantly perturbed the diamagnetic measurement. Treating the diamagnetic signal with a system identification method should allow us to separate the dynamics associated with the power modulation and the ELMs and to measure both the X3 absorbed power and the power loss associated with the ELMs.

To examine the reaction of the ELMs, the X3 launcher mirror was scanned across the resonance layer. As shown in Fig. 2.1.28, with an X3 injected power of 420kW, the absorbed power (TORAY-GA estimate) first increased from 220kW to 300kW (single-pass absorption of 72%) then decreased to below 100kW. Due to the higher electron temperature, the ohmic heating decreased by approximately 100kW at the time of maximum X3 absorption. The ELM frequency increase associated with the X3 absorbed power increase is typical of the so-called type III ELMs. Further results related to H-mode studies and ELM dynamics with this heating scenario are given in Section 2.1.3.

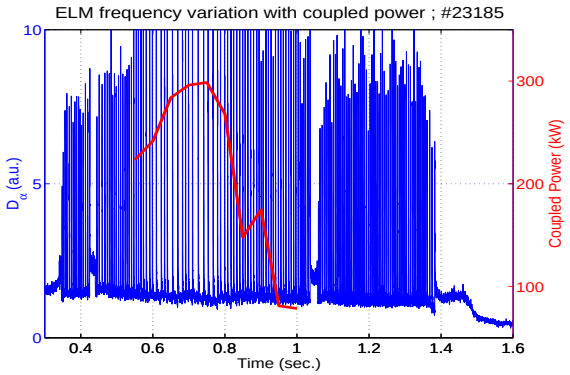

Fig. 2.1.28 *Power coupled to the plasma (from TORAY-GA) and D_α signal. In this experiment the launch mirror angle is swept across the resonance layer resulting in a heating power that first increases from 220kW to 300kW, then decreases to below 100kW. These variations are followed by the ELM frequency.*

Suprathermal electron dynamics in ECH and ECCD discharges

Evidence for the creation of a suprathermal electron population is provided by two diagnostics on TCV, a multi-chord hard X-ray spectrally resolving camera and an Electron Cyclotron Emission (ECE) radiometer with 24-channels in the frequency range 87-115GHz. The two diagnostics have previously been used to provide information on suprathermal electrons produced by X2 ECCD and X3 ECH in

steady state conditions. Recently, both instruments have also been used in perturbative experiments for assessing the transport of suprathermal electrons, which is of paramount importance for the understanding of the ECCD efficiency.

The ECE radiation is collected from antennas on the high field side (HFS) of the vacuum chamber. This arrangement avoids absorption of relativistically downshifted ECE from suprathermal electrons by thermal electrons near the 'cold' resonance layer, as occurs when ECE is measured from the low field side. The emission seen from the HFS is the sum of downshifted suprathermal ECE and a partly absorbed component emitted by thermal electrons.

Before a Fokker-Planck code for reliably calculating the electron energy distribution produced by ECH and ECCD and a coupled ECE code become available, estimates for suprathermal electron temperature and density profiles are made using a bi-Maxwellian approximation. Under this assumption the X2 ECE intensity received by a high field side antenna at the frequency ω is

$$I_\omega = \frac{\omega^2}{8\pi^3 c^2}\left\{T_b\left(1-e^{-\tau_b}\right)e^{-\tau_s} + T_s\left(1-e^{-\tau_s}\right)\right\} \equiv \frac{\omega^2}{8\pi^3 c^2}\,T_{ECE}$$

The subscripts b and s refer to the bulk and suprathermal electron populations, which are characterised by the temperatures T_b and T_s, optical depths $\tau_b \propto T_b n_b$ and $\tau_s \propto T_s n_s$; T_{ECE} is the apparent temperature measured by the receiver. The simulations use bulk parameters measured by Thomson scattering and assumes temperature and density profiles for the suprathermals of the form

$$T_s = T_s(0)(1-\rho^2)^\alpha \qquad n_s = n_s(0)(1-\rho^2)^\beta$$

where $T_s(0)$, $n_s(0)$, α and β are fitted to the measurements. A typical simulation result for stationary conditions is shown in Fig. 2.1.29 with combined X2 ECCD (150^0 launch angle) and X3 ECH, exhibiting a very peaked suprathermal density profile ($\beta=8$) together with a very flat suprathermal temperature profile ($\alpha=0$). This is consistent with the hard X-ray observations reported in what follows. The suprathermal temperatures inferred using the bi-Maxwellian model are in agreement with the photon temperatures from the hard X-ray camera. This is shown in Fig. 2.1.30a) with combined X2 ECCD (150^0 launch angle) and X3 ECH with an X2 power up to 1.5MW. The same figure (b-c) shows how the suprathermal central density, the apparent ECE temperature and the optical depth vary with X2 ECCD power. Above 1MW the suprathermals are optically thick, screening out most of the thermal radiation emitted at lower toroidal field. The fraction of the total electron energy in the plasma carried by suprathermals is quite substantial, assuming the bi-Maxwellian model, varying from near 15% with 0.15MW of X2 power to 40% at 1.5MW.

The multi-chord hard X-ray (HXR) camera, on loan from CEA-Cadarache (France), has been employed to study the space and energy distribution and the temporal dynamics of bremsstrahlung emission from suprathermal electrons in discharges heated by X2 ECH. A linear array of CdTe detectors with an intrinsic resolution of ~7keV views the plasma vertically along 14 chords that span the outboard half of the cross section with a radial resolution of ~2cm on the midplane. Eight energy channels, with adjustable thresholds within the 10-200keV range, are available for each chord.

Previous work on TCV has shown that a substantial suprathermal component is generated by X2 waves launched with a finite toroidal wave vector component (toroidal injection angle $>10^0$), thus capable of driving a non-inductive current in the plasma, parallel (co-ECCD) or anti-parallel (counter-ECCD) to the plasma current. By contrast, in pure heating mode the distribution remains essentially Maxwellian, consistent with ECE measurements described above.

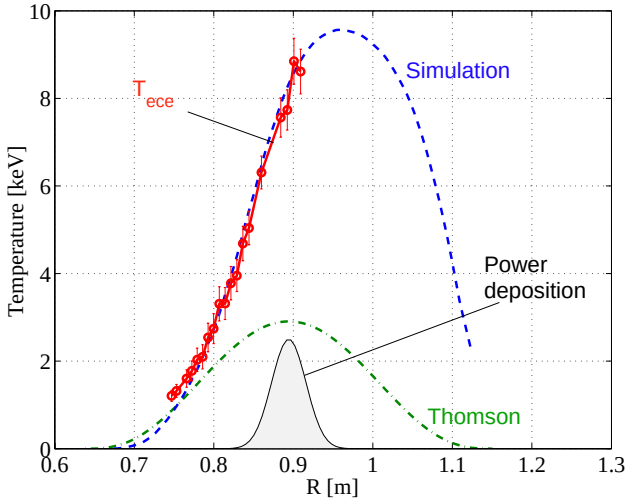

Fig. 2.1.29 *Bi-Maxwellian simulation of ECE spectrum plotted as function of the cold resonance radius for discharge 21732. The plasma was heated with 0.45MW X2 ECCD (15^0 toroidal angle) and 0.47MW X3 ECH. The ECE temperature profile was fitted assuming $T_s(0)=11keV$, $n_s(0)=1.7\times10^{18}m^{-3}$, $\alpha=0$ and $\beta=8$.*

More recent work has specifically addressed the fundamental question of the relative importance of collisional slowing-down and anomalous cross-field transport in the fast electron relaxation dynamics. While in larger devices the former is generally found to be dominant, in TCV even a modest diffusivity could cause a significant spatial broadening of the current-carrying population in relation to the plasma size. Since heating is applied to different velocity classes in different spatial regions, because of the Doppler shift needed to match the local resonance condition, the energy dependence of the HXR signal should generally vary in space as well. Instead, we find that the spectral shape is essentially constant in space, even well outside the theoretical deposition region. This is most naturally interpreted as an equilibration resulting from radial transport, but could also indicate an anomalous deposition profile in both physical and velocity space. To distinguish between these two causes, a time resolved study is required.

To study the evolution at switch-on and switch-off, we applied a square-wave modulation to the EC power (2.35MW) and used coherent averaging on the HXR signals to enhance the photon statistics, taking advantage of the repeatability and precise localisation of the EC waves. As shown in Fig. 2.1.31a) central co-ECCD, immediately after switch-on the on-axis and far off-axis spectra are very different, the former being more pronounced at low energy and vice versa. As time goes on, the spectral shapes become similar. Figure 2.1.31b) generalises this observation by depicting the profile of the photon “temperature” (from a logarithmic fit to the spectra) on the line-integrated signal as a function of the normalised radius. The temperature is initially larger off-axis, but evolves over about 10ms to the constant

profile. This effect strongly suggests fast electron transport. The initially higher off-axis energies are consistent with the larger resonant velocities in that region, while the final relaxed state is everywhere close to the initial temperature on-axis, where most of the power is deposited. From the characteristic times observed in these discharges, we can already set an approximate lower bound for the diffusivity, with $D>1.5m^2/s$.

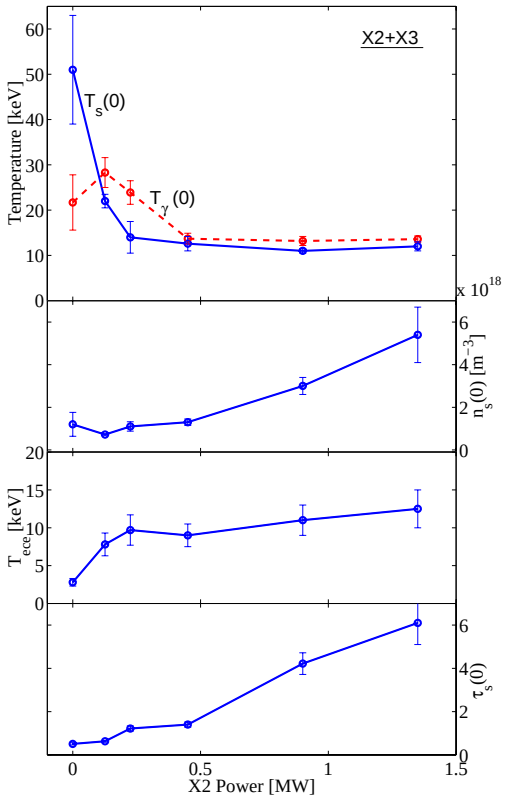

Fig. 2.1.30 *X2 power scan in combined X2 ECCD (15^0 toroidal injection angle), X3 ECH heating experiment (P_{X3}=0.47MW): a) Photon temperature and central suprathermal temperature from bi-Maxwellian calculation;. b) Central suprathermal density; c) ECE temperature d) suprathermal optical depth.*

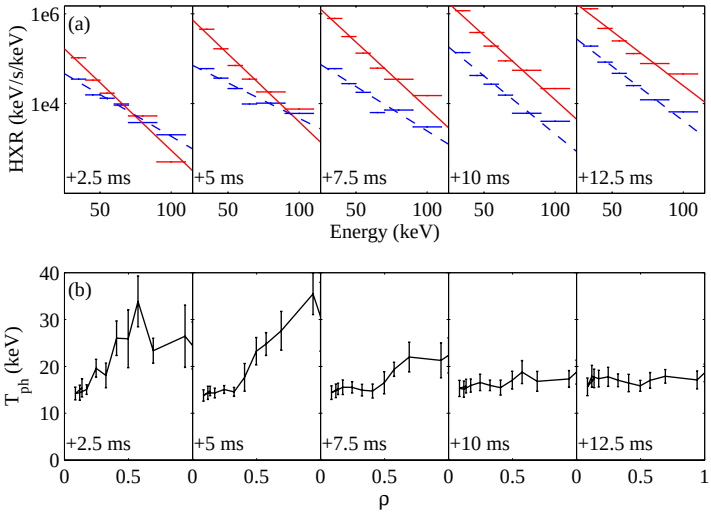

Fig. 2.1.31 *(a) HXR emissivity as a function of energy in 5 snapshots after the ECCD switch-on (t=0), for a central (continuous red line) and an off-axis (dashed blue line, ρ ~0.6) chord; (b) spatial profiles of the photon temperature for the same snapshots (ρ here indicates the minimum normalised radius for each chord, i.e. the point of tangency to the flux surface).*

These results are consistent with our Fokker-Planck modelling using the quasi-linear CQL3D code, which is able to reproduce the ECCD efficiency in TCV only by assuming a diffusivity of the order of $3m^2/s$. CQL3D can also calculate the HXR emission for direct comparison with the experimental data. Without diffusion, not only is the predicted current much too large, but also the predicted HXR signal is far narrower spatially than the measured one. Much better agreement is obtained with $D=3m^2/s$, shown in Fig. 2.1.32 for a discharge with 0.45MW central co-ECCD. Both the amplitude in the centre and the energy dependence are well reproduced.

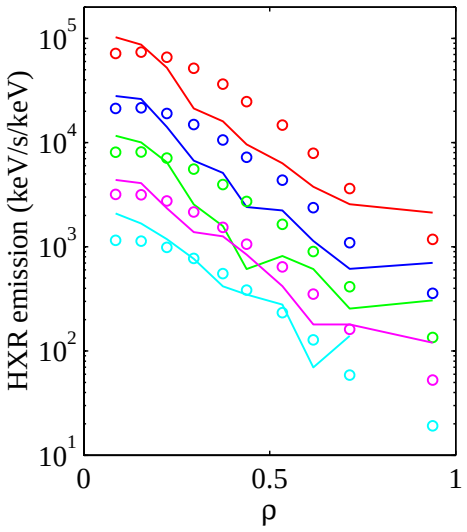

Fig. 2.1.32 *Predicted (lines) and measured (circles) HXR emission as a function of chordal spatial location for 5 energy channels of 8keV width in the 16-56keV range (descending amplitude for increasing energy).*

The high sensitivity and time resolution of the high field side ECE system also allows perturbative studies of the dynamics of suprathermal electrons. We have applied short periodic ECCD pulses to the plasma and studied the ECE response by coherent averaging. Pulses longer than 0.3ms were seen to result in a first peak, followed by a decrease and a further increase until the end of the pulse, indicating that the pulse length exceeded the characteristic RF diffusion time. To avoid this complicating effect, the pulse length was limited to 0.25-0.3ms. The applied power was 0.45-0.9MW with a period of 10ms, corresponding to a 3% duty cycle and an average power <27kW, too low to measurably affect the plasma parameters. Two examples, both with central ECCD, are shown in Fig. 2.1.33. In the case of Fig. 2.1.33a) an antenna with a direct view of the plasma centre is used, whereas in the Fig. 2.1.33b) the antenna is 20cm below the plasma magnetic axis, so that the smallest normalised minor radius from which ECE can be collected is approximately ρ_{min}=0.55.

In both cases the time to peak increases with the ECE frequency, Fig. 2.1.34(I). Moreover, the time lags are clearly larger when the ECE radiometer is aimed off-axis: indeed, when plotted versus the cold-resonance minor radius, the two curves connect smoothly to each other [Fig. 2.1.34(II)]. An increase in frequency can be associated with either a shift towards the high field side (larger minor radius) or an increase in electron energy. However, for equal energy and frequency, the signals from the two chords originate in different spatial regions. This observation corroborates the hypothesis that a transport mechanism is at play and that a non-negligible fraction of the fast electrons generated by ECCD is transported away from the deposition region. The near quadratic increase of the time lag with radius in Fig. 2.1.34(II) is consistent with the diffusion coefficient of a few m^2/s, already shown to reproduce the ECCD efficiency with CQL3D. A more quantitative assessment of transport parameters will require detailed, time dependent modelling, because the evolution of the ECE signals is expected to depend not only on the diffusion time, but also on the slowing-down time. The evolution may even be affected by changes in the power deposition as the electron distribution function changes in velocity and configuration space after the ECH switch-on.

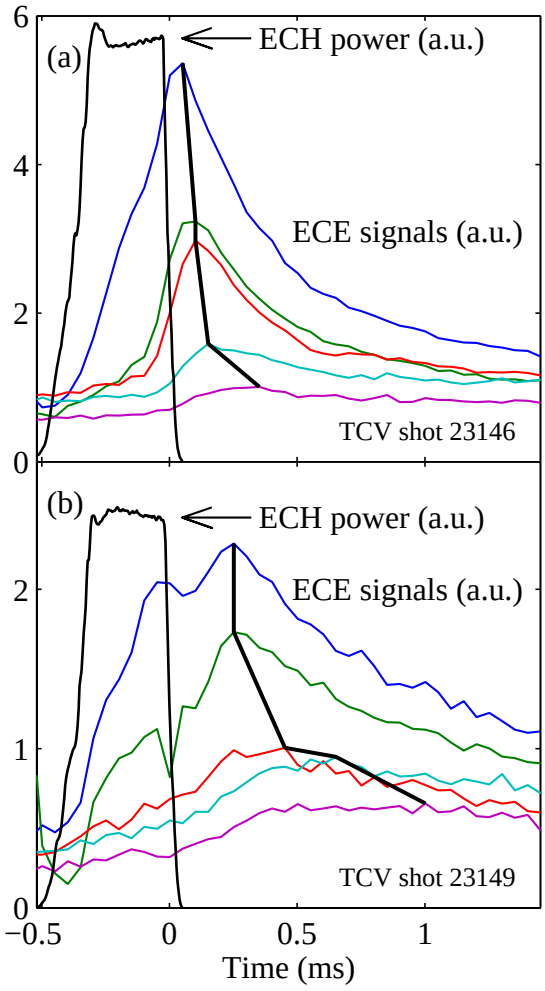

Fig. 2.1.33 *Response of selected ECE signals to a short central ECCD pulse, averaged over 170 coherent pulses; the ECE frequency increases as the peak moves to later times; ECE radiometer (top) on the midplane, (bottom) off-axis (ρ > 0.55).*

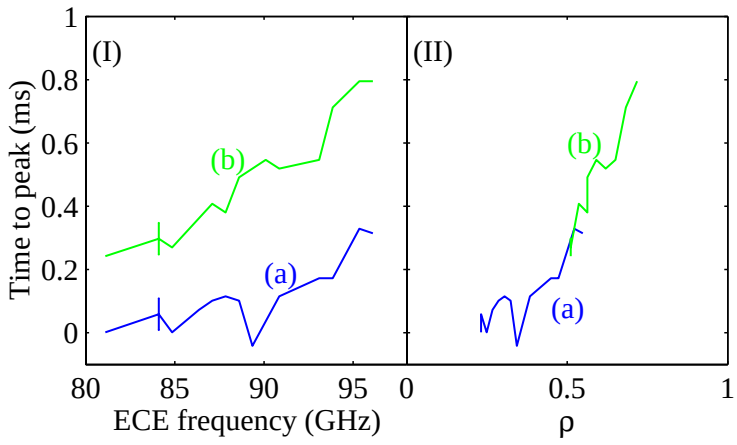

Fig. 2.1.34 *Time lag from the end of the ECCD pulse to the ECE peak, for the two cases shown in Fig. 2.1.33, (I) as a function of ECE frequency, (II) as a function of the cold resonance normalised radius.*

ECH absorption at X2 and X3

Good knowledge of the total absorbed power and of its spatial distribution is crucial for the interpretation of ECH experiments, in particular for determining the effect of ECH on current and pressure profiles in advanced scenarios and for transport analysis. A traditional experimental method is to measure the dynamical response of the plasma to modulated electron cyclotron heating (MECH), which separates heating from transport effects.

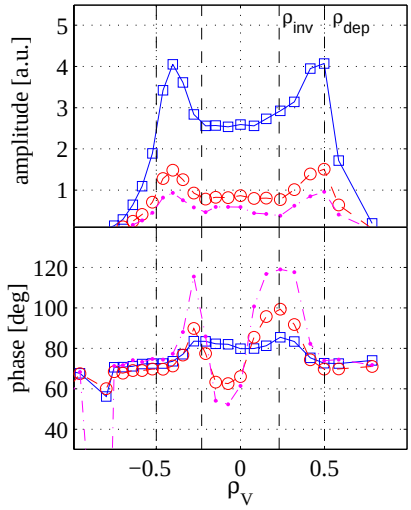

Fig. 2.1.35 *ECH power deposition profile from the plasma response to MECH*

However, this method often encounters the problem of coupling between the MECH and the sawtooth activity, which makes the interpretation of the dynamical response practically impossible. It is therefore necessary to separate the response coming from the sawtooth to that linked to the heating itself. The limitations of previous separation methods based on the Generalised Singular Value Decomposition technique (GSVD) were assessed. In particular, it was demonstrated that the GSVD is incapable of correctly removing this coupling. A new method, based on the Singular Value Decomposition technique (SVD) has been developed. The SVD has the advantage of being able to correctly analyse the phase subspace in which the dynamics of both the sawteeth and the MECH are contained. Treating this reduced problem with a system identification approach allows us to fully separate the two dynamics. This method has been successfully applied on MECH experiments both on TCV and on ASDEX Upgrade.

The experimental determination of the power deposition profile also requires a diagnostic sensitive to the plasma energy content, with appropriate time and space resolution. Several diagnostics were tested on TCV and in collaboration with ASDEX Upgrade. Attention was given to the possibility of using line integrated soft X-ray (SXR) measured both with the diode SXR camera and with the multi-wire proportional X-ray detector chamber. This diagnostic guarantees very good spatial resolution and is not affected by neutrons, a very important feature for future fusion devices. Figure 2.1.35 shows the main results of this study: amplitude and phase profiles of SXR measurements are coherent with electron cyclotron emission (ECE) data and clearly determine the deposition location.

The total ECH power absorbed by the plasma is determined in MECH experiments from the diamagnetic flux of the plasma measured by the diamagnetic loop. This

diagnostic has been extensively used in different heating scenarios of L-mode or H-mode plasmas and with various combinations of X2 and/or X3 with different launching schemes (ECH and/or ECCD). In discharges without suprathermal electrons, the measured value of the absorbed power is in good agreement with the value calculated by the TORAY-GA code, which is based on a thermal electron distribution function. If a suprathermal population exists, the measured value is in general higher than the predicted value, since a significant fraction of the injected power is absorbed by the suprathermal population.

For top launch X3 heating, the diagnostic has been used for measuring the absorption in a variety of plasma conditions with central densities higher than the X2 cut-off. Absorption measurements with X3 heating of ELMy H-mode plasmas were present not yet possible because the ELMs significantly perturb the diamagnetic measurement. Treating the diamagnetic signal with a system identification method should allow us to separate the power modulation and the ELMs in order to measure the X3 absorbed power and the power loss associated with the ELMs at the same time.

Figure 2.1.36 illustrates such an experiment, in which the X3 injected power was 0.9MW (two gyrotrons) and the central electron density, n_{e0}= 4.5-5·$10^{19}m^{-3}$, was above the cut-off density for the X2 system (4·$10^{19}m^{-3}$). The angle of the top launcher mirror was kept fixed at 46.2° (measured clockwise from the vertical). The optimum angle was determined in an earlier shot with same plasma parameters, but with an injection angle swept between 45.5° and 47.5°. The absorption measurement with the diamagnetic loop was made while only modulating one gyrotron (square wave at 237Hz) between t=1.2s and 1.4s. The measured absorbed power of the modulated gyrotron is P_{abs}= 290kW which corresponds to an absorbed fraction of the X3 wave of 66%. A preliminary analysis shows that this value corresponds to single-pass absorption.

With the completion of the X3 top launch system with three gyrotrons injecting a total of 1.35MW, leading to higher electron temperatures, full single-pass absorption is expected even without X2 preheating.

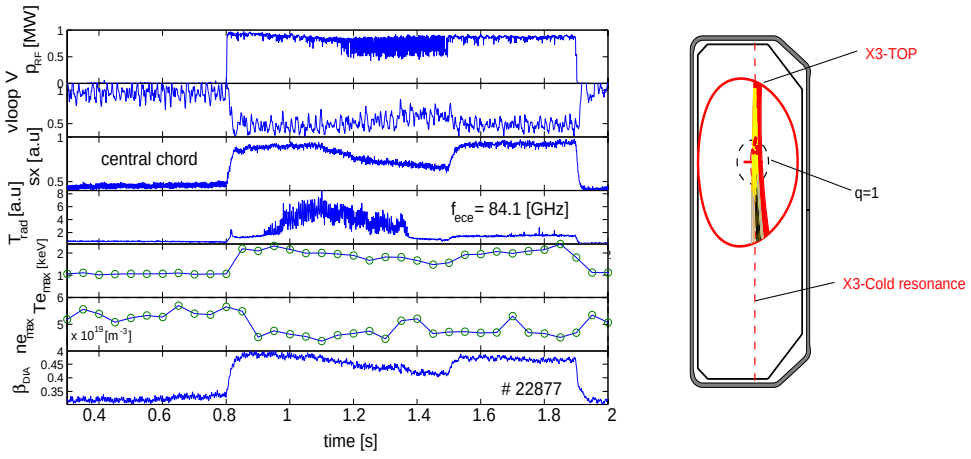

Fig. 2.1.36 *Launching geometry and typical time traces for X3 ECH top launch in Ohmically heated target plasma.*

ECCD physics

During the past few years TCV has become a unique test bed for studying and validating the fundamental properties of ECCD. The exceptional flexibility afforded by the six independently steerable X2 launchers has been used in series of experiments aimed at elucidating both the global properties of ECCD and the dynamics of the current-carrying suprathermal electrons. The main diagnostic tools employed in this effort are the hard X-ray (HXR) camera and the high field side electron cyclotron emission (ECE) radiometer, respectively measuring bremsstrahlung and relativistically downshifted cyclotron emission from suprathermal electrons. Modelling is performed with the linear ray tracing code TORAY-GA, equipped with the Cohen package for current drive estimation, and with the CQL3D code, which solves the Fokker-Planck equation in two velocity and one spatial dimension. The equation includes a quasi-linear EC wave damping term, a relativistic collision operator and a model for radial transport, with an optional linear dependence of the diffusion coefficient on the parallel velocity and a particle-conserving advection term.

ECCD relies on the creation and sustainment of a suprathermal electron population, whose existence has been confirmed by HXR and ECE measurements. The relaxation processes governing this population have a strong impact on the location and magnitude of the driven current. The experimental ECCD efficiency is known to good accuracy in discharges with zero toroidal electric field, when the current is fully non-inductively driven in steady-state conditions. As such discharges are routinely obtained in TCV, we now possess a broad ECCD efficiency database for comparison with theoretical predictions. The experimental efficiency can be between one and three times that calculated by the linear code TORAY-GA. By contrast, the efficiency is greatly overestimated by Fokker-Planck quasi-linear theory, which predicts strong nonlinear enhancement by the unequalled EC power densities achieved in TCV. This discrepancy has been resolved by including a relatively modest diffusion coefficient D~3-5m^2/s in CQL3D as already mentioned.

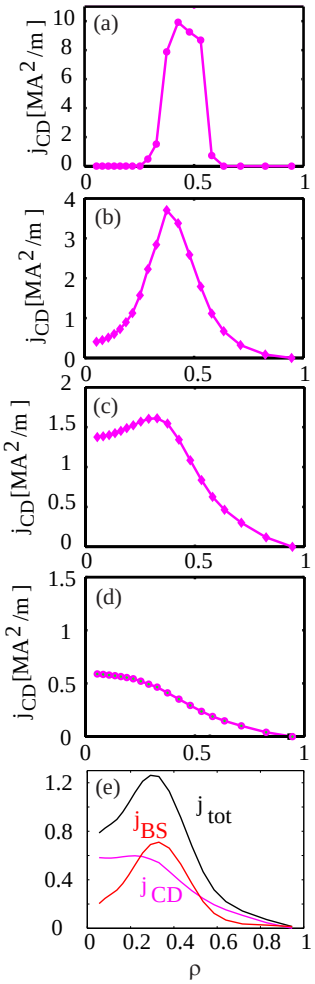

Fig. 2.1.37 *The CQL3D ECCD current profile broadens and the total driven current is reduced as radial diffusion is increased: (a) D=0, I_{CD}=460kA; (b) D=0.05m²/s, I_{CD}=231kA; (c) D=0.5m²/s, I_{CD}=141kA; (d) D=5m²/s, I_{CD}=43kA. The total current density profile (e) is a combination of the lower curve (d) and the bootstrap current calculated from the density and temperature profiles. The power is deposited in the region 0.3<ρ<0.6.*

A striking consequence of this suprathermal diffusivity is the recent achievement of fully non-inductive discharges driven entirely by off-axis ECCD and bootstrap current. The EC-driven current profile calculated by CQL3D is shown in Fig. 2.1.37 for different values of the diffusivity. With the diffusivity required to match the total driven current, the profile is centrally peaked in spite of the power being deposited approximately at half-radius (it should be noted that the total current profile is nevertheless calculated to be hollow, owing to the bootstrap current contribution).

One of the limitations of X2 ECCD is the inaccessibility of high-density regimes, since the cut-off density is $4.2 \cdot 10^{19} m^{-3}$. X3 ECCD on the other hand is beset by very low efficiency. One option to drive current in high-density plasmas with EC waves is to employ the electrostatic electron Bernstein wave (EBW), which can reach in principle current drive efficiencies of the same order as those of X2 ECCD. A study in collaboration with the W7-AS group at IPP Garching (Germany) is underway to explore the possibility of exciting such waves by mode conversion from the X-mode.

2.1.6 ECH-ECCD as tools for advanced tokamak physics

The last two decades of tokamak physics have been marked by the discovery of new modes of operation leading to improved confinement and/or stability. Optimising the performance and limits of operation of these scenarios is one of the major tasks that the fusion community faces at present. Such improvements require the ability

to control, both globally and locally, the plasma pressure and current density profiles. In this respect ECH and ECCD are arguably the best tools available owing to their flexibility, ease of controlling the deposition location and the ability to be absorbed in a very narrow region. This is why ECH and ECCD are being used more and more in worldwide facilities.

Research on TCV is at the forefront of this research, benefiting in particular from the high quality and flexibility of its EC system and the highest power density available. In addition, in the low collisionality TCV plasmas, the heating power that is directly coupled to the electrons cannot be transferred to the ions, making it possible to isolate the transport mechanisms affecting the electrons only. In the last three years, ECH and ECCD have been successfully used for significant local and global pressure and current density profiles modification. Using ECH and/or ECCD as tools for advanced tokamak physics, investigations on TCV have focused on the physics of the improved core electron confinement with central counter-CD, stable steady-state non-inductive discharges, and bootstrap current driven advanced scenarios.

Improved Core Energy Confinement modes

The key to the regime of improved core energy confinement (ICEC) of EC-heated plasmas in TCV is controlling the shape of the current density profile. This has been obtained by a combination of counter current drive and off-axis EC-heating. The best performance in terms of central electron temperature (T_e) and global electron energy confinement time has been obtained with q-profiles characterised by reversed shear. In the presence of an inductively driven current, these conditions can only be achieved with precise alignment of the EC-driven current components. A sufficiently strong counter ECCD component is required to prevent the total current from peaking on axis due to the increase of plasma conductivity with temperature. In the ICEC regime the T_e profiles are characterised by a sharp gradient, which is typical of the formation of an internal barrier for electron thermal transport (eITB) (Fig. 2.1.38).

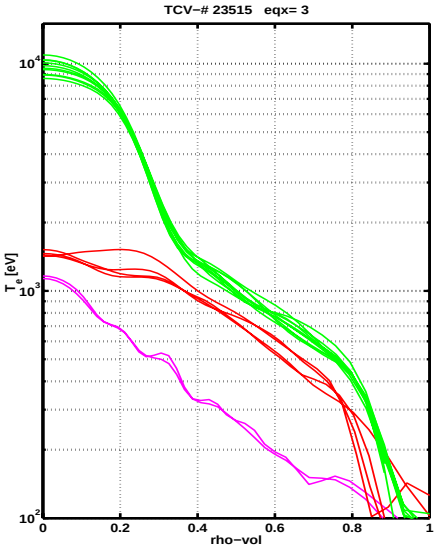

Fig. 2.1.38 *Electron temperature profiles fitted to Thomson scattering data presented on a log scale and in normalised radial coordinates, #23515, Ip=200kA. Magenta: during phase with ohmic heating only;*

Red: during phase with off-axis ECH (1MW at ρ=0.4); Green: during Improved Core Energy Confinement (ICEC) phase (1MW off-axis ECH and 1MW counter ECCD in the centre), showing the formation of an eITB near ρ=0.3.

A series of experiments has been carried out with the plasma current in the range 100 to 200kA and fixed toroidal magnetic field. They reveal the influence of the q-profile on the location of the transport barriers. For a given deposition profile of the ECH and ECCD power the location of the barrier moves outward with decreasing plasma current. In Fig, 2.1.39, the global electron energy confinement time increases by about 20% as a consequence of the widening of the improved confinement region. The correlation between the location of the barrier and the shape of the q-profile is subject to further investigations using the CQL3D code.

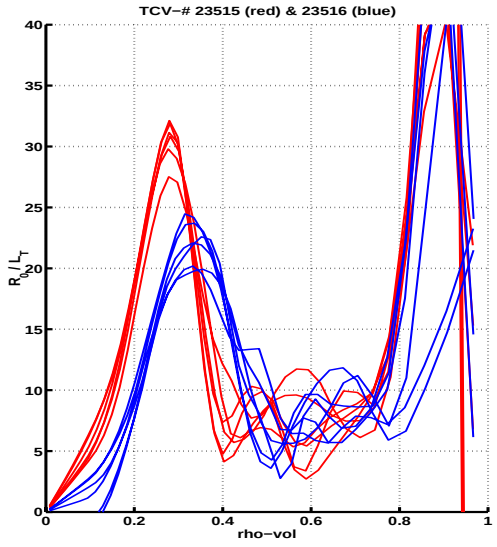

Fig. 2.1.39 *Normalised gradient of T_e versus normalised radius during the ICEC phase for 2 discharges with different total plasma current. #23515 (red), I_p=150kA, and #23516 (blue), I_p=120kA*

Fully non-inductive discharges

The six X2 ECH launchers allow independent steering of the heating sources in both the poloidal and toroidal directions. This high flexibility matches that of the TCV control system, permitting the vast range of shapes that can be created to be heated in an accurately localised manner. The six sources can be employed to tailor the current profile in a stationary state, as will be required in a reactor for MHD stabilisation and performance optimisation. A crucial requirement for the reactor relevance of this scenario is that of stationarity, namely that the ECH pulse length substantially exceeds the current redistribution time from Ohmic to non-inductively driven profiles (for TCV typically <0.5s).

Fully non-inductive operation with a combination of ECCD and bootstrap current has now become routine in TCV, guaranteed by keeping the current in the Ohmic transformer primary constant by feedback once steady-state conditions are reached. Recently, fully non-inductive discharges have been driven entirely by off-axis ECCD and the bootstrap current, with only 0.9MW power. Modelling with the quasi-linear Fokker-Planck code CQL3D indicates that cross-field transport of fast electrons is sufficient to result in a centrally peaked ECCD profile even though the power is deposited approximately at mid-radius.

Operating in the absence of a toroidal electric field offers greatly improved control over the current profile. At the same time, it significantly simplifies physics studies, particularly of fast electron dynamics, as the complicated effect of the toroidal electric field is removed. These benefits are well known from the history of fully non-inductive experiments with lower hybrid current drive, but are significantly enhanced by the high degree of aiming control and localisation of the EC waves. An additional advantage of ECCD is predominant electron heating, which mimics the effect of alpha particle heating in a reactor. The steady state, non-inductive regime is therefore now the starting point for the exploration of advanced modes of operation, such as through the formation of internal electron transport barriers (building on the work described in the previous Section) or through a progressive increase of the bootstrap fraction.

Advanced scenarios with large bootstrap current fractions

Having demonstrated improving the confinement through current profile tailoring and the ability to sustain the full plasma current by ECCD, we have started to develop fully sustained scenarios with non-monotonic current density profiles. Reversed shear scenarios have been shown in other tokamaks to lead to significant confinement improvement and to the formation of Internal Transport Barriers (ITBs). However, until the experiments reported, ITBs were not obtained in plasmas with $T_e >> T_i$, and the barrier was observed mainly in the ion temperature profile.

The experimental method on TCV is based on co-ECCD beams aimed off-axis to maximise the off-axis current density. Simulations indicate that the radial profile of the driven current would be essentially flat due to radial diffusion of fast electrons. Nonetheless, the flat shear is sufficient to improve the electron confinement, as seen in the ICEC regime. Since the current is fully sustained by the off-axis beams, despite the effect of trapped particles, there is no residual electric field that would increase the central current density with increasing central temperature. Therefore, while the pressure builds up in the core region, the current profile remains flat. The bootstrap current increases and in turn leads to an off-axis peaked current profile. This further improves the confinement and an electron internal transport barrier (eITB) is formed. This scenario, illustrated in Fig. 2.1.40, constitutes to our knowledge the first example of a bootstrap-driven ITB. A further advance is that we do not have to use a fast current ramp to form the ITB.

The confinement time does not degrade with respect to RLW scaling with increasing power and actually slightly improves when the third gyrotron (B) aiming in the centre is added Fig. 2.1.40. This leads to a significant increase in the H confinement normalisation factor, which measures the confinement time with respect to the expected value in standard electron heated scenarios as given by the RLW scaling law.

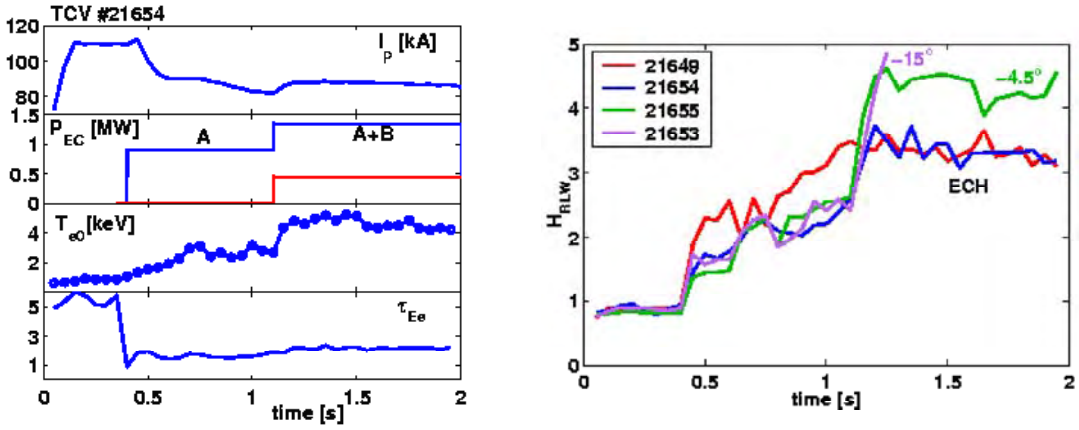

Fig. 2.1.40 *Left: Time traces for advanced scenarios with large bootstrap fraction. First off-axis co-ECCD beams are injected (A) to replace the full current and create a good confinement region in the centre. Power is then deposited in the centre (B) in heating or with a counter-ECCD component. Right: Comparison of the confinement merit* $H_{RLW}=\tau_{Eeexp}/\tau_{EeRLW}$ *with heating and counter-ECCD added in the second phase (B). Adding counter-ECCD in the centre further improves the confinement until the ITB is so steep it becomes MHD unstable.*

In Fig. 2.1.40(right) the H_{RLW} factor is shown for different experimental arrangements. The central EC beam is aimed to provide both heating and counter-ECCD. This discharge shows that a positive feedback loop is generated: the more power is injected in counter-ECCD mode in the centre, the more reversed the central q-profile and the larger the improvement in the confinement time. However, with an angle of -15^{o}, such as in discharge #21653, the eITB becomes so steep that the pressure profile is MHD unstable and the discharge disrupts. As the profiles are fully non-inductively driven, it is easy to stay just below this MHD limit by controlling the amount of counter-CD in the centre and to keep the discharge stable up to the end of the gyrotron pulses. The current profile in the second phase is calculated using the CQL3D code based on the experimental profiles and equilibrium configuration. The bootstrap current density and pressure profile are also calculated from the measured profiles. In this way the equilibrium is fully determined using the derivatives of the pressure profile and the total current (ECCD+bootstrap, as $j_{ohm}=0$, Fig. 2.1.41(left)) as source terms.

An example of the resulting q-profile is shown in Fig. 2.1.41(right), together with the LIUQE reconstruction. The estimated q-profile is reversed, while the LIUQE reconstruction (using only magnetic data as constraints and simple basis functions for the source terms) leads to a monotonic profile.

Discharge #21655 has a bootstrap fraction of about 50%. As mentioned, it is the bootstrap current that sustains the non-monotonic current profile. Preliminary attempts to increase the bootstrap fraction have been performed. A steady-state fully non-inductively driven reverse shear scenario with 80% bootstrap fraction and a clear eITB has already been obtained, showing that it is possible to align the maximum of the bootstrap current density, which depends on the maximum of the pressure gradient and thus on the ITB location, with the position of the minimum

of the q profile, which determines the confinement properties and therefore the ITB position.

This remarkable experimental achievement indicates the way towards the development of advanced scenarios based on steady-state discharges with a large bootstrap fraction, in which the off-axis maximum current density is sustained by the off-axis peaked bootstrap current. This result will certainly motivate concentrated experimental efforts in the future research period and will create significant international interest.

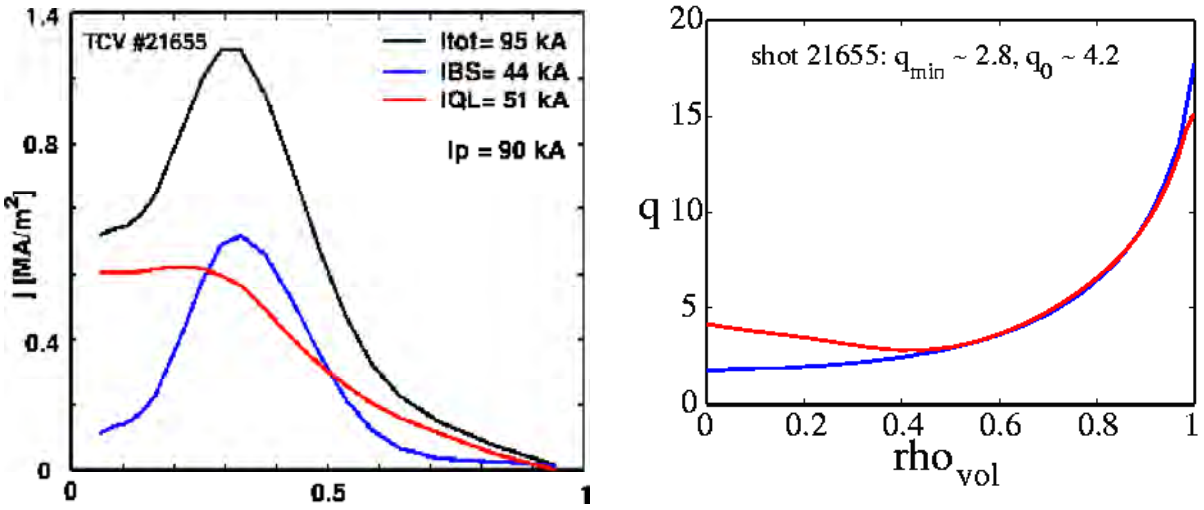

Fig. 2.1.41 *Left: EC current density profile as calculated with CQL3D (I_{QL}), bootstrap current density (I_{BS}) and total current density (I_{tot}). The plasma current in this discharge is 90kA; Right: Reconstructed equilibrium using only magnetic data (monotonic profile) and using the total current density and pressure profiles (reversed shear profile).*

2.2 Theory and numerical simulation

Theoretical activities at CRPP target three main physics objectives:

(1) To improve the understanding of fundamental transport phenomena that take place in magnetically confined fusion plasmas. Most of our efforts are related to anomalous transport and underlying microinstabilities such as the Ion Temperature Gradient mode (ITG).

(2) To explore new 3D configurations for optimised magnetic confinement. The focus of our studies has been on the effect of the bootstrap current in various configurations. The development of a new full wave code for low frequency RF waves (Alfvén and ion cyclotron range of frequencies) has also been pursued.

(3) To contribute to the interpretation and/or the prediction of experiments, such as the modelling of Electron Cyclotron Heating and Current Drive (ECH/ECCD) in TCV or the evolution of Neoclassical Tearing Modes (NTM) in TCV and JET.

In all these activities substantial numerical simulation effort has been made, including new developments or improvements to computational performance. Several of these activities are carried out in close cooperation with other Euratom (Max-Planck IPP in Greifswald and Garching, CEA in Cadarache) or non-Euratom laboratories (PPPL in Princeton, CompX in San Diego, NIFS in Nagoya, Keldysh Institute and Kurtchatov Institute in Moscow).

2.2.1 Physics underlying anomalous transport

Transport in magnetically confined plasmas has its origin in two distinct classes of physical processes. First, particle collisions can lead to particle and energy fluxes: this is the classical (or neoclassical) transport. Second, collective effects in the presence of equilibrium gradients can drive *microinstabilities* that can develop into turbulence and result in high transport levels: this is the *anomalous transport,* which in most experiments significantly exceeds the neoclassical transport. The physical model used for these studies is called *gyrokinetic*. It assumes that the frequencies under consideration are much smaller than the ion cyclotron frequency and leads to perturbations that tend to align with the magnetic field. In all our work leads to a global approach has been followed, i.e. the pertinent set of gyrokinetic equations are solved in the whole plasma volume, in contrast to local, ballooning or flux-tube representations.

Nonlinear gyrokinetic simulations including zonal component

This year, a major step has been made in the understanding of the behaviour and role of purely radial electric fields self-generated by turbulence (called *zonal* ExB flows). Through nonlinear coupling of ITG modes, a component of the electric field purely normal to the magnetic surfaces is driven, called the zonal component. The zonal ExB flow in turn reduces the level of ITG turbulence. Thus, the zonal component of the perturbation appears as a regulator of the ITG turbulence.

The "PIC δf" method of modelling transport consists of choosing points in phase space, or "tracers", and evolving them according to the gyrocentre trajectories. Only the perturbed part of the distribution function (δf) is used in calculating the right hand side of the quasi-neutrality equation. Satisfying energy conservation has proven to be technically rather difficult. The main obstacle is to reduce the numerical noise inherent in such methods down to an acceptable level. In other words, the challenge is to have good enough statistics for the gyrocentre tracers. It was only recently that this collaborative effort resulting in the ORB code has been able to demonstrate energy conservation in nonlinear full-radius gyrokinetic simulations, the result of an optimised loading technique that uses the energy conservation as an indicator of the numerical quality. The optimised loading technique consists of choosing a distribution of the gyrocenters that minimises this statistical noise.

First, a numerical simulation is run with a tracer density proportional to an equilibrium Maxwellian up to a point before the quality of the simulation becomes poor, with the energy conservation serving as an indicator of the quality. Figure 2.2.1 (top) shows the results of such a simulation in a cylindrical plasma with parameters corresponding to the typical properties of the W7-X stellarator which is still under construction: B=2.5T, a=0.55m, T_i=5keV, deuterium, a/ρ_{Li}=135, uniform density and T_e profiles, ion temperature gradient with a/L_{Ti}=3 peaking at

mid-radius. There is clearly a problem of non-conservation of energy in the nonlinear stage of the evolution. The results of the simulation with optimised loading are shown in Fig. 2.2.1 (bottom). Energy conservation is verified to an unprecedented quality. The zonal ExB component E_{r00} shows a remarkable regular and persistent radial pattern. In the non-optimised, non-energy conserving simulation the heat flux is more than a factor of 2 too high in the nonlinear stage at

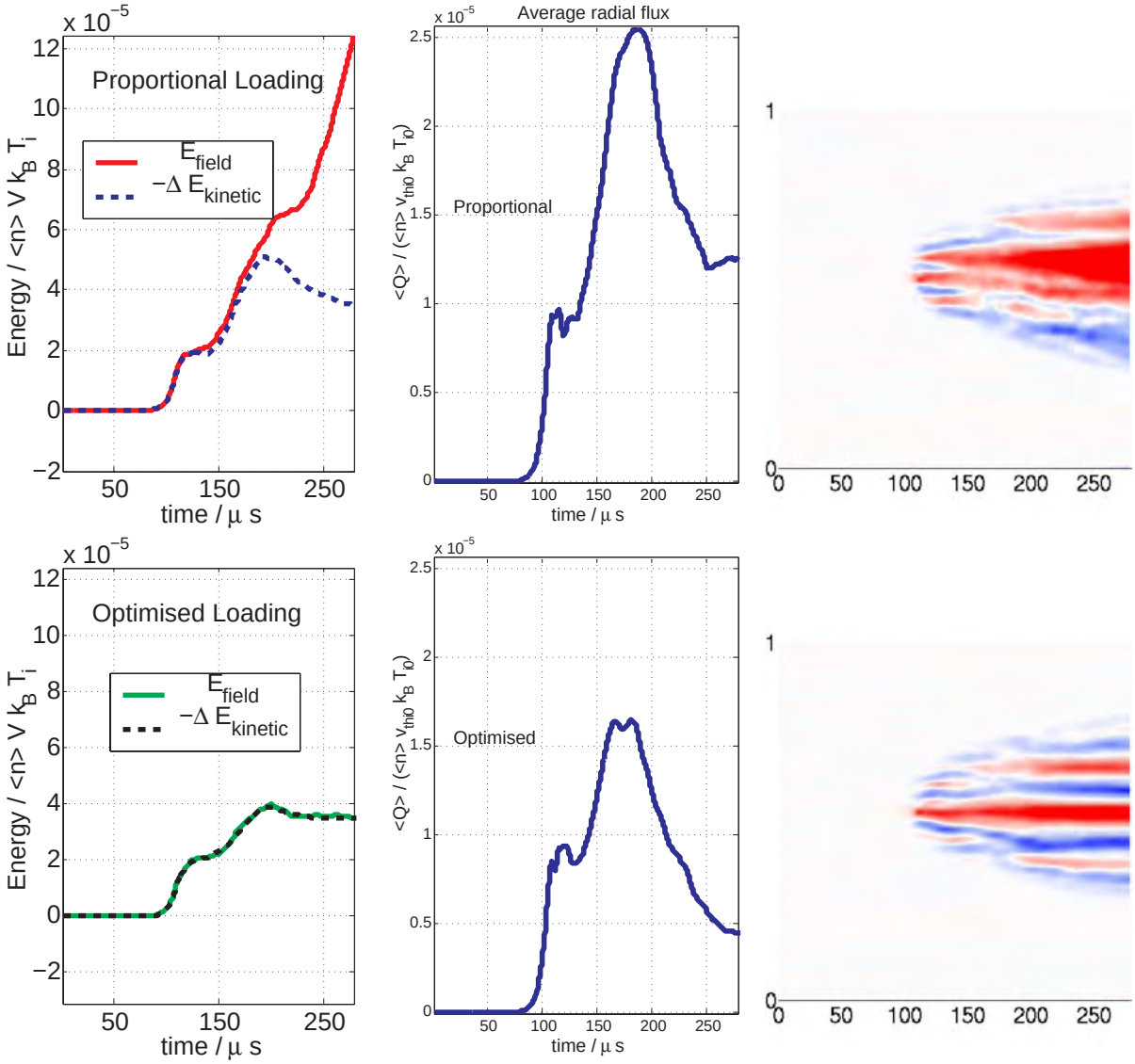

Fig. 2.2.1 *Field energy and change in kinetic energy (left), average radial heat flux (middle) and zonal ExB component $E_{r00}(r,t)$ (right, positive values in red, negative values in blue), for an un-optimised (proportional) loading (top) and after loading optimisation (bottom). Full radius gyrokinetic simulation in a cylindrical plasma with typical W7-X parameters, $a=135\rho_{Li}$.*

the end of the simulation. This large effect on the predicted heat flux level can be attributed to an incorrect calculation of the zonal component of the electric field: we observe that the regular pattern of the zonal component as computed with the energy conserving simulation (Fig. 2.2.1, bottom right), is destroyed at later times in the non-optimised, non-energy conserving simulation (Fig. 2.2.1, top right).

Snapshots in the late nonlinear stage of the ITG and zonal component (Fig. 2.2.2) show a remarkable structure with regions of positive E_{r00} coinciding with suppressed ITG mode activity and regions of negative E_{r00} in which ITG modes have a larger amplitude. The effective ion temperature profile is steepened in the suppressed ITG regions and flattened in the active ITG regions.

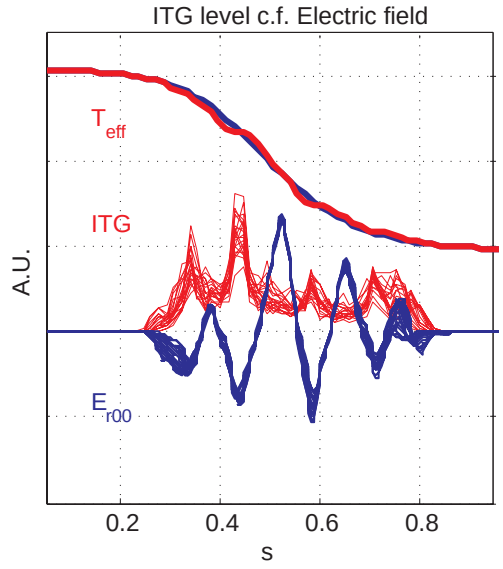

Fig. 2.2.2 *Snapshots of the zonal component E_{r00}, ITG amplitude and effective temperature profile well into the nonlinear stage of the optimised simulation shown in Fig. 2.2.1 (bottom). All quantities are plotted versus s=r/a.*

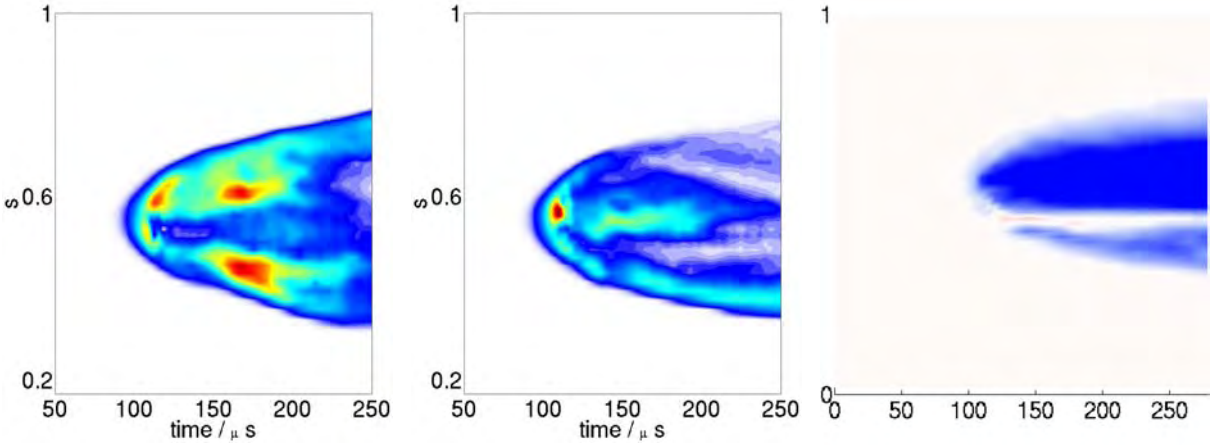

Fig. 2.2.3 *Radial heat flux versus time and normalised radius s=r/a, with (left) and without (middle) $v_{//}$ nonlinearity. Zonal component $E_{r00}(r,t)$ for the simulation without $v_{//}$ nonlinearity (right).*

These results suggest that the strongest nonlinearity in the system is the ExB nonlinearity. However, the nonlinearity in the parallel motion ($v_{//}$) due to acceleration by the parallel electric field is non negligible. The main consequences of ignoring it are the absence of parallel ion trapping, therefore affecting nonlinear ion Landau damping, and also that the energy conservation property is not satisfied and therefore a precious indicator of the quality of the numerics is lost. Figure 2.2.3 shows contour plots of the radial heat flux for simulations with (left) and without (middle) the parallel nonlinearity. The clear difference is related to the zonal component which is strongly affected (Fig. 2.2.3, right) as compared with the case with the $v_{//}$ nonlinearity (Fig. 2.2.1 bottom right).

We have implemented the optimised loading scheme in the toroidal version of the code. First results show that this method is useful in improving the conservation properties of the system. We have investigated the convergence properties of physically relevant quantities such as the field energy and radial heat flux. The results so far are promising, and there is the possibility of further adapting the loading optimisation to the case of toroidal geometry.

An alternative to the PIC-δf method is the semi-Lagrangian approach. This method retains both an Eulerian aspect in that the phase space is discretised on a fixed grid and a Lagrangian aspect in that the gyrocentre trajectories are computed (characteristics) to obtain the evolution of the full distribution function f. We have pursued the development of a new code ORB based on this approach. First results show that the linear properties are well reproduced and confirm that the zonal ExB flows indeed have a prominent role in the saturation mechanism. The behaviour of the nonlinear stage is qualitatively similar to that given by the PIC codes, but there remains a discrepancy to be resolved in the level of the saturated mode amplitudes.

Linear gyrokinetic simulations: effects of an applied ExB flow

We have continued the analysis of a tokamak discharge obtained on ASDEX-Upgrade in which an ion internal transport barrier was formed. (A transport barrier is a region of the plasma in which the usually high level of anomalous heat transport is substantially reduced). We had shown last year that the inclusion of the equilibrium radial electric field has a strong enough effect on ITG and trapped electron modes to completely stabilise them. This discharge showed good confinement in the whole region of negative magnetic shear with the foot of the barrier near the shear reversal region. In order to study the behaviour in the shear reversed region we have produced localised ion temperature gradient profiles, keeping all other parameters as measured in the experiment. Our results show that when the radial position of the maximum gradient is placed in the negative shear region, the growth rates are much smaller than in the positive shear region. We have confirmed the prominent role of the negative shear by considering monotonic q profiles with positive shear: in this case the ITG modes are much more unstable in the plasma core than with negative shear. We conclude from these studies that, in addition to the equilibrium radial electric field, the negative shear plays an important role in the stabilisation of these modes.

We have examined the ExB stabilisation of ITG and trapped electron modes in various configurations (tokamak, heliac and cylinder). While the simplified and often used stabilisation criterion (the ExB shearing rate exceeding the linear growth rate without ExB) appears to be valid for toroidal ITG, helical ITG and slab-like ITG modes, it can clearly be violated when trapped particle effects dominate the instability drive, in which case a *destabilising* effect arises from the value of the ExB velocity rather than its shearing rate.

Linear gyrokinetic simulations: electromagnetic effects at finite β

Increasing the plasma β changes the character of microinstabilities, which acquire an electromagnetic component. The effect of non-adiabatic electron dynamics becomes crucial too. A global eigenvalue numerical code has been optimised through improved parallelisation. This has enabled us to conduct a deep analysis of the numerical convergence properties. In particular the sharp behaviour of the

perturbed potentials in the vicinity of rational q surfaces, a feature which requires a very refined radial mesh resolution, has been confirmed. The Alfvénic ITG mode has been further studied. We have investigated the role of the electron to ion temperature ratio and showed a similar destabilisation effect as for the ITG mode. We have also varied the electron and ion temperature gradients independently. Our results show that the electron temperature gradient contributes as much as the ion temperature gradient to the instability. With an electron temperature gradient equal to the ion temperature gradient, the growth rate is about double that of the zero electron temperature gradient case.

These studies were conducted with a model that neglects the parallel magnetic perturbation, an approximation valid for finite but small β values. In order to extend the domain of validity of the model, we have considered full electromagnetic perturbations in the formulation. The extended model has been written using the same global spectral approach as previously. Adapting it into the numerical code will therefore be possible and attempted in the near future.

Statistical interpretation of non-diffusive transport measurements in tokamaks

Recent measurements in tokamak plasmas provide clear evidence for rapid non-diffusive transport and non-Gaussian fluctuations, which have been widely interpreted in terms of avalanching transport paradigms. Mathematical sandpile cellular automata are employed in this work to assist the characterisation of observed tokamak transport. Cellular automata are attractive because they can model self-regulating, driven-dissipative, non-equilibrium confinement systems that have non-local transport arising from local redistribution triggered by critical gradients. The simple rules that govern the sandpile simulation give rise to a rich phenomenology which displays significant points of contact with fusion plasma data. A detailed examination of the microscopic fluctuations that can occur reveals that diverse behaviour can be generated by well known random processes that are not necessarily associated with self organised criticality. The study is primarily concerned with using the concept of clustering as a basis for the statistical characterisation of non-diffusive transport behaviour. In broad terms, clustering is manifested by correlations between observables measured at different times, different locations, or both. Clustering is both a statistical observable and a physical concept: it originates in the underlying physical processes driving the transport and can be quantified and modelled mathematically. A fundamental message of this work is that, once a critical gradient has been exceeded, clustering of transport events is sufficient to generate much of the avalanching phenomenology and non-Gaussian statistical manifestations observed.

Diagnostics have been used to describe the spatial and temporal evolution of density fluctuations, together with the flux of material throughout the cellular automata, including the amount of matter leaving it and the distribution of times between mass-transfer events. These investigations have revealed new evidence for scale-free correlations in the fluctuations which drive the transport and quantify their distribution in terms of few-parameter non-Gaussian models. The correlation properties of density fluctuations can be interpreted in terms of random walk models, whereas flux fluctuations cannot. Instead they can be described by the discrete negative binomial distribution, which again indicates clustering of events. Some of the spatiotemporal correlations considered emulate multi-channel

measurements in tokamaks, and it is shown how these can be used to characterise the transport of naturally arising coherent structures.

2.2.2 Modelling of sawtooth activity in tokamaks

A semi-analytical approach within the framework of ideal kinetic theory has been employed to model the effect of NBI ions on sawteeth in JET plasmas. Investigations of experimental scenarios have highlighted the importance of sheared plasma rotation and anisotropy, both of which arise as a consequence of the injection of neutral beams. It has therefore been necessary to extend the analysis which describes the toroidal internal kink instability to include these effects self-consistently. For JET NBI discharges with a beam injection angle of about 45°, it is shown that the anisotropic fluid term is more stabilising with respect to the ideal internal kink mode than the kinetic term. The stabilising role of passing ions, often ignored in similar studies, is crucial. For injection which is more perpendicular than in JET, whereby the fraction of trapped fast ions is large, it is found that both co and counter plasma rotation of realistic amplitude and shear can significantly reduce the fast ion stabilisation. The analysis used in our work will also assist in determining the effects of anisotropy on ICRF sawtoothing discharges. This would be particularly important for judging the applicability of auxiliary heated ion behaviour in JET to predict the effects of isotropic α-particles in ITER.

The PRETOR-ST code has also been successful in simulating the combined effects of co-, counter-CD and heating taking place in ICCD experiments at JET where the driven current density profile has a dipole type structure with co- and counter-CD peaking at different spatial positions with respect to the power deposition on electrons. It has been shown that this particular feature is responsible for the two minima observed in the sawtooth period as the resonance crosses the inversion radius. A generic analysis of the best position for stabilising or destabilising sawteeth, using either heating, co- or counter-CD has been performed, depending on the auxiliary heating system used.

2.2.3 Optimisation of 3D magnetic configurations

The design of 3D magnetic confinement configurations is a much more difficult task than for tokamaks. The three-dimensionality, while adding degrees of freedom, requires special care in order that the configuration actually confines particles and energy. One way to overcome this difficulty is to try to obtain "quasi-symmetry" (QS), a 3D magnetic configuration in which the modulus of the magnetic field only depends on two independent variables: a radial variable (magnetic surface index) and a combination of poloidal and toroidal co-ordinates. Among the parameters to be optimised is the plasma β limit imposed by local and global MHD instabilities. We have concentrated our efforts this year on the bootstrap current calculation and its effect on MHD stability.

The effect of the bootstrap current has been investigated in several different types of stellarator systems, all reactor size with a volume ~1000m^3. In a 2-field period quasi-axisymmetric configuration, the bootstrap current at β^*=5% (Fig. 2.2.4) causes the rotational transform ι to increase beyond the critical value ι=1/2 (Fig. 2.2.5). This drives global external kinks (m=2, n=1) unstable (Fig. 2.2.6). These modes can be stabilised by applying counter current drive in the range of 1 MA. In

a 3-field period quasi-axisymmetric configuration, the bootstrap current at β*=5% can destabilise a global external kink mode (m=4, n=3).

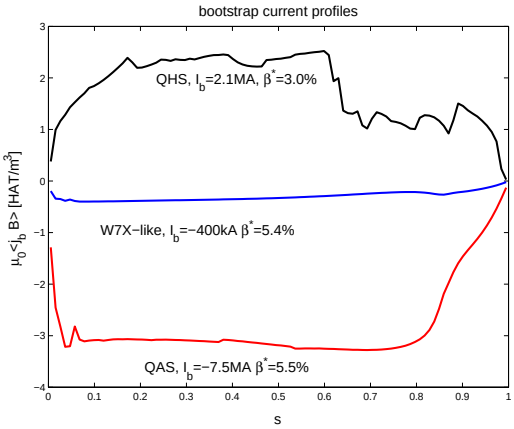

Fig. 2.2.4 *Bootstrap current profiles for quasi-axisymmetric (QAS), quasi-helically symmetric (QHS) and W7-X-like reactor size configurations.*

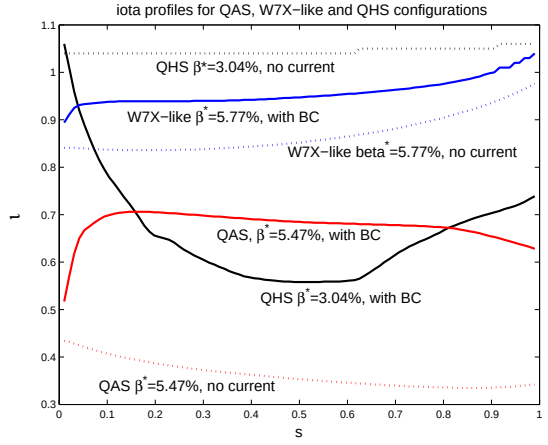

Fig. 2.2.5 *Rotational transform profiles for quasi-axisymmetric (QAS), quasi-helically symmetric (QHS) and W7-X like reactor size configurations, with (continuous lines) and without (dotted lines) bootstrap current contribution.*

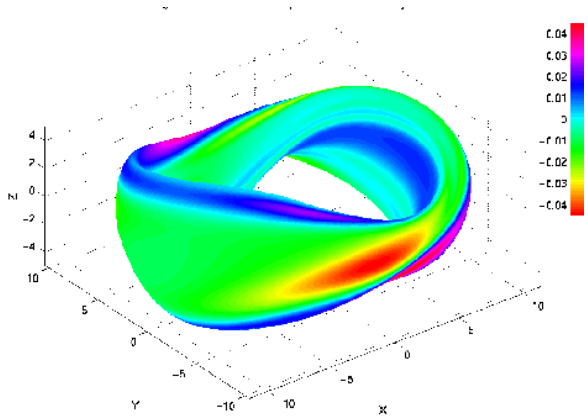

Fig. 2.2.6 *Normal component of the perturbed magnetic field for a global external kink mode in a quasi-axisymmetric configuration.*

Suppressing the bootstrap current slightly stabilises this mode. In a 5-field period system similar to the W7-X device in shape, the rotational transform is enhanced by a factor of only 10% by the bootstrap current (Fig. 2.2.4 and 2.2.5). In a 4-field period quasi-helically symmetric configuration, the bootstrap current is such that it decreases the rotational transform (Figs 2.2.4 and 2.2.5). At β*=3%, a flat ι=1.05 is achieved if zero net current is assumed. With bootstrap current, ι varies a minimum of 1/2 at mid volume and 3/4 at the edge. A pseudo-symmetric 6-field

period system at β*=6% has been shown to preserve the closed contours of the second adiabatic invariant, thus keeping favourable α-particle confinement properties. The bootstrap current is small and decreases the rotational transform only slightly. As a result, only intermediate to high n modes can become weakly destabilised.

2.2.4 Macroscopic stability of tokamaks

Ideal MHD instabilities with large toroidal mode numbers are possible candidates to trigger the Edge Localised Mode (ELM) instability. We have focused our studies on the influence of the presence of a magnetic separatrix and of pedestals in pressure gradient and current density at the plasma edge. External kink modes coupled to ballooning modes set stability limits for the pressure gradient and current density pedestal at the separatrix. (Ballooning means the mode tends to localise in the unfavourable magnetic curvature region at the outboard side of the tokamak.) The KINX ideal MHD stability code has been used to compute the high n kink mode stability of equilibria corresponding to the TCV and Alcator C-Mod tokamaks. We have shown that the β limit imposed by such modes can be lower than those imposed by low n external kink modes and the $n=\infty$ ballooning limit. A current density pedestal at the separatrix adversely affects the edge mode stability. There is also a shift of the range of unstable toroidal mode numbers to higher n values.

Wall stabilisation of external kink modes in steady state ITER scenarios was investigated. It was found that the operating space is rather sensitive to details in the plasma profiles and it could be significantly extended by a relatively small reduction in the pressure peaking factor.

The CAXE equilibrium code was upgraded with a new option for profile prescription in terms of the toroidal flux (instead of the poloidal flux). This option is particularly useful for a description of configurations with very high q in the plasma core (the so-called “current hole”). JET equilibria with extreme shear reversal were reproduced. Stability calculations with the KINX code have shown that for hollow current equilibria with sufficiently high global shear (q_{95}/q_{min} larger than about 2) external kink modes were stable up to values of $\beta_N=4l_i$. To model equilibria with negative core current density and poloidal field reversal the eigenfunctions of the Grad-Shafranov equation were numerically studied. In tokamaks with circular or moderate elongation cross section and finite aspect ratio, the eigenfunctions exhibit poloidal field reversal in the plasma core and $n=0$ island formation with X-points inside the plasma domain.

The quasi-equilibrium evolution code PET was applied to the modelling of a series of vertical displacement events (VDE) in the TCV tokamak in limiter plasma configurations at modest elongation. The accuracy of the plasma position and magnetic measurement prediction, when the flux consumption is matched to that of the experiment, is insensitive to the plasma profile evolution. The obtained values of growth rate agree well with those from DINA code computations in which a more complete transport model is used. The closed loop modelling of shots with highly elongated plasmas (κ>2) requires a higher time resolution to provide the needed accuracy and an adequate choice of the controller model.

The ideal internal kink mode is one of the possible triggers of sawtooth crashes and it is important to know the stability of this mode to be able to predict the behaviour

of sawteeth. We have studied the dependence of the ideal internal kink mode stability limit on the poloidal β inside the q=1 surface in TCV-like equilibria of various plasma shapes and current profiles using the KINX ideal MHD stability code. Plasma elongation was varied from 1 to 2.8 and triangularity from -1 to +1. A stabilisation for both positive and negative triangularities has been calculated. A semi-empirical scaling law for the critical poloidal β value inside q=1 has been proposed which describes satisfactorily the effects of elongation and triangularity. This scaling will be used for the prediction of sawtooth behaviour in TCV experiments.

2.2.5 Radiofrequency waves

Simulation of hard X-ray spectra and the current profile in TCV ECCD experiments

Using the CQL3D Fokker-Planck code including radial transport, modelling of hard X-ray spectra of TCV plasmas has been carried out. Radial diffusion coefficients with different velocity dependencies have been implemented, but there appears so far no conclusive strong evidence in favour of either electrostatic or electromagnetic turbulence. The electromagnetic turbulence model reproduces the measured photon temperature as well as its radial profile, but underestimates the photon intensity by an order of magnitude. In addition, a transport model with different diffusion levels for low and high energy electrons has been introduced to simulate the thermal electron transport barrier in the TCV tokamak. Results with this transport model agree fairly well with the experimental hard X-ray spectra. Photon temperatures agree within error bars but the simulated photon intensities are smaller by a factor of about three. In these simulations, the values of the transport coefficients were adjusted to match the value of the total driven current inferred from experimental measurements. This has proven to be a stringent constraint and as a result the calculated driven current density profile does not depend significantly on the choice of the diffusion model.

Alfvén frequencies and ICRF in 3D configurations

The aim of this work is to calculate the RF wave fields excited by a given antenna in the Alfvén and ion cyclotron range of frequencies in general toroidal 3D magnetic configurations. The newly developed code, LEMAN, uses a finite element discretisation in the radial direction (flux surfaces) and Fourier decompositions in both poloidal and toroidal directions. So far, the cold plasma dielectric tensor has been implemented. The code is linked to the 3D ideal MHD equilibrium code VMEC. Maxwell's equations are solved in terms of vector and scalar potentials to ensure the absence of unphysical numerical solutions. After successfully benchmarking the new code against the LION code in axisymmetric toroidal geometry, we have investigated the plasma response in different geometries: in a mirror configuration we could find the existence of a mirror-induced gap, Fig. 2.2.7a), and a Mirror-induced Alfvén Eigenmode, Fig. 2.2.7c,d), and in a helical configuration a helicity-induced gap and Helicity-induced Alfvén Eigenmode has been found. Unlike the LION code, the new code also includes finite electron inertia and therefore a finite parallel electric field, an example of which is shown in Fig. 2.2.7b).

2.2.6 Simulation of the Neoclassical Tearing Mode time evolution

The nonlinear growth rate of the island width of Neoclassical Tearing Modes (NTM) have been shown to be relatively well predicted by the modified Rutherford equation, which depends mainly on the tearing parameter driven by the current profile, the curvature term, the perturbed bootstrap current, the effect of finite perpendicular transport within the island, the polarisation current and the externally applied current density like ECCD. A systematic test of the modified Rutherford equation in different experimental conditions has been undertaken, simulating the time evolution of the mode island width using experimental initial boundary conditions and the time evolution of the poloidal β. The different terms included in the modified Rutherford equation are evaluated using experimental profiles and equilibria. The main test is in the comparison of the free parameters available in the formulation and the theoretical predictions of the expected range of these coefficients. Previously, the modified Rutherford equation has been shown to be adequate for TFTR, DIII-D and JET discharges. In TCV, we have shown that it can successfully simulate the evolution of the tearing mode from a classical to a neoclassical character. A new term has been proposed for the polarisation current in order to avoid unphysical values at small island width.

Several JET discharges aimed at determining the marginal β limit of NTMs have been simulated as well. It is demonstrated that the main stabilising term for island widths in the 4-6cm range has to be a slowly varying term with respect to island width itself. Therefore, this excludes the polarisation current as the physical mechanism for the stabilisation. It was shown that the perpendicular transport model was adequate in this range. In addition, the modified Rutherford equation has been reformulated through an appropriate normalisation. In this way, specific general constraints on the stabilising terms could be obtained which do not depend on the value of Δ', a term difficult to evaluate from the experimental profiles. The island is expected to be stabilised at typically half the width it would have if only the bootstrap drive and Δ' terms were present.

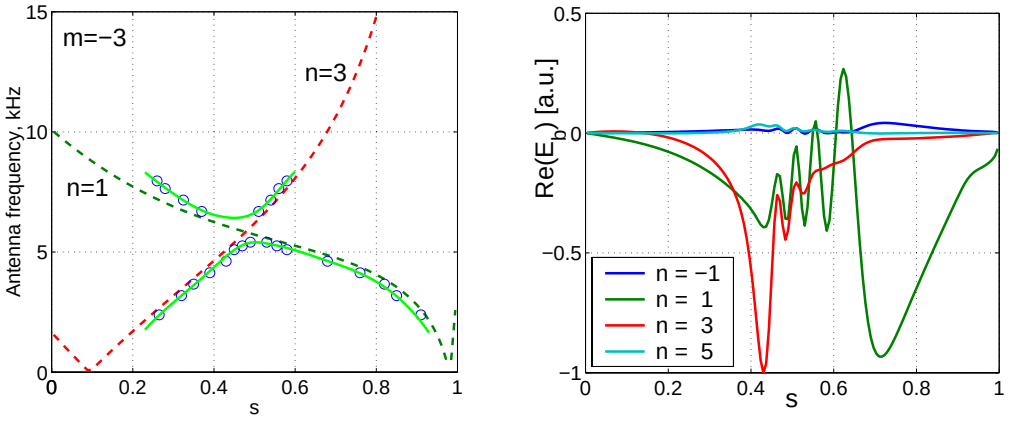

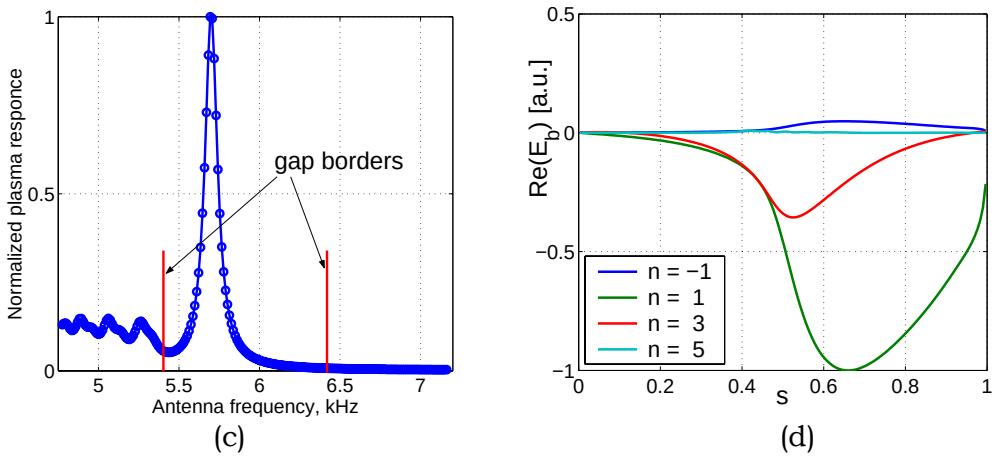

Fig. 2.2.7 *a) Alfvén continuum near the crossing of two cylindrical Alfvén continuum branches (dotted lines). In a mirror-like 2-field period configuration, a mirror-induced gap is formed in the continuum (line with circles); b) Wave field for a frequency below the gap, showing mode conversion to the quasi-electrostatic wave; c) Frequency scan of the antenna resistive power in the gap region. The peak corresponds to a mirror-induced Alfvén eigenmode (MAE); d) Wave field of the MAE.*

A further important test of the modified Rutherford equation was performed by simulating NTMs observed in the tight aspect ratio tokamak MAST. Indeed, this provides a test of the different terms in a regime far from the cylindrical approximation. Using the CHEASE code and formulae valid at arbitrary aspect ratio for the bootstrap current, the different terms have correctly been evaluated. In this way, the time evolution of the observed NTM could be simulated successfully using the same method as for conventional tokamaks. It was shown that stabilising terms are also necessary in MAST to predict the time evolution of the NTM island width (Fig. 2.2.8). In addition, it was confirmed that the curvature term is more important in tight aspect ratio tokamaks and could provide sufficient stabilisation to avoid NTMs in flat q profile scenarios.

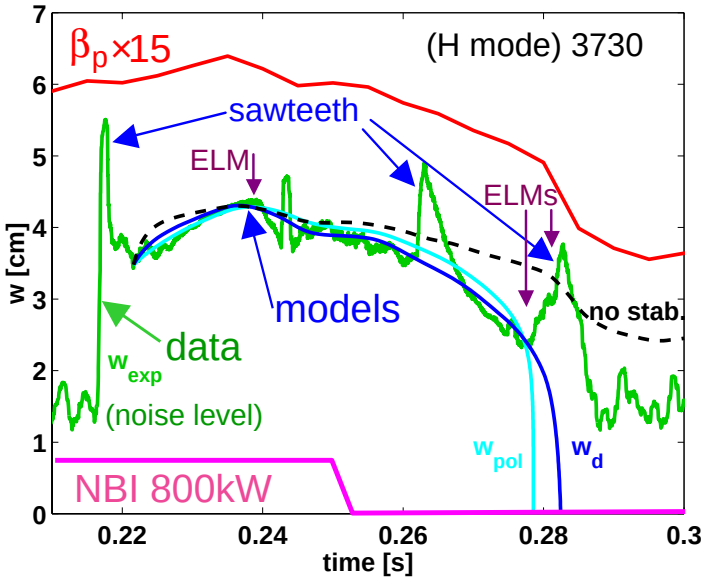

Fig. 2.2.8 *n/m=3/2 NTM amplitude evolution (green) in MAST shot 3730, corresponding to β_p changes (red), after termination of beam heating (magenta). Also shown: results of modelling with ion polarisation current (light blue), finite island transport (dark blue), or no stabilisation effects (dashed).*

2.2.7 Simulations of TCV discharges using the DINA code

Work has continued on the development of the DINA code for simulating TCV discharges, in collaboration with the Kurchatov and TRINITI institutes in Russia and the IPR institute in India. Ohmic discharges were studied in previous reports to show good agreement with the perturbed equilibrium response and the non-linear evolution of VDEs in the elongated vacuum vessel of TCV.

During this past year, we have reimplemented the DINA code in the SIMULINK environment of the Matlab suite, providing an open architecture and transparent implementation of the TCV control system, illustrated schematically in Fig. 2.2.9.

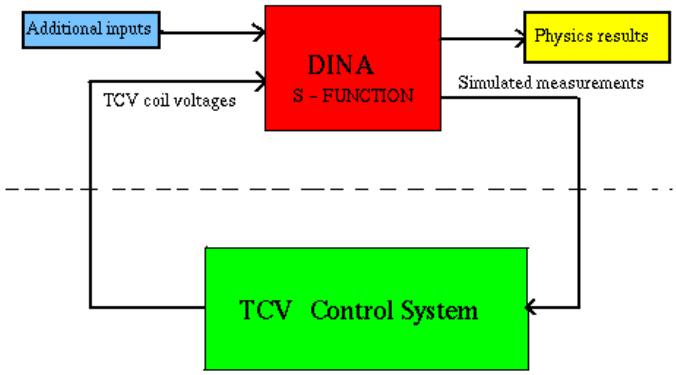

Fig. 2.2.9 *TCV simulations with the DINA-Simulink model.*

The target we set this year was to accurately reproduce TCV off-axis heating experiments previously reported. In these discharges, the plasma shape is not under feedback control. When the off-axis heating is applied, the change to the conductivity profile leads to an evolution towards a broader steady-state current distribution and therefore leads to a change in the plasma elongation in the almost constant quadrupole component of the vacuum poloidal field.

The poloidal angle of the ECH beams can be varied during the pulse and the power deposition varies in time, due to both the plasma shape and/or position variation and the beam launching geometry. Normal analysis of these discharges relies on the TORAY code, which calculates the beam trajectory and absorption for a cold plasma in (R,Z) geometry on the basis of the reconstructed equilibrium, and yields the power deposition in terms of the normalised radius. Using this deposition profile in the simulation would be dishonest, since a very different plasma position in the simulation would still have the experimentally correct deposition in terms of the normalised radius. However, calculating the beam deposition in real-time using TORAY during the simulation would be extremely time-consuming. The compromise

chosen is to convert the TORAY results back into (R,Z) geometry and impose the centroid and width of the power deposition on the simulation. This is still not completely self-consistent, since a different plasma shape would still lead to different diffraction of the EC beam, and therefore a different (R,Z) deposition from that calculated from the measured plasma profiles in TORAY. We consider this as a secondary effect, until proof to the contrary. The input to the DINA simulation is therefore the (R,Z) of the centre of the beam absorption, the width in the same rectangular co-ordinates and the instantaneous power, all imposed with a 1msec time resolution.

We present simulations of TCV discharge # 19692, which is an ECH assisted discharge with far off-axis deposition. The results are shown in Fig. 2.2.10 and we examine the signals in turn. The plasma current is well simulated, since it is fed back in closed loop in both the experiment and the simulation - the close agreement is inevitable. With the modification described above, the comparison of the simulated and measured OH transformer current is reasonable, although work is perhaps needed to improve on the quality of the agreement. The vertical position of the magnetic axis is well modelled, again inevitable since this parameter is also under feedback control. The evolution of κ_{95}, the elongation of the equilibrium at the 95% poloidal flux surface, shows 3 curves, the experiment (dotted line) and two simulation results. In the first simulation, the electron heat conductivity (nominal T-11 scaling) is multiplied by two (grey line) and in the second one, it is multiplied by one (black line). We see a significant difference in the speed of the evolution of the plasma elongation when the conductivity is changed, whereas both simulations tend towards the same elongation. This result shows that DINA is correctly modelling this evolving equilibrium current profile, but that there is a large sensitivity to the evolution of the temperature profile, through variations in the assumed transport. The triangularity δ_{95}, equilibrium parameters (β, li) and q_{95} show good agreement. The evolution of the electron and ion temperatures shows, as expected, significant dependence on the assumed heat transport multiplier, but the simulations are comparable with the experimental values.

There are some other sources of disagreement possible in the DINA simulations. Differences between DINA and LIUQE results for plasma parameters can be due to the different set of equilibrium parameterisation used by these codes. In the case of the LIUQE inverse equilibrium code, reconstruction of the plasma evolution is done by means of a set of parameterised functions for plasma current and pressure profiles and a fitting algorithm calculates the most suitable plasma parameters. However in DINA, the simulation starts with a set of initial conditions and then the plasma profiles evolve in a totally free manner.

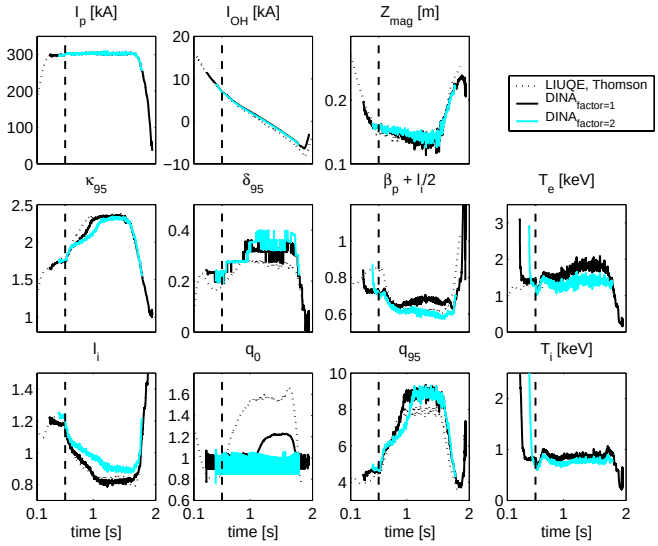

Fig. 2.2.10 *Results of ECH assisted TCV discharge #19692 with two different simulations with electron heat conductivity multiplied by two (grey line) and multiplied by one (black line) compared with the experimental measurements (dotted line). The vertical dashed line indicates the ECH turn on time.*

2.3 Basic Plasma Physics Activities

A basic experimental plasma physics group is being restarted at CRPP. The goal of this group is to isolate and investigate fundamental plasma physics problems of interest for magnetic fusion in a well-diagnosed laboratory plasma. This device will have flexible plasma production systems, such as electron cyclotron resonance heating or tokamak discharge, and magnetic confinement schemes. In addition, such a group provides an ideal environment for training students. The group will investigate linear and nonlinear wave-particle interaction phenomena, transport processes and phenomena related to magnetic reconnection in a magnetized toroidal plasma device.

2.3.1 Aim of first experimental campaigns

Investigations will start from linear and nonlinear wave-particle interaction phenomena related to transport processes. The characterisation and control of turbulence, causing anomalous cross-field particle and energy transport, remains one of the outstanding open issues for fusion, as well as for many space and astrophysical plasma phenomena. An integrated description of how local instabilities arise and combine to give rise to macroscopic behaviour is missing. Recent advances in the theory of turbulent transport and in the development of advanced scenarios in fusion devices have led to the discovery of improved confinement regimes. These are related to the presence of regions of reduced turbulence, characterised by the presence of radial electric fields. The radial field structures can be self-generated (zonal flows), or created by external means. The effects of these electric fields on the nonlinear evolution of drift-wave type instabilities into a turbulent state are important to understand and potentially to limit anomalous transport.

Despite the general relevance of turbulent transport issues, no direct experimental observation of these structures and their dynamical evolution has been made thus far. In particular, almost no experimental benchmark is available for the wealth of accumulated data. In devices oriented towards fusion relevant plasma parameters, the plasma core is not easily accessible for diagnostics with the required time and space resolution, to directly observe the relevant features of turbulence and the related transport. The TORoidal Plasma Experiment (TORPEX) at CRPP, aiming at low density and low temperature plasmas, equipped with modern diagnostics and a highly flexible magnetic field structure, is being designed and built exactly to suit these needs.

The low temperature laboratory plasma produced in TORPEX allows the use of electrostatic and magnetic probes directly inserted into the plasma core, as well as active optical techniques, such as laser-induced fluorescence. A thorough description of the properties of both fields and particles is therefore possible with high spatial and temporal resolution. The relationship between the local turbulence properties and the macroscopic plasma transport should be established experimentally. Subsequently, it will be natural to turn towards searching for possible ways of controlling the turbulence and its effect on the plasma transport.

The nonlinear development of the turbulent structures associated with drift waves is thought to be responsible for the anomalous transport observed in tokamak plasmas, especially for the electron channel. A first-principle simulation of this effect and how the formation of these structures is affected by sheared flows will be undertaken, leading to suggestions on how to limit the growth of these structures, thus limiting their effect on transport. The methods foreseen by theory to control the evolution of turbulence will be tested experimentally. These include the creation of localised shear flows. One way to achieve these is to launch ion Bernstein waves into the plasma core. In the TORPEX device, antennas for direct coupling of IBW can be inserted in the plasma core. Wave characteristics and particle response can be measured directly at the same time as the overall transport properties.

The investigations conducted on TORPEX will naturally fit within the integrated CRPP effort in the domain of cross-field transport, including theoretical developments and experiments on the TCV tokamak. The plasma conditions in the core of the TORPEX device are similar, in terms of temperatures and densities, to those at the edge of the TCV tokamak. Hence novel diagnostic methods aimed at characterising the turbulence and related transport developed and tested on the basic device can be applied to TCV. To highlight this integrated aspect of the experimental efforts at CRPP. Section 3.4 presents details of the TORPEX design and diagnostic systems.

2.3.2 Plasma production scheme

Plasmas of different noble gases will be produced and sustained by means of electromagnetic waves with a frequency in the range of the electron cyclotron (EC) resonance frequency. EC waves will be injected perpendicularly to the purely toroidal magnetic field from the low-field side (LFS), at a frequency f=2.45GHz. The corresponding EC resonance occurs where the magnetic field is B=0.0875T. The maximum output power of the source is 5kW-CW or 50kW for 100ms, with an overall duty cycle of 1 pulse every 30 seconds. During a pulse, the source can be modulated with a maximum frequency of f_{source}=20kHz.

The RF power is injected into the plasma with an O-mode polarization via a 1m-transmission line with a 90^0 twist to obtain the correct polarisation, a quartz pressure window, and a truncated wave-guide as an antenna. The choice of polarisation originates from the presence of a low-density cut-off for the X-mode close to the walls on the LFS. The first pass absorption is poor and the ordinary mode can be partially converted in extraordinary waves after reflection from the inner wall.

EC waves propagate in the vacuum chamber, break down the neutral gas, giving rise to a population of energetic electrons that will ionise the neutrals and build plasma densities up to $10^{17}m^{-3}$, with electron temperatures of the order of 20eV. The exact values of density and temperature will depend on the amount of RF power injected into the chamber.

By varying the magnetic field configuration, the injected power and the neutral density, it should be possible to control not only plasma parameters such as density and electron temperature, but also their typical scale lengths, $L_n$and L_{Te}, which characterise their gradients. The values of L_n and L_{Te} are thought to be crucial parameters in the development of instabilities and play a crucial role in fluctuation induced transport.

The main design values and the expected values of some plasma parameters TORPEX are summarised in Table 2.3.1.

Major radius	1m
Minor radius	0.2m
B_{tor}	0.1T
B_{pol}	0.005T
T_e	20eV
T_i	1eV
$n_e(0)$	10^{17} m^{-3}
β	$8\bullet10^{-4}$
$L_n = 1/n\ dn/dx$	0.04m

gas	**H**	**Ar**
ρe [m]	10^{-4}	10^{-4}
ρi [m]	10^{-3}	$6.5\bullet10^{-3}$
ρ_s [m]	$5.6\bullet10^{-3}$	0.0355
νei [s^{-1}]	$2.3\bullet10^4$	$2.3\bullet10^4$
$\omega_{*,e}/2\pi$ [s^{-1}]	$2\bullet10^4$	$2\bullet10^4$
$\omega_{*,i}/2\pi$ [s^{-1}]	$1\bullet10^3$	$1\bullet10^3$
$v_{th,e}$ [m/s]	$2\bullet10^6$	$2\bullet10^6$
$v_{th,i}$ [m/s]	$1\bullet10^4$	$1.5\bullet10^3$
v_{*e} [m/s]	$5\bullet10^3$	$5\bullet10^3$
$v_{gradB,e}$ [m/s]	500	500
c_s [m/s]	$5\bullet10^4$	$2.3.5\bullet10^3$
f_{ce} [Hz]	$2.8\bullet10^9$	$2.8\bullet10^9$
f_{ci} [Hz]	$1.5\bullet10^6$	$1.4\bullet10^5$
Collisional $\gamma/\omega_{*,e}$	0.02	0.2

Table 2.3.1 *TORPEX design parameters*

2.3.3 Status and Outlook

Most of the hardware development for the construction of TORPEX is being carried out in-house at the CRPP, maximising the use of components used in previous experiments. The main parts of the design, including the mechanical structure and the first diagnostic system, have now been completed. Two major components, the vacuum vessel and the poloidal field coils, are procured from external suppliers. Both items will be delivered to CRPP by the end of 2002, allowing the largest part of the installation, which has already started in terms of mechanical support and electrical infrastructure, to be completed by the end of this year. The first plasmas should be produced by the end of the year 2002 or during the first quarter of 2003.

2.4 Materials for fusion

The main objective of the CRPP Fusion Technology Materials (FTM) group is to investigate the effects of damage produced by radiation in a variety of materials, in particular candidate materials for structural components of the future fusion reactors but also pure metals and model alloys. This group is located at the Paul Scherrer Institute (PSI) in Villigen. It uses the high energy (590MeV) proton beam of the PSI accelerator, through the Proton Irradiation Experiment (PIREX) and the Swiss Spallation Neutron Source (SINQ) facilities, to simulate experimentally the effects of the 14MeV neutrons that are the product, together with energy and helium nuclei, of the envisaged fusion reactions between deuterium and tritium nuclei.

Key parameters for the first wall in fusion power reactors (fusion power: 3-4GW, operational mode: quasi-continuous) are the following: total neutron flux: 10–15x10^{14}n/cm^2.s; neutron wall loading: 2-3MW/m^2; integrated wall load: 10–15MWy/m^2 (100-150dpa in steels); surface heat load: 0.1-1MW/m^2; volume power density: 20-30MW/m^3; maximum irradiation temperature: ≥650°C; gas production rates: 10-15appmHe/dpa, 40-50appmH/dpa (in steels). Note that, in addition to irradiation by 14MeV neutrons, the first wall and breeding blanket components will be also exposed to plasma particles and electromagnetic radiation.

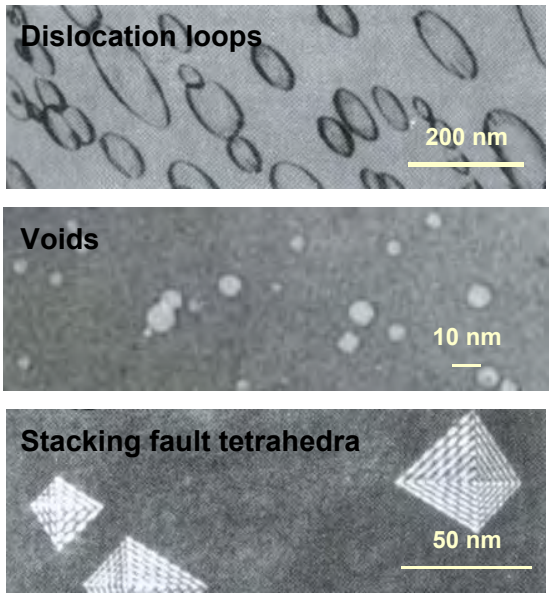

Fig. 2.4.1 *Examples of transmission electron microscopy images of irradiation-induced structure defects.*

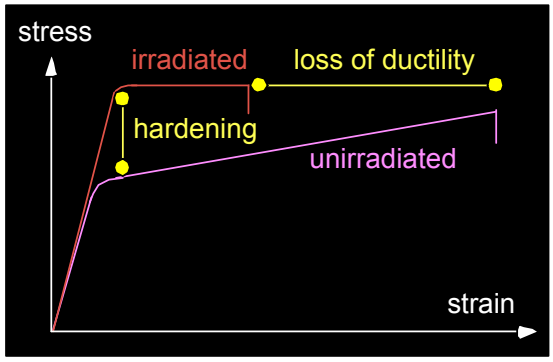

Fig. 2.4.2 *Schematic of irradiation-induced hardening and loss of ductility, measured in tensile tests.*

Like 14MeV neutrons, 590MeV protons produce atomic displacement cascades and transmutation nuclear reactions within the irradiated materials. From the point of view of materials science, atomic displacement cascades induce the formation of point structure defects, that are vacancies and interstitial atoms, while transmutation nuclear reactions yield the production of impurities, such as helium or hydrogen gas atoms. The final microstructure of the irradiated material results from reactions between these different defects. It is formed of defect clusters, dislocation loops, dislocation networks, precipitates, stacking fault tetrahedra (SFT's), voids and/or helium bubbles (see Fig. 2.4.1). This microstructure has an important effect on the physical and mechanical properties of the considered material. It can engender important hardening, loss of ductility and fracture toughness, as well as macroscopic swelling of the material (see Fig. 2.4.3). These effects are the main factors limiting the choice of candidate materials. The residual radioactivity of a large amount of exposed material is also a concern and will govern the handling methods, dictate the storage periods and the overall waste management and recycling scenarios. The development strategy that takes into account these limitations has led to the development of so-called low activation materials.

One of the main advantages of 590MeV protons is to generate a high He/dpa ratio that cannot be achieved with any other currently available irradiation source. While proton irradiations in PIREX produce about 130appmHe/dpa and 800appmH/dpa (in steels), irradiation in SINQ with a mixed spectrum of neutrons and protons produce about 50appmHe/dpa and 450appmH/dpa (in steels). However, in order to investigate the material property changes and degradation under different irradiation conditions, the FTM group is also involved in specific neutron irradiations performed in reactors in Denmark, the Netherlands, Hungary and Sweden.

Candidate structural materials for first wall and breeding-blanket applications include mainly reduced activation ferritic/martensitic (RAFM) steels, vanadium alloys and fibre reinforced SiC/SiC ceramic composites. Each alloy class exhibits some specific problems arising from radiation damage. For the time being, the most promising class of alloys is the RAFM steels for which the greatest technology maturity has been achieved, i.e. qualified fabrication routes, welding technology and general industrial experience are already available.

The design of materials with properties adequate for use in a radiation environment requires an understanding of the effects of irradiation on their physical and mechanical properties. The FTM group has been active in that field for several years within the framework of the European Fusion Development Agreement (EFDA) and collaborates with many research institutes and industries in Switzerland as well as abroad. The research activities of the FTM group include basic research on radiation damage in pure metals and alloys (see Section 2.4.1), characterization and development of low activation materials for fusion power reactor applications (see Sections 2.4.2 and 2.4.3) and characterisation of materials for ITER (see Sections 2.4.3 and 2.4.4). The scientific approach adopted by the FTM group towards understanding the fundamentals of radiation damage in metals and alloys is based on investigating the structure/mechanics relationships at different scalelengths (micro-, meso-, and macroscopical). A range of experimental and numerical tools is used to reach these objectives. The main experimental tools include mechanical testing on sub-sized and standard specimens, scanning and transmission electron microscopy (SEM, TEM) and small angle neutron scattering (SANS). The main numerical tools include molecular dynamics (MD), Monte-Carlo (MC) and dislocation dynamics (DD) simulations and finite element (FE) calculations.

2.4.1 Basic research on radiation damage

Microstructure and mechanical properties of proton irradiated Ni single crystals

Single crystals of high purity (99,999%) Ni have been irradiated to fluences up to 0.13dpa with 590MeV protons in the PIREX facility either at approximately 50°C or at 250°C and the initial dependence of the defect microstructure with dose has been established. The variation of the defect cluster number density on accumulated dose is plotted in Fig. 2.4.3. The densities measured after high temperature irradiation are lower than the ones measured after irradiation at 250°C, but comparable saturation values are obtained. Although the number of doses measured is still insufficient, the behaviour at low dose is linear (in a log-log representation), with comparables rates of accumulation at both temperatures. The size distribution, shown in Fig. 2.4.4, has a mean value of 1-2nm, which is independent of dose. Contrary to what has been observed in other fcc (face centered cubic) metals, such as Cu, both SFT's and dislocation loops are part of the defect population, the latter being about 20% of the total density.

As expected, the irradiation-induced microstructure results in radiation hardening and the measured values of the increase in critical resolved shear stress (CRSS) are plotted in Fig. 2.4.5, where $\Delta t=\tau_0^{irr}-\tau_0^{unirr}$ is the difference between the CRSS after and before irradiation. The linear increase is comparable to that found for other irradiated pure fcc materials. The hardening is controlled by the mean obstacle length $L=(Nd)^{1/2}$, N being the number density of dislocation loops and d their mean

diameter. A typical value of L=57nm was obtained from the TEM results in Figs 2.4.3 and 2.4.4. The main deformation mode is dislocation channelling, which produces a localised strain. The width of the channels is typically 100nm and their accumulation leads to a macroscopic strain localisation, as can be deduced from the results in Fig. 2.4.6. Although at the beginning of a tensile test all the strains are comparable (see Fig. 2.4.6b), a much larger strain develops at ΔL_3 (distance between points 8-10 in Fig. 2.4.6a).

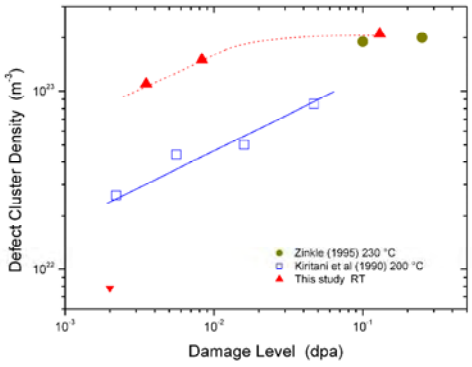

Fig. 2.4.3 *Defect cluster density versus dose. Red: irradiations at 50°C; blue: irradiations at 250°C.*

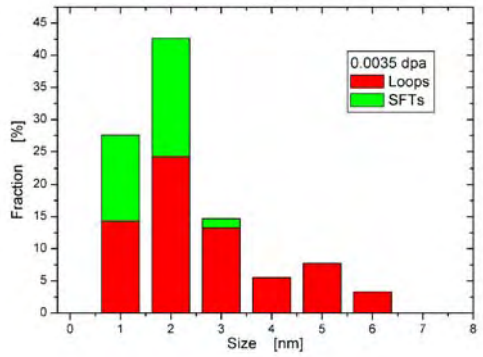

Fig. 2.4.4 *Defect size distribution.*

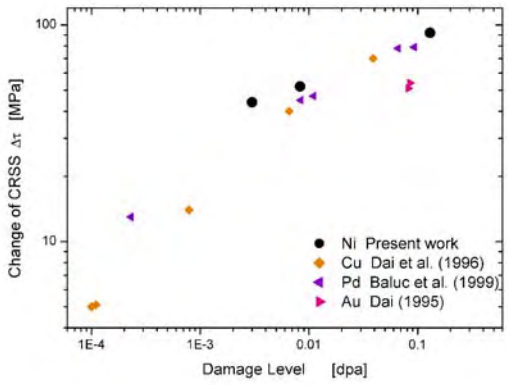

Fig. 2.4.5 *Change of CRSS versus dose*

Additional information on the behaviour of the irradiation-induced defect microstructure as obstacles to dislocation motion is shown in Fig. 2.4.7, where the values obtained for the activation volume (which represents roughly the area swept by the dislocation, as it goes through the obstacles, times the Burgers vector) are plotted as a function of shear strain. While the values for the unirradiated material diminish monotonically with increasing strain, those for the irradiated crystal go through a maximum and then decrease asymptotically to reach the values of the unirradiated ones. As the defects are destroyed as a result of their interaction with the moving dislocations. The mean distance between obstacles increases until it becomes comparable with that between forest dislocations, which are the expected obstacles to mobile dislocations in the unirradiated material.

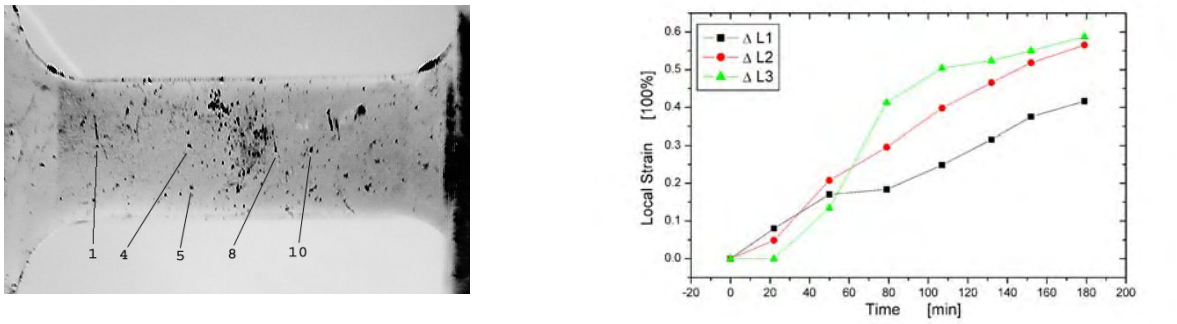

Fig. 2.4.6 *a) (Left) Gauge length of a tensile flat specimen; b) (Right) Local strain versus time. The distances between points 1-4, 4-8 and 8-10 on the left are labeled ΔL_1, ΔL_2 and ΔL_3, respectively, and the time scale is that of the tensile tests.*

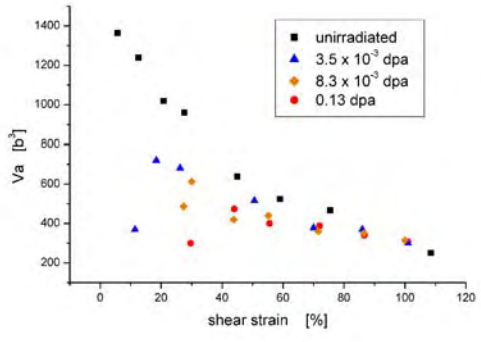

Fig. 2.4.7 *Activation volume versus shear strain.*

Modeling of irradiation of nanocrystalline Ni

The analysis of the cascade evolution in nanocrystalline (nc) materials, has been pursued with the molecular dynamics simulation of cascades produced by recoils of up to 30keV in nc Ni with grain sizes from 5 to 20nm. The investigation has been focused on the role of grain boundaries as sinks for the irradiation-induced defect structure. Earlier work had shown that during the thermal spike phase of the cascade evolution, linear collision sequences move the interstitials produced in the cascade towards the grain boundary, leaving vacancy clusters and SFT's inside the grain. Meanwhile, the grain boundaries themselves do not migrate. Further simulations and their analysis showed that replacement collision sequences (RCS) are the prime mechanism for the removal of self interstitial atoms (SIA). For instance, in a 10keV cascade that develops near a grain boundary, all the SIA leave the grain boundary by RCS even during the thermal spike phase. Furthermore, some grain boundaries seem to attract the SIA in a preferential way, a fact which is usually associated with the presence of free volume or dislocations in the configuration of the grain boundaries and which shows the way for future research on the strength of grain boundaries as sinks.

A small number of SIA left inside the grain after the thermal spike phase are removed from the grain via one dimensional diffusion. The few interstitials still left in the grain after annealing times >50ps have an immobile configuration. It has been shown that truncated SFT's are also left inside the grain during the damage

evolution. They become themselves sinks for SIA shrinking in size as a consequence of SIA absorption.

Heavy ion irradiation of pure NiAl single crystals

A recent analysis of TEM images of pure NiAl single crystals irradiated with 700keV Ni ions in the Tandem facility at the PSI to doses of 10^{14} and 10^{15}ion.cm^{-2} (approximately 0.15 and 1.5dpa, respectively) at room temperature is summarised in Table 2.4.1.

R_p and ΔR_p are the values of the range and the straggle, respectively, calculated using the TRIM code. They are compared with measured (R_p^m, ΔR_p^m) values obtained from TEM weak beam observations using the g(3.1g) imaging condition and the diffraction vector g=(200). It can be concluded from the comparison of calculated and measured range values that channeling (along the [100] direction of the single crystal) has taken place.

ϕ [cm^{-2}]	**G** [dpa]	$\mathbf{R_p}$ [nm]	$\mathbf{\Delta R_p}$ [nm]	$\mathbf{R_p^m}$ [nm]	$\mathbf{\Delta R_p^m}$ [nm]	ρ [10^{23} m^{-3}]
10^{14}	0.15	250	73	506	79	0.7
10^{15}	1.5	250	73	480	94	1.1

Table 2.4.1 *Measured and calculated range and straggle values.*

Furthermore, using the relation $2Dt=\Delta R_p^2(t)-\Delta R_p^2(0)$ measured at different irradiation times, t, values for the diffusion length $(6Dt)^{1/2}$ and the mixing efficiency D/K have been obtained, summarised in Table 2.4.2.

D [nm^2/s]	$\mathbf{(6Dt)^{1/2}}$ [nm]	**D/K** [nm^2/dpa]
0.67	88	957

Table 2.4.2 *Diffusion length and mixing efficiency.*

NiAl has a B2 structure, for which the density of defects is high when compared to that found in other bcc (body centred cubic) crystals at equivalent dose. The reason for this difference can now be explained: channelling prompts a higher density of defects within the straggle band.

Modeling of the damage accumulation in Fe

In order to understand the relatively low defect accumulation rate in RAFM steels, detail of the irradiation-induced dislocation loop structure is needed. MD simulations have been performed in order to clarify the fact that <100>-type dislocation loops are observed at high doses while small <111>-type dislocation loops are observed at low doses. This work is being performed in collaboration with LLNL, USA. Based on extensive MD simulations of <111>–<111> and <100>–<111> loop interactions, a comprehensive mechanism for the nucleation and growth of TEM visible <100> dislocation loops is proposed. This mechanism is consistent with both experimental observations and current understanding of interstitial cluster formation, diffusion and growth from atomistic simulations. SIA produced in collision cascades initially aggregate as small <111> clusters. These clusters either

rapidly migrate to system sinks or interact with each other. <100> nuclei form through the direct interaction of <111> clusters of comparable size via the reaction:

$$1/2\ [111] + 1/2\ [1\text{-}1\text{-}1] \rightarrow [100]$$

Dislocation loops interact according to the following reactions:

$$1/2\ [111] + 1/2\ [00\text{-}1] \rightarrow 1/2\ [110]$$
$$1/2\ [110] + 1/2\ [1\text{-}10] \rightarrow 1/2\ [100]$$

which results in the ultimate growth of a <100>{110} junction until the whole loop is transformed. The resulting loops are metastable with respect to the <111> orientation, but the energy differences can be quite small and the activation barrier to re-orient along <111> quite large.

With increasing size, i.e. SIA number above 68, the <100>{110} loops re-arrange into {100} habit planes. In this configuration, the <100> loops are metastable and practically immobile, allowing the absorption of other small <111> clusters via a direct-rotation mechanism (reaction: <100> + 2 1/2 <111>) -> <211 -> <100>) that allows <100>-loop growth up to TEM observable sizes.

Conventional TEM (Fig. 2.4.8) and weak beam images for a number of loops with different Burgers vectors, habit planes and sizes, have been generated using the g(4.1g) imaging condition and diffraction vector g = (200). Useful information about the induced strain field can be extracted from the conventional TEM simulated images in each case.

The observed strain field of the <111> loops remains mostly confined to the loop glide prism whereas one of the <100> clusters extends beyond the limits of the prism, with the conventional TEM image conditions chosen. Loop shape does not have any significant impact on the simulated images, which all exhibit the well known, double-bean contrast of SIA loops.

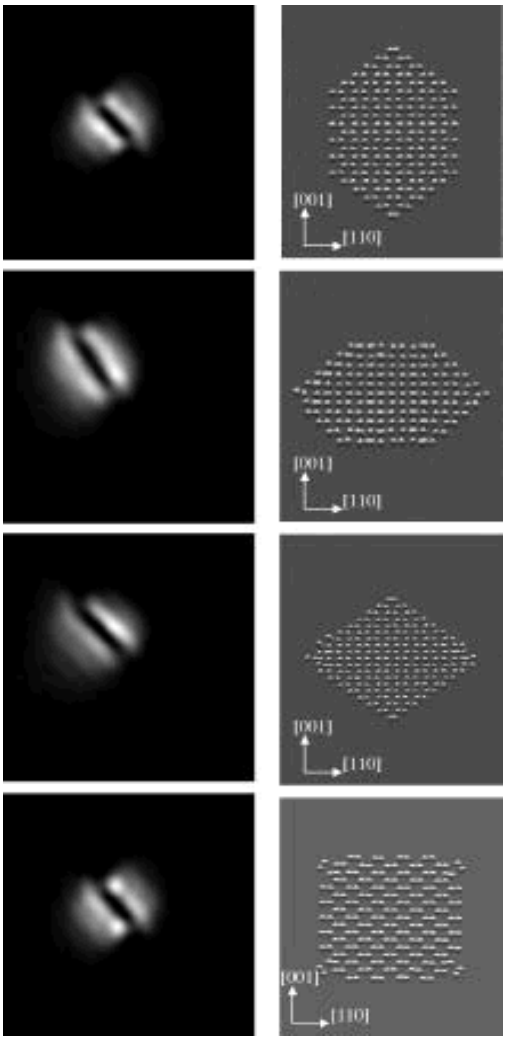

Fig. 2.4.8 *Conventional TEM simulated images (left) of <100>{110} loops with different sizes and shapes (right); hexagonal <111>{110}, rhombic <100>{110} and square <100>{100} loops. The atomic configurations on the right are viewed along the [110] direction*

Finally, the agreement between simulated images and experimental micrographs obtained for an irradiated Fe-9Cr specimen was found the excellent (Fig. 2.4.9), which validates the use of that particular technique to identify the nature of interstitial clusters in irradiated RAFM steels.

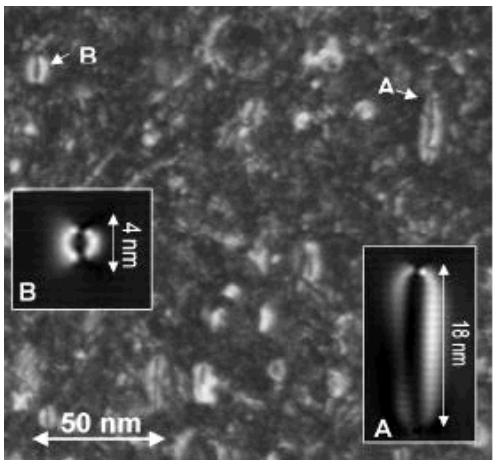

Fig. 2.4.9 *Experimental TEM weak beam image of a Fe-9Cr specimen irradiated with neutrons to 8.8dpa at 302°C. A and B refer to interstitial loops with the [100] Burgers vector and lying in {100} planes. The two insets represent conventional TEM simulated images of (A) a 18nm, rectangular [100] loop and (B) a 4nm, hexagonal [100] loop. The agreement with the experimental images in both contrast and shape is excellent.*

2.4.2 Reduced activation ferritic/martensitic steels

The RAFM steels that are currently under extensive investigation include two large casts of F82H and EUROFER 97 and laboratory casts of, among others, the series of OPTIMAX alloys. The F82H steel was produced in Japan and is investigated as part of the IEA (International Energy Agency) Fusion Materials International Collaboration Program on ferritic/martensitic steels. The F82H steel contains 7.65wt.%Cr, 2wt.%W, Mn, Mo, V, Ta, Si and C below 1wt.% in sum total, and Fe for the balance. The EUROFER 97 steel was developed in Europe within the EFDA Program. Its chemical composition is the following: 8.93wt.%Cr, 1.07wt.%W, Mn, Mo, V, Ta, Si and Cr below 1wt.% in sum total, and Fe for the balance. The RAFM steels known as OPTIMAX steels were developed by the FTM group. They contain about 9wt.%Cr and their detailed composition results from optimisation of previous 12wt.%Cr steels, as MANET for instance, where Ni, Mo and Nb have been replaced by the W, V and Ta low activation elements.

In addition to their favorable cost, availability and engineering data base, the RAFM steels have proven to be a good alternative to austenitic strainless steels for their lower activation, lower damage accumulation and improved thermal properties. At temperatures above 300°C, the RAFM steels are expected to exhibit good resistance to swelling (1vol.% per 100dpa as compared with 1vol.% per 10dpa in stainless steels). However, the RAFM steels exhibit a pronounced drop in tensile strength at about 500°C, a strong reduction in creep strength at temperatures above 600°C and a significant stress softening in low cycle fatigue tests. In addition, the RAFM steels have a bcc structure and, like other materials of this type, they exhibit a ductile-to-brittle transition temperature (DBTT). In the unirradiated state, the DBTT of RAFM steels lies well below room temperature, that is between -80 and -90°C for the F82H, OPTIMAX A and EUROFER 97 alloys.

Effects of irradiation

Irradiation at temperatures below 300-350°C leads to strong hardening and loss of ductility, i.e. to embrittlement. TEM observations showed that the strong radiation hardening shown up for RAFM steels at irradiation temperatures below 300-350°C seems to correlate with the irradiation-induced dislocation loop microstructure (size and density evolution as a function of dose, see Fig. 2.4.10) rather than with the amount of helium produced. The DBTT also increases drastically, for instance up to -5°C for OPTIMAX A neutron-irradiated at 250°C to 2dpa. However, this fast increase is expected to saturate at some intermediate dose. Note that irradiation with fusion neutrons at temperatures below 300°C to 100-150dpa is expected to yield a DBTT well above room temperature. At higher irradiation temperatures (typically above 400°C), the DBTT is not expected to increase significantly. The effects of high He/dpa ratio still need to be investigated in detail. A high density of small cavities (about 1nm), which could be either voids of helium bubbles, has been recently shown up using TEM (see Fig. 2.4.11), SANS and positron annihilation measurements in specimens of the F82H steel that were irradiated in SINQ at about 300°C to a dose of 10-12dpa. The impact of such a distribution of small cavities on the fracture properties of the F82H steel is under investigation. Preliminary mechanical test results seem to indicate that the amount of helium produced correlate well with the fracture behaviour of RAFM steels, i.e. a larger amount of helium yields a stronger rate of increase in the DBTT, at least at irradiation

temperatures below 350°C. It is thought that such a high density of small cavities could also make a further contribution to the overall hardening.

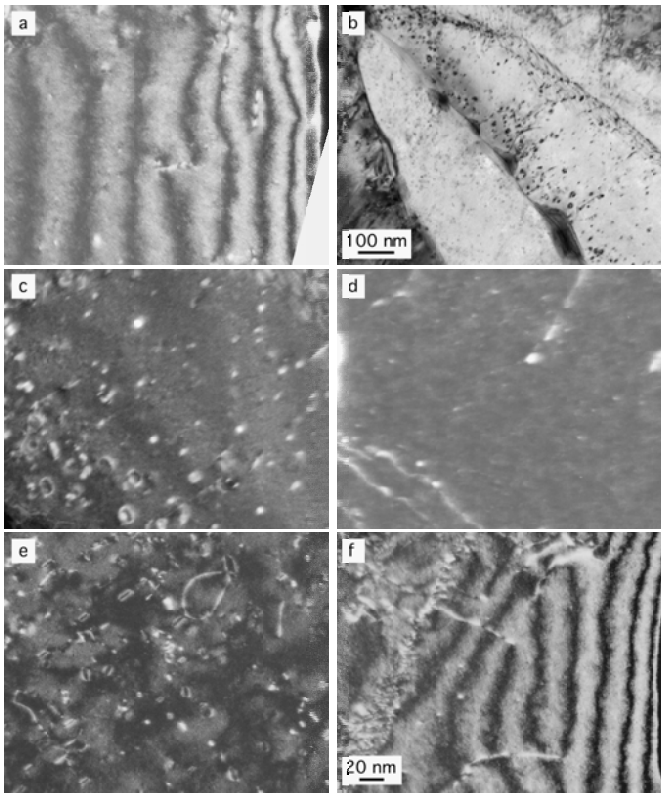

Fig. 2.4.10 *TEM images of irradiation-induced dislocation loops of interstitial type in F82H, for various imaging and irradiation conditions: (a) weak beam image, fission neutrons, 0.7dpa, 250°C; (b) bright field image, fission neutrons, 2.5dpa, 250°C; (c) weak beam image, fission neutrons, 2.5dpa, 250°C; (d) weak beam image, 590MeV protons, 1.7dpa, 40°C; (e) weak beam image, fission neutrons, 10dpa, 310°C; (f) weak beam image, 590MeV protons (0.7dpa) and fission neutrons (0.7dpa), 250°C.*

In summary, the temperature window of use for the RAFM steels is presently approximately 350-500°C, the lower value being limited by irradiation-induced embrittlement effects and the upper limit by a strong reduction in mechanical strength. To decrease the lower temperature limit involves decreasing the DBTT before irradiation. If one may expect to lower the DBTT value by acting upon the composition and/or the impurity level, it seems unrealistic to obtain a DBTT below room temperature after neutron irradiation at temperatures below 300°C to a dose of about 100-150 dpa. One way to get round this problem would consist of maintaining the irradiation temperature above 350°C (with regard to the effect of helium in the lower temperature regime) and/or to regularly anneal the first wall of the fusion reactor at high temperature (but lower than the tempering temperature) to recover the DBTT obtained in unirradiated conditions. On the other hand, it is expected that adding a fine dispersion of strong particles to the RAFM steels (e.g. oxide dispersion strengthened steels) could contribute to increase the upper temperature limit.

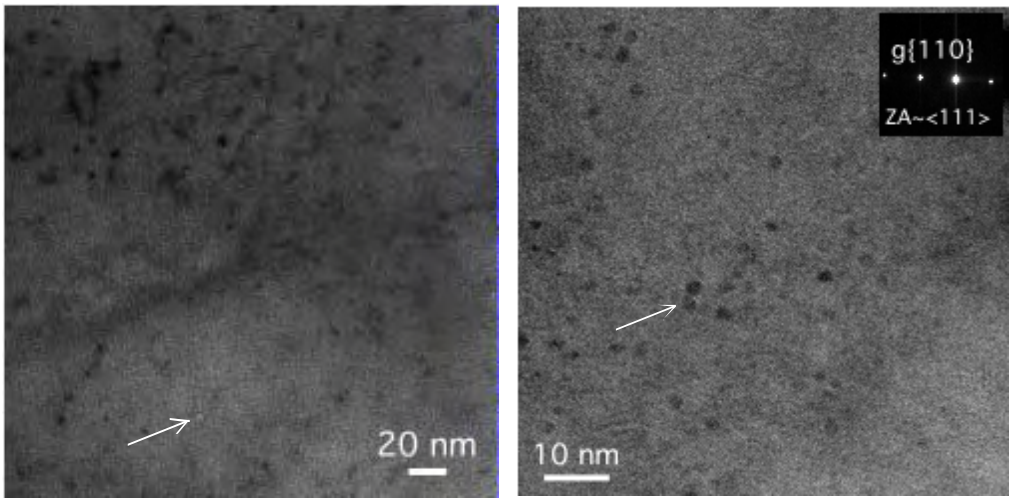

Fig. 2.4.11 *TEM bright field images of irradiation-induced cavities in F82H irradiated with (left) fission neutrons (8.8dpa, 302°C, High Flux Reactor in Petten) and (right) a mixed spectrum of protons and neutrons (10dpa, 300°C, SINQ). On the left the few visible cavities appear in white (overfocused) and on the right cavities appear in black (underfocused).*

In beam fatigue testing

A series of specimens has been *in beam* fatigue tested in the PIREX facility, at 300°C. The dose at the end of life was between 0.2 and 0.3dpa. Four of them were loaded using a symmetrical strain signal (R=-1) under continuous fatigue. The strain rate was varied in order to analyse frequency effects. One specimen has been additionally loaded by a tensile hold of two minutes at the maximum strain. These two conditions have been repeated using a standard testing machine and specimens with the same gauge geometry. Another specimen was irradiated in the *in beam* machine but without simultaneous deformation and the fatigue test was carried out after the irradiation. The dose was the same as in the corresponding *in beam* test, 0.3dpa. As the main result, the radiation-induced hardening was absent under *in beam* loading; it only appeared in the specimens tested at high frequency at their end of life but in a reduced amount. Despite the absence of radiation hardening, it was found that the fatigue life was shorter for the *in beam* specimens, the shortest life being found for the specimen loaded with tensile holds.

SEM analyses have shown that the mechanism of crack initiation is the same for all conditions, i.e. the cracks are generated at the lath boundaries. A systematic gas analysis has been conducted in the post mortem specimens and it was found that some amount of hydrogen (resulting from spallation reactions) is retained in the specimens, despite the elevated testing temperature. Therefore it is believed that the shortage of the fatigue life of the F82H steel is probably due to its high hydrogen susceptibility. The *in beam* testing of the F82H material is now completed. A similar simplified program will be conducted on the EUROFER 97 steel to confirm the above results.

Fracture toughness characterisation by fracture reconstruction and fractography

The mechanical testing was carried out on a modified vanadium-niobium-stabilised RAFM steel. The alloy is close to the ASTM designation T91 (Fe-8.26Cr-0.1C-0.95Mo-0.2V-0.075Nb). It was normalised for 2.5 hours at 1070°C and tempered for 4.75 hours at 765°C. The fracture tests were carried out on fatigue pre-cracked, 20% side-grooved, small compact tension specimens, with crack length (a) to specimen width (W) ratios of about a/W=0.5 and a specimen thickness (B) to width ratio of B/W=0.5 (B=5.0mm (0.2T CT)). Static tests, at a ram speed of about 4μm/s, were performed under displacement control using a servo-hydraulic load frame at temperatures ranging from -196 to –85°C. Temperature control was provided by either a liquid-nitrogen-cooled alcohol bath or a regulated N_2 gas environment. Test and analysis procedures to determine K_{JC} or K_Q, representing valid small scale yielding elastic-plastic toughness and large scale yielding toughness, respectively, were based on the ASTM Standard Practices E813 and E1921-97 which take into account the specimen geometry.

The fraction reconstruction technique was used to determine the sequence of events leading to fracture. It uses the topographic maps of two conjugate fracture surfaces. The topographic maps have been obtained using a confocal scanning laser microscope 1LM21. The optics of the microscope are configured to provide a very shallow depth of focus so that only the points on the focal plane can be imaged. In order to determine the height of a given point on the surface, the specimen is moved up and down at a fixed focal length. The maximum intensity of a pixel of the surface is then recorded and corresponds to the height of that specific point of the surface. In order to get a precise topographic map over a significant fracture area (several mm^2), it is necessary to assemble smaller confocal fields, whose characteristic dimensions are about 200μm x 300μm. A computer-controlled stage is used to move the specimen horizontally in order to acquire the series of confocal fields in sequence. The confocal fields are taken in such a way that they overlap over the four adjacent ones on a strip of about 10μm so that assembling can be made accurately. Finally, the height of a given point of the surface is represented by a grey level ranging between 0 and 255. The resolution in the horizontal plane is about 0.3μm while the vertical resolution between two gray levels depends evidently on the height difference between the lowest and highest points of the surface area investigated. For the specimens studied here, it was possible to build the topographic maps with a vertical resolution of the order of 1μm. The last step before running the fraction reconstruction itself consists of computational overlapping and matching the conjugate surfaces. The difference between both surfaces is calculated and set to zero on the pre-cracked area. Finally, the surfaces are separated by an amount corresponding to the crack tip opening displacement. At a given crack tip displacement, spots develop on the surfaces where the profiles cross each other. These black spots correspond to material separation areas. So, the nucleation and evolution of the damage preceding the macro-crack initiation can be followed and the critical crack tip opening displacement determined.

The analysis programs were lifted from the original codes developed at the University of California in Santa Barbara. However, they had to be adapted to our own acquisition equipment. Furthermore, modifications of the code were necessary to recompile all the libraries and routines to make them compatible with the computer platform we are using.

The 0.2T CT fracture test results obtained for the T91 steel are shown in Fig. 2.4.12 where the fracture toughness-temperature curve is presented. It is an important result that all the specimens failed by a quasi-cleavage fracture mode. The data plotted in Fig. 2.4.12 have to be interpreted as an effective static fracture toughness, K_e, which intrinsically depends on the metallurgical state, loading rate and specimen size and geometry factors. Only for restricted conditions (plane strain, mode I of loading, and much smaller plastic zone than the characteristic specimen dimensions), can K_e be considered as a material property. For the 0.2T CT geometry used here, the K_e data are reasonably valid up to about 100MPa.m$^{1/2}$ where in-plane constraint is maintained. Constraint loss is primarily associated with plasticity encompassing a large fraction of the uncracked ligament. The few data points lying above 200MPa.m$^{1/2}$ underwent extensive loss of constraint, even out-of-plane constraint loss was shown up by optical microscopy observations of the specimens whose fracture toughness is higher than 200MPa.m$^{1/2}$. The issues of loss of constraint can be mitigated by assessing local properties at the crack tip that do not depend on the deformation level. This can be done by locally evaluating the stress/strain fields by finite element analysis to define a critical condition for cleavage. Furthermore, it is also important in this modelling to understand how the macro-crack responsible for the failure of the specimen is initiated and evolves as a function of the local stress/strain field. In order to get some insight into that process, the technique of fraction reconstruction was applied and two analyses are given in detail below.

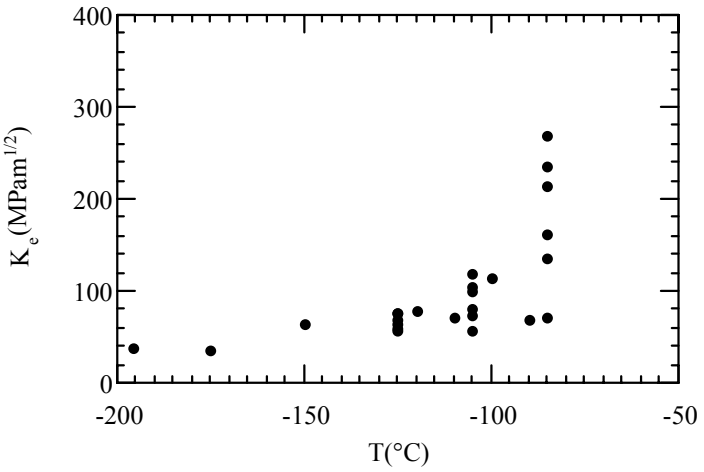

Fig. 2.4.12 *Fracture toughness–temperature curve for the T91 steel, measured on 0.2T CT specimens.*

Two different specimens were selected for fraction reconstruction: one, tested at T=–105°C, which exhibited an almost completely elastic loading and failed at 118MPa.m$^{1/2}$ and one at T=-85°C whose loading curve was elastic-plastic and failed at 270MPa.m$^{1/2}$ after having undergone a significant loss of constraint. The corresponding load-displacement curves are shown in Fig. 2.4.13. The fraction reconstruction sequences are given in Figs 2.4.14 and 2.4.15. The δ-value indicated below each field is the crack tip opening displacement. The black areas correspond to the spots where the material is separated while the white ones refer to zones where the material is still intact. In Fig. 2.4.14, it can be seen that the crack does not propagate and that the initial damage appears for δ equal to about 20μm. The damage zone size increases with δ and it is very important to emphasise that the

damage initiates ahead of the crack tip. This observation is confirmed by the images corresponding to δ=28μm and 32μm where a white strip separates the crack tip from the damage process zone in which micro-cracks nucleate. Increasing δ above 36μm leads to a full separation between the two surfaces. Hence, the critical opening displacement for that specific specimen is of the order of 40μm. Interestingly, the same qualitative sequence of events occurs for the tougher specimen. In this second case, however, the damage initiates between δ=220μm and 230μm. It has to be noted that, in the latter case, an important crack blunting is taking place which results in an overall crack tip advance of about 200μm. Above δ=230μm the crack continues to blunt and the damage zone containing the bridged micro-cracks increases until all the micro-cracks coalesce into a large macroscopic and unstable crack. This happens for a critical crack tip opening displacement of about 260μm.

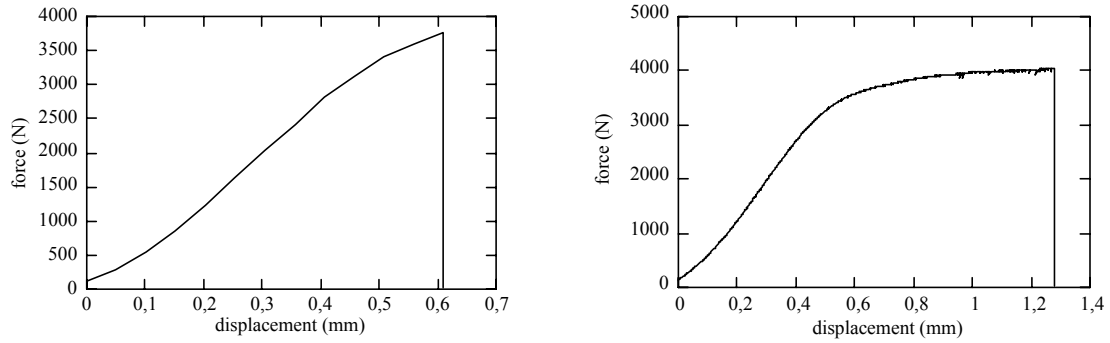

Fig. 2.4.13 *Load-displacement curves, 0.2T CT specimens tested at (left) T=–105°C; (right) T=-85°C.*

Values of the critical opening displacements obtained from fracture reconstruction can be used to recalculate the fracture toughness by using the following relation:

$$K_\delta = (2E'\delta^*_c\sigma_y)^{1/2}$$

where E' is the plane-strain Young's modulus, δ^*_c is the critical crack tip opening displacement and σ_y is the yield stress. Good agreement between the values of K_δ and those of K_e (determined from the mechanical tests) was found, summarised in Table 2.4.3.

T = - 105°C	δ_c^* = 40μm	K_δ = 106MPa.m$^{1/2}$	K_e = 118MPa.m$^{1/2}$
T = - 85°C	δ_c^* = 260μm	K_δ = 264 MPa m$^{1/2}$	K_e = 270MPa.m$^{1/2}$

Table 2.4.3 *Fracture toughness as determined from the critical opening displacements obtained by fracture reconstruction, K_δ, or from the mechanical tests, K_e.*

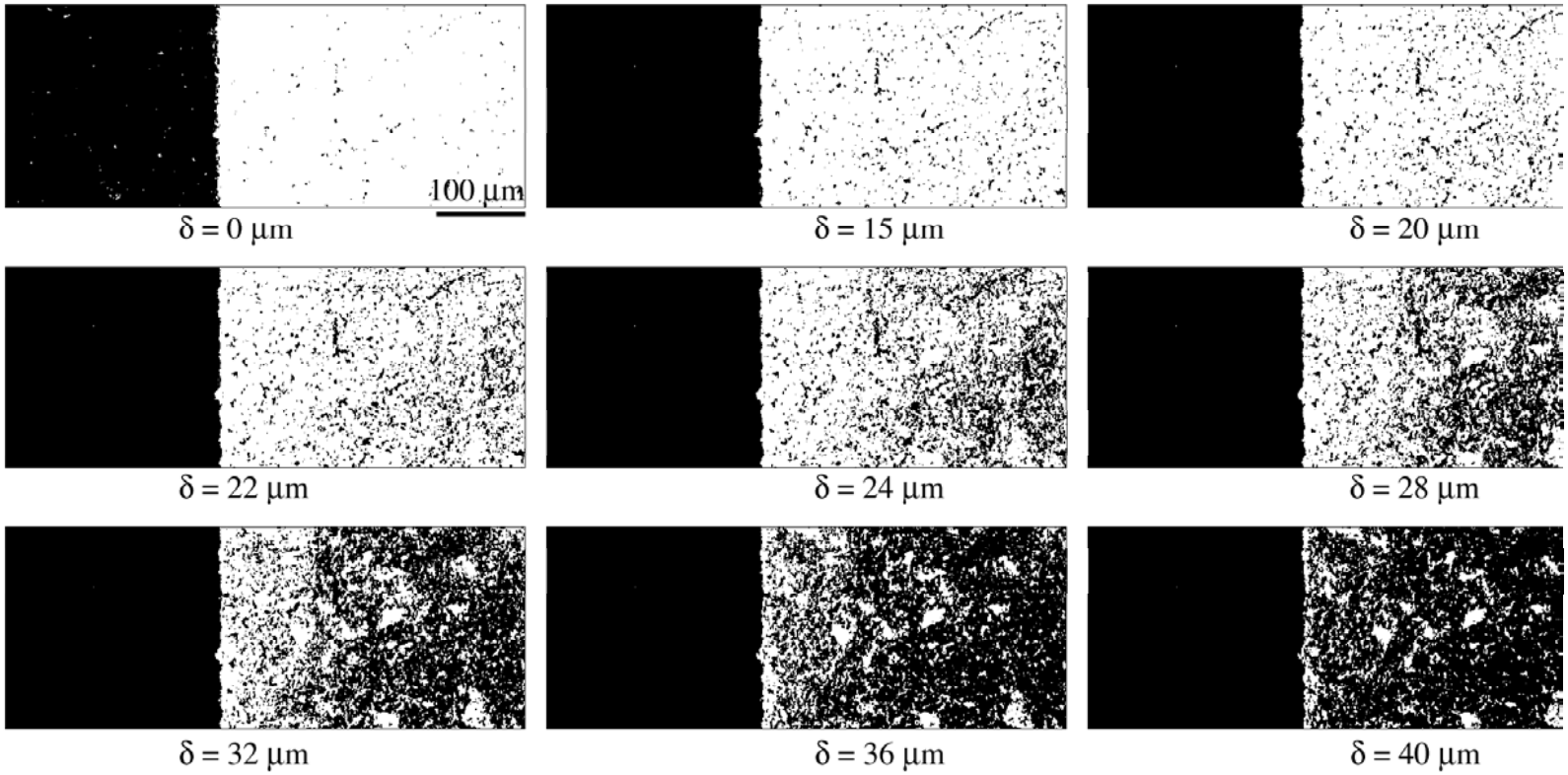

Fig. 2.4.14 *Example of fracture reconstruction; 0.2T CT specimen of T91 at T=-105°C exhibiting a limited amount of plastic deformation before failure.*

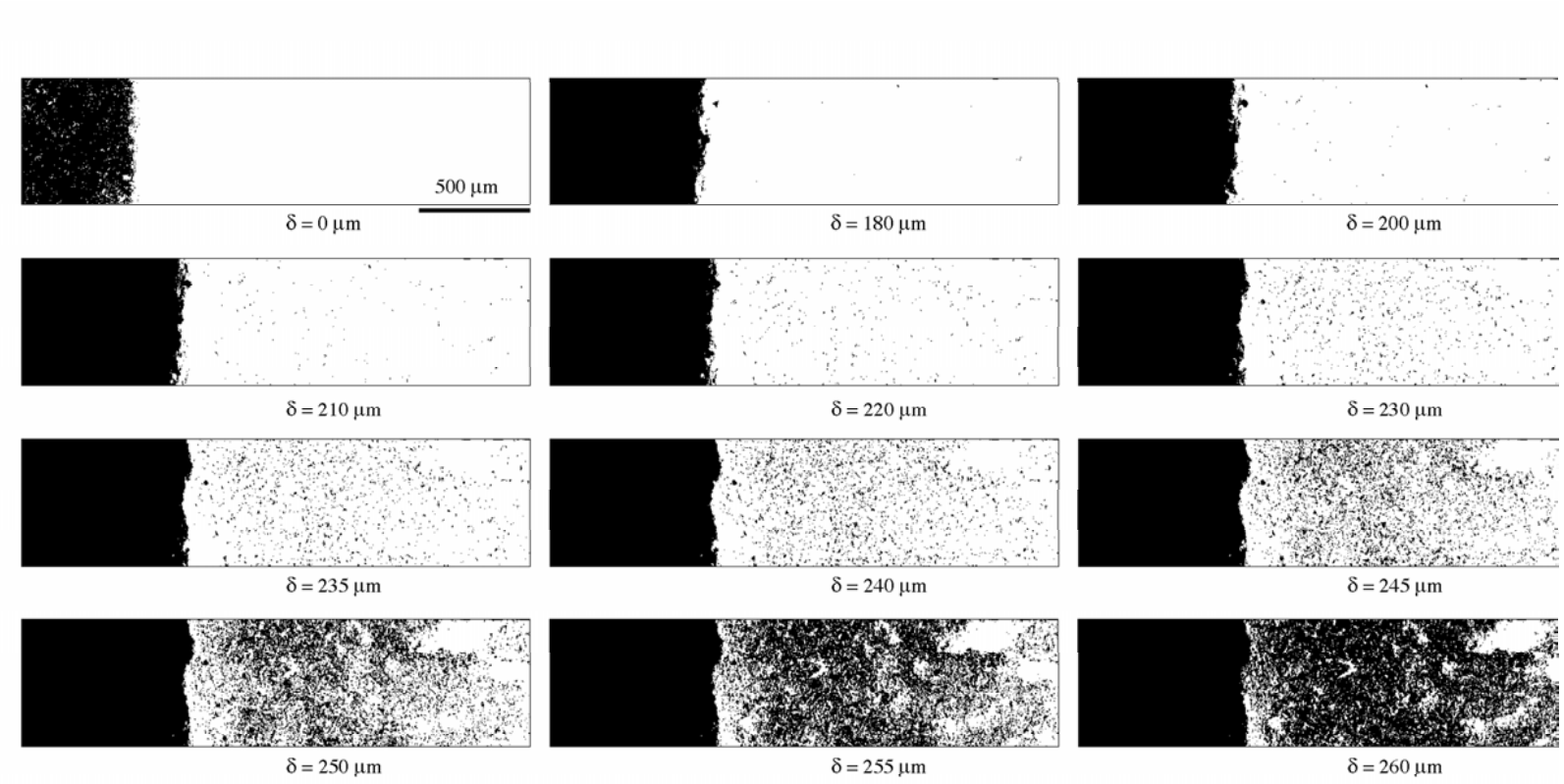

Fig. 2.4.15 *Example of fracture reconstruction; 0.2T CT specimen of T91 at T = -85°C exhibiting a large amount of plastic deformation before failure.*

Finally, in Fig. 2.4.16, we present an SEM image of the fracture surface of the specimen tested at T=-85°C in conjunction with the corresponding topographic map obtained by confocal microscopy. A selected area of the SEM image is compared with the topographic map whose horizontal resolution is 0.34μm/pixel and vertical resolution is 1.06μm by grey level. A careful observation of both images reveals a very good one-to-one correspondence between them. It is important to emphasize that SEM images and topographic maps carry different but complementary information. On the one hand, from the SEM image in Fig. 2.4.16, one can conclude that in that specific specimen which underwent a huge amount of constraint loss, the fracture mode remained unstable and was quasi-cleavage. On the other hand, from the topographic map, it is possible to extract profile lines across the fracture surface. The different heights between the cleavage facets can be precisely measured and the amount of ductile tearing between them determined.

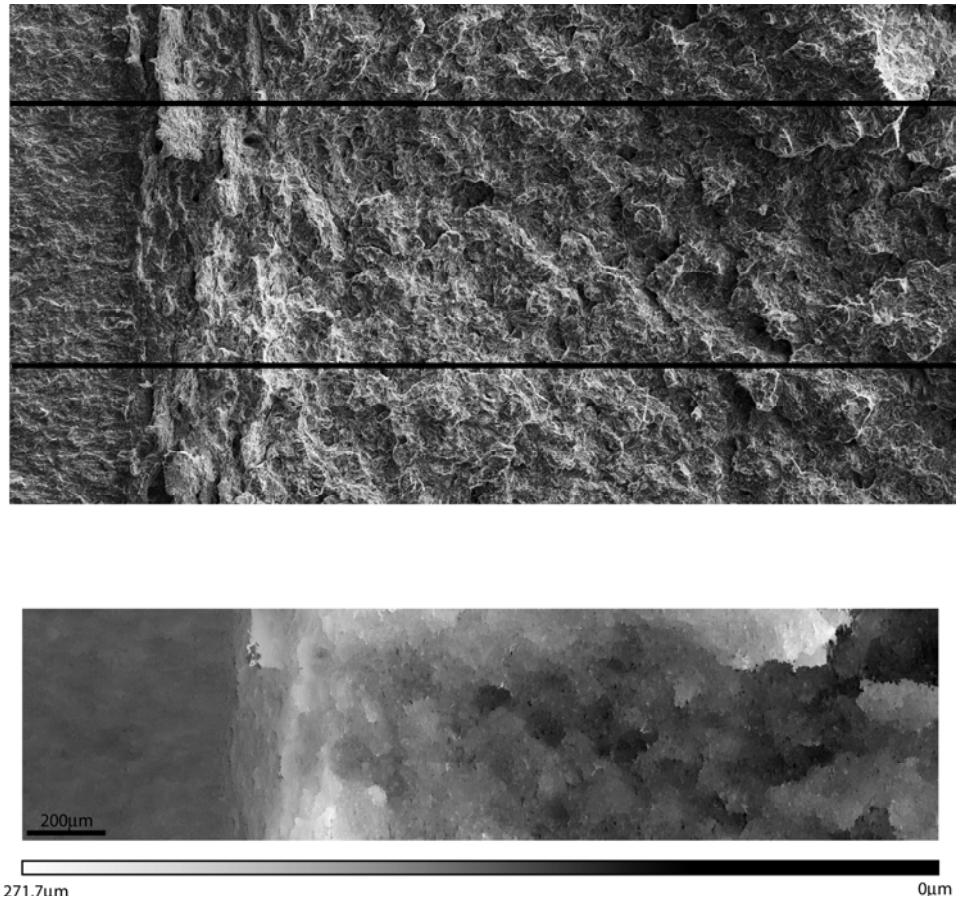

Fig. 2.4.16 *SEM image (upper part) and topographic map (bottom part) of a 02T CT specimen of the T91 steel tested at T=-85°C. The black frame in the SEM image relates to the topographic map below.*

In summary, the technique of fracture reconstruction was used to understand the effects of specimen size/geometry on fracture toughness better. A scanning laser confocal microscope 1LM21, with a computer controlled stage, was used to acquire a series of small confocal fields from two conjugate fracture surfaces, which are later assembled into large fracture areas. The topography of the fracture surfaces is represented by 256 gray levels. After a careful computational alignment of both surfaces, they are separated by a given displacement reflecting the crack tip

opening displacement. Following the overlapping of the surfaces, it is possible to determine the evolution of damage and the nucleation of micro-cracks as a function of the crack tip opening. Two examples were given for 0.2T CT specimens of the T91 RAFM steel; one with a level of in-plane constraint well maintained and another one exhibiting a huge amount of constraint loss. It was possible to localize at which crack tip opening the damage ahead of the crack tip appeared and to relate the critical opening to fracture toughness. Good agreement was found with the fracture toughness data resulting from the mechanical tests. The information obtained from the fraction reconstruction is of primary importance for the development of a local criterion for cleavage and for the modelling of the fracture toughness-temperature curve.

2.4.3 Titanium-base alloys

Titanium alloys exhibit a number of properties that make them attractive candidates as structural materials for fusion reactors, including: high strength-to-weight ratio, plasticity, good fatigue and creep rupture properties, small modulus of elasticity, high electrical resistivity, heat capacity, small coefficient of thermal expansion, low long-term (> 10 years after shutdown) residual radioactivity (after V and Cr, Ti exhibits the fastest decay rate), compatibility with coolants such as lithium, helium and water, corrosion resistance, high workability and good weldability, commercial availability with established mine and mill capacity, together with good resistance to void swelling under a wide variety of irradiation conditions. Titanium alloys are basically low temperature alloys, however, having a maximum working temperature in the neighborhood of 500°C. In addition, titanium and its alloys have a high chemical affinity with hydrogen which, in the fusion environment, leads to hydrogen embrittlement and tritium inventory. Therefore, in order to make practical use of titanium alloys for increased fusion applications, hydrogen barrier coatings are required to prevent hydrogen intake and subsequent hydrogen isotope induced deterioration of the material.

Titanium alloys can be divided into three major classes determined by phase constituency, that are referred to as α, β and α/β, where the α phase is hcp (hexagonal compact) and the β phase is bcc (body centered cubic). The alloying elements used in the titanium system can be divided into two classes upon the basis of which phase the element stabilizes. The α stabilizers are Al, Zr and Sn, while the β stabilizers are V, Cr, Mn, Fe, Co, Ni and Mo.

Titanium-base alloys for ITER

An assessment of the tensile, fatigue and fracture toughness performance under irradiation of two titanium alloys for the flexible connectors attaching the ITER–FEAT blanket modules to the vacuum vessel is under progress. The two candidate alloys considered are: a classical α/β alloy, Ti-6Al-4V, and an α alloy, Ti-5Al-2.5Sn. Tensile and low cycle fatigue mechanical tests revealed that the resistance to radiation damage at 350°C is superior for the α alloy compared with the more complex α/β alloy. The α/β alloy has been found to be unstable when irradiated at 350°C. A fine precipitate distribution is generated within the α grains, which results in reduced ductility and strong hardening. Hydrogen has been loaded in mini-Charpy specimens of both materials, using a Sievert's apparatus, to amounts ranging between 0 and 400ppm (0.04wt%). The specimens were then irradiated in

the DR3 reactor at Risö, Denmark, to 0.12dpa at 60°C and 350°C. Small fatigue cracks have been introduced in the specimens after irradiation. The specimens were tested in a three-point bend fixture, in order to determine the crack initiation fracture toughness. The effect of hydrogen was found similar in both unirradiated materials. At room temperature, the fracture toughness diminishes with increasing hydrogen content, from about 120 to 60kJ/m^2. At 400ppmH, the fracture toughness is slightly higher for the α/β alloy, but at 150ppm it is lower, as compared to the α alloy. At 350°C, there is no dependence on the hydrogen content and the α/β alloy shows fracture toughness values around 120kJ/m^2, whereas the α alloy exhibits values around 140kJ/m^2.

After irradiation to 0.12dpa, there is a strong reduction in fracture toughness for the α/β alloy with values around 20-40kJ/m^2, but the behaviour of the α alloy is much better, especially at 350°C with fracture toughness values still as high as 80J/m^2. Despite the better mechanical resistance shown by the α alloy, the ITER team has decided to manufacture the connectors using the α/β alloy. The main reasons are that this alloy is already widely available from the industry and that it fulfills the ITER requirements.

Development of new titanium-base alloys

Our efforts concentrate on the development of new α titanium alloys. Having chosen the promising alloy Ti-5Al-2.5Sn as a reference, a series of five alloys has been prepared in which first the substitution of Al and Sn has been tested and also where an attempt was made to vary the associated impurities (O, N, Fe) to detect their influence on the properties. Al has been substituted with Zr, to create a Ti-5Zr-2.5Sn alloy, then Sn was removed and two binary alloys were developed, containing 5wt.%Zr and 22wt.%Zr, respectively. The Charpy impact properties of these new alloys have been determined between -150°C and 350°C. It appears that the alloys can be divided in two categories, depending mainly on their composition and impurity level: some alloys show an increased impact energy as temperature decreases, while others show the reverse behaviour, namely a decreasing impact energy with decreasing temperature.

2.4.4 Other materials

The object of this additional research is to investigate the mechanical behaviour of the CuCrZr alloy in the condition of *in beam* fatigue. The fatigue behaviour of this alloy has been previously extensively studied within the framework of the ITER technology program. The fatigue properties of CuCrZr are already known in the unirradiated and irradiated conditions. Since this alloy will be placed in the first wall of ITER, it will be subjected to *in situ* fatigue, due to the pulsed operation of ITER. It is therefore necessary to investigate the behaviour of CuCrZr when fatigue deformation is imposed simultaneously with irradiation. Fatigue specimens have been manufactured and extensometers have been prepared. A reference fatigue test has been performed, using the *in situ* machine without proton beam. This test has then been compared with a test performed under *in beam* conditions, using the same mechanical parameters. Two interesting results have been obtained: as in the case of RAFM steels, there is no radiation-induced hardening, even after about 0.4dpa; on the contrary proton irradiation yields cyclic softening. More interesting

for ITER, the fatigue life is improved under *in beam* fatigue conditions. The results can be understood in terms of better plasticity and dislocation flow.

2.5 Superconductivity

Research and Development on cable-in-conduit superconductors for fusion magnets is the core of our activity in 2002. Conductor development focuses on an improved layout for Nb_3Sn TF coils: a new conductor sample is in preparation and will be tested in 2003. The test activity in the large SULTAN installation in 2002 included five NbTi conductors with parametric variations, developed and manufactured in 2001, as well as the test of a full size poloidal field conductor prepared under a joint effort by CEA and ENEA.

The results of the critical current test on individual Nb_3Sn strands, extracted from cable-in-conduit samples tested in SULTAN in 2001, opened a new, lively discussion on the rules of performance extrapolation from single strands to large cables.

In the framework of a collaboration with Forschungszentrum Karlsruhe, the design of large, 70kA High Temperature Superconductor Current Leads was carried out and the preparation of a prototype, to be tested in Karlsruhe in 2003, was started.

2.5.1 NbTi Conductor Optimisation

An R&D program on NbTi cable-in-conduit superconductors started in 2001 at the CRPP with the aim of selecting the design parameters for the ITER poloidal field conductors. Five, medium size, NbTi cable-in-conduit samples with parametric variations has been designed and procured in 2001 to investigate the role of strand coating, subcable wraps and copper segregation on the overall performance.

Three types of NbTi strand have been procured from Alstom. The table below summarises the strand characteristics

Strand Identification	*Strand Diameter*	*Cu:non-Cu*	*Twist pitch*	*Total Length*
ZR500191	0.87mm	≈ 1.12	7mm	≈ 2 180 m
ZR500192	0.70mm	≈ 1.05	7mm	≈ 19 150 m
ZR500193	0.70mm	≈ 7.5	7mm	≈ 9 100 m

Table 2.5.1 *Characteristics of the NbTi strands for the five parametric samples.*

Five cable-in-conduit conductor sections, each about 18m long, have been cabled and jacketed at VNIIKP (Moscow) on CRPP specification. The strand coating (either SnAg solder or Ni electroplating) was also applied at VNIIKP. The conductor characteristics are summarised below

CICC	*Strand Type*	*Strand Coating*	*Cable pattern**	*Cable space ø*	*Outer diameter*
# 1	ZR500191	Ni	(1+**7**) x 3 x 4 x 4	16.5mm	18.5 ± 0.1mm

# 2	ZR500192	Sn base	(**1**+6) x 3 x 4 x 4	16.5mm	18.5 ± 0.1mm
# 3	ZR500192	Ni	(**1**+6) x 3 x 4 x 4	16.5mm	18.5 ± 0.1mm
# 4	ZR500192	Ni+subcable wraps	(**1**+6) x 3 x 4 x 4	16.5mm	18.5 ± 0.1mm
# 5	ZR500193	Ni	(**1**+6) x 3 x 4 x 4	16.5mm	18.5 ± 0.1mm

Table 2.5.2 *Layout of the five cable-in-conduit NbTi conductors.*
Bold *figures are segregated copper wires. For conductor # 1, the copper wires have ø=0.62mm. For conductors # 2-5 the copper cores have ø=0.70mm*

From the five conductor sections, five hairpin samples with a U-bend replacing the bottom joint have been prepared and instrumented. The testing of the five samples formed the core our the experimental activity in 2002. Testing started in February 2002, was discontinued in June and was resumed in October until the end of 2002. A few highlights of the test results are quoted below.

The AC loss before any load, after I_c test and after 1400 load cycles is compared in Fig. 2.5.1 for NbTi #2 and #3, two conductors only distinguished by the strand coating. The ac loss per cycle is here normalised to the cable volume including the copper wires. The loss in the SnAg coated conductor is considerably larger than in the Ni coated conductor. The first loadings, due to the I_c test, led to reduced coupling loss in both conductors. However, in contrast to the SnAg coated conductor, the AC loss of the Ni coated conductor is not further reduced by the 1400 load cycles. The coupling loss constants nτ, measured from the initial slope of the loss curve, are also listed in Fig. 2.5.1. The nτ value of the SnAg coated conductor is over a factor of 5 larger than that of the Ni coated conductor NbTi #3 of identical cable layout, even after 1400 load cycles. In NbTi CIC, the Ni strand coating is effective at reducing the interstrand coupling loss well below the level of the interfilament loss, i.e. nτ≈10ms. The loss does not substantially change after cyclic load and is not affected by the operating current, i.e. the transverse resistance does not change significantly when the strand bundle is under compressive load. A sub-cable wrap, which is a disadvantage for stability and the helium flow, is not required to reduce the AC losses.

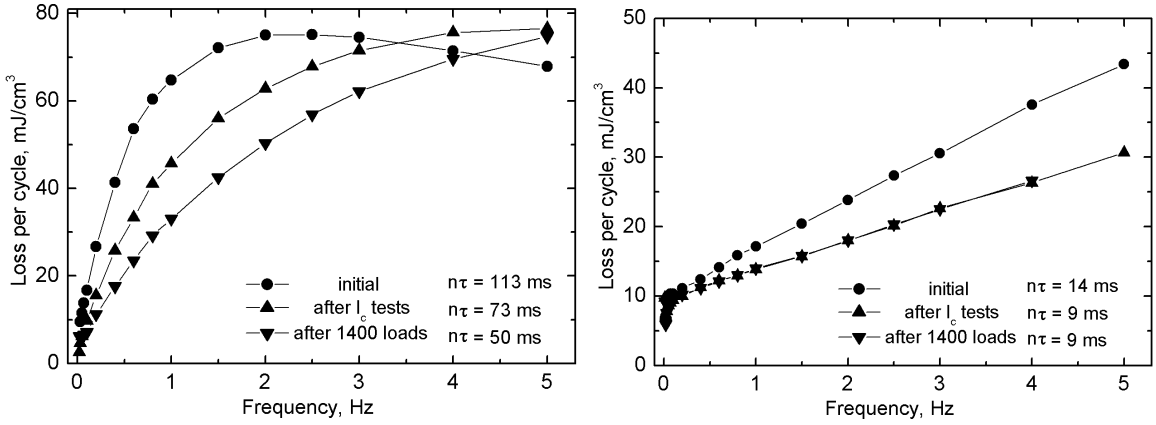

Fig. 2.5.1 *AC loss of two NbTi CICC with either SnAg coating (left) or Ni coating (right) at different steps of the load history. Background DC field 2T, applied AC field ± 0.2T.*

Transient field stability experiments have been performed at a background field of 6T. The results vs. temperature margin are shown in Fig. 2.5.2 for the conductor NbTi #3 before and after 1400 load cycles, for two levels of operating current, in the range of the design values for the ITER poloidal field (PF) coils. The open symbols indicate the largest transient that can be withstood before a quench occurs. The filled symbols are for quench. In agreement with the nearly unchanged AC loss, Fig. 2.5.1, there is no significant change in the transient stability before and after cycling. The minimum field integrals required to cause a quench are much larger than the maximum disturbance predicted at the ITER PF conductors at a plasma disruption ($\int \dot{B}^2 dt < 1 T^2/s$). The temperature margin necessary to withstand a plasma disruption in a Ni coated, NbTi CICC is negligibly small and does not need to be retained in the design criteria, i.e. it is buried in the engineering margins.

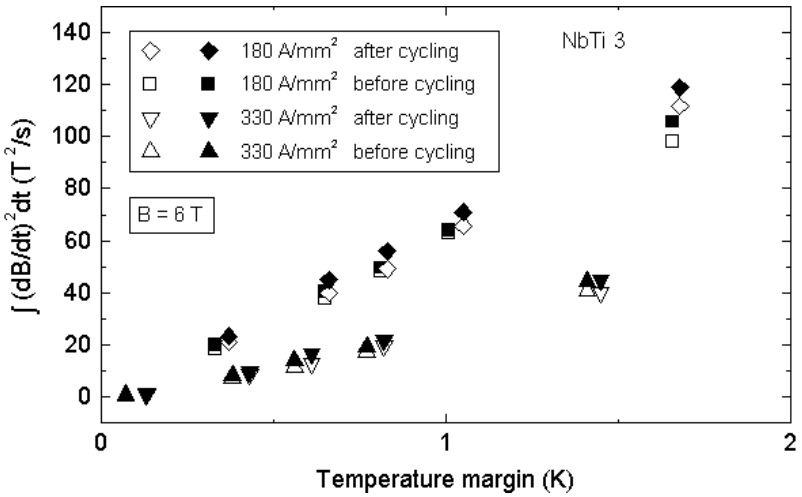

Fig. 2.5.2 *Minimum field integrals required to quench NbTi #3 before and after 1400 load cycles for currents of 10kA (180A/mm²) and 18kA (330A/mm²).*

The transient stability results vs. the normalised operating current at constant operating temperature are shown in Fig. 2.5.3 for both conductors, NbTi #2 and #3. The stability of the SnAg coated conductor is much poorer because of the higher AC loss. The limiting currents calculated according to the Stekly stability formula for heat transfer coefficients of 600 and 1000W/m²K are also indicated. In the ITER PF coils, the ratio I_{op}/I_c is designed between 0.127 and 0.365. The following measures are recommended for the ITER NbTi conductor:

- Ni strand coating with no subcable wraps
- No temperature margin to be retained for transient stability
- Design coupling loss $n\tau$=15ms suggested

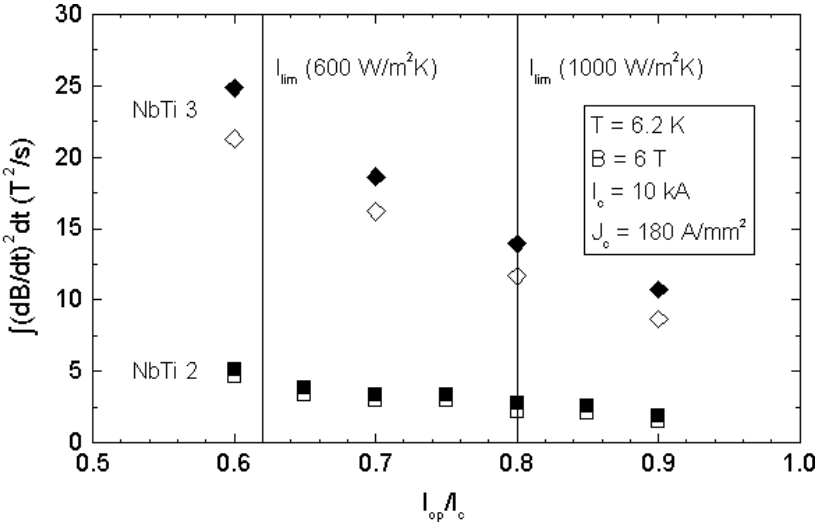

Fig. 2.5.3 *Field integrals required to quench NbTi #2 and #3 (solid symbols) versus the ratio of operating to critical current after 1400 load cycles.*

The critical current measurements in Nb_3Sn cable-in-conduit conductor are always stable. A smooth transition, with extended current sharing, is observed between the superconducting and normal regime. In NbTi CICC, unstable transitions are observed above a threshold current density. Two examples of such a transition are shown in Fig. 2.5.4. Whenever the transition is smooth, the voltage-current characteristic can be fitted by an exponential curve with index *n*. In 2001, extensive measurements on Nb_3Sn CICC proved that the index *n* cannot be scaled from the strand results to the CICC results. For NbTi conductors, we found that the index *n* measured on CICC matches the strand results satisfactorily, suggesting that current unbalance in the CICC, if there is any, has no significant impact in the voltage-current characteristics, in the electric field range of 10 to 100μV/m. The results of the index *n* are gathered in Fig. 2.5.5 for strand and CICC.

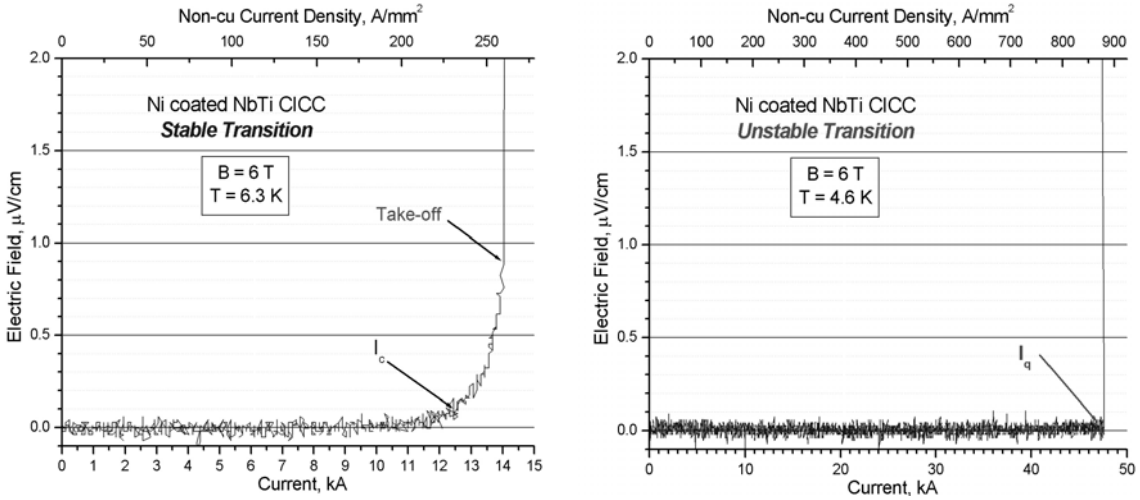

Fig. 2.5.4 *Examples of voltage-current characteristic of NbTi CICC, showing stable and unstable (sudden) transitions*

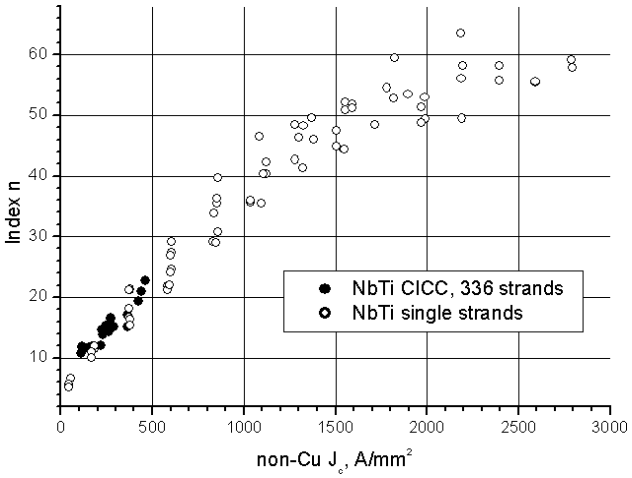

Fig. 2.5.5 *Results of index n for a NbTi strand and cable-in-conduit conductor. The results come from a large number of I_c measurements over a broad range of field and temperature.*

In Fig. 2.5.6, the I_c and I_q results of NbTi #2 and #3 are compared with the strand performance. Below the stability threshold, open symbols in Fig. 2.5.6, the CICC results scale satisfactorily compared to the strand J_c (continuous lines). At higher J_c, the CICC performance (full symbols = I_q) deviates progressively from the strand data. The CICC with low transverse resistivity (SnAg coating) has a higher threshold for unstable transition, 800 vs. 550A/mm^2, which is evidence of a more effective interstrand current sharing (on the other hand, the CICC with SnAg coating has much higher AC loss and hence very poor transient field stability). The presence of a pressure release channel in the CICC drastically reduces the coolant speed in the strand bundle area for the same overall mass flow rate. The impact on the stability is dramatic. A NbTi full size ITER conductor with a central hole (Section 2.5.2) showed a threshold for stable to unstable transition in the range of 150A/mm^2 compared to the 550-800A/mm^2 observed in the conductors without a central hole, i.e. #2 and #3. Systematic measurements of the critical current as a function of the mass flow rate, i.e. increasing the heat transfer coefficient, showed a shift of the stable-to-unstable transition at increasing helium speed.

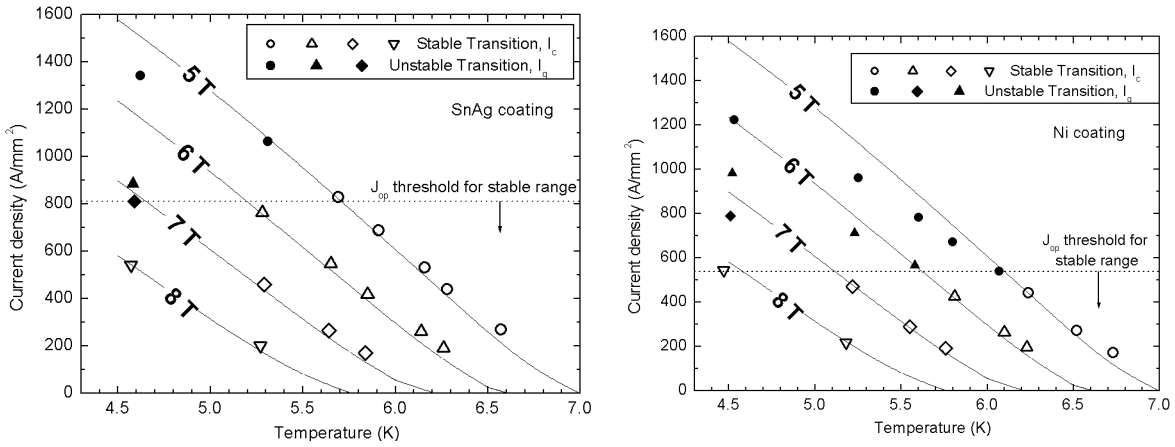

Fig. 2.5.6 *DC performance of two NbTi CICC, identical except for the strand coating (i.e. the transverse resistance), revealing the threshold between stable and unstable transitions.*

2.5.2 Test of a Full Size NbTi Sample

The conductor for the poloidal field coils of ITER is a NbTi cable-in-conduit superconductor. A Full Size Joint Sample of a PF conductor (PF-FSJS) was manufactured by the industry under monitoring by CEA and ENEA. It was delivered to the CRPP in July 2002 for testing in the SULTAN facility.

The sample, prepared according to the user interface document for SULTAN short samples, consists of two legs made of jacketed NbTi full size cables, of a lower joint, and of two upper terminals. The geometrical parameters of both legs are identical, but the strands in the cables were different. One cable contained nickel-coated NbTi strands (fabricated by Europa Metalli, Italy) with a pure copper matrix, while the other cable was composed of non-coated NbTi strands (fabricated by Alstom, France) with a Cu/CuNi matrix (internal CuNi barrier). The purpose of the nickel coating and the CuNi barrier was to reduce the coupling current loss by increasing the inter-strand resistance.

The sample is equipped with temperature sensors in the high field region of both conductors and at the helium outlet. Hall sensors and pick-up coils were installed in the high field regions of the conductors and the joint. Voltage taps were located symmetrically along the two conductors and the joint. Ohmic heaters were attached on each conductor below the upper clamps. The sample is depicted below, along with the main parameters of the two conductors.

Strand manufacturer	Alstom	Europa Metalli
Strand barrier	Internal CuNi barrier	Ni coating
Strand diameter	0.81mm	
Ratio Cu/non-Cu	1.54	1.9
Cable pattern	3x4x4x4x6	
Number of Sc strands	1152	
Number of Cu strands	0	
Cable diameter	38.7mm	
Conductor dimensions	51mm x 51mm	
Jacket material	AISI 316LN	

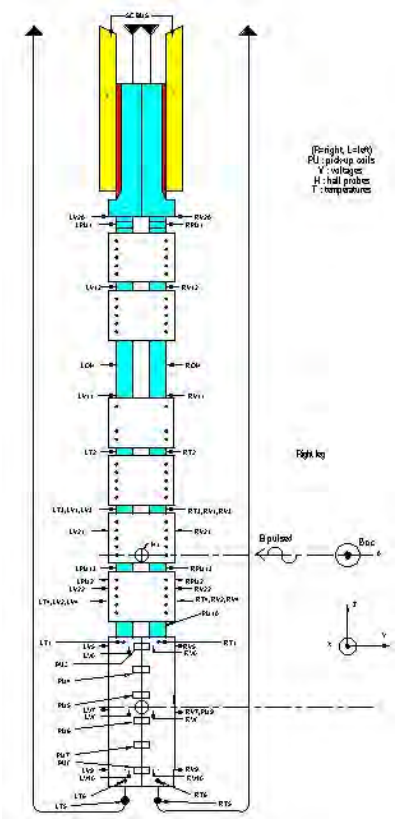

Fig. 2.5.7 *Main data of sample PF-FSJS and sketch of the sample assembly and cooling circuit*

The objective of the experiments in SULTAN is to characterise the DC behavior, the AC losses and the transient field stability of the conductors and joint. The experimental period lasted from the end of July until early October 2002. The DC tests consisted of measurements of the critical current I_c and the current sharing temperature T_{cs} on the sample in virgin state and after cyclic loading. The experiments were carried out at magnetic fields of 4, 5, 6, and 7T and a helium flow rate of 4g/s. Cycling load was performed by ramping the transport current 500 times up to 50kA at a magnetic field of 6T. The plots in Fig. 2.5.8 show the DC results for both conductors and the performance (critical and limiting current) predicted by the CEA from the strand characteristics. The extrapolation at zero current, i.e. the critical temperature is several tenths of degree higher than expected, casting a shadow on the reliability of the predictions.

Measurements of the AC losses were carried out at magnetic fields of 2 and 6T on the sample in its virgin state, after the DC tests, and after 200, 400 and 525 loading cycles. The amplitude of the sinusoidal pulses, perpendicular to both the magnetic field of SULTAN and the vertical axis of the sample, is ±0.1T and the frequency ranges from 0.06 to 6.0Hz. The loss is measured by the magnetisation method in arbitrary units and calibrated over a limited range of frequency by gas flow calorimetry. The loss decreases drastically after cyclic load of the conductor with an internal CuNi barrier, see Fig. 2.5.9.

In the stability measurements the conductors were exposed to a transverse field transient of 140ms duration and increasing amplitude until a quench was observed. Magnetic fields of 4, 6 and 7T and transport currents of 0, 40, 50 and 60kA were applied. Experiments for studying the effect of helium mass flow on stability were added to the program.

In DC tests the resistance and the quench temperature of the joint were studied. Experiments on the AC loss were conducted at magnetic fields of 2 and 5T and frequencies between 0.02 and 5.0Hz by means of the calorimetric and magnetisation methods. At the end of the experimental session, the stability of the joint during exposure to trapezoidal pulses was investigated. In these tests, ITER relevant scenarios like plasma disruptions and fast normal operation were simulated.

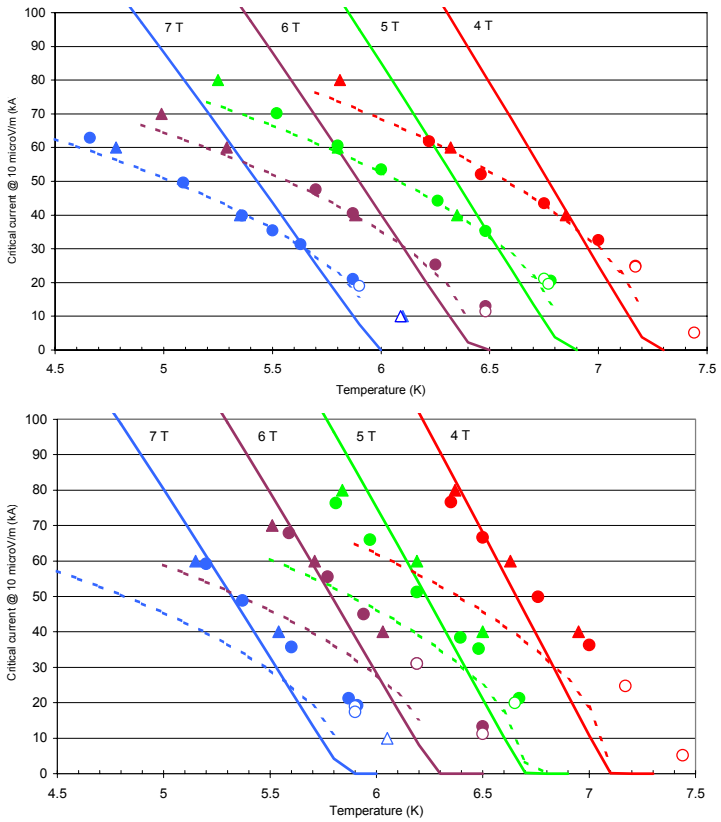

Fig. 2.5.8 *DC performance of the Europa Metalli (top) and Alstom conductor (bottom). The solid and dotted lines are the critical and limiting currents extrapolated from the CEA strand results. Experimental data from I_c and I_q measurements are represented by open and solid*

circles, while the data points from T_{cs} and T_q measurements are shown by open and solid triangles.

An interesting (and alarming) effect was observed during the AC loss measurements, with a 2 minute long applied field sweep. The temperature increase of the overall mass flow at the outlet pipe of the sample (T5) had a moderate increase, about 0.2K, because of the modest AC loss deposited power. However, the local temperature at the strand bundle (T3 and T4) kept increasing slowly, well above 0.2K, till the critical current was locally exceeded and a quench occurred, see Fig. 2.5.10. The local temperature runaway is evidence of the poor mass and heat exchange between the central channel and the bundle region. The flow in the bundle becomes stagnant for very modest, constant power load and the heat removal takes place only through the (poor) transverse conductivity of the bundle.

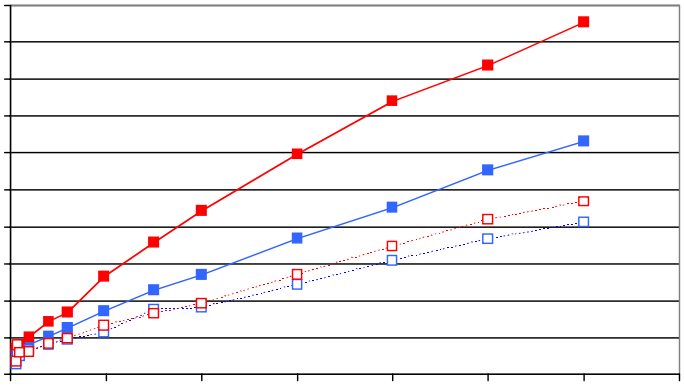

Fig. 2.5.9 *AC loss estimated by the magnetisation method in the Europa Metalli conductor (blue) and the Alstom conductor (red) at B_{dc}=2T and B_{ac}=±0.1T. Results from the conductors in virgin state are represented by solid squares, while data measured after the DC tests are shown by open squares.*

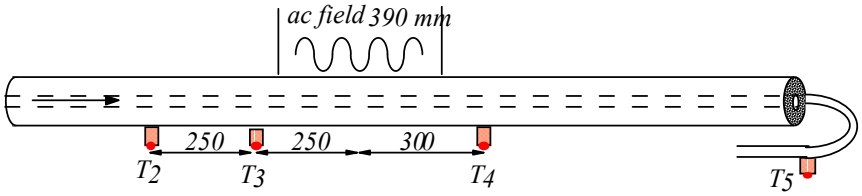

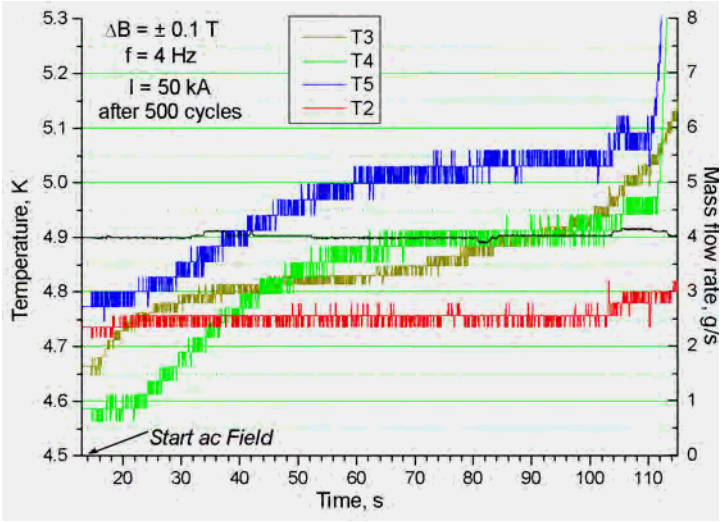

Fig. 2.5.10 *Evolution of the local and overall temperature during a long AC field sweep, with thermal runaway and eventual quench*

2.5.3 Development of a new Full Size Nb_3Sn Conductor for ITER

A drawback of present ITER conductors is the inhomogeneous current distribution mainly caused by uneven contact resistance and high current transfer resistance in the cable preventing current redistribution. This behavior is a limiting factor for conductor performance and there is a clear need to solve this problem. As a step in this direction, the CRPP designed and is presently preparing two lengths of full size Nb_3Sn conductors to be tested in the SULTAN test facility in 2003. The task attempts not only to optimise the design to improve the current distribution in cable-in-conduit conductors but wants to make use of the lessons learned during the last 8 years of R&D within ITER, i.e. after freezing the layout of the model coil conductor.

In general terms, the new conductor should combine improved current distribution among the strands by lower transverse resistivity in the cable, tolerable transient AC loss and stress tolerance to transverse load. On the whole, the conductor follows the specifications of the TF conductor.

As a first measure destined to improve the current distribution, the subcable wraps were removed. The initial purpose of the resistive strips around each subcable was to reduce the coupling currents between substages. However, recent results revealed that no such wraps are necessary to reduce the coupling current losses in multistage Nb_3Sn cabled conductors and we strongly expect that the absence of the wraps will have thoroughly positive effects on the conductor performance. Another effective way to improve the current distribution is reducing the interstrand resistance in the cable by decreasing the thickness of the Cr coating from 2-3μm as presently applied, to 1-1.5μm. Coating of the strands by a thin layer of Cr is the standard approach used to increase the transverse resistance between Nb_3Sn strands. The reduced layer thickness is certainly not beneficial for interstrand coupling current loss but there is some allowance for higher transient AC loss in the cable-in-conduit Nb_3Sn conductors for ITER.

Evaluation of the role of segregated copper for stability further guided the design of the new conductor. While segregated copper makes little contribution to current

transfer within the cable, the Cu:non-Cu ratio in the Nb_3Sn ITER strand can be reduced to 1 or even less, while maintaining high transient stability. Evidently, the cable layout must include sufficient segregated copper for quench protection.

Cyclic load tests performed with the CS Insert Coil and transverse cycling load subsequently applied to medium size Nb_3Sn CICC conductors in SULTAN caused a degradation of DC performance (see below). We expect that among other factors, the cabling pattern, void fraction and strand design can significantly affect the magnitude of the transverse stress effect in CICC conductors. These considerations have led to the selection of a cable configuration based on a braid. Compared to a twisted cable, the interlocked structure of braids provides higher transverse Young's modulus for the same overall void fraction.

Regarding the superconducting strand, we want to make use of a post model coil advanced strand with improved properties. The target values of non-Cu critical current density J_c(12T, 4.2K) and non-Cu Hysteresis loss at a field of ±3T, are 800A/mm^2 and ≤400 mJ/cm^3 respectively.

To comply with these considerations, a circular cable-in-conduit type conductor was selected with a central cooling channel and a thin circular jacket, both in Titanium. The reference operating conditions are those of ITER TF conductor: I_{op}=68kA, T_{op}=5K, B_{op}=11.8T and temperature margin ΔT=1K. The selected jacket material whose thermal contraction matches that of Nb_3Sn, allows the superconductor to operate at strains close to the intrinsic strain of the Nb_3Sn strands, thus avoiding the detrimental high compressive thermal strain of the filaments present with stainless steel jacketed conductors. The maximum temperature reached inside the conductor in the case of a quench has been estimated by the classical hot spot method, considering that only the cable material and the annular helium have the ability to absorb the energy generated by ohmic heating. With 230K, the present design reaches a temperature value close to the maximum allowable temperature set for ITER.

The cable configuration is a multistage arrangement of Nb_3Sn and pure copper strands. The Cu:non-Cu ratio in the superconducting strand is reduced to a value of 0.8 with the consequence that a large amount of segregated copper is present, offering an enhanced cost advantage. The first cable stage is a braid containing 14 superconducting and 15 pure copper wires, Fig. 2.5.11. The second cable stage consists of 7 braids twisted around a core of 49 copper strands. The core is manufactured from 0.7mm copper wire in two subsequent cabling operations both based on 'six around a core' patterns. The third and last cable stage consists of six second stage cables twisted around the central cooling channel. No wrapping is applied to the last but one cable stage.

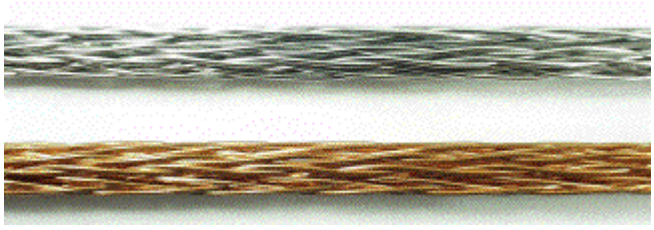

Fig. 2.5.11 *Samples of the 29-strand braids, Cr plated (top) and bare (bottom)*

However, the 'new full-size' project provides an interesting opportunity to compare directly a full-size CICC and a solder-filled conductor of similar cable pattern. Consequently, two conductor pieces, one for each leg of SULTAN, will be manufactured with the only difference being that the strand used in one piece has no chrome coating. After reaction heat treatment, the conductor piece without coating will undergo an additional manufacturing step consisting of filling the annular space of this conductor with solder, thus leaving only the central channel for helium flow. Evidently, in order to assure the wetting of the cable surface, the strands used in this conductor must be bare strands. To avoid solder penetration from the annular space into the central channel, the central channel of the soldered conductor will be a tube instead of a spiral.

Although solder-filled conductors have the potential to (i) eliminate internal disturbances caused by strand movement, (ii) enhance local and global current sharing and (iii) reduce the transverse pressure on filaments due to the hydrostatic effect of the filler, there is no direct relation between the soldered conductor and the manufacturing technique elaborated for ITER magnets based on Nb_3Sn. The preparation of this conductor for testing in SULTAN is rather an attempt to answer the question whether solder-filled conductors have an improved stress tolerance during transverse cyclic load compared to CICC. An equally important issue which we might be able to solve by comparing filled and unfilled CICC is whether a solder-filled cable has the capability of mitigating the decrease of the *n* index of the strands after cabling.

The procurement contract for the Nb_3Sn strand was awarded to Outokumpu (former IGC) as best bidder from four companies. Half of the length produced has been Cr-plated and half was left bare. The main characteristics of the manufactured Nb_3Sn strand are summarised in Table 2.5.1. With 45% Cu, a very low copper content was achieved in the strand. The average Cr thickness is 1.3μm with a remarkably small tolerance of ± 0.1μm. The strand was delivered in June 2002.

Strand diameter [mm]	0.7 ± 0.003
Cu:non-Cu ratio	0.8 ± 0.07
Non-Cu J_c(12T, 4.2K) [A/mm^2]	≥ 750
Non-Cu Hysteresis Loss, ±3T [mJ/cm^3]	≤ 300
RRR	> 100
Twist pitch, right hand [mm]	10
Cr-plating thickness [μm]	1.3 ± 0.1

Table 2.5.3 *Nb_3Sn strand specification*

	Conductor A	Conductor B
Type of strand	Cr-coated	bare
Cable configuration	29 x (49 + 7) x 6	
Cable twist pitches, right hand (mm)	350/160/390	
Cu-core twist pitches, right hand	40/80	
No. of superconducting strands	588	
No. of copper strands	924	
Diameter of SC and Cu strands (mm)	0.7	
Total non-Cu cross section (mm^2)	126	

Total Cu cross section (mm^2)	456	
Titanium central channel	Strip spiral 8x6	Tube 8x6
Cable space void fraction (%)	~37	
Cable diameter (mm)	~36.4	
Ti-jacket wall thickness (mm)	2÷2.5	

Table 2.5.4 *Conductor layout*

Two companies are involved in the cable manufacturing. The braiding was completed in August 2002 by Marti-Supratec on a prototype braider first used in 1990 by ABB during development of CICC for NET. This company produced two lengths of 29-strand braid, one with Cr-coated wires, one with bare wires. For the subsequent cabling and jacketing operations, the Russian company VNIIKP was awarded a fixed-price contract to manufacture two conductor lengths based on the two types of braids. A major factor in the choice of VNIIKP was their experience in fabricating the conductor for ITER TF Insert Coil. Table 2.5.2 summarises the layout of the two conductor lengths, denoted A and B, as they were specified for the manufacturer. Twist pitches, cable diameter and void fraction are target values. The conductor delivery from VNIIKP is expected at the end of 2002.

2.5.4 High Temperature Superconducting Current Leads

The CRPP and the Forschungszentrum Karlsruhe (FZK) are developing a 70kA current lead for the toroidal field coils of ITER using high temperature superconductors (HTS). In the first phase of this program two 10kA current leads fabricated from AgAu/Bi-2223 ($(Bi,Pb)_2Sr_2Ca_2Cu_3O_{10+x}$) tapes have been already successfully tested at the CRPP. These binary current leads consist of a conduction-cooled HTS and a wire bundle heat exchanger, partly actively cooled by 60K He gas. Using HTS current leads, Joule heating can be eliminated in the temperature range of 4.5 to 70K, which provides the possibility of reducing the heat load at 4.5K by a factor of 10. The difference of 10K in the He and the conductor temperature leads to a negligible heat flux at the cold end of the heat exchanger. The 10kA HTS current leads have been found to consume only 1/3 of the refrigerator input power necessary to cool metallic current leads. Presently, the inlet temperature of the He gas required to cool the Cu parts of the current leads of the TF coils has not been fixed in the ITER design. Furthermore, studies performed at CERN indicate that the optimum temperature at the warm end of the HTS of the 13kA current leads for the Large Hadron Collider (LHC) is 50K for a He inlet temperature of 20K. Consequently, the effect of both the He inlet and the warm end HTS temperature on the performance of the 70kA current leads for the TF coils of ITER has been investigated.

T_i (K)	Int_{AgAu} (W/m)	Int_{steel} (W/m)
40	1614	83
50	2385	136
60	3243	202
70	4181	277
80	5192	359

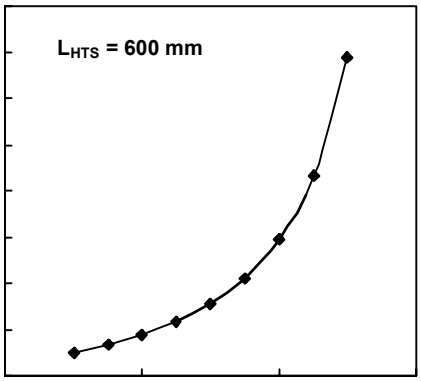

Fig. 2.5.12 *Heat load at 4.5K versus the HTS warm end temperature for an overall J_c = 16kA/cm²(77K, B=0), an HTS portion 600mm long, and a stainless steel cross-section of 40cm².*

The input power necessary to cool a binary HTS current lead depends on the heat load at 4.5K, the He mass flow rate required to cool the Cu part, and the refrigerator efficiency. The heat load at 4.5K caused by heat conduction is proportional to the conductor cross-section and the thermal conductivity integrated from 4.5K to the temperature T_i at the warm end of the HTS. In addition to the HTS, the stainless steel support structure contributes to the heat load at 4.5K. The HTS cross-section is selected in such a way that the critical current for the expected magnetic field B = 68mT perpendicular to the broad face of the Bi-2223 tapes reaches 95kA at T_i. Typically the AgAu:Bi-2223 ratio in the tapes is as large as 7:3. The contribution of the Bi-2223 filaments to heat conduction is negligible because of their extremely small thermal conductivity. The values of the integrated thermal conductivity of Ag 3% Au and stainless steel are listed in Table 2.5.3. Due to the considerably higher critical current of the Bi2223 superconductor and the reduced values of the integrated thermal conductivity, the heat load at 4.5K is reduced for lower values of T_i, see Fig. 2.5.12.

To determine the mass flow rate necessary to cool the heat exchanger part of the current lead the steady state thermal behavior has been simulated numerically. The input values selected for these calculations are summarized in Table 2.5.6.

Copper	*RRR* = 50
Current density	1.07kA/cm²
Copper cross-section	63.6cm²
Nominal current	68kA
Specific heat of helium	5.21J/g K
T_{in} (He inlet temperature)	20 - 70K
T_i (cold end of heat exchanger)	45 – 80K
T_{end} (warm end of heat exchanger)	293K
Product of heat transfer coefficient *h* and cooled perimeter *P*	20000W/mK

Table 2.5.5 *Design parameters for the 70kA HTS current leads*

The optimum length of the heat exchanger part of the current lead varies between 500 and 1400mm. Generally, the optimum length decreases with both lowered He inlet and enhanced Cu cold end temperature. The heat flux at the cold end of the

heat exchanger is equal to the heat load at 4.5 K. The minimum mass flow rates required to cool the Cu part of the binary current lead at a current of 68kA are shown in Fig. 2.5.13 (left). The smallest mass flow rate is for the lowest He inlet temperature of 20K and the highest copper cold end temperature of 80K. In the present simulations connections between the heat exchanger and the HTS part have not been taken into consideration. Thus, the temperatures at the cold end of the heat exchanger and the warm end of the HTS are equal.

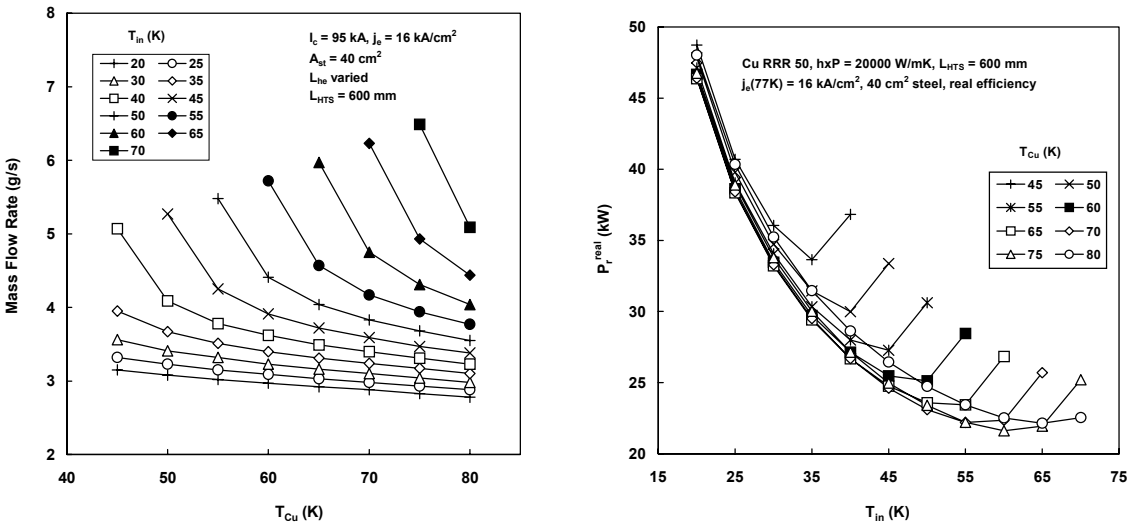

Fig. 2.5.13 *He mass flow rate needed to cool the heat exchanger part of the binary current lead for I = 68kA (left). The resulting refrigerator input power required to cool the whole current lead is shown on the right.*

To determine the refrigerator input power needed to cool the whole current lead, the efficiencies of the two cooling cycles have to be taken into account. A large refrigerator needs an input power of approximately 400W to remove a heat load of 1W at 4.5K. The helium gas, used to cool the heat exchanger part of the current lead, is warmed up from the inlet temperature T_{in} to room temperature. Reasonable values for the minimum work required to cool helium gas from 300K to T_{in} vary between 3350 and 15300J/g for T_{in} values of 70 and 20K, respectively. These data are based on the assumption that a large refrigerator can reach 32% of the efficiency of an ideal, reversible cooling cycle for T_{in}=70K, while only 19% of the ideal efficiency is obtained at T_{in}=20K. The refrigerator input power necessary to cool the whole current lead is shown in Fig. 2.5.13 (right). The minimum required refrigerator input power is reached for T_{in}=60K and T_{Cu}=75K at the cold end of the heat exchanger.

However, even for T_{in}=50K and T_{Cu}=65K, the required refrigerator input power is only slightly enhanced. The optimum difference of the He and Cu temperatures at the cold end of the heat exchanger is approximately 15K. Reduced critical current densities as well as an enhanced cross-section of the stainless steel support would favour slightly reduced values of T_{in} and T_{Cu}.

The results of the present study indicate that the optimum He inlet temperature for a binary HTS current lead is in the range 50–60K, while the optimum temperature at the warm end of the HTS is 65–75K. In spite of slightly enhanced refrigeration costs, a temperature close to 60K at the warm end of the HTS, which is below the

optimum value, may be preferable because of the considerably enhanced critical current.

2.5.5 Strands extracted from loaded Nb_3Sn cables

To confirm the reason for the low *n* index observed in the Nb_3Sn cable-in-conduit samples in 2001, the strands from the cable section exposed to cyclic, high transversal load have been extracted from the CICC and tested as individual specimens. The performance comparison of strands extracted from loaded and non-loaded CICC sections is a crucial test to assess permanent damage of the strands.

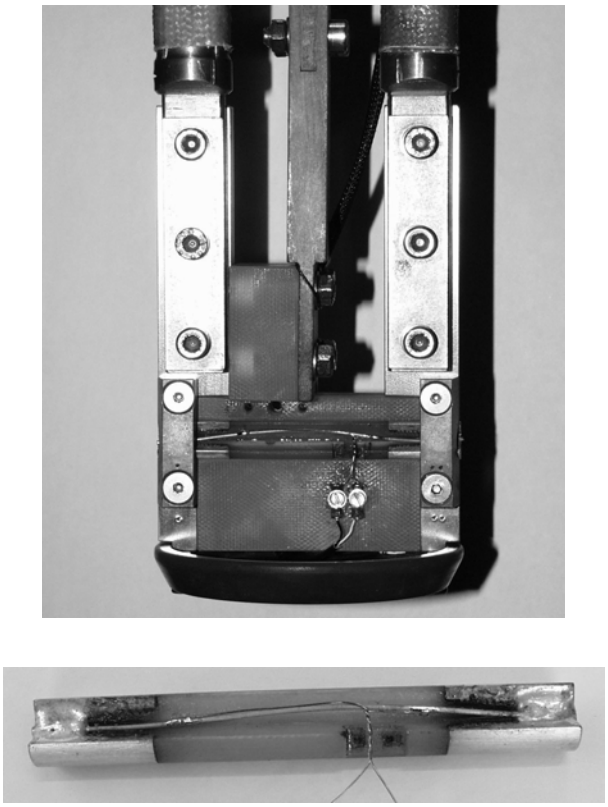

Fig. 2.5.14 *Sample holder for short length, straight strand and (bottom) a strand extracted from a cable, soldered to the Cu/glass-epoxy supporting cylinder*

The test of Nb3Sn strands extracted from a section of heat treated cable is a challenging task and a number of preliminary investigations has to be carried out to guarantee the reliability of the results. The test is at liquid helium, in 12T background field from a 80mm bore solenoid. The sample holder, Fig. 2.5.14, allows the testing of straight (or almost straight) strand specimens, with a 78mm total length. The specimen is soldered at both ends of a copper/glass-epoxy cylinder, which is finally bolted into the sample holder. In the twisted strands extracted from the cable, a gap of variable width is left between strand and cylinder. To conveniently support the non-straight specimens against the Lorenz force, the gap is filled by grease or Stycast (both have been shown to have the same effect). The voltage taps are placed in the central 30mm long section of the specimen, to allow sufficient length for current transfer at the ends. Due to the short length of the

voltage taps, the noise in the electrical field is large and the critical current can be reliably measured starting upwards from 50μV/m. The *n* index is evaluated over the electric field range 50-200μV/m. From the measured I_c at 50μV/m and *n*, the I_c@10 μV/m is extrapolated. For each specimen, five I_c runs are measured. The standard deviation of the results from run to run, i.e. the reproducibility, is better than 1% for I_c and up to 10% for *n*, which is estimated from the linear fit of Log E vs. Log I between 50 and 200μV/m.

Initially, six specimens were measured, from strand sections separately provided by the strand supplier. The six sections are from three different manufacturing batches (billets). To obtain straight specimens, the strands are inserted into quartz glass capillary tubes during the heat treatment. Strands from the same billet gave identical results within 1%, but the scattering of the results billet-to-billet, i.e. the minimum scattering to be expected for strands randomly extracted from the cable, is as large as 13%. The I_c and *n* results are shown in Fig. 2.5.15 and 2.5.16, with the label "original strand". The I_c extrapolation at 0.1μV/cm criterion is in good agreement with the results from coiled specimens measured at the University of Twente. Seven specimens were prepared from strands extracted from a cable section and straightened before heat treatment. The results, labeled as "extracted before h.t.", are identical to the "original strand" in terms of *n*, average I_c and standard deviation (13%), proving that mechanical deformation before heat treatment does not affect the strand performance.

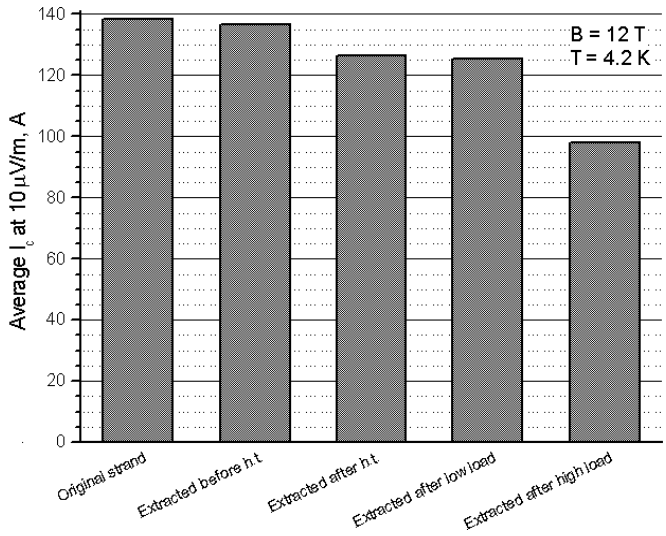

Fig. 2.5.15 *Average critical current on short strand specimens, extrapolated at 10μV/m, for the five groups of tested strands.*

Another seven specimens were prepared from strands extracted from a heat treated short cable section which was never loaded (label "extracted after h.t."). Five more specimens were from strands extracted from a cable section cut from the same sample in the low load region (label "extracted after low load"). These two groups of specimens present very similar results, with high *n* and average I_c only 7% lower than the former series. The scattering of I_c is larger than the expected 13%. Rather than the extraction procedure, the twisted geometry of the specimens (with the field not perfectly perpendicular and non-identical load distribution) can be considered to be responsible for the small, apparent performance drop.

The crucial series of seven strands was extracted from a sample section exposed to the highest transverse, cyclic load, (label "extracted after high load"). Contrary to the strands extracted from a low load section, clear friction marks (bright spots) have been detected at the crossovers, Fig. 2.5.17. The average spacing between friction marks is of the order of 6mm. The Cr plating is not damaged from wear. The local displacement by friction at the crossover has been estimated by eye to be of the order of 0.1-0.2mm. The scattering of *n* and I_c results is extreme, ranging from one specimen with almost intact performance to one with an *n* value as low as 5, i.e. a very early resistive slope.

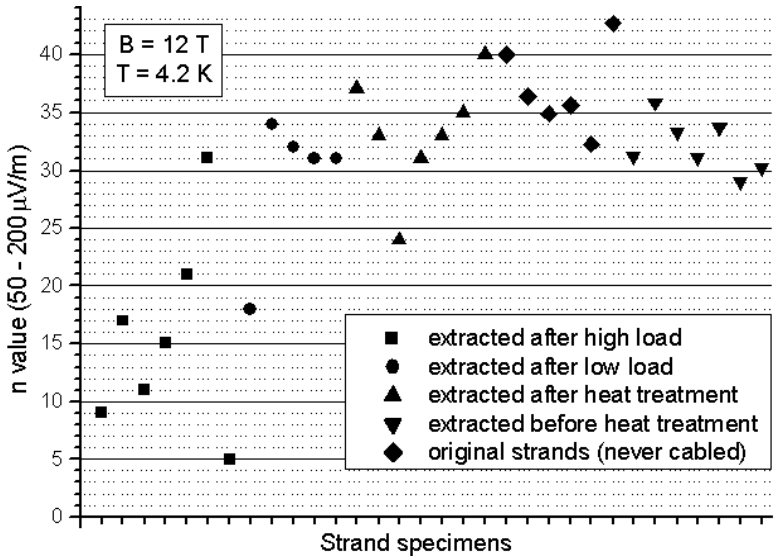

Fig. 2.5.16 *Results of the n index for all the strand specimens. Each dot is the average of at least three consecutive I_c test runs.*

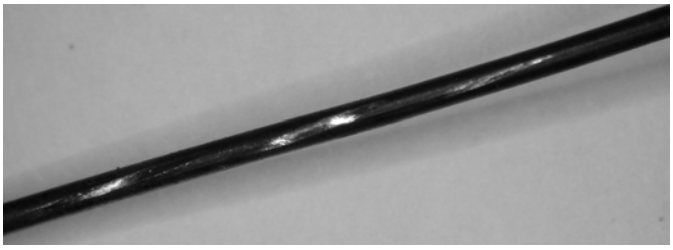

Fig. 2.5.17 *Friction imprints (bright spot) at the strand crossovers, observed only at strands extracted from the high load section, o.d. =0.82mm.*

2.5.6 Superconductivity Studies

Electric, thermal and hydraulic analysis of the Nb_3Sn CICC experiment

In the scope of the test campaign for Nb_3Sn cable-in-conduit conductors, completed in SULTAN in 2001, a transient, interstrand current redistribution was induced by firing a localised heater and bringing part of the conductor into current sharing. The current redistribution was qualitatively inferred from the signals from Hall

plates arranged around and along the conductor. The goal of this study is a quantitative assessment of the current redistribution to obtain a deeper understanding of the experiment characterised by the local transient energy deposition, i.e. with thermal, hydraulic and electric transients. The approach is based on (1) the reconstruction of the current displacement from experimental self-field measurements, and (2) simulations with a coupled and consistent thermal, hydraulic and electric model (THEA® code by CryoSoft). From the reconstruction we draw conclusions on the time constants and characteristic length for the current transfer. The first THEA simulation model consists of the last-but-one cable stage as 4 twisted superstrands with uniform properties. The superstrands are independently cooled by a single helium flow, and are coupled electrically through mutual inductances and interstrand conductance. The matrices related to these electrical properties are generated by the Conductor Interactive Designer (CID® code by CryoSoft). The electrical joints are included using a simple approximation of ideal conditions, i.e. perfect contact between the superstrands or zero joint impedance. Preliminary results show that the model with 4 superstrands, although capable of matching the orders of magnitude and the global behaviour during the evolution following the heat pulse (e.g. the stability margin), is inadequate for a detailed comparison of the measured resistive voltages and Hall probe signals, including amplitude and dynamics. These results call for a more detailed modelling with more superstrands, a fine tuning of the thermal resistance network, as well as multiple hydraulic channels. This activity is in progress and preliminary results are shown in Figs 2.5.18 and 2.5.19.

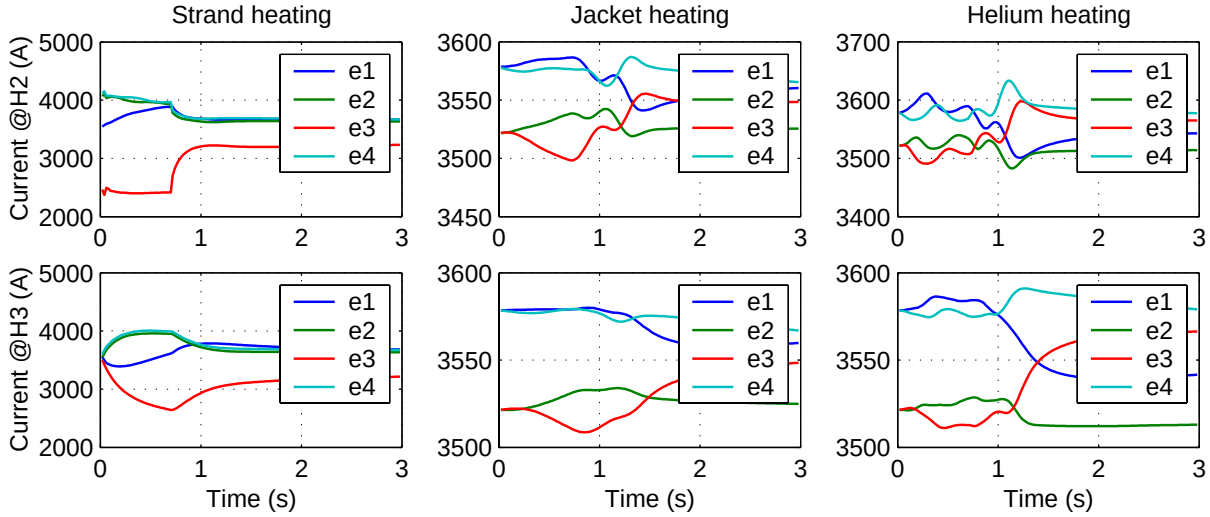

Fig. 2.5.18 *Time history of the current in the 4 superstrands at the Hall arrays H2 and H3. The duration of the heat pulse is 0.7s. Comparison of the heating modes correlates current displacements with thermal gradients, i.e. decreasing from strand to helium heating.*

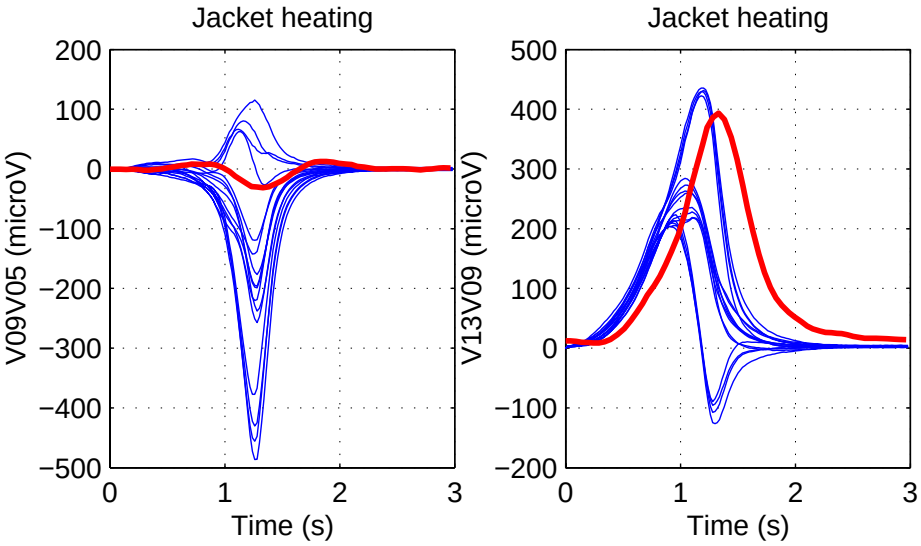

Fig. 2.5.19 *Time history of the resistive voltage V13V09. Simulated results (blue) for jacket heating are in agreement, i.e. amplitude and time scale, with the experiment (red).*

Analysis of the TFMC current sharing temperature with ramp heating

The ITER Torodial Field Model Coil (TFMC) was tested (phase I) as single coil in the TOSKA facility of the Forschungszentrum Karlsruhe in 2001. The racetrack coil, which uses a circular Nb_3Sn cable-in-conduit conductor, is equipped with external heaters for the evaluation of the current sharing temperature (T_{cs}). Since there are no sensors inside the coil, the only possibility to assess the coil temperature is to use the measured inlet temperature and to estimate the down-stream propagation of the temperature profile. To heat the TFMC up to T_{cs}, ramp heating was proposed by the CRPP as a compromise between heat slug injection and the steady state heating. The analysis of the ramp heating was completed by combining simulations, superconducting strand data and results of an experimental run.

The thermal hydraulic code Gandalf® of CryoSoft was used to extrapolate, from the experimental inlet temperature, the conductor temperature downstream at the maximum field (B_{max}), where the quench occurs (T*). At the ITER criterion of 50mV/m the current sharing power in the short length exposed to B_{max} is negligible and the resulting estimated range of T* is 9.4-9.8K. The expected T_{cs} based on strand data is 8.8K, obtained using the Summers law and assuming a longitudinal strain of -0.61%. This overestimation of the cable performance compared to the strand performance is likely to be due to heat diffusion from the heated conductor into the coil through the radial plates, a feature not included in this model.

A simple model for the prediction of the quench point in cable-in-conduit conductors

There are two standard DC experiments performed on short samples of the future conductors for ITER-FEAT: the critical current (CC) and the current-sharing temperature (CS) measurements. In the critical current runs, the sample is exposed to a given magnetic field, is maintained at constant temperature by a constant helium mass-flow and the current in the sample is increased slowly from zero up to

a value where an accelerated and irreversible increase of the sample voltage appears. This value of the operating current is named “the quench current” and is a function of the applied field and temperature. Although it has become standard to document the quench current measurements, up to now there has been no theoretical model explaining this effect. Such a theoretical model has been developed to explain the quench behaviour of CICC.

The main assumption of the model is that the current-voltage characteristic of the cable can be described by a power-law, parameterised by the electric field criterion E_c (10μV/m in most practical cases) and the power index (or power exponent) n

$$E(I_{op},T_{cond},n) = E_c\left(\frac{I_{op}}{I_c(T_{cond})}\right)^n \qquad (\mathbf{1})$$

where E is the electric field, I_{op} the operating current, T_{cond} the conductor temperature and I_c the critical current.

We observe that both CC and CS measurements are in quasi steady state. The current or temperature increases slowly and we can assume that the conductor and helium are always at thermal equilibrium. The thermal equilibrium of the conductor is controlled by the power generated in the conductor (index heating)

$$W(I_{op},T_{cond},n) = E(I_{op},T_{cond},n)I_{op} \qquad (\mathbf{2})$$

and by the cooling capacity (available cooling power) of the helium

$$G(T_{con},T_{He},h) = hp_w(T_{cond} - T_{He}) \qquad (\mathbf{3})$$

W is a function of the operating current, conductor temperature and the power-law index while G depends on the conductor temperature, helium temperature T_{He} and the heat exchange coefficient between conductor and helium, h. The p_w is the wetted perimeter of the conductor.

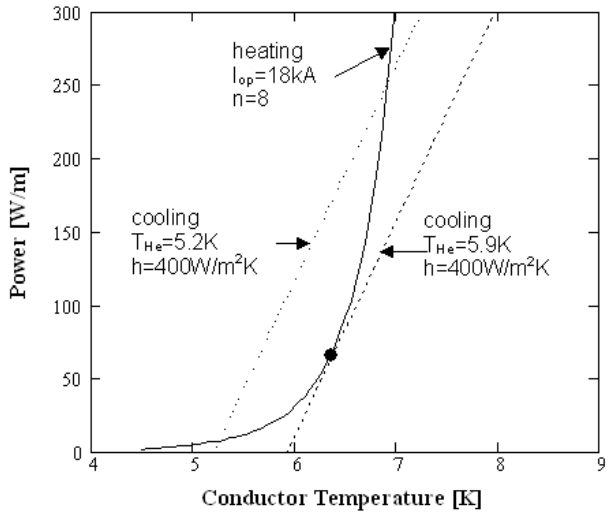

Fig. 2.5.20 *Thermal equilibrium (steady-state) conditions in a current sharing experiment. The helium temperature is increased from 5.2K to 5.9K at a constant I_{op}=18kA.*

A typical situation encountered in a CS experiment is illustrated in Fig. 2.5.20. The generated power W and the cooling power G are plotted as a function of the conductor temperature for two different helium temperatures. The continuous line is the power generated in the conductor for I_{op}=18kA and n=8 and the two straight lines represent the cooling power for T_{He}=5.2K and T_{He}=5.9K. The heat exchange coefficient is the same in both cases, h=400W/m^{2}K. The situation corresponds to an increase of the helium temperature from 5.2K to 5.9K. At lower temperatures (T_{He}=5.2K) there are two intersection points between the generated power and the cooling power line but only one point (the lower one) is a thermal-equilibrium point. When the helium temperature T_{He} is increasing (the G line moves to the right), the two crossing points will come closer and closer, up to the point where they collapse in a common contact point. The second G line in Fig. 2.5.20 illustrates this limiting situation. Any increase of the helium temperature beyond this point will result in the disappearance of the contact point i.e. of the stable solution for thermal equilibrium. The cable will quench. This limiting point defines unequivocally the quench point.

Based on this model, the quench parameters of Conductor A from the SeCRETS experiment were parametrised and compared with the experimental ones. As seen in Fig. 2.5.21, there is a good agreement.

Next, assuming a linear dependence of the critical current on temperature and based on the observation that at the quench point the slopes of the cooling and heating curves are equal, a fully analytical model was also developed. A collection of the most important relations obtained in the frame of the linear model is given in the table below.

The model gives a good estimate of the quench point parameters of CIC conductors. For a linear dependence of the critical current on temperature, a fully analytic model was developed. Useful relations for the calculation of the quench point parameters in the framework of the linear model are given and it was shown that they could be expressed with the help of a new nondimensional group called “the quench number”. The calculations with the linear model also show good agreement with the experimental results. Experimental data can be used to assess the value of the heat exchange coefficient from DC experiments and offer an alternative to assessment through stability experiments. This analysis can be extended straightforward to NbTi and High-T_c superconductors, which have a different scaling of the critical current or to the exponential form of the voltage-current characteristic.

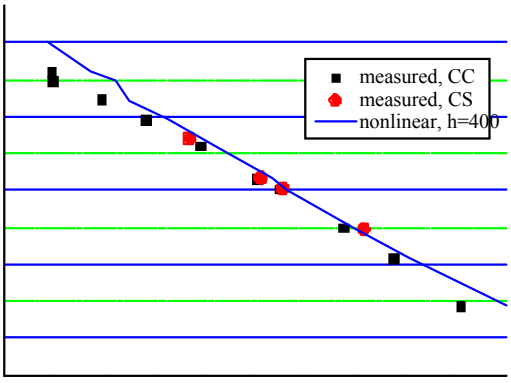

Fig. 2.5.21 *Comparison between the measured and calculated quench parameters for the SECRETS conductor.*

Analytical relations for the quench point

Current Sharing	Critical Current
$T_{q\_He} = T_c\left(1-\frac{n+1}{n}\frac{I_{op}}{I_{c0}}\frac{1}{\left(\frac{\Phi}{n}\right)^{\frac{1}{n+1}}}\right)$	$I_q = \frac{nI_{c0}}{n+1}\left(\frac{\Phi}{n}\right)^{\frac{1}{n+1}}\left(1-\frac{T_{op}}{T_c}\right)$
$T_{q\_cond} = T_c\left(1-\frac{I_{op}}{I_{c0}}\frac{1}{\left(\frac{\Phi}{n}\right)^{\frac{1}{n+1}}}\right)$	$T_{q\_cond} = \frac{T_c}{n+1}\left(1+n\frac{T_{op}}{T_c}\right)$
$E_q = E_c\left(\frac{\Phi}{n}\right)^{\frac{n}{n+1}}\frac{hp_wT_c}{nI_{c0}}$	$\Phi = \frac{hp_wT_c}{E_cI_{c0}}$ quench number

2.5.7 Testing of MgB_2 High Temperature Superconductor

In contrast to cuprate high temperature superconductors, the current flow in the intermetallic compound MgB_2 is not affected by the grain boundaries. Therefore, MgB_2 is a promising conductor for high current applications in spite of the modest critical temperature of 39K.

The research division of Edison Spa developed a new wire manufacturing technique based on reactive infiltration and the powder-in-tube (PIT) method. The field and temperature dependences of the critical current of a mono- and a multicore wire prepared by Edison Spa have been investigated at the CRPP. Using a temperature variable cryostat the critical current of the MgB_2 wires was measured in magnetic fields up to 10T at temperatures between 4.2 and 30K. The critical currents can be well represented by the scaling law

$$I_c(B,T) = \frac{C_0}{B}\left(1-\left(\frac{T}{T_c}\right)^{\beta}\right)^{\gamma}\left(\frac{B}{B^*(T)}\right)^{p}\left(1-\frac{B}{B^*(T)}\right)^{q} \quad \text{with} \quad B^*(T) = B^*(0)\left(1-\left(\frac{T}{T_c}\right)^{\alpha}\right)$$

where B* is the irreversibility field and T_c=39K. The scaling parameters obtained for both MgB_2 wires are listed in Table 2.5.6.

	p	q	α	β	γ	C_0 (AT)	B*(0)(T)
1-filament wire	0.8	5	1.08 ± 0.05	1	0.82 ±	8830 ± 160	11.39 ± 0.24

					0.03		
7-filament wire	0.5	5	1.2 ± 0.1	1.55 ± 0.37	1.89 ± 0.45	28900 ± 2000	13.5 ± 0.5

Table 2.5.6 *Definition of parameters and correlation for the quench point.*

The critical currents (1μV/cm criterion) found for the monocore MgB_2 wire are shown in Fig. 2.5.22. The critical current densities achieved are high enough to be of interest for applications at moderate magnetic fields up to 2-3T and at intermediate temperatures accessible by the use of cryocoolers.

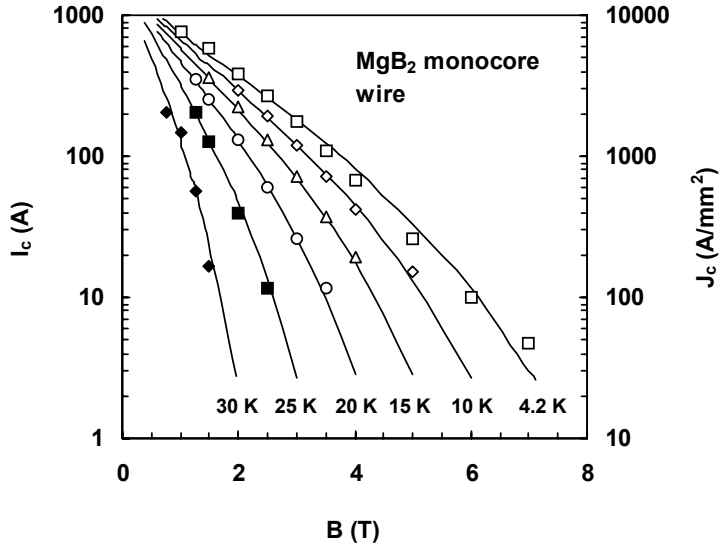

Fig. 2.5.22 *Critical current versus applied magnetic field for selected temperatures. The MgB_2 cross-section of the monocore wire is 0.1mm².*

2.6 Gyrotron development

2.6.1 118 GHz Gyrotron development

The three 118GHz/0.5MW/2s gyrotrons produced by Thalès Electron Devices within the framework of a collaboration between Thalès, CRPP, FZK-Karlsruhe and CEA-Cadarache have been installed and operated on TCV between the end of 2001 and April 2002.

At this time, the first X3 gyrotron installed on TCV suffered from a window failure during a 2s/500kW pulse. This cryogenic window is designed for CW operation with an RF output power of 500kW. The tube has been sent back to Thalès for repair and the window has been investigated by the institute of "Material Science" at FZK, showing no degradation of its transmission and absorption properties. The failure cause is not yet clearly established. The repair of the gyrotron and reinstallation in the TCV-ECH system is planned for the first half of 2003.

In parallel, a contract between CEA-Cadarache, Thalès and CRPP has been placed to improve the tube performances (210s pulses are required from the same gyrotron for operation on Tore Supra) by suppressing the parasitical oscillations in the mode converter which where found to be responsible for the power degradation over time. Among the modifications, a conical mode converter has been designed by Thalès to replace the existing cylindrical one, and the cooling of the mirror box and of some othe components such as the ion getter pumps will be improved.

2.6.2 140 GHz Gyrotron development

After the successful operarion of the so-called 'maquette' tube, modifications (mainly in the quasi-optical mode launcher and in the cooling circuits) were made to the design of the 140 GHz 1MW/CW Gyrotron to be used on W7-X. On this basis, a 'prototype' tube was built, delivered and operated at FZK. This tube has routinely achieved an output power of 0.85MW in 180s pulses, limited by the cooling capability of the power supply. At reduced power level, the 'prototype' reached 900s/0.5MW and 1320s/0.25MW, limited by the pressure increase in the tube.

Experiments carried out by the CRPP at FZK in the autumn of 2002 have encouragingly shown that the tube performance is not limited by any form of malfunction, nor are they degrading with time. Even though a milestone on the way toward CW operation has been met (the energy per pulse has been multiplied by a factor of 6 with respect to the 'maquette' tube), technological improvements to the cooling are still needed to extend the pulse length further. On this basis, it has been decided to end the R&D phase of the collaboration. Negociations between IPP Garching and Thalès Electron Devices are underway to lay out the future of the project.

2.6.3 Gyrotron mode converter

Generally, the high order TE_{mn} modes generated by gyrotrons are not suitable for long path transmission and plasma heating. Both transmission and heating require conversion to Gaussian-like beam (in free space). For a 170GHz, $TE_{34,19}$ gyrotron, the conversion can be performed by a conical (with linearly increasing wall radius) mode converter with a helically rippled wall. This type of converter couples the power in the $TE_{34,19}$ mode to other TE modes. The interference between the TE modes results in the formation of a microwave bunch – Gaussian beam. Expressions for the coupling coefficients have been derived. Preliminary versions of two computer codes have been developed. The first mode calculates the power contained in each TE mode as a function of the converter longitudinal coordinate, while the second simulates the microwave bunch formation. For the future, improved versions of these codes will be used to optimise the converter parameters for efficient transformation into Gaussian-like microwave beam.

2.6.4 Second Harmonic Quasi Optical Gyrotron

A proof of principle was carried out for the use of a grating in a Littrow mount to excite oscillations at the second harmonic of the cyclotron frequency in a quasi-optical gyrotron. The existing grating of the 115GHz quasi-optical test stand was replaced by another grating designed to operate at 2x70GHz. Gyrotrons oscillations at 140GHz were clearly identified, as nothing was observed at 70GHz, indicating

that the emission only occured at the second harmonic. Since the tube characteristics (gun geometry, magnetic field profile) were not designed for operation at this frequency, no attempt was made to optimise the output power.

*2.7 Industrial process plasmas**

During 2002 several CTI (Commission for Technology and Innovation) projects ended and the industrial plasma group succeeded in obtaining new CTI projects on various topics. In one case a CTI project was prolonged for one more year, concerning the production of large area solar cells, an important project for the photovoltaic community in Switzerland. This project is of particular interest since it may allow Swiss industry to enter into the new and expanding market for equipment for thin film solar cell production.

In addition several new CTI projects have been proposed and have been accepted by the industries concerning despite the difficult economic situation in Switzerland. Many of these new projects are starting activities in new areas. Discharge plasmas physics is the main topic in the EMD (electrical discharge machining) project and in the project investigating atmospheric pressure plasmas. An opening towards modelling is underway by proposing a collaborative project with industry dealing only with the modelling of the process plasmas, in particular of large area RF plasmas. All these new activities will clearly allow the industrial plasma group at the CRPP to broaden its scope and competence.

2.7.1 The physics of plasma enhanced CVD for large area coating

The aim of this CTI project is to develop a large area, high throughput coating system for mass production of silicon thin film solar cells, based on plasma enhanced chemical vapour deposition (PECVD) in a single chamber reactor. As foreseen in the project planning, the work is carried out in a collaboration between CRPP Lausanne, IMT Neuchatel, and Unaxis Truebbach.

Boron contamination reduction for single chamber operation

In a single chamber reactor a critical issue is boron contamination of the intrinsic layer after deposition of the boron-doped p-layer, even when using thermally-stable TMB (trimethylboron) as the boron source gas. Many different scenarios were evaluated for their effectiveness in inhibiting boron contamination without damaging the final solar cell. Sandwich structures of p- and i-layers were deposited using various interface treatments, and the depth profile of the boron concentration was analysed by secondary ion mass spectrometry (SIMS).

It was previously seen, a simple flushing of the reactor with gases such as argon, hydrogen, and oxygen is not effective in reducing the contamination. The origin of the contaminating boron was checked not to be from outgassing of physisorbed TMB, nor from the boron in the p-layer of the film itself. A in situ oxidation process developed at IMT Neuchâtel strongly reduces the boron contamination compared to a single short pumping period. A unique gas treatment, recently discovered at the CRPP, also eliminates boron contamination and will provide an effective solution to the contamination problem, provided tests currently underway assure that the final cell performance is not adversely affected. To conclude, various innovative

* The work described under this section was not performed within the frame of the Association Euratom – Confédération Suisse.

techniques have been developed to avoid the contamination, and the method to be finally used will depend on the preference of the industry.

Deposition rate and quality of the intrinsic layer

Another key point was to increase the deposition rate. It was found that higher rates are accompanied by an increase in film porosity, which appears to be linked to excessive degradation of the cell efficiency. Ellipsometry was shown to be sensitive to the residual porosity in the high density range appropriate for solar cells, and this diagnostic technique was used for quality control of the films. A previous observation was that the i-layer density is principally determined by two parameters: the substrate temperature and the deposition rate. Since then, a systematic comparison has shown that the film density also depends on the substrate surface roughness. The physical reason for this is most likely due to shadowing effects and inhibition of surface mobility of radicals during film growth. This is an important issue since quality control is usually performed on silicon wafers, whereas the final solar cell is generally produced on glass, coated with rough transparent conducting oxide to enhance light trapping. Studies are underway to determine whether the degradation of the final cell is also linked to the roughness of the substrate surface via the porosity effect.

2.7.2 Plasma spraying

Low Pressure Plasma Spraying (LPPS) or Vacuum Plasma Spraying (VPS) make use of plasma torches operated inside a vessel under reduced pressure. In contrast to Atmospheric Plasma Spraying (APS) these processes offer the advantage of a controlled atmosphere to avoid oxidation or contamination of the powders and sprayed deposit. This also allows an extension of the specific operation parameter space by controlling the chamber pressure.

At lower chamber pressure (below 10mbar), the plasma jet exhibits unconventional behaviour related to very weak collisionality and large dimensions. In this regime a new process (LPPS Thin Film) has been shown to rapidly deposit thin dense layers of metals or ceramics over large areas.

The plasma gun investigated is a Sulzer Metco F4-VB gun with different conical nozzles. It is mounted inside a $2m^3$ vacuum vessel and the vessel pressure is regulated in the range 2–100mbar by means of a 3-stage pumping system. A modified enthalpy probe system is used to measure the stagnation pressure and enthalpy in low pressure plasma jets. The operating parameter range investigated is 400-600 A current, 40–60SLPM Ar flow and 2–100mbar chamber pressure.

During this 3rd year of the project, advanced diagnostic techniques were specially developed to characterise the plasma jet flow at the lowest pressure range. In particular, the use of double electrostatic probes and Mach probes has allowed the measurement of key plasma jet properties, such as the Mach number, electron density and temperature.

Investigation of different nozzle geometries

Several investigations using plasma jet imaging have been conducted to determine the effect of the nozzle shape and dimensions on the flow characteristics in terms of aerodynamic equilibrium with the surrounding chamber atmosphere, positions of the shock waves, and optimum operating pressure. All the nozzles investigated have been equipped with pressure taps to measure the static pressure at the exit and inside the nozzle. These pressures are important parameters to optimise the flow characteristics (design pressure). This led to recommendations for the various specific spraying processes, requiring either high enthalpy and moderate velocity for the spraying of ceramics, or moderate enthalpy and velocity for low melting temperature metals like copper.

Imaging of the plasma jet has also been extensively used to show up the jet flow structure (shocks and successive compression/expansion zones) for different operating pressures, gas flows and currents. These images have been used to identify the regions with the strongest variations of the jet properties, to be further investigated with other local, quantitative diagnostics such as enthalpy or electrical probes or emission spectroscopy.

Electron density and temperature and Mach number from electrostatic probes

For the characterisation of plasma jets expanding at the low pressure range (1–40mbar), two dedicated measurement techniques based on small electrical probes have been developed: the double Langmuir probe and the Mach probe. These techniques are usually used in low density plasmas, but rarely in thermal plasma jets because of the high heat load and highly collisional regime. However, these can be used in our plasma jets provided that the pressure is low enough (below 40mbar).

The double probe is made of two small cylindrical tungsten rods (0.15mm diameter, 1.5mm long). The rods are mounted parallel to each other, separated by 1mm, their axes perpendicular to the plasma jet axis. The current circulating between the probes immersed in the plasma jet is measured as a function of the probe voltage difference. The probes are quickly swept radially throughout the plasma jet by a rotating arm with calibrated position to obtain radial profiles. A suitable theory for electrostatic probes in plasmas is used to infer the electron temperature and number density profiles from the current-voltage characteristics.

The Mach probe construction is similar, except that the two probes are mounted with their axes perpendicular to each other. Therefore one probe is parallel to the plasma jet flow, the other being perpendicular. Each probe is polarised at the same potential in the ion saturation current region of the Langmuir characteristic. The ratio of the currents collected by the two probes is measured and allows us to determine the ion Mach number of the plasma flow. Figure 2.7.1 shows a drawing of the two kinds of probes.

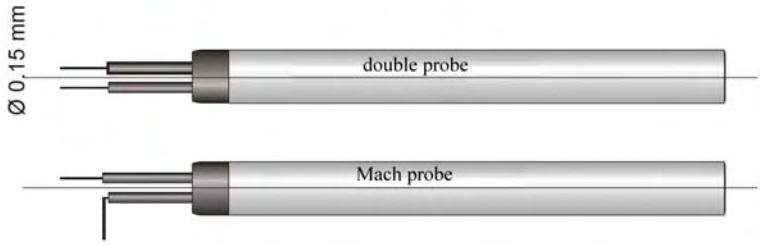

Fig. 2.7.1 *Double probe and Mach probe construction*

Extensive mapping of the plasma jet Mach number, electron temperature and density profiles has been performed for different chamber pressures between 2 and 40mbar and various torch currents and argon gas flows. Figure 2.7.2 shows Mach number radial profiles at different axial positions in plasma jet at 2 and 10mbar, corresponding to the middle of successive expansion/compression zones. This shows how the jet flow accelerates in the expansion, where thermal energy is converted into kinetic energy, and slows down in the compression zones due to the opposite effect.

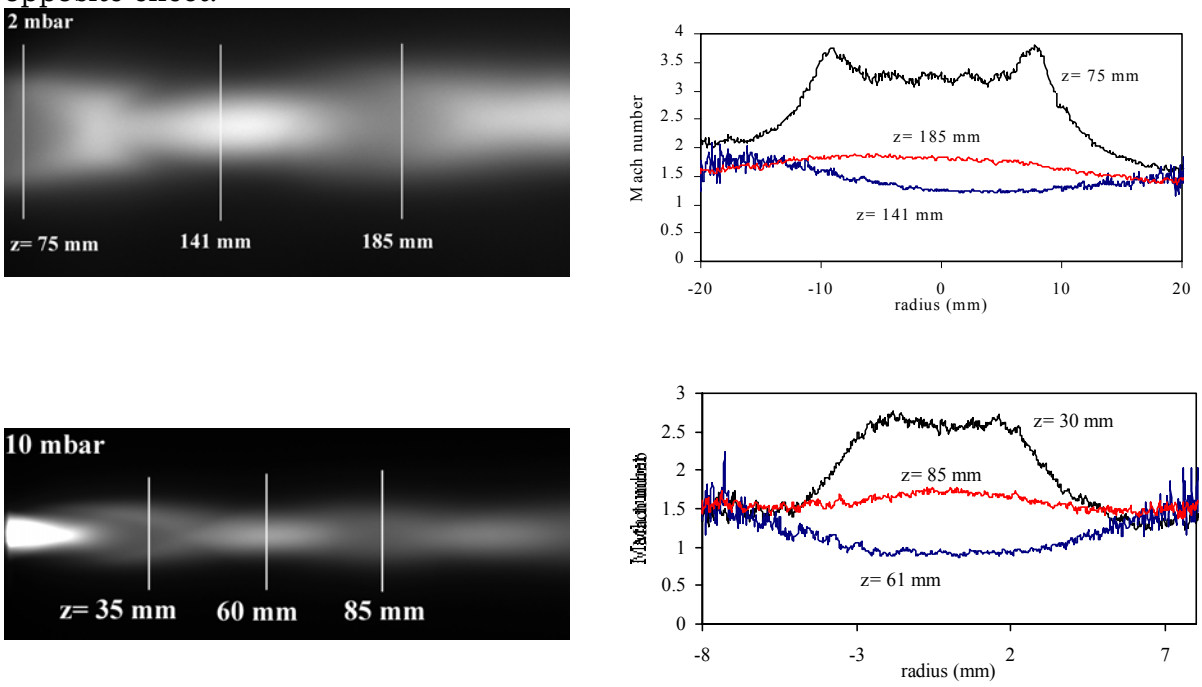

Fig. 2.7.2 *Plasma jet image at 2 and 10mbar and Mach number profiles obtained with the Mach probe at the axial positions shown on the image.*

The electron density and temperature radial profiles, obtained from the double probe at the same axial positions are presented in Fig. 2.7.3. This reveals that the electrons are also compressed and heated up as the flow slows down in the compression zones.

These results, combined with the optical emission spectroscopy data described below, contributed to improve the understanding of the supersonic plasma jet behaviour at very low pressure. They are used to demonstrate the non-applicability

of the enthalpy probe technique for low pressure jets (below 40mbar), because they allow to quantify the deviation from the LTE.

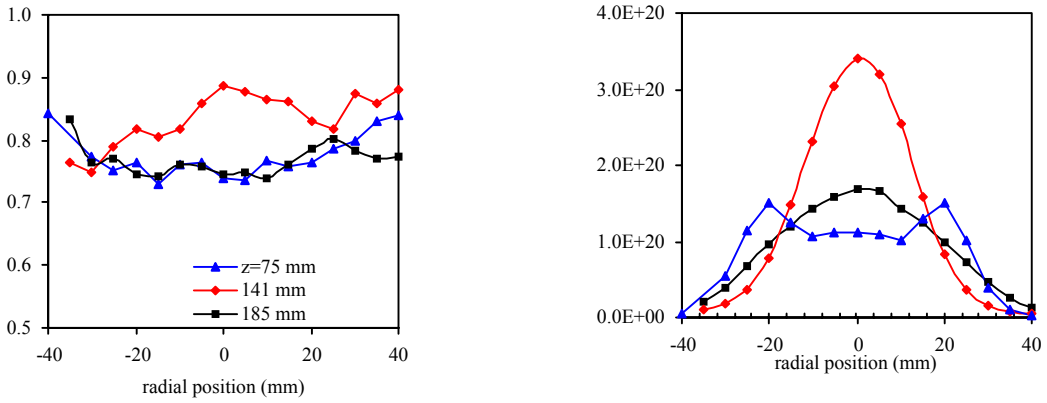

Fig. 2.7.3 *Electron temperature (left, degrees Kelvin) and density (right, m^{-3}) radial profiles throughout the successive expansion/compression zones of Fig. 2.7.2 (argon plasma jet at 2mbar).*

Optical emission spectroscopy

Special optical emission spectroscopy techniques have been developed and used to characterise the non-LTE plasma jets at low pressure. Here, the standard techniques based on the ratio of different spectral lines or line to continuum, to infer the plasma temperature or density, are no longer applicable. This is why we used line broadening measurement techniques, which do not rely on the LTE assumption. Two broadening mechanisms are dominant and can be exploited in these kinds of plasmas : Doppler broadening due to the thermal motion of the emitting species (excited atoms of argon or hydrogen), and Stark broadening due to the micro-electric fields from the surrounding charged plasma species (ions and electrons), which modify the energy levels of the emitting species. Suitable theories can be applied to determine the heavy particle (ions and neutrals) temperatures from the Doppler width, and the plasma density from the Stark width. Both techniques are not applicable simultaneously throughout the whole pressure range, because Stark broadening dominates at elevated pressures (or densities) and masks the Doppler broadening, which can only be shown up and used at low pressure (or density). In the intermediate pressures (2–10mbar) and in certain regions of the jets, the spectral line shapes can be numerically deconvolved to extract the respective Doppler and Stark widths.

Profiles of the plasma jet temperature and density have been done for different operation pressures and compared with the results of electrostatic probes. Figure 2.7.4 shows axial profiles of the heavy particle temperature and electron density for a 2mbar argon/hydrogen plasma jet. This shows the strong density drop in the first expansion at the nozzle exit and the consecutive density increase in the normal shock around z=150mm.

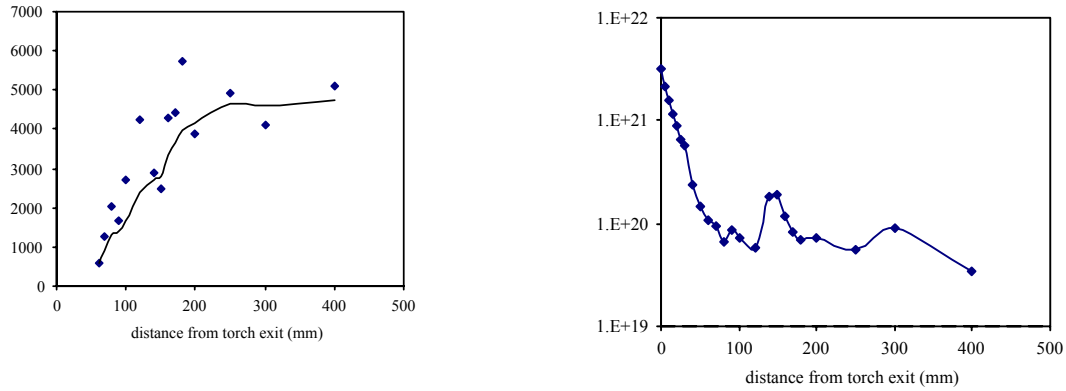

Fig. 2.7.4 *Heavy particle temperature (left, degrees Kelvin) and electron density (right, m^{-3}) axial profiles for a plasma jet at 2mbar (600A torch current, 60SLPM argon, 1SLPM H_2 flows).*

Enthalpy probe

The low-pressure enthalpy probe system has been further improved by the addition of a second heat exchanger. It is now able to sustain the very high heat loads produced by the high enthalpy LPPS plasma jet in spraying conditions using either a mixture of argon and hydrogen or of argon and helium. A new design of enthalpy probe tips for the "high" pressure range (around 100mbar) has been done, the probes have been constructed and tested on the LPPS spraying booth at Sulzer Metco. These new probe tips have the special feature of a large diameter core for increased sample gas flow with a smaller diameter at the tip for improved spatial resolution (Fig. 2.7.5).

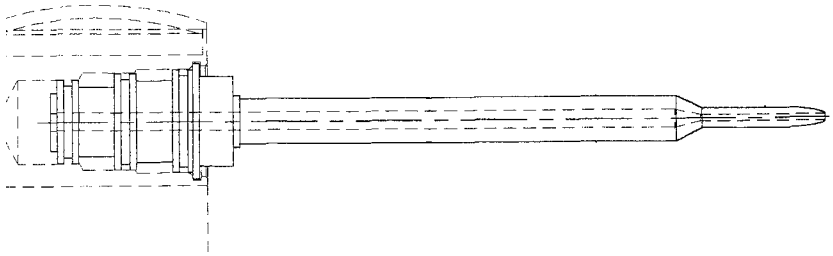

Fig. 2.7.5 *Two-step enthalpy probe tip used for the high pressure range.*

These new probes have been used to characterise the plasma jet of the new Sulzer Metco process at 100mbar for the spraying of ceramics.

The interpretation of the enthalpy probe measurements has been carried out with the help of further improvements of the iterative numerical calculation technique, developed at CRPP, for the case of supersonic jets. In particular, the local static pressure in the free jet is determined indirectly, from the measurement of the static pressure after the shock in front of the probe tip. This has been made possible by numerical simulations of the stagnation process at the probe tip, within the framework of a collaboration with Prof. Bertrand Jodoin (Mechanical Engineering Dept., Ottawa University, Canada).

Perspectives

The experimental characterisation of LPPS plasma jets, carried out in the framework of the present project, has produced physically significant results, which can be used as input for future modelling of the spraying processes. These are required for a more complete understanding of the phenomena involved. In particular, the plasma-particle interaction modelling (acceleration and heating of the powders, and plasma cooling and slowing down by the particles) requires detailed knowledge of some key plasma flow properties, such as jet velocity and specific enthalpy, which have been measured here.

On the other hand, immediate benefits to the present LPPS processes can be obtained from the plasma jet characterisation performed in this project. For example, the optimum spraying distance can be determined, taking into account the balance between the heat load to the substrate, and the heat and momentum transferred to the sprayed particles. Other recommendations for an improved spraying efficiency can be made, regarding the effect of the operating pressure and the nozzle geometry on the uniformity of the plasma jet properties. Strong deviations from an aerodynamic equilibrium of the jet with the surrounding atmosphere lead to shock waves which scatter the sprayed particles and result in poor deposition efficiency and bad layer properties.

2.7.3 Design of a new large area high density source (HDS)

Plasma processing, whether film deposition or etching, is generally more efficient when using high density plasmas. Such plasmas can be obtained using high power inductively-coupled plasma (ICP) at 13.56MHz, or by microwave discharges working at an excitation frequency of 2.45GHz. However, these sources are not suited to large-area plasma processing of solar cells or flat panel displays. Conventional 13.56MHz large area RF parallel plate sources cannot be operated at higher power levels because higher sheath voltages lead to ion bombardment damage of the material.

An alternative way to achieve high density plasmas consists of using very high RF excitation frequencies while keeping the design similar to parallel plate reactors. Much higher RF power can be coupled into the plasma while keeping a moderate sheath voltage thus preventing substrate damage. The problem is that, as the frequency increases, the RF quarter wavelength becomes comparable to typical reactor dimensions, causing standing wave non-uniformities. We have demonstrated that a solution of Maxwell's equations for specially shaped electrodes suppresses this non-uniformity even when the lateral dimension of the reactor becomes comparable or larger than a quarter wavelength. The main aim of the present work is to verify this theory experimentally and to finish up with a new industrial high density plasma source for deposition and etching purposes.

The first step was to construct a cylindrical reactor (whose geometry lends itself to an analytical solution of the electromagnetic fields), vacuum chamber and associated RF matching circuit and stripline. Secondly, the RF electric field in the reactor was mapped out by means of a probe, and found to agree with the theoretical values. Possible perturbations due the presence of imperfect dielectric substrates were also quantified. The next step, currently underway, is to verify that the plasma density and temperature faithfully reproduce the uniformity of the

electric field. With this aim, special arrays of fibre optics and ion flux probes were installed in the electrode surface. Initial problems of parasitic plasmas, which can ignite in very small gaps at these high frequencies, were solved by plugging all volumes with Teflon. Following this, intense edge plasma due to fringing fields at the RF and ground electrode boundaries have been mostly solved by constructing symmetric electrode sidewalls, and further experiments are being carried out. Parallel to this, the design and construction of a large area rectangular reactor with numerically-designed shaped electrodes is underway for etching and deposition tests.

2.7.4 Plasma diagnostics for the electrical discharge machining (EDM)

The main aim of the TOPNANO 21 project is to increase the basic understanding of electrical discharges during machining. Application of plasma emission spectroscopy was chosen as the starting plasma diagnostic method in order to obtain first indications on the plasma parameters of the discharge.

In collaboration with Agie-Charmilles SA a small EDM machine dedicated to plasma investigation was designed and constructed. A lot of care was taken in the design of the lab device for the required flexibility for diagnosing the plasma, in particular to access of the optical fibre for plasma emission spectroscopy. Aside from this particular feature, the device can run with the same machining parameters as the commercial machines from Charmilles SA. The discharge current, current form and the on/off time are computer controlled. The simple construction of the electrode arrangement allows easy positioning of the optical fibre and as well easy replacement of the electrode itself. The dielectric (oil or water) can also easily be changed, thus giving the possibility to investigate the influence of different dielectrics. Figures 2.7.6 and 2.7.7 show the constructed Lab-EDM device from Charmilles SA installed at the CRPP.

Fig. 2.7.6 *Lab-EDM device*

Fig. 2.7.7 *Electrodes and fibre optics*

After delivery of the Lab-EDM machine to the CRPP, the device was equipped with a quartz fibre which transmits the emitted light from the discharge to a monochromator. This 0.275m monochromator works in the visible with wavelength from 300nm-900nm and is equipped with a sensitive CCD camera. Furthermore a differential voltage probe and a high frequency current probe allow simultaneous, accurate measurements of the discharge voltage and current (Fig. 2.7.8.).

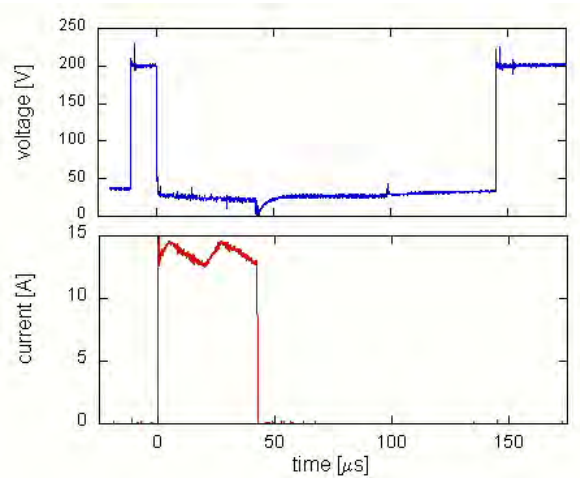

Fig. 2.7.8 *Voltage and current during an EDM discharge*

The first light emission spectra of the EDM discharge plasma have been obtained. Figure 2.7.9 shows a typical plasma emission spectrum obtained by integration over several seconds. In the present case, a copper anode and a stainless steel cathode immersed in the oil dielectric were used. The spectrum in Fig. 2.7.9 clearly shows that the plasma discharge is contaminated by both electrode materials. The atomic hydrogen line and the strong hydrogen continuum most probably originate from the completely cracked oil which was used as dielectric in the present case.

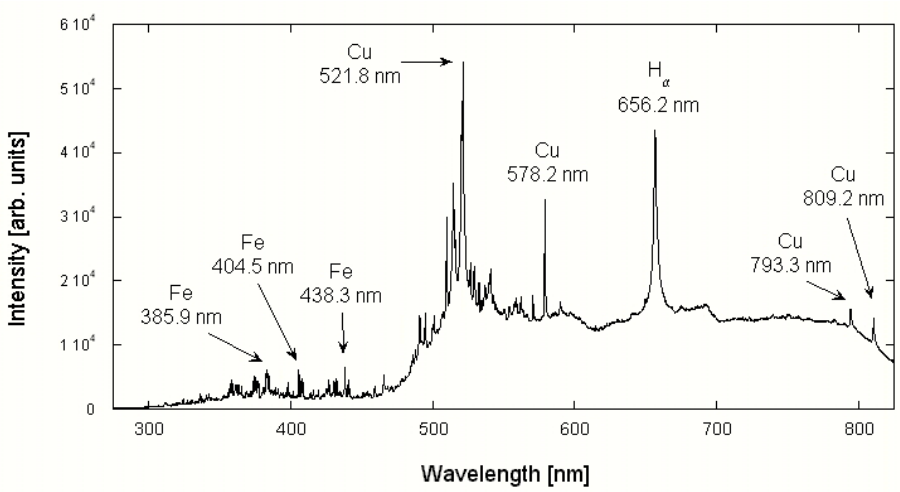

Fig. 2.7.9 *Emission spectrum of EDM discharges*

Assuming local thermal equilibrium, the electron temperature can be determined from of the ratio of different copper lines. Typically, an electron temperature of 0.75eV was found. Astonishingly, only the H_α line is detected in the hydrogen Balmer line series with the H_β and H_γ lines completely absent. The H_α line shows considerable broadening (Fig. 2.7.10.a) resulting from interactions between the excited hydrogen atoms and the background ions and electrons (Stark effect). The electron density can be estimated from the line broadening. In the case of the EDM discharge high electron densities (Fig. 2.7.10b) of the order of 10^{18}-10^{19} cm^{-3} have been obtained.

It is planned to continue the time-integrated measurements of the emission spectra. In particular the dependences on the process parameter and configuration (dielectric) will be investigated. Time-resolved spectroscopy measurements are also planned for next year.

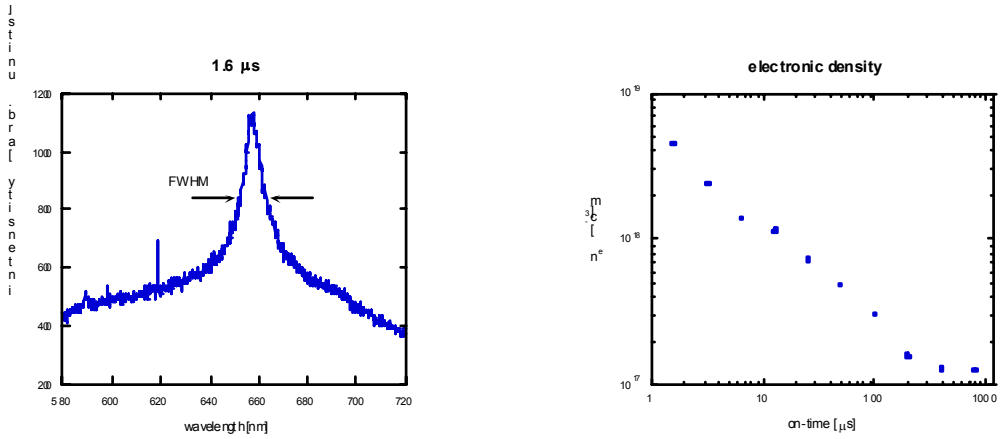

a) b)

Fig. 2.7.10 *a) Stark broadening of the H_α line in the EDM discharge.*
b) Electron density vs plasma on-time as determined from Stark broadening

2.7.5 Atmospheric plasmas for thin film coating

During the year a new CTI project on investigating atmospheric plasmas has been accepted and started. Avoiding vacuum technology for depositing coatings on polymer films is certainly one possible route to cost reduction. Vacuum technology has several economical drawbacks: the process for coating deposition is not continuous, the machine has to be stopped and opened for loading and unloading film reels, and the pumping down time is tightly linked to the pumping speed and cleanliness of the pumping system. The maintenance of equipment in a production status is costly and time consuming. Plasmas at atmospheric pressure are thought to be an alternative for the production of coatings for various applications.

However there are different problems related to RF plasmas at atmospheric pressure. First of all, the applied RF voltage must be in the kV range, giving rise to considerable problems in the design and construction of the RF generator, circuit and of the RF electrodes. RF plasma discharges at this pressure often show a discharge consisting of many different discharge filaments similar to the one observed in the so-called silent discharges. However, under certain conditions a uniform plasma can be obtained, required for uniform film deposition. The control of the discharge type is one of the difficulties in atmospheric RF plasma applications. The control parameters for the discharge transition are the plasma excitation frequency and the electrode gap distance.

In the new CTI project the parameters to be varied are the working pressure, gas flux, excitation frequency and electrode gap distance to establish a stable glow discharge which yields fast deposition of good quality films, in particular SiO_x films. As well as an optimal choice of the electrode insulation material, particular attention must be paid to impurities. It is well known that impurities from the

electrode material have a considerable influence on the discharge type. Different gas mixtures shamustll be tried since the addition of gases with metastable states is considered essential for obtaining a discharge which fills the whole discharge volume. The importance of the metastable states lies in the fact that their high excitation energies lead to Penning ionisation. This induces additional ionisation and increases the ionisation coefficient, in particular at low p·d "Paschen" products.

Preliminary experiments showed that high powder production takes place in an atmospheric RF plasma for the deposition of SiO_x. This powder formation currently limits the application of the atmospheric RF plasmas.

As plasma diagnostics, optical emission spectroscopy, infrared absorption spectroscopy and, if possible, mass spectrometry, will be applied to the RF plasma. The films obtained will be analysed ex-situ by AFM (atomic force microscopy), permeation measurements and other material characterisation methods if necessary.

2.7.6 Nano powder synthesis by thermal plasmas

In the frame of TOPNANO 21, a project has been started on the nano-powder synthesis in thermal plasmas in collaboration with the EMPA in Thun. The project will contribute to the understanding of nanometer-sized powder formation and production in RF thermal plasmas through a multidisciplinary approach involving material scientists (EMPA-Thun) and plasma physicists (CRPP-EPFL).

In recent years, several methods have been studied to produce nano-sized particles of metals or ceramics. As well as colloidal precipitation and mechanical grinding, various plasma processes and in particular RF plasmas have been shown to have a high potential and flexibility for manufacturing nano-particles with different morphologies and compositions. For many potential industrial applications (ceramics, catalyzers..) controlled, high-rate synthesis of nano-powders is needed. Controlled powder synthesis includes uniform particle size, composition, morphology and, in particular for metallic nano-powders, also contamination (oxidation) free processing.

Thermal reactive plasmas are used in ultra fine particle synthesis and coating deposition. In ultra fine particle production gaseous or liquid reactants are injected into the plasma, or solid material is evaporated in the thermal plasma. The species produced in the plasma react with the plasma gas or the quenching gas in the condensation region of the reactor. The high cooling rate due to the quenching guarantees homogeneous nucleation.

The project triggered the development and application of *in situ* powder monitoring techniques during non-oxide nano-powder processing in inductively coupled RF plasmas. To produce the nano-powders with the desired properties and high reproducibility it is necessary to understand the interior of the plasma where reactions between powders and different plasma components take place. In the thermal reactive plasma, and in the following quenching area of the plasma reactor, different chemical reactions and physical phenomena may influence the formation and growth of the nano-powders. These reactions and phenomena include phase transformations, particle melting, evaporation and recondensation just to name a few. In addition particles in the plasma will also chemically react with the injected gases. Depending on the kind of gases and their flow, different chemical reactions

between molten particles and the gas molecules are expected to occur. As well as the temperature of the plasma, the heat flow might play a significant role in the formation and distribution of the nano-powders. In this project the fundamental study of these chemical, physical and thermal reactions and phenomena in the plasma will be carried out by applying various *in-situ* particle monitoring methods.

A very important goal of the project is to monitor *in situ* the nano-particle formation by various *in situ* particle diagnostic methods. We aim to understand the nano-particle production and growth mechanism in such a device and to develop *in situ* process monitoring for nano-particle processing in thermal RF induction plasmas. *In-situ* diagnostic methods are of prime importance to guarantee high purity, good dispersion and ultra fine size.

The project started late in 2002 and the first experimental work will take place at an existing inductively coupled RF plasma device at EMPA in Thun, whereas it is planned that the CRPP will design and apply different plasma and particle diagnostics.

2.7.7 Plasma induced surface modifications for biomedical applications

Different studies on surface modifications for biomedical applications have been performed in a CTI project in collaboration with Prof. H.J. Mathieu from the Laboratoire de métallurgie chimique (LMCH) of the Faculté STI Sciences et Techniques de l'Ingénieur.

RF plasmas are widely used to modify and functionalise surfaces, in particular polymer surfaces. The modifications mainly looked for are hydrophilic or hydrophobic surfaces, frequently needed in biological or medical applications. The desired surface modifications can be obtained by noble gas plasmas (Ar or He) often admixed with reactive gases such as oxygen. One of the big problems in transferring the plasma process for surface modifications of polymers to an industrial scale is that the basic plasma and relevant process parameters are unknown in most of the cases and little precise literature is available. The aim of the present project is to diagnose the RF plasma used for surface modifications of polymers for biomedical applications in great detail in a collaboration with Prof H.J. Mathieu. For this reason various commercial plasma diagnostic methods are being applied to processing plasmas.

As well as the electrical parameters of the discharge such as bias voltage, RF power and amplitude, process relevant plasma parameters such as the type of bombarding ions and their ion energy distribution are monitored. Basic quantities such as the fluence and dose of the impinging ions on the polymer surface is of great importance for reproducing the surface modifications in other larger plasma devices. The results obtained are correlated with different surface relevant parameters of the polymer used, such as the contact angle and, if available, the composition changes of the polymer surface obtained from XPS measurements.

In addition, another biomedical application of plasma treatment has been worked at in the framework of this collaboration. *Pseudomonas aeruginosa* is one of the most prevalent bacterial strains in a clinical environment, responsible for 30% of nosocomial pneumonia cases occurring in intubated and mechanically ventilated patients. Colonisation of the intubation device leads to mortality for over 40% of these cases, despite aggressive antibiotic therapy. Therefore, a strategy to reduce

bacterial adhesion to intubation tubes would be a breakthrough. This project investigates a method to prevent protein adsorption and eventual bacterial adhesion, as protein adhesion is believed to be a key event responsible for specific adhesion of bacteria to a surface. The strategy is to mask the PVC substrate with a chemically inert Teflon-like fluoropolymer layer deposited by plasma, which serves as an ideal platform for further surface modification due to its low surface energy properties. By exploiting hydrophobic-hydrophilic interactions, we then bind protein and bacterial resistant molecules to the fluoropolymer film. The films are deposited in an RF plasma reactor, using C_2F_6 as a precursor and H_2 as a carrier gas. The PVC substrates were $1cm^2$ sections cut from endotracheal tubes, which were flattened to allow subsequent microscopic counting of bacteria. XPS analysis and contact angle measurements confirms Teflon-like films are capable of producing surfaces resistant to protein adhesion. As protein adhesion is believed to be the triggering event in the inflammatory response and eventual failure of biomaterials, this method could prove to be critical in creating anti-fouling surfaces.

2.7.8 Modelling of industrial plasmas

In collaboration with Unaxis a new project on the modelling of industrial plasmas has been elaborated and proposed to the CTI.

During the last decade, the substrate size used for the fabrication of thin-film-transistor-liquid-crystal-display (TFT-LCD) has increased from about 0.5m diagonal length to about 1.5m with a time interval of about 2 to 3 years between each substrate generation, and this growth will continue to about 2m diagonal length for the next substrate generation. This growth is motivated by the fact that larger individual displays are now produced and that it is more economical to produce several displays on the same substrate. At the same time, the specifications for the thin film used such as the thickness and composition uniformity over the substrate area have been maintained or even increased.

Up to now, the development of each reactor generation has essentially been empirical, based on the experience acquired with the preceding reactor generation. Due to the larger size of the present reactors, it becomes more and more costly and time consuming to develop a new reactor generation, especially if technological innovations have to be tested and introduced to reach the required specifications. The aim of this project is to develop numerical models for large area PECVD reactors, first to reproduce the performance of the existing equipment, essentially the deposition rate and film composition uniformities over the substrate area, and then to predict the performance and to evaluate the effect of potential innovations on the uniformity for the next still larger reactor generation.

Over the last 20 years, the development of PECVD applications has been followed by the development of numerical modelling techniques for the plasma physical properties and gas phase chemistry and flow. These numerical modelling techniques have now been integrated into commercial packages such as CFD-RC which could in principle be used to model commercial PECVD equipment. However, the use of these commercial packages still requires considerable effort and development together with deep knowledge of the numerical methods to model specific equipment and processes. The main technical and scientific goals of this project are to apply and develop these numerical models for large area PECVD equipment. The main objective of these calculations will be the prediction of the deposition rate and film composition profiles over the substrate area for a given

reactor geometry and process condition. These two parameters are the most important for the reactor performance and can also be directly compared with experimental measurements. The different points that have to be treated to reach this goal are modelling the working gas injection into the plasma reactor, modelling the gas phase chemistry for the different processes used (essentially, deposition of a-SiN:H (amorphous silicon nitride film) or a-Si:H (amorphous silicon film) and μc-Si (microcrystalline-silicon film)), and modelling the plasma physical properties. Special effort will be concentrated on the validation of the models by comparing the numerical results with experimental results performed in existing PECVD large area equipment.

2.7.9 Other collaborations and industrial mandates

Several industrial mandates have been carried out during 2002. These mandates essentially involved basic research and development of new processes or improvement and control of existing plasma processes. However it has been agreed with the different industries to keep the contents of these research activities confidential.

Numerous industries consulted the CRPP during the last year and this resulted in many small experiments and tests which have been carried out on the existing plasma reactors at the CRPP.

At this point it should be added that the collaboration with industry is excellent and a high degree of confidence between the collaborating industry and the plasma processing group exists. This working atmosphere is extremely stimulating for both PhD students and senior physicists.

3 TECHNICAL ACHIEVEMENTS OF THE CRPP IN 2002

3.1 TCV operation

During the period covered by this report, TCV did not undergo any planned shutdown. In March 2002, operation was interrupted for two weeks following a minor air inlet implying a short intervention and a vessel baking. Apart from this incident, no major problem was encountered.

During operational periods, TCV was run on a basis of three weeks of scientific operation followed by one week of maintenance. Statistics in term of successful plasma shots are reported in Fig. 3.1.1.

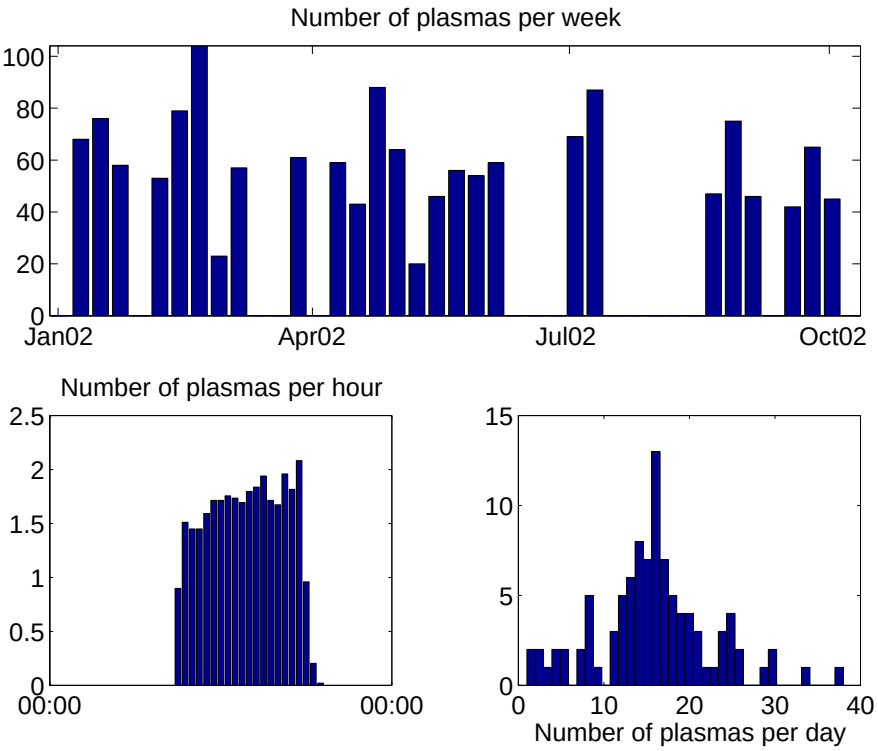

Fig. 3.1.1 *Statistics of TCV operation from January 2002 to October 2002.*

3.2 TCV diagnostics

The regular upgrading of TCV diagnostics has continued over the last year with a greater emphasis on improving the quality of existing measurements to satisfy the demands of present and future physics programmes. Many of these diagnostics require considerable study of their design and feasibility before implementation and installation on TCV. Since the material and manpower costs of these improvements is often high, possible solutions are often tested on TCV for a short operational

period before a major change is implemented. In this light, an increasingly larger proportion of the diagnostic enhancements are part of a longer term design.

3.2.1 Magnetic measurements

Together with the magnetic probes and flux loops for equilibrium reconstruction and MHD measurements, a Diamagnetic Loop is mounted on TCV. This measurement of the linked flux, when compensated for externally imposed magnetic flux, gives a measurement of the stored plasma energy as a function of time. Several compensation coil measurements have been constructed and are now used to extract the plasma energy component of the DML flux from the initial measurement for a wide range of plasma configurations. A method based on the temporal variations of the diamagnetic flux of the plasma during Modulated Electron Cyclotron Heating (MECH) has been developed and was first used to measure the absorbed power with X2 ECH, Fig. 3.2.1.

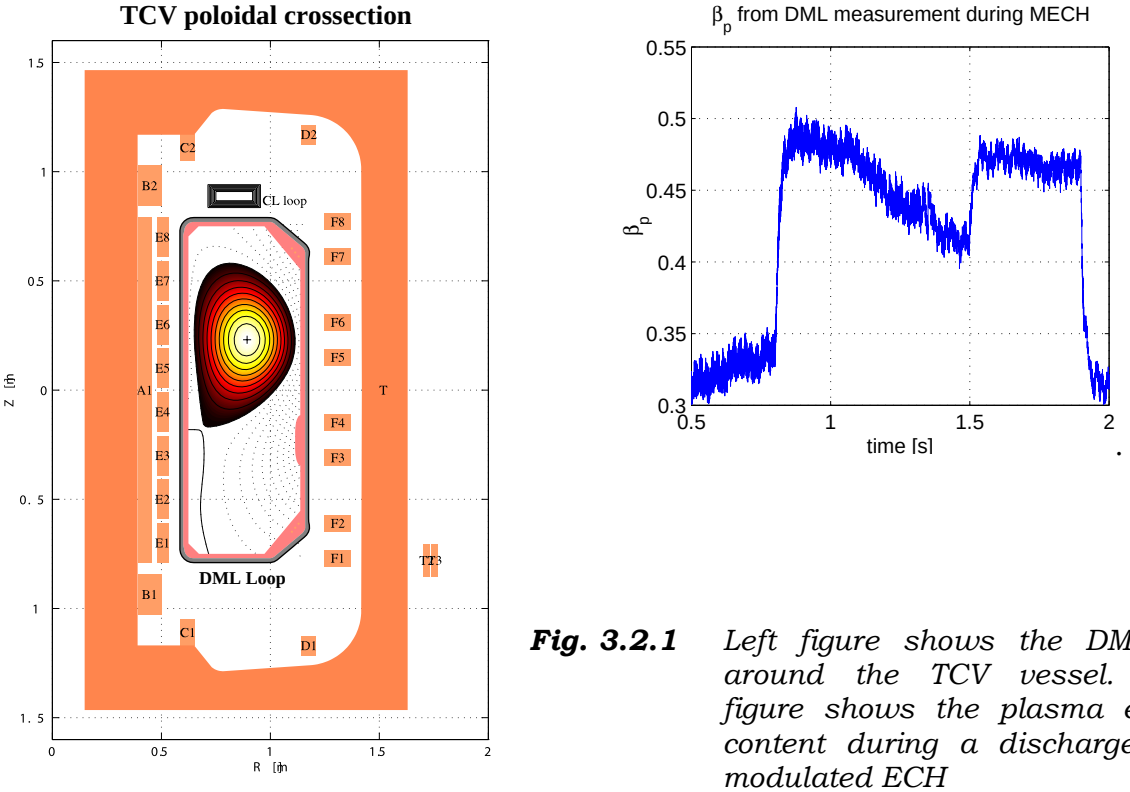

Fig. 3.2.1 *Left figure shows the DML coil around the TCV vessel. Right figure shows the plasma energy content during a discharge with modulated ECH*

This diagnostic was used to measure X3 absorption, showing that full single-pass absorption of the injected X3 power was achieved with the X2 pre-heating in co-current drive.

3.2.2 Thomson scattering

The set of 3 Nd:YAG lasers was replaced by new, more powerful models during the TCV shutdown period at the end of 2002. With these lasers, the single pulse energy is a factor of 2 higher, which will result in a substantial improvement in signal-to-noise ratio. In particular, measurements on low density EC heated plasmas will benefit from this enhancement.

For measurements of Te and ne profiles near the plasma edge, additional channels with a spatial resolution of ~10mm (instead of 30mm) have been installed, Fig. 3.2.2, as a collaboration with Consorzio RFX, Padova, Italy, including the loan of 9 spectrometers and their data acquisition system. This system has been implemented in summer 2002 and first encouraging results have already been obtained.

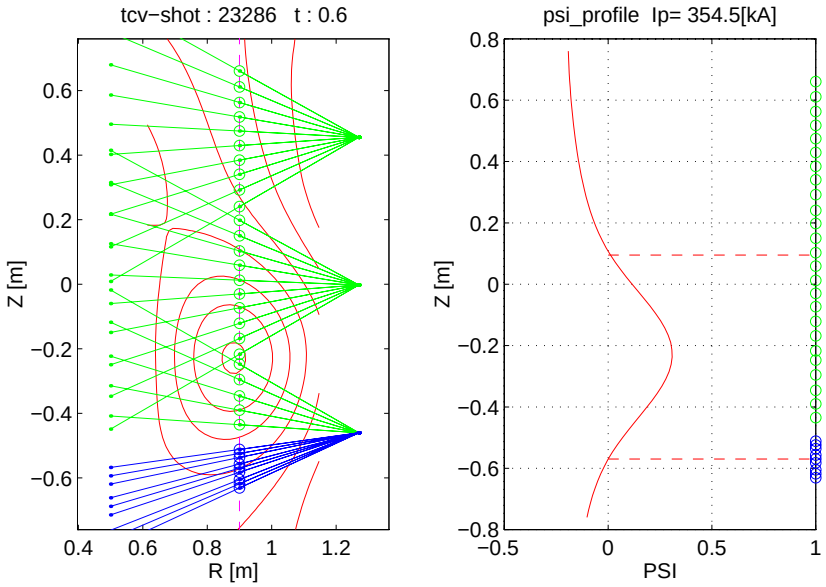

Fig. 3.2.2 *Green lines indicate the current Thomson observation chords and the blue lines the initial positions of the RFX spectrometers. The temperature trace on the left shows the higher spatial resolution obtained in the plasma edge.*

3.2.3 Plasma core diagnostics

Diagnostic neutral beam

Following poor emissivity and an unexpectedly high passive emission from TCV, both the Diagnostic Neutral Beam Injector (DNBI) and the associated spectroscopic diagnostic systems have been upgraded.

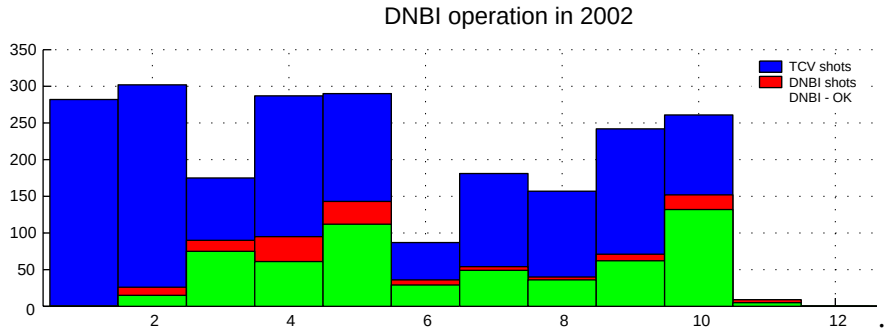

Fig. 3.2.3 *Availability of the DNBI month by month through the 2002 operation period*

In the first stage of the beam upgrade, which was completed in July 2002, the beam current from the source was increased to nearly 2.9A and the beam extraction optics were optimised to maximise the full energy component in the neutral beam. This upgrade included a more powerful plasma source power supply and a new extraction grid assembly. The improved signal-to-noise is illustrated in Fig. 3.2.5. Further improvements to the beams are under discussion with the Budker Institute of Nuclear Physics (BINP) following this upgrade, with the goal of increasing the injected neutral particle density in the region of spectroscopic observation. Improvements under consideration include: further increasing the beam current, improving the beam charge fraction using an arc source, or changing the beam geometry, thus increasing the injected beam density. Recent results from Charge Exchange simulation codes also indicate a possible improvement in beam penetration and spectral line excitation rate by increasing the primary beam energy to ~60keV from the current value of ~50keV.

A new visible spectrometer, designed for charge exchange spectroscopy, is being commissioned at the end of 2002 and features a large numerical aperture, a high reflectivity grating and a specially developed front illuminated CCD detector from Xcam (UK) which is 4x more sensitive than the current back illuminated CCD, Fig. 3.2.5.

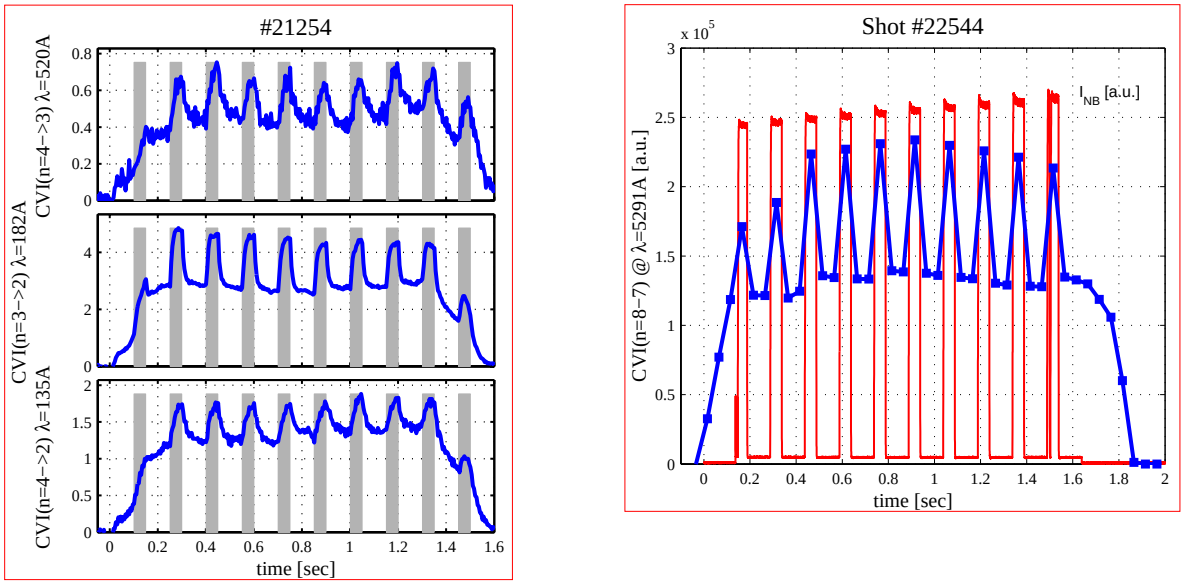

Fig. 3.2.4 *On the left, three spectral line intensity evolutions from SPRED spectrometer observing the neutral beam injection. On the right the integrated intensity of the main visible Charge Exchange excited spectral line after the upgrade was completed. Note the large increase in the line intensity during beam injection (indicated by the blue trace)*

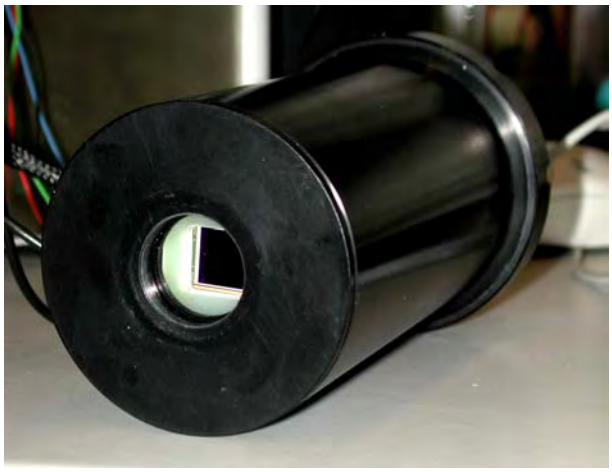

Fig. 3.2.5 *Photograph of the Xcam CCD detector head showing the 1024x1024 pixel front illuminated CCD chip with Peltier cooling. This CCD also features two channel readout and highly flexible programming controlled by an on-board CCD system. Using a parallel acquisition board over 2Mpixels/s can be read into host computer memory (usually following pixel binning of the regions of interest)*

SPRED spectrometer

The SPRED VUV spectrometer test stand was completed and is able to provide an absolute intensity calibration, Fig. 3.2.6. Following some doubts about the focussing of the SPRED, as delivered from the manufacturer, the lamp illumination was scanned across the spectrometer étendue to examine the spectrometer focussing properties. A preliminary 30% decrease of the spectrometer line width has already been achieved and there are hopes of improving this further by better grating alignment and/or an improved detector design.

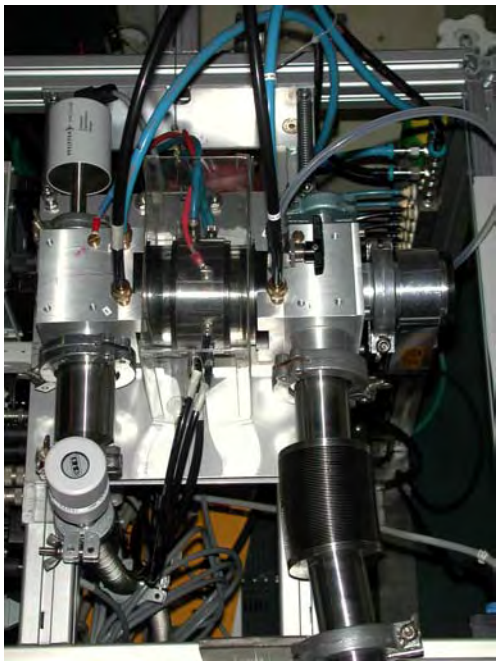

Fig. 3.2.6 *Photograph of the calibration source for the SPRED spectrometer calibration. The lamp itself is in the middle of the image with the gas supply system on the left. On the right is the final pumping system after which the emitted light is directed towards the spectrometer. For calibration purposes the lamp is normally filled with Neon or Helium at a pressure ~1torr and a current of 1-2A applied which requires a voltage ~500V.*

Edge Profiles

Using the method of a separate fibre optic telescope coupled to the entrance slit of an imaging spectrometer, a multi-chord spectrum of the TCV edge plasma region

has been installed, Fig. 3.2.7. Currently this system uses the same spectrometers

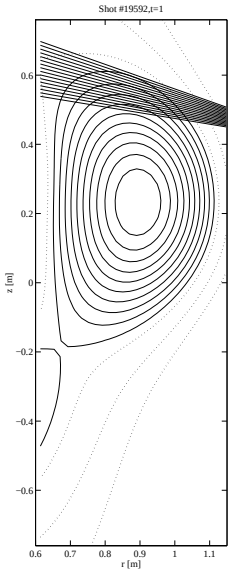

Fig. 3.2.7 *The chords for edge observation are shown for a plasma configuration where H-mode is obtained on TCV*

as the CXRS, already described in the DNBI, as a result of only changing the spectrometer entrance slit optics. In the current arrangement, there are 16 chords observing the outer 30% of the plasma volume. This is intended for experiments during which a strong change in the temperature and density edge profiles are observed such as H-mode transitions. A similar system is still in the design phase for installation in a lower TCV port to observe the spectral emission during plasma detachment.

Soft X-ray Pulse Height Analysis (PHA)

A Roentec Xflash Silicon Drifted diode detector has been tested together with a commercial DSP pulse treatment and histogramming module, (Xia, DXP-2X, USA). Using a high flux Fe^{55} radioactive source, and X-ray tube fluorescence radiation from an Iron or Aluminium target, this combination has demonstrated count rates exceeding 300kHz with 100eV spectral resolution and 2MHz with 800eV resolution. A thin beryllium window is being installed on TCV at the end of 2002 and a filter wheel/aperture control mechanism is under design to hold the diode to observe the TCV plasma along a vertical chord thus permitting data collection from all TCV plasma configurations.

To demonstrate the higher data rate of the DSP signal treatment, the present liquid nitrogen cooled Ge diode detector was operated with the DSP processor. With no other change in the analogue electronics scheme, a maximum count rate of over 100kHz was achieved compared with the previous value of 30kHz, Fig. 3.2.8.

SDD + traditional dedicated analogue electronics

SDD + DXP CAMAC Unit

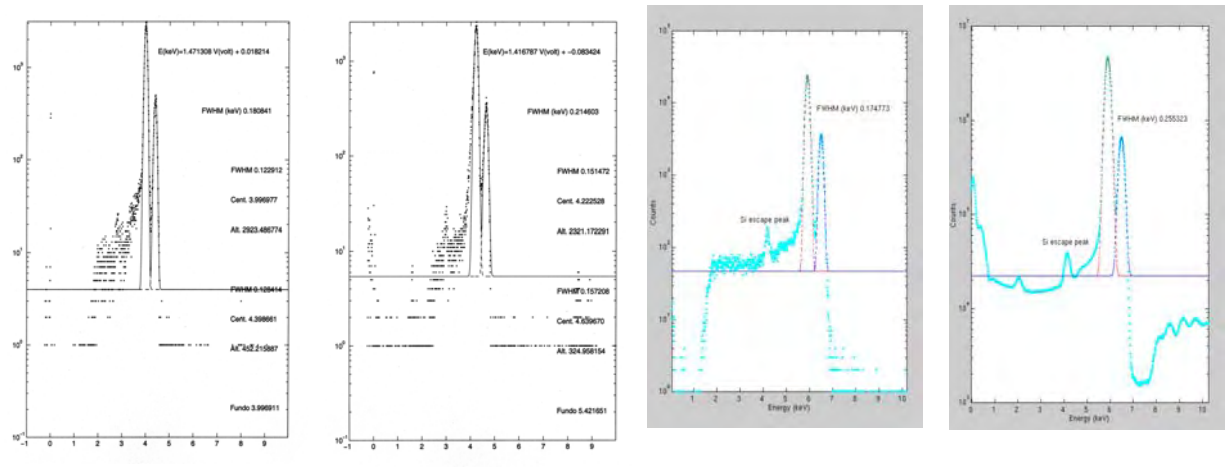

a) Low throughput: 5 kHz
Energy Resolution: 181 eV

b) Maximum throughput: 50 kHz
Energy Resolution: 214 eV

c) Low throughput: 3.7 kHz
Energy Resolution: 175 eV

d) Throughput: 110 kHz
Energy Resolution: 255 eV

Fig. 3.2.8 *Performance spectra of the present PHA diode: a) shows the spectrum with standard analogue electronics; b) IATG electronics (CFN, Portugal); c) performance of DSP system with low signal rate; d) example of acquisition at over 100kHz whilst retaining good spectral resolution*

Rotating Crystal Spectrometer

After a complete vacuum system upgrade of the Bragg crystal spectrometer on loan from the Princeton Plasma Physics Laboratory, it was determined that the MicroChannel plate detectors were not operational. Both sides of the spectrometer are equipped with 3 pairs of rectangular plates in a chevron configuration. Their replacement using up to date MicroChannel plates with enhanced soft X-ray sensitivity with reduced Ultra-Violet sensitivity has been undertaken. This combination will help reduce the problem of scattered Ultra-Violet light within the compact spectrometer body which will in turn increase the available dynamic range.

MultiWire Proportional X-ray detector (MPX)

The Multiwire Proportional X-ray (MPX) detector has been operated on TCV during 2002 and its high spatial resolution has proven useful in the identification of small spatial changes in the X-ray emissivity, especially during ECH mirror sweeps. In order to increase the spatial coverage, the current detector is being remounted closer to TCV and the entrance slit X-ray filter will be changeable remotely. In a later development, a stack of 2 or more such detectors with different working gases and intermediate X-ray filtering will replace this detector providing high resolution spatial coverage with two or more channel X-ray energy resolution.

Impurity laser ablation

The Ruby laser ablation system injection chamber was upgraded and equipped with a CCD camera to observe the injection target, Fig. 3.2.9. This diagnostic uses the 10x20 channel soft X-ray photodiode array to measure the change in X-ray emissivity following light impurity injection. These measurements are supplemented with line resolved measurements from the SPRED spectrometer and in the future from the crystal X-ray spectrometer. Targets of a thin layer of Aluminium and Silicon have been installed and operated on TCV and there is a future possibility of using targets in which small micro-pellets of trace impurity can be injected using the same technique.

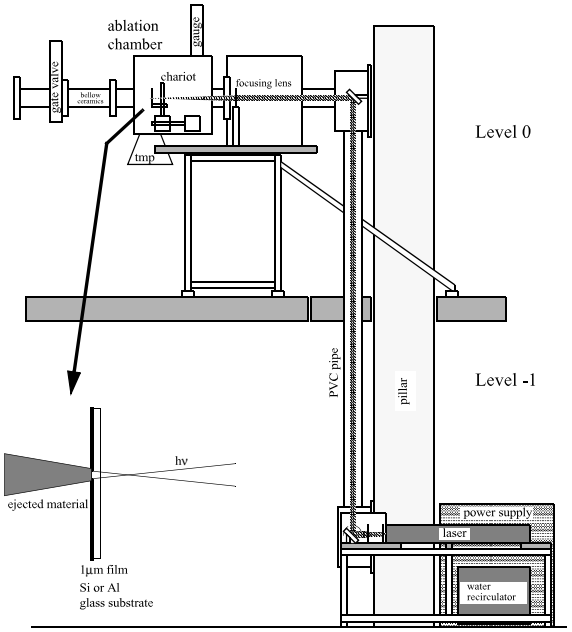

Fig. 3.2.9 *Schematic view of the ablation system. At level -1 of the TCV hall inside the restricted area there are the laser body, the power supply and the cooling water re-circulator. In front of the laser output an optical table is placed. At level 0 the main component is the vacuum ablation chamber, containing the target and its motion system.*

Neutral Particle Analyser (NPA)

Following the observation of a tail and other small features in the emitted neutral particle energy spectrum using the present NPA analyser, have investigated a possible improved diagnostic with the following features: Low sensitivity to magnetic fields, to avoid large magnetic shielding requirements, mass selection to differentiate between working gas (Deuterium) and injected fast particles (Hydrogen) and increased energy range to investigate the slowing down characteristics of the beam particle slowing. A development device (CNPA) from the A.F.Ioffe Physica-Technical Institute, St-Petersburg, Russia, is being considered since it features a compact design, a high detection efficiency with a number of microchannel plate detectors. In this system the deflection is achieved with permanent magnets and the incoming neutrals are ionised (stripped) by a thin carbon foil.

Fast Bolometry (AXUV)

Before the final design of the new 7 camera fast bolometer/ionisation source bolometer array is finalised, the test camera is being equipped with a Lyman Alpha filter at ~122nm, Fig. 3.2.10. This band-pass absorption filter will avoid the

problems associated in more typical Balmer Alpha visible range interference filters where the filter characteristics depend on the incidence angle. The Lyman alpha emission line was chosen because of its strength, and the fact that it is well separated from expected impurity lines from the plasma.

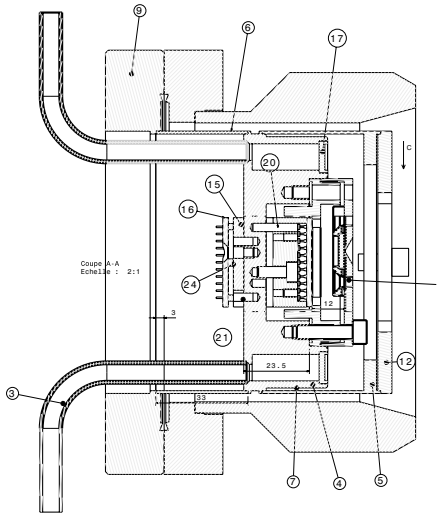

Fig. 3.2.10 *Section of one of the new AXUV camera heads. The plasma radiation enters the camera from the right through an entrance slit onto an unfiltered diode array (bolometer) and an array with an absorption or interference filter (Deuterium radiation)*

3.2.4 Plasma edge diagnostics

Fast reciprocating Langmuir probe

On long term loan from the University of California, San Diego (UCSD), a fast reciprocating Langmuir probe system has been installed on TCV since late 1999 and has provided valuable measurements of scrape-off layer T_e and n_e profiles. The device is a 5 tip system optimised for fluctuation measurements, with coaxial cables right up to the probe tips themselves, allowing fast sweeping and high frequency acquisition rates. Preparations began in 2002 to provide new electronics for turbulence analysis. This will include DSP based electronics and associated amplifiers for real time analysis of the plasma sheath harmonic response to a fast sinusoidal sweep (100-400 kHz) on a single probe tip. Simple combination of these harmonics yields a real-time high frequency measurement of T_e, a rarely available quantity in most fluctuation experiments and important for computation of the cross-field turbulence driven energy flux. A new data acquisition unit was implemented. The system can provide up to 10MS/s for 2 channels, but will be typically used at 6MS/s for up to 8 channels. To improve the measurement quality, the probe head has also been modified this year (Fig. 3.2.11) by shaping the head to match the angle of the separatrix at the probe position for a specific diverted plasma equilibrium of particular interest. When complete, the new system will allow simultaneous direct measurements of the turbulence in particle flux, radial and poloidal electric fields and T_e. Preliminary measurements for the turbulent particle flux and potential fluctuations during ELMs on TCV were obtained just before the machine shutdown in October 2002.

Fig. 3.2.11 *The reciprocating Langmuir probe head following modification in early 2002. The 5 graphite pins are 1.5mm in diameter and mounted in a boron nitride (BN) insulating base, itself protected by a graphite housing. The BN base has diameter 10mm. The probe head is positioned by a slow drive and then reciprocates over a stroke of 15 cm on a fast timescale (~200ms) driven by a pneumatic system under 4bar of helium pressure.*

Fast pressure gauges

Divertor detachment in TCV is anomalous in the sense that under certain conditions it appears to occur at plasma densities that are too low for classic processes of electronic recombination to result in significant ion loss. To complement existing Langmuir probe measurements, and to assist in the significant modelling effort underway to understand this phenomenon, two new in-vessel fast pressure gauges are now functioning routinely. These are ASDEX Type ionisation gauges, specially designed to operate in high magnetic fields. They are modified hot cathode ion gauges able to tolerate both high magnetic fields (1-10T) and relatively large changes in these fields on fast timescales. The gauge head consists of a large diameter filament, acceleration and control grids and ion collector. To suppress background in the ion collector signal, the control electrode voltage is chopped at a frequency of several kHz allowing the ion density to be measured from the modulation amplitudes of the emission and ion collector currents. Typical ion currents on TCV are <10μA. A protective shield is welded onto the gauge head to allow for thermalisation of atoms and molecules entering the device. Considerable effort was required to adapt the gauge and two iterations were required on TCV, in particular owing to initial inadequate feed through design that is critical for these devices – low collected currents must be measured whilst simultaneously applying high sweeping voltages. Figure 3.2.12 shows the divertor gauge just before installation. A second gauge is located in a port at the outside midplane of the machine.

Fig. 3.2.12 *One of the two ASDEX type fast ionisation gauges (this one is installed under the lower floor tiles) on its mounting flange.*

IR Thermography

Two new IR systems were developed in 2001 and have now (end 2002) reached the stage of commissioning. The first is a new diagnostic, designed for heat flux surveillance of a part of the TCV central column tiles during high power ECH experiments and for divertor physics studies with suitable magnetic equilibria. The second replaces the previous system used for some years to monitor the heat flux to a part of the vacuum vessel floor. In each system, the field of view encompasses in-vessel thermocouples and tile embedded Langmuir probes.

The two new IR cameras at the heart of these thermography diagnostics are based on state-of-the-art microbolometer technology consisting of focal plane arrays (FPA) of 320x240 pixels operating in the long wavelength IR range from 7-14μm. These cameras have the advantages of requiring no active cooling, being less sensitive (but not completely insensitive) to the tokamak magnetic fields and providing digital 12 bit output. They have the disadvantage of being bolometric by nature and therefore of reduced time resolution with respect to the faster (and more expensive) medium wavelength IR systems, typically employing InSb FPAs. Each camera is equipped with a set of Germanium relay optics designed in collaboration with Opto-System-Technik, Eppelheim, Germany and custom built digital acquisition systems based on the S-Link data link technology developed at CERN. The acquisition electronics also contain RS-232 serial links for camera function control and the whole (digital acquisition and control) is managed by a Matlab GUI interface running on a dedicated Linux PC. Separate electronics ensure that IR frames are synchronised with the TCV master clock.

Digital CCD cameras

The four 12-bit Digital CCD cameras, purchased to replace the analogue CCD camera observation of the divertor visible radiation, have been installed on a custom designed optical bench can be installed close to the machine while retaining the system alignment. After detailed optical modelling, the beam splitters and interference filters were placed as close as possible to the coherent fibre-optic bundle that carries the image from the tokamak plasma to the multi-camera detection system. A lens at the tokamak focuses light from the plasma onto the input end of the fibre bundle so that each camera observed the same image through an interference filter with a different selection wavelength, see Fig. 3.2.13.

Acquisition software has been installed on two dedicated PC computers permitting the acquisition from the four cameras to be synchronised with each other, and the TCV discharge, and then forward them to a remote controlling computer with user control of the camera's features situated outside the experimental hall.

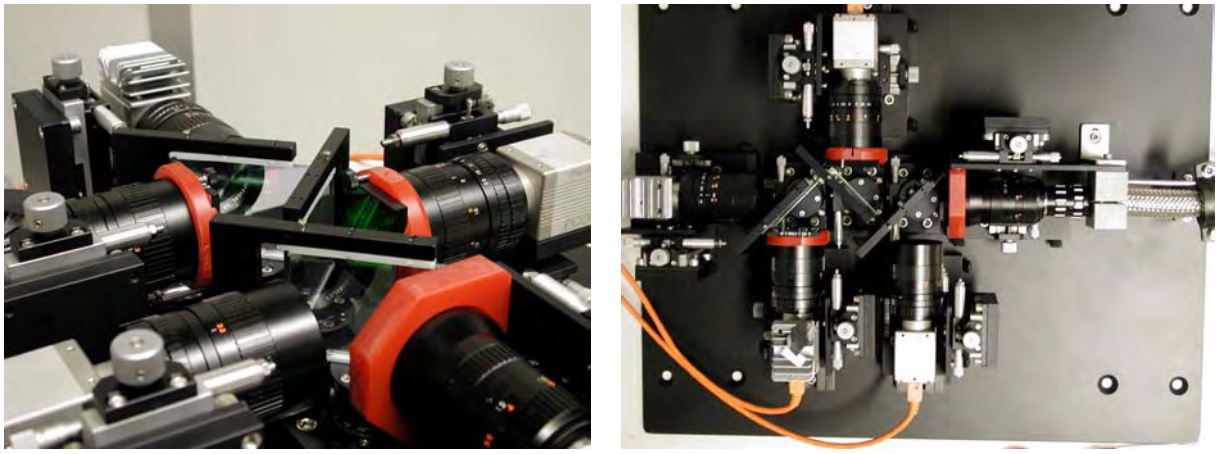

Fig. 3.2.13 *Photographs of the 4 camera observation system showing the incoming beam from TCV on the right beam-split onto 4 CCD cameras which are all equipped with Interference filters.*

3.3 TCV Auxiliary heating systems

3.3.1 X2 electron cyclotron heating system

The X2 heating system has reached its full maturity. During 2002, the X2 system operated routinely providing from 0.1MW to 2.8MW of power (DC, modulated or power ramps) for a variety of pulse lengths as required by the physics experiments.

Gyrotrons

The X2 gyrotron average age is, at present, ~5 years. During the initial phase of the 2002 operating campaign, the 5th tube began to exhibit evidence of poor vacuum conditions. The high gas pressure resulted in the electron beam ionising the background gas, the resulting ions bombarding the cathode thereby increasing the cathode temperature, and in turn the beam current, which further increases the

ionisation, resulting in a run-away beam current. This was circumvented by a 10% decrease in the beam current (resulting in a 25% decrease in the output power). Any further degradation in the tube vacuum will mean repair at the factory.

The Matching Optics Unit (MOU) located between the output of the gyrotron and the beginning of the transmission line is used to: filter out unwanted modes from the gyrotron; provide optimum coupling into the HE_{11} corrugated waveguide; change the beam's polarisation for optimum coupling to the plasma via a universal polariser. The universal polariser consists of two grating mirrors, which provide either rotation of the polarisation plane or introduction of circular beam polarisation elipticity. The grating mirrors are rotated about their axis to change the beam polarisation. One of the rotation mechanisms failed, causing its mirror to 'wobble' about its axis. The reflected beam from the mirror was deviated from its normal path and resulted in poor coupling into the waveguid,e depending upon the rotation of the grating mirror. At the beginning of 2002, the mechanism was repaired and the output power was measured as a function of mirror rotation angle. No variation of power was observed. The rotation mechanism that failed was a prototype design; all other MOUs use an improved design.

Control system

A new control system for the X2 ECH system was included into the control system in 2001. A single GUI window (MATLAB based) now creates all of the waveforms and settings used to characterise the operation of the gyrotron for a given discharge. This includes the waveforms used for the cathode voltage, launcher mirror angle sweeps, universal polariser angles for optimum coupling for the given target plasma. The control of the gyrotron auxiliary systems (water cooling, power supply status, cathode heating) is still performed using VSYSTEM GUIs, which are monitored throughout the TCV shot cycle. The control system was intensively used during 2002 and has simplified the operation of the X2 system to the extent that a single operator is required to control the six gyrotrons, including start-up, conditioning, operation and shutdown.

3.3.2 TCV X3 electron heating system

The integration of the X3 ECH system into the TCV environment is now complete. The control and acquisition systems dedicated to the X3 heating have been implemented and tested and the X3 system is now routinely used for the TCV research program. The accessible regions with the X3 top-launcher and the upper lateral launcher are shown in Fig. 3.3.1.

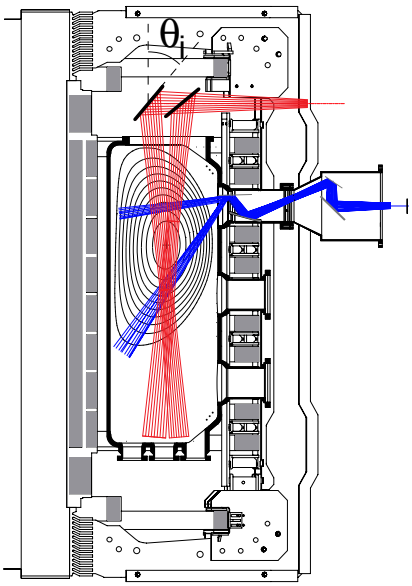

Fig. 3.3.1 *Accessible regions with the X3 top-launcher (in red) and with an upper lateral launcher (in blue).*

During the top-launch commissioning, particular attention was paid to the mechanical accuracy of the aiming parameters. A set of experiments was devoted to studying the plasma response with respect to the poloidal aiming angle in order to assess the mechanical aiming accuracy. In Fig. 3.3.2, a central soft X-ray signal (left y-axis) is plotted as function of launcher poloidal angle where an increased soft X-ray signal indicates increased absorption. From this type of experiment a mechanical setting accuracy better than 0.1° was demonstrated. For comparison, the predicted absorption curve versus launching angle, calculated with the ray-tracing/absorption code TORAY-GA (continuous line, right y-axis), shows good agreement with the experimental measurements.

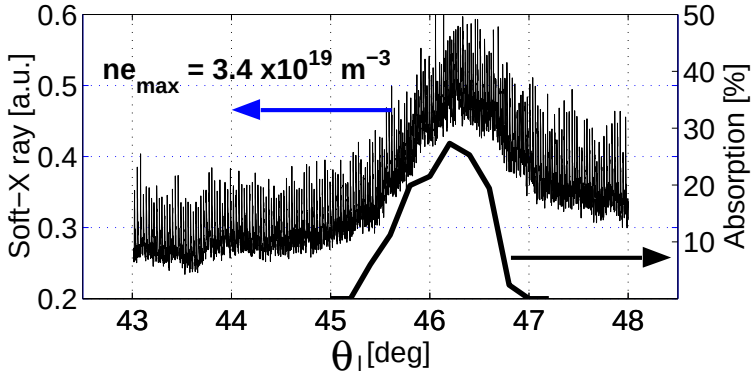

Fig. 3.3.2 *A central soft X-ray signal plotted with the TORAY-GA absorption prediction as a function of the launcher poloidal injection angle.*

In April 2002, the first X3 gyrotron installed on the tokamak suffered of a window failure during a 2s/500kW pulse. This cryogenic window is designed for CW operation at an RF output power of 500kW. The window failure on the gyrotron is presently not clearly understood and detailed investigations are underway both by the gyrotron manufacturer and at the insitute of "Material Science" at FZK (Germany). The repair of the gyrotron and reinstallation in the TCV-ECH system is planned for the first half of 2003.

3.4 TCV control system and data management

Over the years, the data acquired for each TCV discharge has risen from 10MB to reach the 200MB mark in 2002. To store these data, two racks of hard disks were installed, with a capacity of 0.5TBytes each. This allows all TCV data to be kept on line.

An update of the TCV Control System was necessary because it had reached the resource limit, in both CPU and IO, of the machine on which it was running. Moving it from a VAX computer to another AXP multiprocessor architecture implied a revision and recompilation of the locally developed software, and an upgrade of the database application used, which itself forced the revision and upgrade of many configuration files. Another change to the local code was made to double the number of BITBUS field bus nodes that can be controlled. All these changes were successfully implemented during the summer of 2002.

3.5 The TORPEX project

3.5.1 The TORPEX experimental apparatus

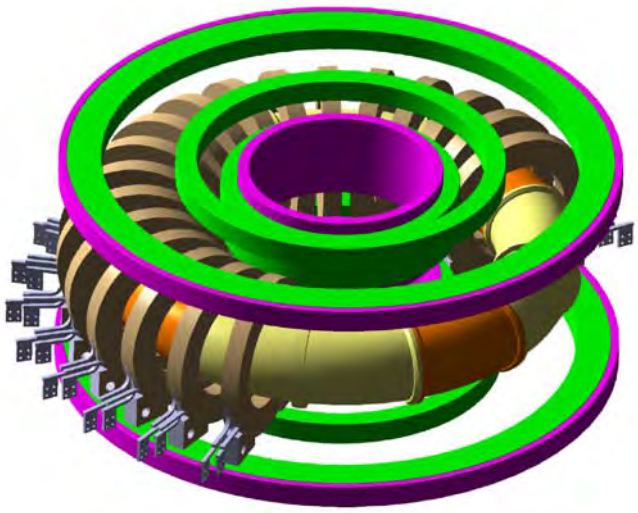

Fig. 3.5.1 *Sketch of the TORPEX experimental apparatus*

The activities of the basic experimental plasma physics group will be concentrated on the TORPEX toroidal device of which sketch is shown in Fig. 3.5.1. The TORPEX vacuum vessel has a major radius R~1m and is made of 12 sectors spanning an angle of 30° each and a circular cross section with an open diameter of approximately 0.4m. The wall is made of stainless steel DIN 1.4435 (X 2 CrNiMo 18143) ~5mm in thickness. The fourfold symmetrical vessel is segmented into 4 pairs of electrically insulated sectors to limit the induced eddy currents and 4 extractable sectors, with removable UHV seals and spacer rings. The retractable sectors enhance the ease and duration of interventions such as the installation or the modification of diagnostics. The outside of the vessel will be equipped with electrical heating and thermal insulated sleeves, so that it can be baked to 150°C. 48 port-holes give access for diagnostic instrumentation and pumping. The vacuum vessel is fixed to the toroidal field coils by feet designed to allow for thermal expansion and is supported by a crossed structure of metal beams to spread the floor load. A picture of the vessel is shown in Fig. 3.5.2.

The TORPEX magnetic field coil system will allow a variety of configurations and includes a toroidal coil system, a poloidal coil system, and an ohmic coil system. The toroidal system is made of 28 equally spaced coils, salvaged from a previous linear plasma experiment at CRPP. The toroidal field can be varied up to 2kG on axis. The poloidal coil system has 10 different coils, and can produce a cusp field (with the magnetic null at the centre of the vacuum vessel) and a purely vertical field. The current in the poloidal field set can vary from 100A (vertical field operation) to 4500A (cusp field operation), producing a vertical field up to 0.005T, and a cusp field up to 1kG about 10cm from the centre of the vessel.

The typical operation cycle foreseen is based on a 0.5s plasma discharge every 30 to 60s, for 8 hours a day. Special care was taken in the design of the coils and their connections to minimise the effect of the ohmic-ally nduced voltage. Figures 3.5.3 and 3.5.4 show the calculated magnetic field structure for the case of cusp field and vertical field, respectively.

Fig. 3.5.2 *The TORPEX vacuum vessel*

The ohmic system includes a central column composed of two solenoids with 2x28 turns each and two correction coils attached to the outer poloidal coils (1x7 turns each) to divert most of the magnetic field lines around the plasma region, maximizing the induced voltage and guaranteeing its homogeneity. A loop voltage of the order of 100V can be generated for approximately 3ms. Several pulses per discharge can be obtained using a periodic power supply that drives an oscillating LRC-circuit. The capacitors have been recovered from the TCV 39GHz gyrotron bank and are charged up to 9 kV each.

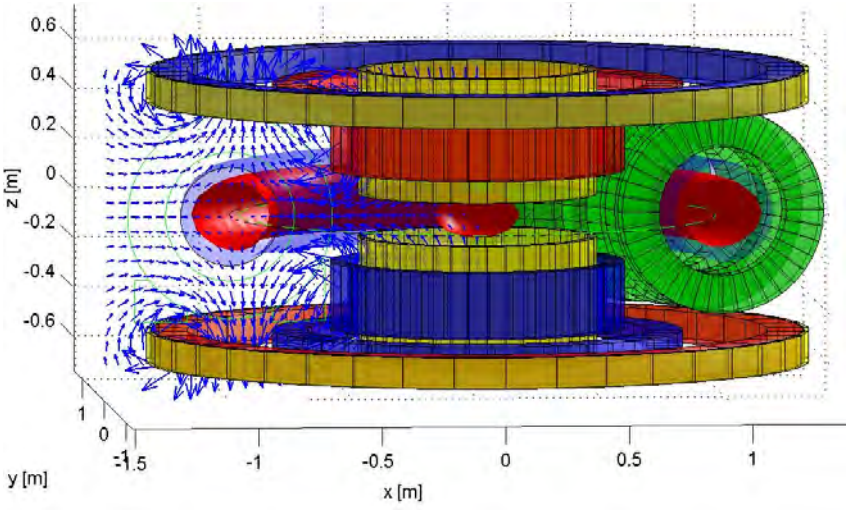

Fig. 3.5.3 *General plan of the cusp-field operation mode of TORPEX with simplified coil design. Toroidal coils are green, ohmic coils yellow and poloidal coils red/blue according to the direction of the current. The resulting magnetic cusp field is shown on a poloidal plane (blue*

arrows). We also indicate the resonant surface, corresponding to 2.45GHz Electron Cyclotron Resonance (red "egg-shaped" tube) inside the vacuum vessel (blue transparent), the X-point circle (green dashed line) and the centre of the vacuum vessel (black dot-dashed line)

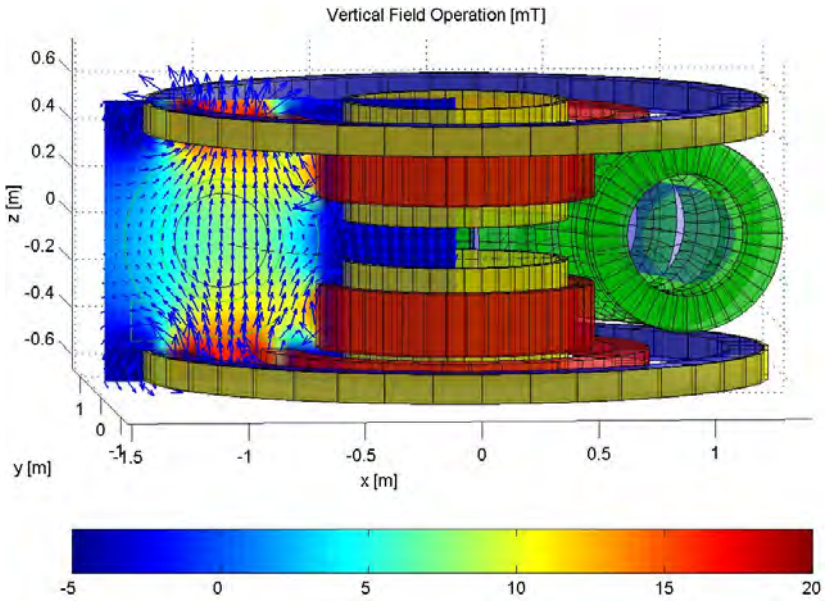

Fig. 3.5.4 *General plan of vertical field operation of TORPEX*

3.5.2 Initial diagnostics and data acquisition

Two 8-pin arrays of Langmuir probes will be installed from the start of the experimental campaign on TORPEX for the measurement of plasma background parameters, including electron temperature, density and plasma potential. The current-voltage characteristic is measured by sweeping the input voltage (100V amplitude, with triangular waveform) at a frequency of 1kHz. The probes are mounted on a remotely controlled movable shaft and introduced horizontally from the low-field side. The probe holder can translate radially across the whole poloidal section and rotate over 180° about its axis (Fig. 3.5.5). The tips are cylindrical, have a length of 4mm and a diameter of 1.5mm. They are mounted on a ceramic tube of 14cm in length. By moving the whole probe structure on a shot-by-shot basis along the major radius, a 28cm vertical strip can be explored in the poloidal section.

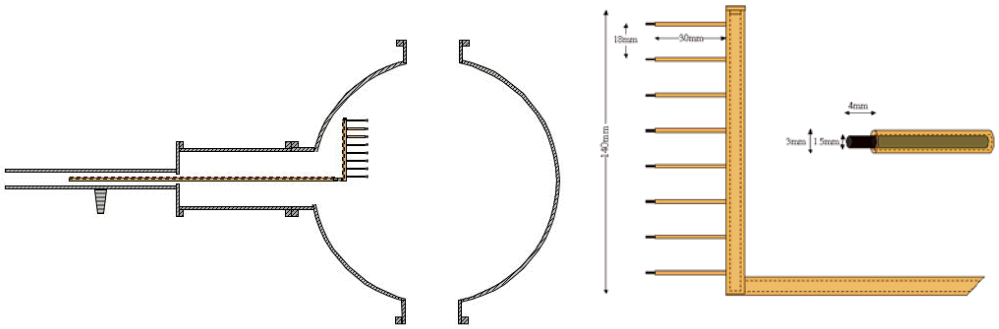

Fig. 3.5.5 *View of the low frequency Langmuir probe array*

For the fluctuation measurements, three arrays, each containing 11 pairs of tips (5mm length and 0.5mm diameter), 8.5mm apart, will also be installed for the first experimental campaigns (see Fig. 3.5.6). The distance between two adjacent tips (same pair) is about 2 mm, and the length of each probe has been chosen so that all the tips are at the same radial distance from the plasma centre.

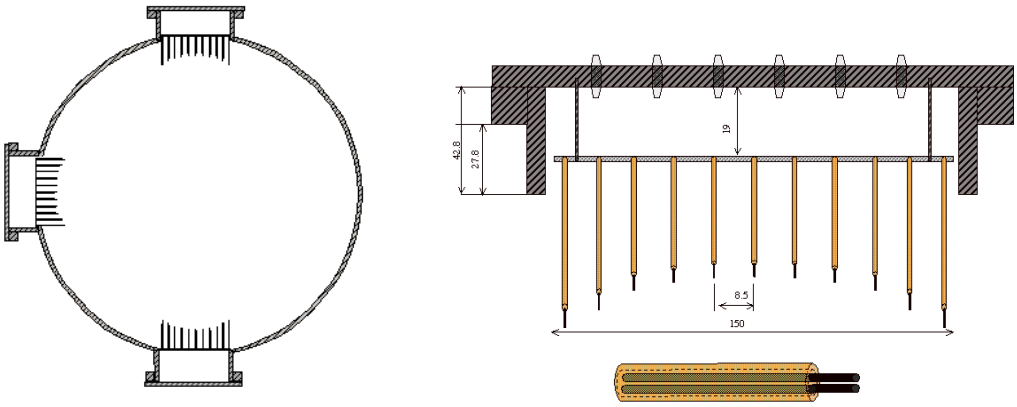

Fig. 3.5.6 *View of the electrostatic probe array for fluctuation measurements*

This geometry will allow the study of waves propagating perpendicularly to the toroidal field. The localisation of the dominant modes along the minor radius depends on the value of the density gradient, which needs to be determined experimentally.

A combination of three systems is foreseen for data acquisition, at low, intermediate and high frequency. The low and high frequency systems, 1kHz and 25MHz, are CAMAC based and include 64 channels (originally from the TCV tokamak) and 8 channels, respectively. The intermediate (250kHz) system is based on three C-PCI modules, for a total of 96 channels differential-input channels.

3.6 Superconductivity

3.6.1 The SULTAN facility

After the January shut down of the PSI services, operation of the SULTAN facility was resumed at the beginning of February 2002. The shut down was also used to replace all the instrumentation cold-connectors for the short samples, as the old connector series (SOURIAU) are no longer manufactured. After thermal cycling trials, the cheap, compact “subminiature” connectors were selected. The total number of channels for the short sample instrumentation has been upgraded by almost a factor of two. Now 42 4-wires sensors (e.g. thermometers and Hall sensors) can be wired to seven Sub-D-25 connectors and 60 2-wire sensors (voltage taps, pick-up coils) can be wired to five connectors, see Fig. 3.6.1. The instrumentation of the short samples prepared by external users must use the male subminiature connectors as described in the user interface document.

At the end of May, a current lead of the pulsed field coil broke and the facility had to be warmed up for repair. The same current lead had already broken in 2001 due to a displacement of the pulsed coil assembly during operation. The reason for the last failure was imperfect alignment of the current leads and the main field of SULTAN: the small, non-parallel field component caused a bending load on the lead, which eventually ended in the mechanical failure of the support assembly after many hundred cycles of operation. The damage was repaired and a new assembly was inserted. Operation was resumed after cool-down at the end of July 2002. A total of six short samples have been measured in 2002, with nine warm-up and cool-down cycles.

An update of the user interface document "User Specification for Conductor Samples to be Tested in the SULTAN Facility" was written in June 2002. The report gives a brief survey of the SULTAN facility. The superconducting magnets, the pulse coils and the associated power supplies, the cryogenic system, and the data acquisition system are described. Furthermore, the requirements on the geometrical dimensions and the instrumentation of samples to be tested in SULTAN are discussed, and the operating range for experiments is outlined.

Fig. 3.6.1 *The five Sub-D-25 connectors for 2-wire sensors*

3.6.2 A new Facility for Resistance Distribution Test on Joints

A new test facility for resistance distribution measurements on termination and joints of large superconducting cable has been built under an EFDA contract in 2002. The facility is nicknamed JORDI.

In ideal conductors operating in purely DC mode, the series resistance of the individual current carrying elements at the electrical termination (joint) affects the current distribution among the superconducting strands. The resistance between a superconducting strand in a cable and the equipotential surface defined by the symmetry plane of the joint is a mix of series and parallel paths, where the prevailing component depends on the joint layout (such as void fraction, resistive barriers, soldered contacts). A direct, experimental assessment of the contact

resistance distribution at the joints is of primary importance to correctly analyse the current distribution in the conductors and to qualify the joint layout.

In JORDI, a half joint (referred as the conductor termination) is prepared according to the reference procedure, specified by the coil manufacturer. Adjacent to the termination, the cable is opened down to the first cable stages, which are individually connected to the positive lead of a current source (all cable stages may be supplied simultaneously with the same current source). The negative lead is connected to the copper side of the termination, which is coated with a special superconducting alloy to obtain a true equipotential surface. The voltage drop, and hence the resistance, is sensed between each first cable stage and the equipotential surface. A key issue for the correct assessment of the resistance distribution, is that each cable element (e.g. each first cable stage) must simultaneously carry the same current during the test. To obtain this, the DC current from a 12kA current source is shared among the cable elements by precision, 70μΩ shunt resistors developed for this purpose. The voltage drop is sensed by a multi-channel data acquisition system. As the contact resistance is in the range of few tens of nΩ, the shunt resistors guarantee an imposed, balanced current distribution even in the case of an unbalanced resistance distribution in the termination. JORDI is designed for up to 100 current carrying elements, i.e. 100 shunt resistors in parallel, each provided with a voltage pair over the shunt and a voltage pair to sense the resistance in the termination. Using all the 100 resistors and the highest current from the power supply, the maximum power dissipated in the helium bath is 100W. The current in the individual elements is up to 120A and the voltage is sensed with an accuracy of ≈0.1μV, giving an accuracy of ≈1nΩ for the resistance measurement.

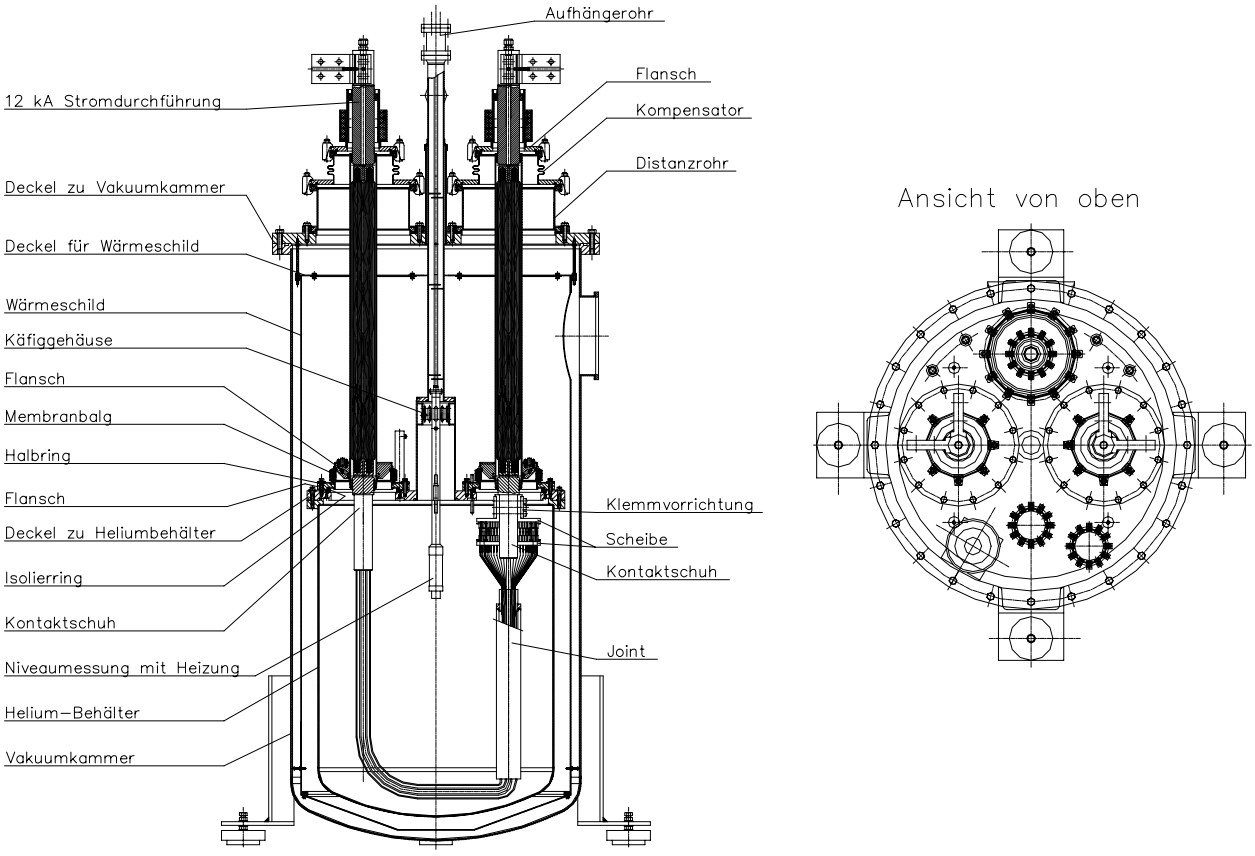

Fig. 3.6.2 *Elevation view and top view of JORDI*

JORDI consists of a vacuum chamber, 800mm indiameter x 1650mm tall, Fig. 3.6.2, with a radiant heat shield of copper inserted, cooled by Helium gas at 80K. In the cover flange of the vacuum chamber two 12kA current leads, a Joule Thompson (JT) valve and different measurement wires and safety valve feed-throughs are built in. A 300 liter liquid He container is suspended in the vacuum chamber over a central tube. The cold ends of the current leads are provided with insulated feed-throughs in the He container flange and plunge into the liquid He. The termination sample can easily be exchanged after lifting the main flange along with the current leads out of the main vacuum chamber and then sliding out the bolted He container from the bottom. The length variation during cool down and warm up is compensated by flexible bellows.

Fig. 3.6.3 *Vacuum chamber, copper shield and He container before final assembly*

JORDI is continuously supplied by supercritical Helium at 10bar, flowing over a transfer line from the cryoplant over a valve box to the He container through the JT valve and on the other hand for two current leads. The JT valve is controlled by a level measuring probe in the He container. The He flows back from the Hecontainer over the transfer line and the valve box to the cryoplant. Likewise, from the He-container a safety line leads to a relief valve and to the warm gas recovery. The mass flow of the two conventional current leads is regulated by a mass flow meter with a control valve at room temperature.

The facility has now been completed. The first termination samples will be prepared and tested in 2003 from full size ITER conductors.

*3.6.3 Commissioning of the Cryogenic System for the SLS Superconducting Cavity**

The main trend in the development of third generation synchrotron radiation facilities is to increase the brightness of the radiation, achieved mainly by reduction of the electron beam dimensions. The disadvantage of increasing the brightness is however a significant reduction in the beam lifetime. A method to overcome the lifetime limitation is the use of a passive superconducting 3rd harmonic radio-frequency cavity. With a passive 3rd harmonic cavity, a flat portion in the machine voltage around the phase position at which the electrons are injected is created. The flat portion can accommodate more electrons in stable orbits, thus enlarging the bunch length and increasing the lifetime without reducing the brightness.

The Swiss Light Source (SLS) in Villigen, Switzerland and Elettra in Trieste, Italy have decided to upgrade their facilities with such a superconducting cavity in order to increase the beam lifetime. The solution with a passive (idle) cavity was found to be optimal for the conditions at the two storage rings. Therefore the two institutions, in collaboration with CEA Saclay France (cavity design and manufacture) and CRPP-Fusion Technology, Villigen Switzerland (cryogenic system) started a joint project called SUPER-3HC which aimed at designing and manufacturing two complete cryomodules based on a scaling-up to 1.5GHz of the 350MHz two-cell cavity developed for the SOLEIL project. Each cryomodule consists of two Nb/Cu cells, enclosed in their LHe reservoirs. Each cell is equipped with a mechanical frequency tuner driven by a stepping motor, which changes the cell length within the elastic limit (±500kHz, 10Hz accuracy). At the nominal cavity voltage of 800kV (4MV/m) a bunch lengthening of a factor of three is anticipated, resulting in 2-3 times longer beam lifetimes (depending on the vacuum quality in the beam line). The first cryomodule was delivered to SLS in June 2002 and is shown in Fig. 3.6.4. Beside the design of the cryomodule, the design of the cryogenic system was a challenge too because at both synchrotrons there was no LHe facility and no gas management system installed or planned. A completely new LHe/GHe infrastructure was designed in the very restrictive space conditions of the operational storage rings. Several layouts were considered for placing the coldbox, He compressor and LHe storage. Different cooling schemes were analysed including pure liquefaction mode, pure refrigeration mode and mixed mode cooling of the cryomodule. The final decision was a scheme with a storage Dewar and operation in mixed mode at a moderate warm gas return level, which represented a compromise between system complexity and operational stability.

---

* The work described in this section was not performed within the frame of the Association Euratom – Confédération Suisse. It was supported by and performed for the Paul-Scherrer-Institute.

Fig. 3.6.4 *The SUPER-3HC cryomodule installed in the SLS ring*

A schematic of the cryogenic system is shown in Fig. 3.6.5. The cryogenic system is composed of a He refrigerator (Air Liquide, Model HELIAL-1000), a 500 liters storage Dewar, the cryomodule with the two superconducting cavities, a cryogenic valve box and two transfer lines. The He refrigerator consists of a cold box accommodating the heat exchangers and the two high performance turbines, a He screw-drive compressor and purification system and a fully automatic control system cabinet. The He liquefaction takes place in the storage Dewar. Two-phase He is transferred after expansion in the Joule-Thomson valve to the Dewar through the central pipe of a short coaxial transfer line. The cold gas is returned to the cold box through the external concentric pipe of the same transfer line. Through a second transfer line, LHe from the storage Dewar is transferred to the valve box, where a cryogenic valve LCV5 regulates the mass flow required by the cryomodule. The valve box is connected to the cryomodule by a 10m long multiple transfer line. In a phase separator included in the cryomodule, LHe is separated from the gas phase, which returns at about 20K to the valve box. Before leaving the valve box the He cools a radiation shield inside the long transfer line. LHe from the phase separator fills bottom-to-top the two reservoirs surrounding the resonant cavities and accumulates up to a certain level in the collector vessel placed above the cavities. The main part of the cold gas produced here by the thermal load is returned to the cold box through the long transfer line, valve box and a fourth simple transfer line. Regulated amounts of cold gas are stripped from the collector and used to cool a 60K radiation shield and the two extremity tubes connecting the cavity to the beam line. The cold gas at 60K from the shield is returned back to the valve box and is used to cool a second radiation shield in the long transfer line after being returned as warm gas to the low pressure circuit of the refrigerator. The mass flow through the extremity tubes is returned directly as warm gas. A view of the system installed is presented in Fig. 3.6.6.

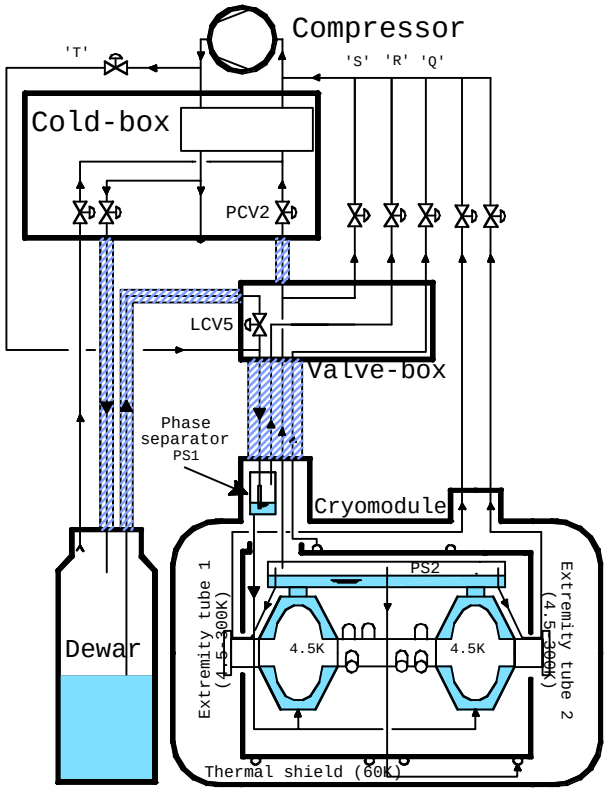

Fig. 3.6.5 *Schematic of the cryogenic system for SUPER-3HC*

The factory acceptance test of the refrigerator was performed at SLS in July 2002. The measured performance of the refrigerator was excellent. In pure liquefaction mode a liquefaction rate of 48 l/hr (rising level) was measured and in mixed mode a combined liquefaction rate of 9.7 l/hr and 150W refrigeration power were measured. In order to spare electrical energy, over the compressor pressure was reduced from 15 to 12bar and with this 50% performance overhead in mixed mode was still measured. The specified performance (nominal +50% margin) could be obtained at a compressor pressure as low as 11bar.

Fig. 3.6.6 *Installation of the HELIAL-100 coldbox and the 500 liter Dewar*

Commissioning of the cryogenic system was performed successfully between 23 and 27 September 2002 during one of the planed shutdowns of the SLS ring. In the month before, operation of the cavity was tested in warm modes. The cavity was detuned and kept at room temperature by helium gas circulation. Commissioning started with the test of the automatic conditioning system followed by a controlled cooldown with a cooldown overhead of –50K (later increased to –100K). In less than 24hr the first indication of the presence of liquid helium in the cavity was observed. After stabilisation of the liquid level in the cryostat, on 30 September 2002 tests with the cold cavity and the beam were started. For the first time, the beam intensity at SLS could be increased and maintained for hours at 400mA, indicating stable operation of the whole system at the highest level of performance. The beam lifetime, which, without the cavity was limited to 4hr at 400mA by the Toucheck effect, was increased to 9hr with the cavity. The theoretical beam lifetime with the cavity is 12hr. The measured beam lifetime increase was less than the factor of three as theoretical predicted, due to additional beam scattering on residual gas in the beam line. The bunch lengthening has already reached the factor of three expected. An additional benefit of the resonant cavity is an increased dumping effect, stabilising the longitudinal oscillation of the beam.

4 INTERNATIONAL AND NATIONAL COLLABORATIONS

4.1 Exploitation of the JET facilities

4.1.1 Collaboration with the JET-EFDA Task Force M (MHD)

CRPP collaboration with the Task Force MHD for JET-EFDA experiments has focussed on leading experiments and finalising analyses of experimental data and of simulations of 2001 experiments. Due to the lack of enhanced injected power in the first campaigns of 2002 and the cancellation of the autumn campaign, relatively few new experimental results have been obtained.

The main experiments in 2002 in which the CRPP was directly involved in coordinating the sessions for TF M were related to sawteeth, NTMs and TAE physics. Otherwise CRPP collaborators have continued to offer expert analyses of MHD phenomena of discharges produced by other Task Forces.

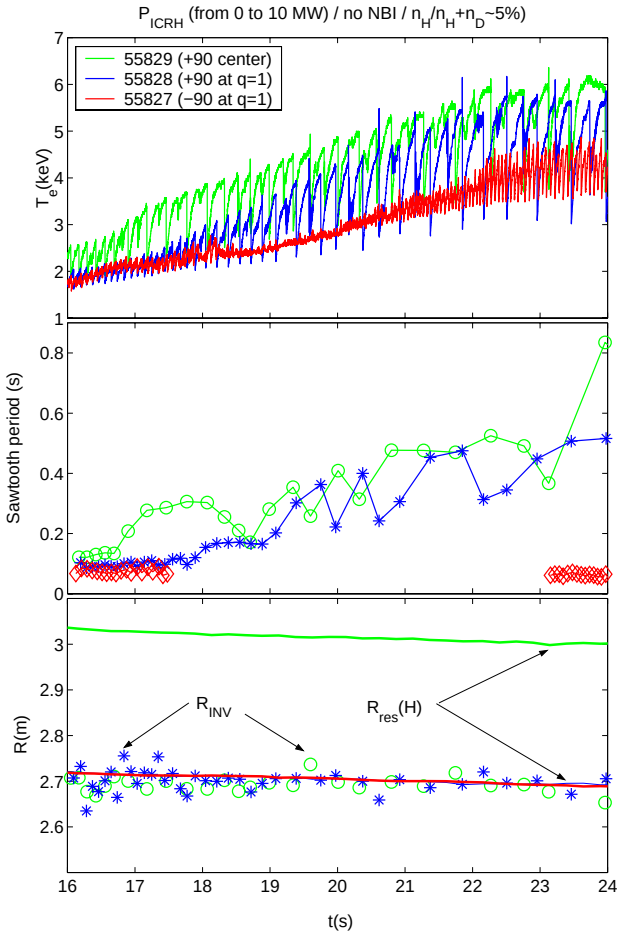

Fig. 4.1.1 *Power ramp of ICRF with different antenna phasing and deposition location. With –90° phasing, near the inversion radius, sawteeth are*

destabilised and very small sawteeth with short period are obtained even up to about 10MW

In the first set of experiments, ICRH and ICCD were used to modify the sawtooth period with both 1st harmonic and 2nd harmonic minority heating. The dependence on the resonance location, both near the LFS and HFS inversion radii, on the Hydrogen concentration and on the ICRH power have been studied. In the 1st harmonic, clear sawtooth destabilisation has been obtained with very small and regular sawteeth being generated (Fig. 4.1.1), which should be of interest for NTM avoidance schemes.

The NTM experiments concentrated on testing real time control algorithms, where the capability to change plasma conditions triggered by the appearance of either 3/2 or 2/1 modes has been demonstrated. A campaign to compare JET and DIII-D marginal beta limits with power ramp-down experiments in similar plasma conditions has started. Both of these projects will need additional JET experiments in 2003.

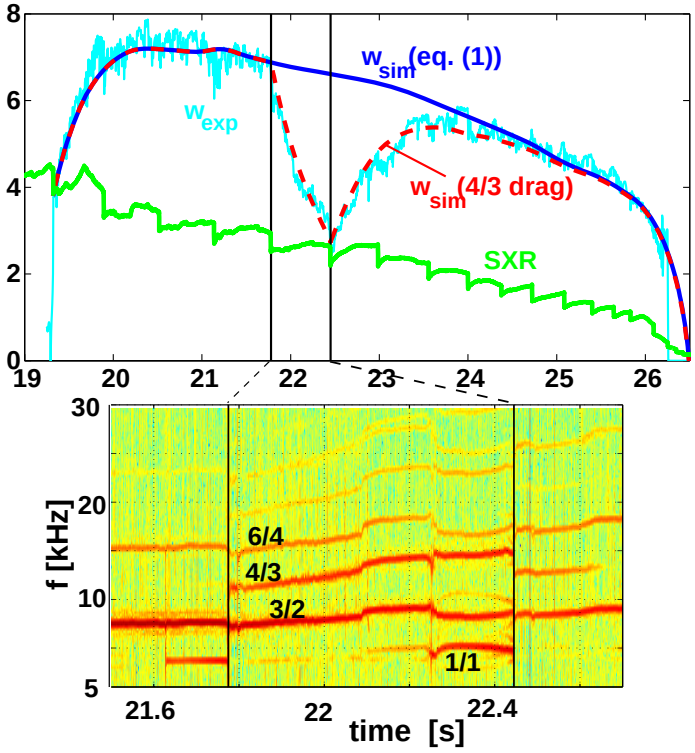

Fig. 4.1.2 *Experiment to measure the marginal beta limit. The power is slowly ramped-down after the 3/2 NTM is triggered, until the mode stabilises at low beta (near 26s in this case, JET #53290). In this discharge a 4/3 mode exists between two consecutive sawtooth crashes. Consequently strong stabilisation of the 3/2 mode is observed. The full time evolution of the 3/2 island width cannot be simulated with the modified Rutherford equation alone (labeled eq.(1)) but requires an extra stabilising term representing the interaction with the 4/3 mode (labeled 4/3 drag).*

Detailed analysis has been carried out for discharges where the power was slowly ramped down once a NTM had been triggered. A scaling of the marginal beta limit for the 3/2 mode proportional to $\rho^{*1.1}$ was found while no significant dependence on collisionality was observed. The lower onset beta measured in discharges with $q_{95}<3$ was demonstrated to be due to the stronger trigger mechanism related to sawteeth activity and not to a lower marginal beta limit. A strong interaction of the 4/3 and 3/2 modes was observed in the saturated phase of a 3/2 mode. This was observed for a long phase on JET as seen in Fig. 4.1.2. While the 3/2 mode amplitude was slowly reduced due to a slow power ramp-down, a 4/3 mode was triggered by a sawtooth crash. At this time the 3/2 island width growth rate became very negative and the mode amplitude decreased sharply, shown in Fig. 4.1.2. At the next sawtooth crash the 4/3 mode is stabilised and the drag on the 3/2 mode disappears, allowing the 3/2 mode to grow back to its saturated state. The full time evolution of the 3/2 island width has been simulated, requiring an additional drag in between the two sawtooth crashes to represent the stabilising contribution of the 4/3 mode on the 3/2 mode. Using a bicoherence analysis, it has been possible to show that a strong nonlinear three wave coupling exists between the 3/2, 4/3 and 7/5 for the whole time interval in between the two sawtooth crashes.

The study of Alfvén waves and their interaction with fast particles continues to be an important topic in the JET programme. Various dedicated experiments have been performed within the framework of the Task Force activities during this period. This work has mainly concentrated on the following issues:

- studying the dependence of the frequency and damping rate of stable, externally driven, Alfvén Eigenmodes (AEs) with low toroidal mode number upon the ion Larmor radius, the bulk plasma beta and the core safety factor and magnetic shear;
- studying the instability threshold for AEs driven by resonant fast particles as function of the edge magnetic shear;
- using AEs to infer information on background plasma parameters at the mode radial location, such as the safety factor and toroidal rotation, the so-called *MHD spectroscopy technique*;
- designing a new dedicated antenna system for the excitation of AEs with high toroidal mode number, to be installed on JET during the 2004 shutdown

4.1.2 Collaboration with the JET-EFDA Task Force E (Exhaust)

Building on the efforts of the previous two years, support for the JET Exhaust Task Force (TFE) by CRPP staff during 2002 concentrated on the analysis and presentation of results from the JET pure helium plasma campaign and on final commissioning and first physics operation of the new retarding field analyser edge probe, developed by the CRPP in conjunction with the UKAEA as a JET enhancement project.

Pure helium plasmas

Analysis of the March 2001 JET pure helium campaign continued throughout 2002, with many of the key results presented at major conferences.

Helium plasmas are one option for the low activation phase of ITER, but little effort has sp far been devoted to studying them in a large, diverted tokamak. They are also of considerable interest from the point of view of divertor and edge plasma physics, particularly in a graphite containing machine in which the absence of carbon chemistry in a pure He plasma should significantly modify the source of impurity production, providing an excellent tool for assessing the role of chemical sputtering in equivalent deuterium discharges. In combination with the modified impurity source distribution, the differences in He atomic physics in comparison with D has a strong impact on divertor physics, affecting the balance of particle fluxes and radiation and hence the character of detachment and density limits

Much of the analysis relies on matched pairs of D and He discharges, an example of which is shown in Fig. 4.1.3 for two L-mode discharges with identical magnetic configuration. During the period of He neutral beam heating (NBI), the total input power (Fig. 4.1.3b) is similar in both He and D, albeit it for a 20% higher D plasma density (Fig. 4.1.3a).

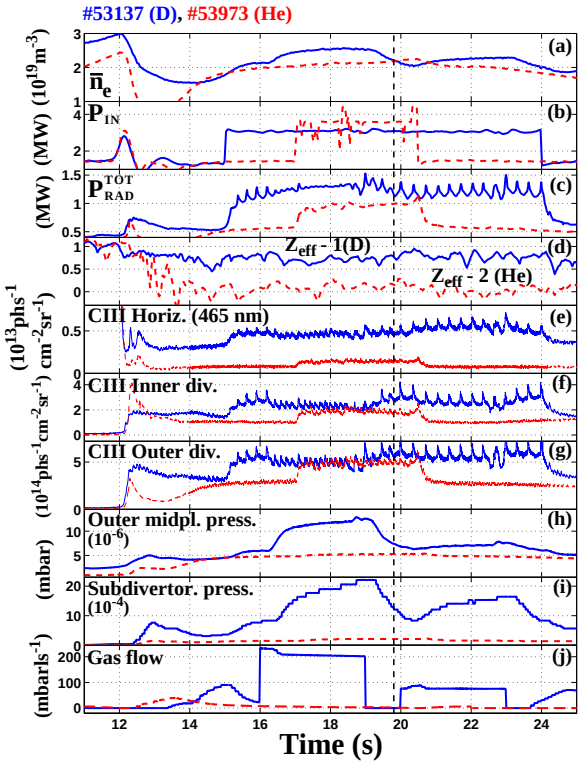

Fig. 4.1.3 *Comparison of matched JET L-mode, low wall clearance D and He shots at I_p=2.4 MA, B_T=2.5 T: full blue lines D (#53137), dashed red lines He (#53973). The dashed vertical line at 19.8s shows how when the plasma density is very similar and the D gas fueling is low, midplane pressures are almost the same but subdivertor pressures are about a factor 6 lower in He compared with D. Note also the similar levels of CIII emission in D and He at the divertor targets, implying that physical sputtering in He efficiently replaces chemical sputtering in D for medium to low density. This does not occur at higher $\bar{n}_e$ (see Fig. 4.1.4)*

The incremental Z_{eff} in Fig. 4.1.3d demonstrates the cleanliness with respect to core carbon content of these He discharges. This is correlated with a reduction by a

factor 3 in the intensity of inner midplane CIII (465nm) emission (Fig. 4.1.3e), whilst inner and outer divertor CIII signals are of similar magnitude in D and He during the beam heating phase (Fig. 4.1.3f,g). The midplane and subdivertor pressures in Fig. 4.1.3h,i vary strongly in the D plasma owing to the intense gas puffs, but at ~19.8s into each discharge (marked by the dashed line), there is a point where $\bar{n}_e$ in both cases is identical. Inspection of the SOL profiles at this time using three separate diagnostics shows them to be remarkably similar in D and He, despite the differing ionization energies and charge-exchange dynamics of the two species. Mach number profiles of the SOL flow are also reasonably similar, with the anomalously large parallel flow always observed in D plasmas also present in He.

Qualitatively, the observations described above for L-mode diverted plasmas are consistent with a picture in which carbon chemical sputtering accounts for a large fraction of the divertor impurity source in D plasmas, particularly at medium to high densities. Quantitatively, this has been demonstrated using UEDGE code simulations of these He plasmas to provide correction factors for line of sight diagnostic views of CII and CIV emission from the inner and outer divertors. Simulations and comparison with He plasmas have also been used to demonstrate the importance of main chamber impurity production in determining the discharge purity in deuterium and the dominance of the inner divertor over the outer as an impurity source. In H-mode, the presence of ELMs renders the task of quantifying the relative importance of divertor and main chamber impurity sources much more difficult. It is clear, however, from Fig. 4.1.4, that CIII intensities are comparable at all locations in the machine for matched Type I ELMing H-modes in D and He. The competing roles of physical and chemical sputtering in this case cannot be extracted from the available data, but physical sputtering is likely to be dominant.

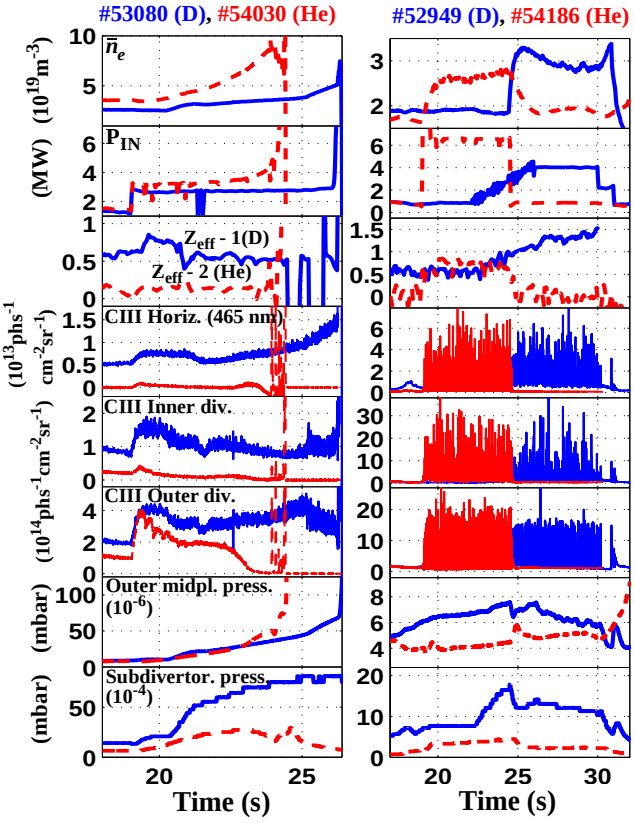

Fig. 4.1.4 *Comparison of matched L-mode D and He density limit shots at at I_p=2.4MA, B_T=2.5T (left) and matched Type I ELMing H-mode discharges at at I_p=1.0MA, B_T=1.0T (similar pulses at higher current*

did not access the Type I regime owing to the higher L-H transition threshold and the lower available NBI power in He). Both pairs of discharges are low wall clearance equilibria. Note how with rising density in the He plasma, CIII emission falls to undetectable levels everywhere and that in the H-mode pulses, how the ELMs provoke similar carbon emission to that observed in D plasmas.

The observed enhanced density limit in L-mode He plasmas (up to a factor 2.8 higher than in D depending on plasma-wall clearance in the main chamber – see Fig. 4.1.4), is, partly, a consequence of reduced ionisation rate coefficients (longer mean-free paths for He neutrals in the cold divertor plasma at high density) and significantly lower charge exchange and elastic collision rates in He. This combination leads to an increased neutral penetration depth (enhanced neutral leakage from the divertor) such that, although an X-point MARFE forms at similar densities in both D and He, in the He plasma the density can be increased continuously until the radiative power fraction reaches 100%. In H-mode, it appears that the D and He density limits (defined as the density at the H-L-mode back-transition) are very similar.

The increased He neutral penetration in comparison with D also produces significant differences in the divertor detachment behaviour of He plasmas. Detachment begins at much higher upstream densities and is similar to that in D only in the sense that the inner target appears to detach first. What is different is the decrease in power flux, especially at the inner target, long before the particle flux. Such behaviour is in contrast to the general picture in D whereby ion-neutral frictional processes at low divertor T_e and eventually recombination reduce the target ion flux. These effects in He are qualitatively reproduced by the first attempts at modeling of these discharges, performed at CRPP using the SOLPS5.0 (B2.5-Eirene) code package. The modeling has shown directly that recombination processes cannot play a role in He owing to the low residence times for He^+ in the divertor region, itself due to the lack of sufficient momentum removal by ion-neutral in comparision with D plasmas.

In addition to the question of impurity production, density limits and detachment, a number of other important edge physics research areas have been addressed by these helium discharges. Of note is the question of net redeposition of carbon at the inner divertor, revealed by IR camera surface temperature response to He NBI power steps and the rapid disappearance of hydrocarbon species during D-He changeover. Progress has also been made on understanding SOL cross-field transport through the extension made possible with the addition of points at different (A,Z) and the use of helium has allowed choices to be made with regard to the current thinking as to how ELM energy is transported from the main to SOL to the divertor target plates. As shown in Fig. 4.1.5, the characteristic time for the ELM released energy pulse in pure He to propagate to the divertor targets scales with power deposition time at the target similarly to the situation in D. This indicates strongly that the key element determining the transmission of energy to the targets is simply the arrival time of the ion pressure wave front, with SOL collisionality playing a minor role.

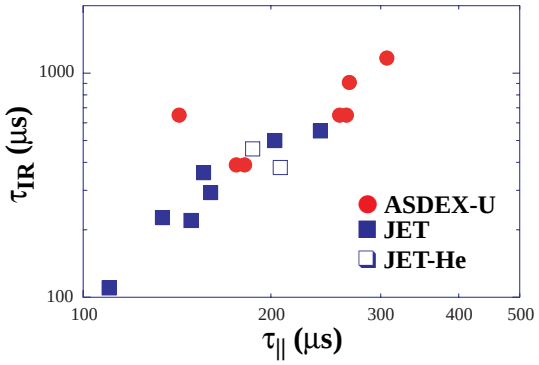

Fig. 4.1.5 *Variation of ELM divertor target power deposition times measured by IR thermography with time for parallel propagation of the SOL pressure wave traveling at sound speed from the upstream location of the ELM event to the outer targets in the JET and ASDEX-Upgrade tokamaks.*

Retarding field analyser enhancement project

Over the period 2000-2002, the CRPP managed a JET Enhancement Project (JW-OEH-SWIS-03) to provide a new Retarding Field Analyser (RFA) probe head for the fast reciprocating probe drive system KY3-A. Details of this design process and of the new probe (for measurements of SOL ion temperature and plasma flow) appeared in the 2001 report. Following successful commissioning in early 2002 of the new diagnostic manufactured principally at the CRPP, first physics operation was possible during a dedicated JET experimental session in September 2002. Analysis of the results is already underway, but Fig. 4.1.6 illustrates the excellent quality of the raw data obtained in a diverted discharge using neutral beam injection to provide power steps during each of which the RFA is inserted. The device is bi-directional, allowing ion temperature measurements in directions facing both the inner and outer divertors, in addition to the plasma flow velocity parallel to the total magnetic field. These tests have shown that although the new CRPP device is a significant improvement on previous attempts at JET, functionality of this rather delicate diagnostic is impaired beyond certain limits of plasma density and input power. Nevertheless, the 2002 experiments, and those planned in 2003, will provide a wealth of new information not previously available on JET.

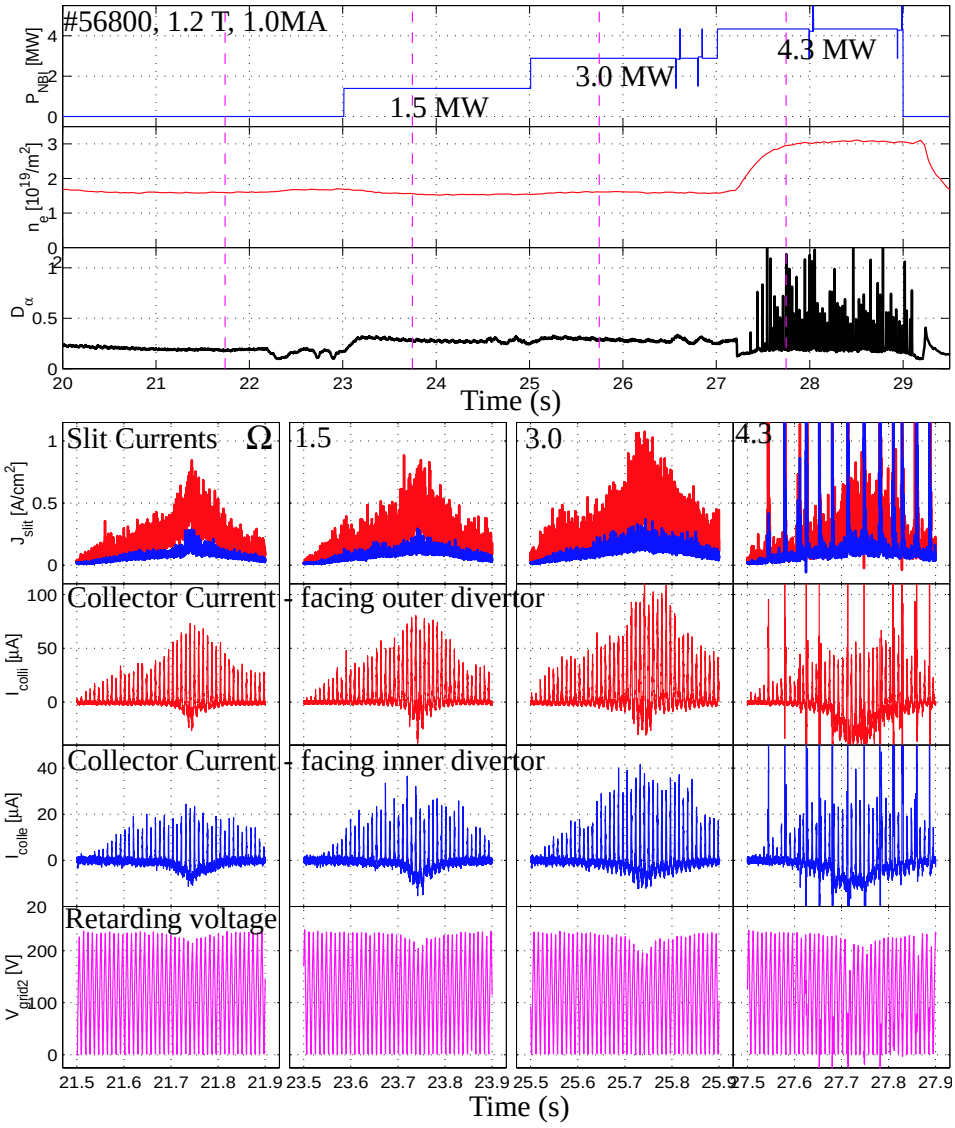

Fig. 4.1.6 *The RFA slit currents, slit voltages, ion retarding voltage sweep and ion collector current characteristics during a JET discharge dedicated to physics operation of the new probe head. The probe reciprocates 4 times into this 1.0MA discharge, including in the Type I ELMing H-mode phase obtained at 4.3MW of injected NBI power. Although somewhat perturbed, the ion characteristics during this latter phase should allow analysis for the first time of the SOL ion transport during ELMs. The very different slit currents for directions facing towards and away from the outer divertor demonstrate the existence of strong SOL flow in JET.*

Divertor detachment without septum and plans for 2003

In addition to the RFA experiments described above, the CRPP also conducted an exploration of divertor detachment physics in October 2002 with the aim of characterising the differences with respect to operation with the divertor septum which was removed in the interval between Campaigns C4 and C5. Unfortunately, in view of the technical difficulties experienced at JET at the end of Campaign C6,

the experiment was conducted with only ohmic heating, making comparison with previous beam heated shots difficult. However, first analysis has clearly demonstrated how septum removal leads to greater symmetrisation of the inner and outer divertor plasmas. Detailed SOLPS5.0 modelling of these discharges will be performed at CRPP.

Task Force E will take a leading role in experiments with reversed toroidal field that will comprise the JET Campaign C9 in 2003. Considerable effort has already been invested by CRPP during 2002 in planning for these experiments, which will include investigation of the effect of field reversal on edge plasma flows, fuel retention, ELM power flux transit times, impurity screening, erosion and redeposition, divertor detachment, helium operation and the search for the QH mode on JET.

4.1.3 Collaboration with the JET-EFDA Task Force D (Diagnostics)

A CRPP staff member was seconded to JET as Task Force D (TFD) deputy leader, with the role of coordinating diagnostics services to the work programme during the C5 & C6 campaigns, including as small number of specific TFD experiments. The job also included the selection (together with fellow task force leaders) and subsequent promotion of the proposals made for 2002 campaigns by the associations in the frame of TFD.

The deputy TFD leader implemented a scheme by which Diagnostics Coordinators are fully integrated into the control room team and encouraged to actively engage in the physics of the experiments in addition to providing the service of coordinating and supervising diagnostics during operation. In order to obtain a direct assessment of the situation of the Diagnostics Coordinators in the control room, the deputy himself played the role of Diagnostics Coordinator on many occasions.

4.1.4 JET-EP: Heating and current drive calculations for sawtooth control in JET and TCV

Calculations have been made to determine the JET ECH system power and launcher angles requirements for sawtooth control to avoid seeding NTMs with large sawteeth. Sawtooth stability is highly sensitive to the localisation of the EC power deposition in the q=1 surface region. As shown in TCV, a deposition close to q~1 destabilises sawteeth (short periods) and a deposition slightly further out ($+\Delta q \sim 0.05$) stabilises sawteeth. It was also shown that the stabilisation depends on the local EC driven current density and not on the total driven current I_{CD}. Ray-tracing calculations have been undertaken for the JET ECRH launcher geometry and different JET equilibria using TORAY. The maximum driven current density is reached at a relatively small toroidal injection angle, Q_{max}, leading to a requirement in injection angles that is reduced from the case of maximising the total driven current. This range of angles is easily covered by the present JET launcher design. Typical total driven currents of I_{CD}=0.1-0.15MA can be obtained at φ_{max} for 5MW EC power, representing 2.5-5% of the plasma current, a power which is sufficient to obtain a significant sawtooth stabilisation/destabilisation effect according to TCV results.

4.1.5 JET-EP:Extreme Shape Controller

Work is being carried out on JET to develop an Extreme Shape Controller, in collaboration with ENEA-CREATE consortium, ENEA-Frascati and UKAEA-Fusion. As part of this project, experiments were carried out this year to measure the dynamic response of the plasma equilibrium to the poloidal field coil power supply demand voltages. To date, two discharges were produced, exciting all coil supplies with two frequencies, from which the full response model can be deduced for all coils at these two frequencies, following on from earlier work carried out on TCV. The next step will be to compare these measured responses with the CREATE-L model on the basis of which the Extreme Shape Controller is being developed.

4.1.6 LIDAR diagnostics

Several different tasks were achieved by a secondee. The first was to be trained on all the diagnostics of the LIDAR-microwave group in order to be a diagnostic expert during JET operation days. The second was to study, from a statistical point of view, the discrepancies between central electron temperatures measured by the LIDAR and by the ECE Michelson diagnostic. The last one is related to the edge LIDAR diagnostic measurements. We have add a new Processed Pulse File (PPF) in JET data that gives the line integrated density of the diagnostic on one line of sight of the FIR interferometer.

4.2 ITER Tasks and Research & Development

4.2.1 Superconductivity

Most of the activities at Fusion Technology - Superconductivity are carried out under EFDA contract in fulfillment of ITER relevant R&D actions agreed between the JCT (now IT) and EFDA.

The contract 00-518 (SULTAN operation) includes development and characterization of NbTi cable-in-conduit conductors, see Sections 2.5.1 and 2.5.2.

The contract 01-586 covers the design of 70kA High Temperature Current Leads and is carried out in collaboration with Forschungszentrum Karlsruhe, Section 2.5.4.

Under Task TW1-TMC-JSPREP, various R&D activities are carried out, including the development of a new full size Nb_3Sn cable-in-conduit conductor, Section 2.5.3, the set-up of a new facility for resistance distribution at joints, Section 3.5.2, and the critical current tests on Nb_3Sn strands extracted from loaded cable-in-conduit, Section 2.5.6.

The recently started task TW3-3.1-TMSC-ELRES is devoted to the investigations of the effect of the joint resistance distribution on the voltage-current characteristic of cable-in-conduit conductors.

4.2.2 ITER 170GHz gyrotron development (TW2-TPHE/ECRDEV)

The 2MW coaxial 170GHz gyrotron for ITER will require a superconducting magnet. The magnet must meet mechanical, electrical and physics constraints in order for the gyrotron to operate successfully. The design of both the magnet and gyrotron must be carried out in concert for operation at 170GHz. The beam parameters necessary for proper interaction with the selected gyrotron cavity mode are taken as a design goal. Using the DAPHNE code, a suitable preliminary design fulfilling the beam requirements has been established for both the gun cathode-anode geometry and the magnetic field shape. An iterative process has begun in which the design is reviewed by the other task partners and further calculations with respect to the beam transport after the interaction region are carried out. At the same time, calculations related to the feasibility of construction of the desired magnet winding are carried out. Finally, the technical details related to construction of the gun will be discussed with an industrial partner as a prelude to actual fabrication and testing.

4.2.3 Design Task on Plasma Control Issues (Task FU05-CT2001-00018 EFDA/00-551)

Work was performed in the context of the D424-E ITER Design Task on Plasma Control Issues as Design Task FU05-CT2001-00018 (EFDA/00-551). The work comprised 4 components, namely:

"The Effect of the Feedback Controller on the Superconducting Tokamak AC losses"
"AC-CRPP User Manual"
"Sensitivity of the ITER tokamak closed loop control system to variations in the assumed model"
"ITER divertor sweep AC loss Estimation"

and was performed by members of the CRPP, in collaboration with E. Zapretilina (from JCT Naka and Efrimov Institute, Russia).

The CRPP is active in both plasma shape and position controller design and superconductor development and it was natural to attempt to produce a simplified model of the AC losses in ITER. These losses are due to a) hysteresis losses (a property of the superconducting material when the transverse magnetic field changes) and b) coupling losses (essentially the skin effect in the normally conducting material which makes loops which intersect the changing transverse magnetic flux where the filaments touch). Their precise calculation is normally quite onerous and we developed a simplified model for these two losses and calibrated it against the detailed calculations, to generate the "AC-CRPP" model. Such a simple calculation is required for studying the properties of feedback controller design, since a long calculation cannot be used in any reasonable iterative design procedure. The first phase of this work was therefore the development and documentation of the AC-CRPP model, Part 2 of this work. The model was implemented within Matlab software, for ease of interface to the controller design tools in this same package and for portability.

Having established a benchmarked fast estimate of the AC losses, the primary goal was addressed, namely the sensitivity of the AC losses to the feedback controller design parameters, Part I of the work. The distribution of the two AC losses was studied for fixed perturbations (minor disruption, compound ELMs and Type I

ELMs, all defined as conventional in ITER work). The calculations were cross-checked against calculations made in Naka. The feasibility of optimising with respect to the closed loop performance and the AC losses was thereby demonstrated. In the next step, the feedback controller parameters were varied in the presence of a mixture of perturbations and during a 430 second plasma current flattop during an 1800 second full pulse. The results were as expected, namely reducing the responsivity reduces the AC coupling losses, but that the feedback controller parameters are not crucial for the hysteresis losses unless the closed loop response is oscillatory. In a final step, a proposition for a more benign controller was made using an adaptive controller. Finally optimising such a trade-off between performance and AC losses reduction will require experimental determination of the perturbations during ITER operation and this Task demonstrates a suitable approach.

In Part 3 we studied another open question, namely the variation of the closed loop performance in the presence of uncertainties in the open loop model on which the feedback controller was designed. This work was further enhanced by considering a more realistic case of saturation of the power supplies, which can cause a poorly performing feedback loop to actually become uncontrolled, thereby exaggerating the effect. This part of the design task was intended to demonstrate the method, based on Monte Carlo simulations with random variations of the parameters of the open loop system. The algorithm for modifying the open loop parameters was taken directly from experimental studies on JT-60U performed as a collaboration between CRPP and JAERI. Again a suitable methodology was demonstrated. The results indicate that the vertical instability is the primary parameter which causes changes to the closed loop performance, as expected. No other single parameter was identified to have a similar effect.

A final contribution in this task was to use the AC-CRPP model to examine the limits of divertor sweeping, from the point of view of the ELM heat load on the divertor plate. The amplitude, frequency and waveform of the sweeping were varied and the AC losses were estimated. The perturbation due to the ELM was also included in the closed loop modelling. The results were qualitatively as expected, with high AC losses at high frequency and high amplitude. However, the AC losses are only increased by a small factor above the losses due to the perturbation itself for the lower frequencies and the results suggest that there could be a window in which the power spreading might contribute to protecting the divertor. The results suggest that optimising such a strategy would be quite creative and would depend on the ELM character found in ITER. This work therefore suggests the methodology for implementing such a strategy. The next step would be to improve the reference ITER controller to reduce the cross-coupling between the reference signals for the divertor strike-point and the other gap parameters.

4.2.4 H-Mode database

New TCV data were contributed to the ITPA H-mode Threshold Database (ITPA = International Tokamak Physics Activity). They were selected in discharges with an L-mode to H-mode transition occurring at a high safety factor value (q95>2.6) in opposite to previously sent data. The new data present threshold powers lower than those from previous data and are in better agreement with the fit based on the multiple machines data. This result confirms the necessity of accessing the H-mode in a future reactor while the safety factor remains around 3, in order to maintain the threshold power as low as possible.

4.2.5 Diagnosing the ITER Divertor region using EC Absorption

The diverted region of ITER plasmas presents an enormous challenge to diagnosticians and at the same time is of crucial importance to ITER operation. It is essential to measure, with high spatial and temporal resolution, as many divertor plasma parameters as possible. It is, in principle, possible to measure the electron pressure in the divertor region using electron cyclotron absorption of electromagnetic radiation at a frequency near the fundamental (ordinary mode) and first harmonic (extraordinary mode) of the local cyclotron frequency. A feasibility study has been undertaken to study this. At this time codes are being developed to facilitate such a study. It is expected that a significant contribution to the ITER diagnostic effort will come from this work.

4.2.6 EC systems

R&D for ITER was focused on the development of the Electron Cyclotron wave system. Three main projects are presently still under development: design of a 2 MW-CW-coaxial gyrotron (see Section 4.2.2), design of the upper launcher and contribution to the design of various power supplies for the ITER gyrotron.

Regarding the design of the upper launcher which in ITER will be essential for the control of the neoclassical tearing mode, the CRPP completed a first assessment of the so-called “front steering mirror” concept. In this concept, the required steering of the millimetre wave beam is provided by movable mirror placed in front the plasma behind the neutron shield. The final report on the assessment of this concept was delivered to the EFDA-CSU in Garching. In collaboration with the Associations FZK (Germany), FOM (The Netherlands) and the Institut für Plasmaphysik (Univ. Stuttgart), a comparative assessment of the “front steering mirror” concept and of the “remote steering” concept was initiated and will be completed in 2003. In the so-called “remote steering” concept, the millimetre wave beam is steered by mirrors located outside the ITER vessel and propagated to the plasma using a specially designed waveguide.

The power supply system for ITER electron wave system will include high voltage, high power elements to be developed by industry and to be tested in an actual test stand by an Association. In view of their implementation on an European gyrotron test stand to be installed at the CRPP, our laboratory has been collaborating with the Associations ENEA (Italy) and FOM (The Netherlands) in the definition of these elements. The preliminary specifications of the test stand have already been defined.

4.3 Collaborations with other EURATOM Associations

R. J. Buttery and M. Hole, UKAEA, Culham, GB, *"MHD ideal stability limit and NTM studies of MAST discharges"*

M. Ciotti, P. Gislon, Association EURATOM-ENEA, Italy **D. Ciazynski, L. Zani**, Association EURATOM-CEA, France*, "Test in SULTAN of the PF-FSJS sample",* see Section 2.5.2

G. Cunningham, G. McArdle, Association UKAEA Fusion, UK, **J. Qin**, Imperial College, London, UK, *"Comparing the plasma equilibrium control of tight and conventional aspect ratio tokamaks"*

V. Grandgirard, P. Gendrih, X. Garbet, Y. Sarazin, Association EURATOM-CEA, France, *"Gyrokinetic theory and code development"*

Y. Ilyin and A. Nijhuis, University of Twente, Holland, *"The assessment of current distribution results from test in SULTAN"*

A. Jaun, Royal Institute of Technology, Association Euratom-NFR (Sweden), *"Kinetic theory of Alfven waves in toroidal plasmas"*

S. Kuhn, D. Tskhakaya, Association Euratom ÖAW, Innsbruck, Austria, **A. Loarte**, EFDA/CSU Garching, Germany, **L. Popova**, Bulgarian Academy of Sciences, Sofia, Bulgaria, *"PIC Simulations of ELM-produced particle and energy pulses and their effect on the SOL"*

M. Maraschek and S. Guenter, IPP, Garching, D, *"NTM marginal beta limit on AUG Tokamak"*

T. Madeira, **P. Amorim**, CFN/IST, Lisbon, Portugal: *"X-ray spectroscopy of the TCV plasma"*

A. Mück, C. Angioni, F. Ryter, H. Zohm, Max-Planck-Institut für Plasmaphysik, EURATOM-Association, Germany, and **E. Westerhof**, FOM-Instituur voor Plasmafysica "Rijnhuizen", Ass. EURATOM-FOM, Holland *"Sawtooth control experiments on ASDEX-Upgrade using ECRH"*

P. Nielsen, R. Pasqualotto, G. Manduchi, Consorzio RFX, Padova, Italy, *"Thomson scattering from the edge plasma of TCV"*

J. Nuehrenberg, S. Sorge, R. Hatzky, A. Peeters, V. Kornilov, Max-Planck IPP Greifswald and Garching, Germany, *"Development and upgrade of nonlinear global electrostatic PIC-finite-element gyrokinetic codes"*

Y. Peysson, Association EURATOM-CEA, France, *"Temporary installation of imaging hard-X-ray camera"*

D. Reiter, IPP, Forschungszentrum Juelich, Germany, *"Extension of B2.5 simulation grid for Eirene simulation of molecular reactions in TCV"*

A.P. Rodrigues, CNF/IST, Lisbon, Portugal: *"Multiple DSP based controller for TCV digital control system"*

TFMC test group included representatives of the German, Austrian, French, Italian and Dutch Associations, *"Toroidal Field Model Coil (TFMC) Test and Analysis Group"*
R. Heller, Association EURATOM-FzK, Germany, *"EFDA task on design of High Temperature Superconducting Current Leads"*

G. Zvejnieks, V.N. Kuzovkov, Institute of Solid State Physics, University of Latvia, Latvia, **O. Dumbrajs,** Helsinki Univserity of Technology, Finland, **H. Zohm** Max-Planck-Institut für Plasmaphysik, EURATOM-Association, Germany, *"Dynamical properties of Edge Localised Modes (ELMs) occurring in the ASDEX Upgrade and TCV experiments"*

4.4 Other International Collaborations

L. Bottura, CRYOSOFT and CERN, *"Development of finite elements codes applicable to the analysis of cable-in-conduit conductor behaviour"*

J.Egedal, M.Porkolab, J.Nazemi, Plasma Fusion Science Centre, MIT, USA, *"Collaboration on magnetic reconnection"*

G. Giunchi, Edison, Milan, Italy *"Test of MgB_2 high temperature superconductors"*

R. W. Harvey, CompX, San Diego, USA, *"Radial transport effects on electron cyclotron current drive efficiencies"*

R. La Haye, General Atomics, San Diego, USA, *"NTM studies on the DIII-D tokamak and cross-machines scalings"*

V.E. Lukash, RRC Kurchatov, Institute of Nuclear Fusion, Moscow, Russia, **R.R. Khayrutdinov**, TRINITI, Troitsk, Russia, **D. Raju**, IPR, Bhat, India, *"Simulation of TCV experiments using the non-linear DINA code"*

S.Yu. Medvedev, A.A. Martynov, A.A. Ivanov, Yu. Yu. Poshekhonov, V.V. Drozdov, Keldysh Institute of Applied Mathematics, Moscow, Russia, **M.Yu. Isaev, M.I. Mikhailov, V.D. Shafranov, A.A. Subbotin**, RRC Kurchatov Institute, Moscow, Russia, *"Stability of tokamaks including consistent description of the magnetic separatrix. Investigation of novel 3D magnetic configuration concepts and their optimisation"*

J. Minervini, PFSC, MIT, USA and **N. Martovetski**, LLNL, USA, *"Preparation and test of two subsize Nb_3Sn cable-in-conduit superconductors"*

G. Moritz and M Wilson, GSI, Darmstadt, Germany, *"Conceptual design of a superconductor of the new accelerator ring"*

W. Peide, Academia Sinica Institute for Plasma Physics, China, *"Evaluation of the test results of the Chinese superconductor sample in SULTAN"*

V.D. Shafranov, Kurchatov Institute, Moscow, Russia, **S. Medvedev**, Keldysh Institute of Applied Mathematics, Moscow, Russia, **V. Nemov**, Kharkov Institute of Physics and Technology, Ukraine, **J. Nuehrenberg**, MPIPP Teilinstitut Greifswald, Germany, *"Novel Approaches to Improve Confinement in 3D Systems"* (INTAS grant)

J. Snipes, M. Porkolab, P. STitus, D. Schmittdiel , Plasma Fusion Science Centre, MIT, USA, *"Alfven Eigenmodes and fast particle physics on JET"*

A. Sushkov, V. Andreev, K.A. Razumova, RRC Kurchatov Institute, Moscow, *"Implementation of a multiwire proportional X-ray detector for high sensitivity, high speed, high time resolution in TCV"*

M. Svandrlik, Elettra, Trieste, Italy, *"Commissioning of a new cryoplant system"*

K. Yamazaki, K.Y. Watanabe, Y. Narushima, S. Okamura, C. Suzuki, National Institute for Fusion Science, Toki-shi, Japan, *"MHD Stability in Heliotron and Quasiaxisymmetric Systems"*

4.5 Collaborations within Switzerland

Ph. Mullhaupt, D. Bonvin, B. Srinivasen, Laboratoire d'Automatique, EPFL, *"Development of saturating controller algorithms for ITER"*

L. Rivkin, Paul Scherrer Institute, *"SUPER-3HC Project"*

D.M. Semadeni and D. Spring, CEPE, *"Socio-economic studies for fusion"*

T.M. Tran, SIC-EPFL, *"Parallelisation of CRPP codes"*

J. Vos, Enterprise CFS, Parc Scientific PSE, Lausanne, *"Computational fluid dynamics of plasmas at atmospheric pressure, in particular applied to plasma torches"*

Many industrial collaborations are underway with the plasma processing group, see Section 2.7.

5 THE EDUCATIONAL ROLE OF THE CRPP

The CRPP plays a role in the education of undergraduate and postgraduate students, particularly in the Faculté des Sciences de Base (Faculty of Basic Sciences) of the EPFL. Advanced education and training in fusion and plasma physics topics is carried out as part of the research activities of the Association. Section 5.1 presents the 7 courses given to physics undergraduates and to engineering undergraduates. In their fourth and final year, physics undergraduates spend time with a research group at the EPFL, typically 12 hours per week for the whole year. During this period, they perform experimental or theoretical studies alongside research staff, discovering the differences between formal laboratory experiments and the "real" world of research. After their final examination at the end of the 4th year, physics students are required to complete a "diploma" work with a research group, lasting a full semester. This diploma work is written up and defended in front of external experts. The CRPP plays a role in all of these phases of an undergraduate's education, detailed in Sections 5.2 and 5.3.

As an academic institution, the CRPP supervises many Ph.D. theses, also in the frame of the Physics Section of the EPFL. 8 PhDs were awarded in 2002. At the end of 2002 we had 29 Ph.D. students supervised by CRPP members of staff, mostly in Lausanne but also 5 at the PSI in Villigen. Their work is summarised in Section 5.4.

5.1 Undergraduate courses

K. Appert, *Chargé de cours, and* **A. Fasoli,** *Assistant Professor – "Plasma physics II"*
One semester option course presented to 4th year Physics students, introducing the theory of hot plasmas via the foundations of kinetic and magnetohydrodynamic theories and using them to describe simple collective phenomena. Coulomb collisions and elementary transport theory are also treated. The students also learn to use various theoretical techniques like perturbation theory, complex analysis, integral transforms and solution to differential equations.

N. Baluc, *Chargée de cours – "Material Physics"*
Basic course on material physics, presented as an option to 4th year Physics students. The course covers the theory of diffusion, dislocation and plasticity as well as the characterisation of materials. Experimental techniques used in materials studies, as well as analysis methods are presented for super-alloys, quasi-crystals, ceramics, composites and polymers.

J.B. Lister, *Chargé de cours – "Plasma Physics III"*
An introduction to controlled fusion, presented as a one semester option to 4th year Physics students. The course covers the basics of controlled fusion energy research. Inertial confinement is summarily treated and the course concentrates on magnetic confinement from the earliest linear experiments through to tokamaks and stellarators, leading to the open questions related to future large scale fusion experiments.

M.Q. Tran, *Professor – "General Physics I"*

Winter semester 2001-2002 (2 hours of lecture and 2 hours of exercises) for the "Communications Systems" section. The course covers kinematics and basic Newtonian mechanics of material points.

M.Q. Tran, *Professor – "Plasma Physics I"*
An introduction to basic plasma physics, presented as a one semester optional course to 3rd year Physics students. The course treats the fundamental physics of magnetised and non-magnetised plasmas.

L. Villard, *Maître d'Enseignement et Recherche (MER) – "General Physics II"*
Summer semester (4 hours/week lecture and 2 hours/week exercises). Introductory course in physics for students in the "Communication Systems" section. The course covers Newtonian systems dynamics, special relativity and thermodynamics.

5.2 Undergraduate work performed at the CRPP

EPFL Students (2002 Summer semester)

Chong DING: *"Diagnostics of RF Plasma"*
During the first semester, the practical work consisted of getting to know the diagnostics of RF plasmas at 13.56MHz. At first, it started with getting to know the experimental set-up, i.e. the RF plasma reactor, the pumping system and the gas control system. Then, by studying the RF voltage and also by using several diagnostic probes such as Langmuir and ion flux probes, argon and oxygen plasmas were investigated in detail. Finally, an investigation of the species present in argon and oxygen plasmas was carried out using optical spectrometry. The objective of the TP was to compare the results obtained from the different diagnostics techniques and being capable of choosing the adequate technique for a specific plasma investigation.
During the second semester, the investigation of argon and oxygen plasmas was continued by in-depth understanding of the ion flux probe, which allowed a better measurement than the other probes during the first semester. Secondly, the ion species present in argon and oxygen plasmas were identified using a mass spectrometer. Then the ion species in a oxygen plasma under two different experimental conditions were identified for polymer surface modification.

Nicolas FREMAUX: *"Etude de système d'inversion d'image pour diagnostic TCV"*
This was the second semester during which the inversion of CCD camera images from the TCV divertor region was examined. The images are obtained from interference filtered CCD cameras equipped with a wide-angle viewing permitting observation of the entire plasma divertor plasma. During high density experiments, the plasma temperature and density in the plasma edge change and greatly modify the spectroscopic emission profiles from intrinsic impurities such as carbon and the deuterium working gas. The images obtained from the camera are integrated across chords intercepting the plasma. By applying tomographic inversion techniques similar to those used in medical imaging, the emission profiles during the plasma gas injection experiments can be calculated as a function of time. These are then used as input to edge modelling codes which examine the relative importance of the plasma processes during these experiments.

Joël GROGNUZ: *"Electron Bernstein Wave Heating"*
A means of heating overdense magnetically confined plasma is to couple ordinary mode electromagnetic radiation to the electrostatic Bernstein mode via the evanescent extraordinary mode. Work started in this field by attempting some Bernstein emission measurements (the reverse process to absorption and heating) and moved on to examine the feasibility of heating TCV plasmas using Bernstein waves, adapting both analytical and numerical models for use on TCV.

Christian SCHLATTER: *"Rapid tomographic inversion of bolometric data"*
A previous version employed a regular mesh of rectangular pixels to get the plasma emissivity cross-section (as is the case in most present plasma tomography algorithms). In a new version, we tried to apply the principles of rapid tomography on an irregular mesh with pixels shaped according to the plasma magnetic flux surfaces. This second approach has its origins in reconstruction routines written for the CRPP by colleagues from the Hungarian Association. Some defects in the flux shaped pixels algorithm were discovered while upgrading some functions. We succeeded in putting the routine into a usable form, although it unfortunately turned out that rapid tomography principles are not particularly efficient in this case. Finally, we applied the new routines on real bolometric data and tested the reconstruction quality as a function of the position error of magnetically determined flux surfaces. The results proved that the bolometric tomography was robust to these errors.

Daniel TAMBURRINO: *"Characterisation of powders in a circulating fluidised bed of a RF inductive plasma discharge by CCD imaging and laser scattering"*
RF inductive plasma discharges can be used to produce thin-film deposition on powders by Chemical Vapour Deposition (CVD). During the second semester the aim was to study the effect of powders circulating in the plasma on the electrical characteristics of the discharge and to characterise the powder circulation. Modifications of the exciting coil were necessary to produce homogenous plasmas. This required the development and improvement of the RF matching device. A fast 12-bit CCD camera was used to study the radial distribution of the powder for different pressures and various gas flows without plasma. Images of the powder illuminated by a laser sheet were taken with short exposure time (~300μs). The velocity could be determined by calculating the ratio of the length of the illuminated trails to the exposure time. The number density of the powder was also measured for different circulating conditions. The light of a laser beam is diffused through the powders, which we consider to be spherical, and is attenuated due to their presence. The concentration is determined by calculating the ratio of the intensity of the transmitted beam to the intensity of the beam without powder.

Themistoklis VASCO BOUTOS: *"X-ray measurements with a multiwire proportional counter (MPX)"*
With its 64 channels, the MPX diagnostic provides the best spatial resolution in the soft X-ray range in TCV and allows unprecedented MHD activity measurements, at a sampling rate of 200kHz. Measurements with an important high absorber thickness and Xenon gas in the wire cell yielded promising signals for the detection of the emission from supra-thermal electrons. The evolution of soft X-ray profiles of high elongation, high q discharges was studied.

Pierre WEBER: *"Etude et réalisation d'un prototype d'analyseur électrostatique d'énergie des ions pour l'expérience TORPEX"*
A gridded energy analyser has been designed for the new plasma device TORPEX. The relatively low density and temperature of the plasmas produced in TORPEX

allow measurements of the energy distribution of ions and electrons in the core of the plasma. Special care was taken in guaranteeing a good spatial and temporal resolution in view of the use of the probe for the characterisation of particle transport, a central goal of TORPEX experiments. The design of the probe was performed on the basis of calculations of the predicted plasma parameters. The major mechanical and electrical parts of the probe, including the system of multiple grids, have been constructed and tested. The probe is ready to be installed on the TORPEX device ready for the first plasma measurements.

EPFL Students (2002-2003 Winter semester)

Lukas DERENDINGER: "*Development of an RF plasma source for powder processing"*
In collaboration with the Institute für Verfahrenstechnik (ETHZ) an RF plasma for plasma treatment of various powders will be developed.

Sébastien JOLLIET: "*Trajectoires des particules dans un champ curviligne: méthode perturbative"*
This work will familiarise the student with techniques for following the guided centre orbits in an in-homogeneous magnetic field.

Nicolas MELLET: "*Résolution des équations pour les surfaces magnétiques resonantes d'Alfvén"*
This work will familiarise the student with the nature of the Alfvén Wave resonant surfaces in toroidal geometry.

Samantha PAVON: "*Powder production in the BAI plasma reactor"*
It is well known that powder formation takes place during microcrystalline silicon deposition. The aim of this TP work is to characterise the parameter space over which powder formation takes place.

Karin SCHOMBOURG: "*Construction and installation of a Gridded Electron Analyser for TORPEX"*
This work will familiarise the student with the instrumental and analysis techniques of this important diagnostic for TORPEX.

Francesca PALAZZI: *"Hot plasma effects on ray-tracing for 2nd harmonic X-mode heating in TCV Tokamak"*
The ray-tracing/absorption code TORAY-GA which is used for calculating the RF deposition profile with the ECH system installed on TCV does not take into account hot plasma effects in the ray-tracing part of the code. With a low-field side injection of the electron cyclotron waves, the hot-plasma effect on the refraction near the resonance layer (anomalous dispersion) can be such that the rf wave is refracted out of the plasma and is therefore not absorbed. In a simplified slab model (1D), a ray tracing code including hot-plasma effects is in development. This code will be used to study the relevance of these effects in typical TCV plasmas.

Exchange students

Sophie MOUSEL: from ESPEO – Université d'Orléans, France, *"Development of a numerical simulation tool to study uniformity of large area PECVD thin films"*

Plasma enhanced chemical vapour deposition (PECVD) of thin films such as silicone nitride is used for the fabrication of active matrix liquid crystal displays. During the last decade, the substrate size used by industry has increased from about 0.25m^2 to more than 1m^2 while the film thickness uniformity requirement has been increased. In order to help industry in the design of the new generation of PECVD reactors, a numerical model has been developed to predict the deposition uniformity in a large area rectangular reactor. This model solves the gas flow and species continuity equations for silicon nitride deposition in the geometry of a KAI type reactor developed by UNAXIS. The results of the model have been compared with experiments performed at UNAXIS. As its major result to date, this model has allowed us to understand the role played by the working gas injection geometry on the final uniformity obtained.

Alberto ALFIER: from Padova University, Italy for his "laurea thesis", *"Density limits in TCV"*
A collaboration with the Consorzio RFX group aims at improving the Thomson scattering diagnostic covering the edge region of TCV plasmas in a configuration typical for H-mode studies. For this purpose 9 spatial channels have been added providing a spatial resolution of $\Delta z \sim$ 1cm over the range -0.51cm < Z < -0.63cm, along a vertical chord at R=0.9m. The necessary spectrometers and data acquisition channels have been obtained on loan from the RFX team. The particular contribution of this work consisted of the analysis of Raman calibration data and preliminary analysis of data from a series experiments with ELMy H-mode plasmas in a SNU configuration, with the plasma centred in the bottom part of the TCV vessel. First results are presented the section on TCV physics.

Claire HOWARTH: Imperial College, London, UK, *"Calculation of Plasma Ion Temperatures"*
This third year physics exchange student diagnosed the electronic performance of a neutron detector on TCV and compared the measurements on the TCV tokamak with other ion temperature diagnostics. A ^{3}He filled gas proportional detector was used to detect the neutrons resulting from D-D fusion reactions. After analysis of the analogue amplifier electronics of this system, a digital filter was designed to compensate a strong over-shoot in the pre-amplifier section. The detector is now operational on TCV and was used to deduce an effective ion temperature and to detect the existence of a fast ion velocity tail that has been observed in previous ECH experiments.

External students

Sébastien GELIN from Lausanne and **Etienne STALDER** from Geneva chose to devote their school project ("travail de maturité") to controlled fusion. Both were introduced to this subject with equal emphasis on general fusion physics and tokamak physics. They wrote a mémoire and presented their work in their school. S. GELIN performed a personal piece of work during which he calculated the trajectory of charged particles in different magnetic field configurations.

5.3 EPFL Diplomas awarded in 2002

Steve GIRARDIN: *"Equilibre magnétohydrodynamique des miroirs couplés toroïdalement"*.
A 4-field period toroidal linked mirror system was conceived by splitting a regular torus into 4 quarters which are separated uniformly to produce straight segments. The coils in the corners are tilted with respect to the vertical and poloidal field coils and are introduced to help generate a toroidal linked mirror system with vacuum flux surfaces. Using LMP model coils that carry up to 36kA, it was demonstrated that a significant volume is enclosed by the last magnetic surface and that rotational transform values of the order of unity can be attained, though they are more typically about 0.2. Magnetic well values of 35% can be achieved. If the straight segment length becomes too long, the volume of closed magnetic surfaces vanishes. The VMEC code has been applied to compute MHD equilibria. Though this code failed to exactly duplicate the shapes of the vacuum flux surfaces obtained with field line ray tracing, the general tendencies of enclosed volume, rotational transform and magnetic well were reproduced with variations of coil currents and straight segment length.

Martin FOCKETYN: *"Etude comparative du courant "Bootstrap" dans le régime faiblement collisionel d'un stellarateur"*
A comparative study of the bootstrap current in stellarators in the collisionless regime between formulations that differ in the degree of analytic approximation has shown quite good agreement in quasiaxisymmetric (QAS) systems while in quasi-helically symmetric (QHS) systems the current, though reversed, differs by a factor of 2. In Wendelstein 7X (W7X), the difference is much more significant. The formulation adopted in the TERPSICHORE code yields results much closer to the nearly vanishing bootstrap current anticipated in this device. Nevertheless, some useful information is garnered from the more heavily analytic approach. The geometrical factor comprises three main terms. The first term depends almost entirely on the plasma current profiles. The second term depends strongly on the geometry of the fields and the third term is virtually negligible in all configurations. In QAS devices, the first term dominates. In QHS and W7X-like devices, the second term contribution to the bootstrap current becomes increasingly relevant.

5.4 Postgraduate studies

Postgraduate course in the 3rd cycle *"Applied Superconductivity II"*, R. Wesche and P. Bruzzone
This 39-hour course started in the winter semester 2001/2002 with "Applied Superconductivity I" and has been completed by "Applied Superconductivity II" in the summer semester 2002. The two main subjects of the course are large low temperature superconductors for fusion magnets and the metallurgy of high temperature superconductors.
In the introductory part of the course, an overview on the different classes of superconducting materials is given, including critical state model, Ginzburg-Landau and BCS theory. Because of their importance for applications of superconductivity, the AC loss behaviour, the stability and the effects of mechanical loads on the current carrying capacity are examined in depth. Relations between the microstructure and the transport critical current density are considered for low

and high temperature superconductors. The consequences of the anisotropic physical properties of high temperature superconductors on magnet design are discussed. The reduction of the refrigeration operation and investment costs provided by the use of high temperature superconductors is estimated.
After the discussion of technological aspects (conductor and winding manufacture) an overview on magnet (accelerator magnets, nuclear magnetic resonance, magnetic separation) and power applications (fault current limiter, transformer, power cables, superconducting magnetic energy storage, magnetic levitation) is given. The magnet system of the International Thermonuclear Experimental Reactor (ITER-FEAT) is described in detail. In addition, design considerations for superconducting current leads and power cables including economic aspects are presented. The results of performance tests of superconducting power cables and current leads are discussed. The subjects covered by the course provide an introduction to advanced research and development in the field of applied superconductivity.

International WE-Heraeus Summer School in Bad Honnef Germany, 8-13 September 2002 - Ch. Hollenstein
A course entitled "Dusty plasmas" was given in the postgraduate course on Low Temperature Plasma Physics and Applications (CLTPP-7).

2nd Summer School on Advanced Matrials, Politehnica University of Timisoara, Timisoara, Romania, September 2002 - N. Baluc
A course entitled "Structural materials for fusion reactors" was given at this Summer School.

Doctorate degrees awarded during 2002

Patrick BLANCHARD: *"Study of the supra-thermal emission in TCV with electron cyclotron heating"* EPFL PhD thesis no. 2606(02)
This work made use of a 24-channel high field side ECE radiometer in the frequency range 78.5-114.5GHz. Observation from the high field side allows the relativistically downshifted supra-thermal ECE to propagate towards the receiver without being reabsorbed by the thermal population. This diagnostic played an important role for the interpretation of combined second harmonic X-mode ECCD and third harmonic X-mode ECH experiments, where it measured supra-thermal ECE intensities up to six times above the thermal level. No supra-thermal emission was observed with pure second harmonic ECH, while third harmonic ECH on its own led to the production of supra-thermals. The plasma emission was interpreted using the bi-Maxwellian approximation, which provides estimates of the supra-thermal electron densities and effective temperatures, which are presented in more detail in the section on TCV results of this report. The bi-Maxwellian estimates are in good agreement with observations using a hard X-ray camera.

Christian DESCHENAUX: *"Etude de l'origine et de la croissance de particules submicrométriques dans les plasmas radiofréquence réactifs"* EPFL PhD thesis no. 2590(02)
The formation of sub-micron particles has been studied in a low pressure (0.1mbar) radio-frequency (13.56MHz) capacitively coupled dicharge. The growth of particles in silane plasmas, monitored with Infrared and Cavity Ring Down Absorption Spectroscopy, allowed us to make out changes in the structure of the particles during their growth. The hydrogen content of powder formed in silane plasma was estimated and changes in the absorption spectrum could be observed for silane diluted with hydrogen and argon. In particular, photoluminescence has been

detected for particles at 2.15eV that is attributed to crystalline structures in the particles. We showed that acetylenic compounds are preferentially produced in methane, ethylene and acetylene plasmas and that the hydrogen content of the other species produced in these plasmas depends on the initial gas hydrogen content.
Negative ions were shown up in these plasmas and a polymerisation reaction is proposed between acetylene and C2nx-negative ions to explain the formation of the particles' precursors. The formation of aromatic is suggested for n>3. The different relative production of C2Hx- ions is proposed to explain the different powder production rates with different initial gases or different fluxes. Particle heterogeneity, studied ex-situ with Transmission Electron Microscopy (graphitic onions, multiwalled nanotubes, flakes and agglomerates) is attributed to the erosion or the delamination of the deposited carbon layer.
Keeping in mind that the control of the powder production implies a control over the reactor contamination and its history, we concluded that an important fraction of the particles formed in the discharges studied depends on the gas phase reactions, determined by the plasma chemistry.

Florian DALLA TORRE*: "Microstructure and mechanical properties of nanocrystalline Ni produced by three different synthesis techniques"* EPFL PhD thesis no. 2713(02)
This work is a contribution to the characterisation of the microstructure and mechanical properties of nanocrystalline (nc) Ni produced by inert-gas condensation (IGC), electrodeposition (ED) and severe plastic deformation (SPD) via high pressure torsion (HPT).
The microstructure of the nc Ni samples as investigated by transmission electron microscopy (TEM) and X-ray powder diffraction (XRD) shows very small mean grain sizes, between 10 and 65 nm, a high degree of internal strains, a high quantity of impurities and in one type of sample (IGC), a large amount of porosity. The mechanical properties of nc Ni are characterized by a strong increase of strength (~1GPa) and a substantial reduction of ductility, when compared to conventional coarse grained Ni. Differences in microstructure and mechanical properties have been observed both as a consequence of the different synthesis techniques and of the synthesis parameters.
Regarding the deformation mechanisms, it is concluded that nc Ni deforms by three concurrent processes: (a) in the largest grains, deformation proceeds by lattice dislocations interacting with each other, (b) in the smaller grains, the grain boundaries play an active role in the nucleation, emission and absorption of lattice dislocations and (c) in the smallest grains, plastic strain is concentrated at the grain boundaries and is carried by grain boundary dislocations or other processes as atomic shuffling. There is a smooth transition from one mechanism to another, which strongly depends on the grain size, the microstrain and the characteristics of the grain boundary. The nucleation and emission of lattice dislocations are regarded as the rate controlling processes in nc Ni.
Differences were found in the thermal stability of the three types of nc Ni. Grain growth in nc Ni starts at temperatures considerably lower than in cg Ni. The deformation behavior at elevated temperatures, where strong grain growth occurs concurrently with the deformation, is significantly different in ED nc Ni as compar5ed to HPT Ni. It is concluded that ED Ni, that shows the typical features of superplasticity, deforms by grain boundary sliding of micron sized grains. The grain boundary sliding is controlled by the presence of a second Ni/S phase, while HPT Ni deforms by normal dislocation interactions.

Gloria FALCHETTO: *"Electromagnetic effects on micro-instabilities in tokamak plasmas"* EPFL PhD thesis no. 2524(02)
Electromagnetic micro-instabilities in tokamak plasmas are studied by means of a linear global eigenvalue numerical code. The development of this code is the extension of an existing electrostatic global gyro-kinetic spectral toroidal code. The model includes both non-adiabatic electron and ion responses. The parallel component of the magnetic perturbation is neglected, thus the model applies to finite but small beta plasmas. The geometry is a large aspect ratio configuration with circular magnetic surfaces. Trapped electrons are described by the bounce-averaged drift-kinetic equation. The system is closed by the quasi-neutrality equation and the parallel component of Ampere's law.
The electromagnetic effects on toroidal Ion Temperature Gradient (ITG) driven modes were studied. The stabilisation of these modes with increasing beta, predicted in previous work, was confirmed. The effects of finite beta were considered together with those of different magnetic shear profiles and of the Shafranov shift. Trapped electron modes, on the other hand, are rather insensitive to beta.
At a value about half the ideal MHD ballooning limit, another mode, the Alfvenic Ion Temperature Gradient (AITG) mode becomes unstable. Its global radial structure was shown up for the first time. It has both a global, ballooning-like radially extended structure and a sharp behaviour at rational values of the safety factor.

Xuejun JIA: *"The effects of simultaneous radiation damage and helium production on the microstructure and resulting mechanical properties of spallation source candidate materials"* EPFL PhD thesis no. 2702(02)
In this work the defect microstructure, irradiation hardening and helium embrittlement produced by high energy proton irradiation in 304L austenitic steel and martensitic steels F82H, T91 and OPTIMAX are studied.
The defect microstructure in the as irradiated and deformed and irradiated 304L as been investigated by TEM after irradiation to 0.7-7dpa at 250^{0}C with 800MeV protons. Irradiation induced small defect clusters characterize the structure of the as irradiated steel and faulted Frank loops. About 25% of the small clusters can be resolved as stacking fault tetrahedra (SFT's). The mean size of the small clusters and SFT's is 1.5nm. At the temperature and dose range investigated, both the size and density are insensitive to radiation dose. The size of the Frank loops, on the other hand, is larger than that of the clusters and is approximately proportional to the irradiation dose, reaching a mean size of 20nm at 7dpa. Although the high energy protons produce 170appm/dpa, no He bubbles were observed, probably due to the low irradiation temperature. Then again, the pre-existing carbides transformed to an amorphous structure as a consequence of the proton irradiation. In the deformed samples, the main feature is the presence of dense twin lamellae, which is the main deformation mode of the steel irradiated at this temperature, with characteristics comparable to dislocation channeling: no irradiation produced defects are observed in the twins. Radiation hardening is measured in the irradiated steel. As the defect density saturates, further hardening above 0.5dpa is believed to be due to the growth of the Frank loops.
TEM observations of the ferritic/martensitic steels after irradiations in the SINQ Target-3 to doses up to 11.8dpa at temperatures between 70^0-360^{0}C show the presence of a large density of small clusters and faulted loops The density increases rapidly with dose, but after 1-2dpa, the rate of increase diminishes to saturate at 11.8dpa. At the same time, the cluster size remains constant up to 235^{0}C, but it increases rapidly at higher irradiation temperatures. Their density, on the other hand, decreases above 255^{0}C. A high density of 1 nm He bubbles have been observed in samples irradiated at temperatures higher than 175^{0}C. Their size

increases slightly with increasing irradiation temperature, while their density decreases. Once again, carbides amorphise and it has been shown that the irradiation temperature controls this process, the amorphous temperature in this case being 235^{0}C.
Small punch tests (SPT) have been used to establish the mechanical properties of irradiated steels. An increase in the brittle-ductile temperature (ΔDBTT) has been measured that, contrary to the saturation observed after neutron irradiation, increases continuously with dose. There is a linear increase ΔDBTT with increasing He concentration and this increase is not reflected as comparable hardening due to He. In fact, the hardening observed can be explained by the presence of the cluster defect microstructure with the addition of a high density of nanovoids (which produce additional hardening even when no He is present). This hypothesis is confirmed in part by the observation under scanning electron microscopy of an intergranular type fracture in the T91 steel after low temperature testing of a sample irradiated to 8.6dpa and 720appm He.

Laurent KLINGER: *"3D numerical simulation of a plasma torch using a finite volume method"* EPFL PhD thesis no. 2678(02)
With a view to obtaining numerical simulations of a DC plasma torch, used for atmospheric pressure plasma spraying, we developed and implemented a numerical model based on the assumption of a one-species, local thermodynamic equilibrium flow. The model uses the complete Navier-Stokes equations and the current continuity equation to describe the flow inside a torch and the electric arc. The main feature of the flow is its cross-flow aspect, which requires a 3D model. After we added the electrical part and arc-specific aspects to the NSMB flow solver, we finally dealt with the implementation of the real gas equation of state in the code. The completion of that last step in our model enabled us to perform simulations for two main configurations: an arc in a cross flow in a square duct and an arc in the torch geometry. The simple geometry of the former allows relatively quick runs, while the latter is more computationally intensive. The results exhibit the basic features of an arc in a cross-flow that are observed experimentally, such as maintaining a fixed electric current while increasing the flow velocity results in a more deflected arc that dissipates more power.

Adriano MANINI: *"Analysis and interpretation of the plasma dynamic response to additional heating power using different diagnostics"* EPFL PhD Thesis no. 2599(02)
The spatial distribution of the absorbed power is a crucial ingredient for the interpretation of experiments with electron cyclotron heating (ECH), determining its effect on current and pressure profiles in advanced scenarios and for transport studies. A powerful method is to measure the dynamical response of the plasma to modulated electron cyclotron heating (MECH). Practically, however, this method encounters the problem of coupling between the MECH and the sawtooth activity, making the interpretation of the dynamical response impossible. A new method based on the singular value decomposition to determine the phase subspace containing the dynamics of both the sawteeth and the MECH, coupled with system identification, has been developed and successfully applied on both TCV and ASDEX Upgrade. This determination requires a diagnostic which is sensitive to the plasma energy content with an appropriate time and space resolution. Several diagnostics were tested on TCV and ASDEX Upgrade, with attention given to line integrated soft X-rays measured both with the diode SXR camera and with the multi-wire proportional X-ray detector chamber. A special effort was also made to develop a robust and routine method of experimentally assessing the total ECH power absorbed, from the time derivative of the thermal energy measured by the diamagnetic loop. This approach was first used to determine the absorbed power for

third harmonic X-mode heating in TCV and is now routinely used in various ECH experimental scenarios.

Edgar SCAVINO: *"Impurity transport measurements using laser ablation of impurities"* EPFL PhD thesis no. 2677(02)
This project, completed this year, investigated the transport of trace amounts of non-recycling impurties, Si and Al, injected into the plasma by means of a laser ablation system. The laser was a resuscitated pulsed ruby laser which had been used on the TCA tokamak 20 years ago and was installed onto TCV a few years ago, together with a target chamber supplied within the framework of a collaboration with KFKI, Budapest. The experimental work consisted mostly of several series of parameter scans in Ohmic L-mode discharges, including elongation, triangularity, plasma current, magnetic field and plasma density. Impurity penetration and the subsequent outflow phase were mainly diagnosed using the 200-channel X-ray tomography system. One of the most intriguing and least expected results was that the Si impurity residence times decrease by a factor of 2.5 as elongation was increased from 1.6 to 2.3. More importantly, the ratio of impurity to electron energy confinement time decreased from 3 to 1.2 during this scan, suggesting that operation of a fusion reactor at high elongation may be beneficial from the point of view of avoiding fuel dilution by reducing impurity content. The experimental results were interpreted using the STRAHL code to obtain estimates for the local transport parameters, shown in more detail in the section on TCV results.

Ph.D. Theses supervised by CRPP staff at the end of 2002

Paolo ANGELINO: "*Gyrokinetic model for electron and ion dynamics in axisymmetric plasma configurations"*
Electromagnetic microinstabilities in tokamak plasmas are studied by means of the linear global eigenvalue numerical code, EM-GLOGYSTO. An optimisation of the code running on parallel machines has been carried out with the aid of the MPI library, which allows for high portability and scalability. Thanks to the reduction of memory requirements obtained, we have been able to conduct a deeper analysis of the numerical convergence of the code. The electromagnetic code implemented has been applied to the study of ion temperature gradient (ITG) driven instabilities in tokamak configurations and Alfvénic Ion Temperature Gradient (AITG) modes. The effect of varying the ratio between the electron and ion temperature on these modes has been investigated, showing a stabilising effect at low ratio values. The behaviour of AITG instabilities for different electron temperature profiles has also been analysed. The evolution of the spectrum of these modes has been studied for varying magnetic shear configurations. The model has been further improved removing the drift kinetic approximation for electron dynamics, passing electrons now being treated with a full gyrokinetic model. This extension will allow us to study the Electron Temperature Gradient (ETG) driven modes.

Gilles ARNOUX: *"Plasma heating at the 3rd harmonic of the electron cyclotron frequency"*
The main feature of using X3-ECH on TCV is its ability to heat higher density plasmas since the cut-off density at the 3rd harmonic (1.1×10^{19} m^{-3}) is a factor of 3 higher than the 2nd harmonic. The first studies on the heating in X-mode top launch configuration have shown that the absorption efficiency was strongly dependent on the launcher poloidal angle. These results suggest install a real time feedback control. Experiments have been successfully performed to identify possible plasma signals to be used in the feedback loop.

To study the physics of the X3 heating more precisely, it is possible to determine the absorbed power by measuring the diamagnetic flux with a diamagnetic loop during modulated power experiments (MECH). MECH experiments allow us to determine not only the absorbed power, but the deposition profile by using singular value decomposition and a system identification.
These diagnostics have been used for quantitative studies of the single pass absorption in a variety of plasmas conditions with central densities above the X2 cut-off. In these experiments heating at L-mode plasmas with purely X3 heating or both off axis X2 and central X3 have shown single pass absorption as high as 100%. Single pass absorption as high as 80% has been measured in X3 heating of ELMy H-mode plasmas. Experiments with X3 top launch combined with high field side electron cyclotron emission have shown the potential of the X3 top launch to study the dynamics of supra-thermal electrons.

Juliette BALLUTAUD: *"Study of high deposition rate amorphous silicon in a Plasma Enhanced Chemical Vapour Deposition (PECVD) reactor for silicon thin-film solar cells"*
During the last year, we have carried out a systematic study of the influence of process parameters (pressure, power, gas flows, RF frequency) on the deposition rate of an aSi:H layer and on the layer qualities, namely layer density and defect absorption. This study used a standard inter-electrode gap reactor, 2.4cm. We obtained layers with a good deposition rate of 7Å.s^{-1} and higher. Solar cells made with this porous aSi:H layer have very bad degradation with time. An explanation for this phenomenon is that at a high deposition rate, radicals involved in the layer growth have less time to diffuse and react at the surface, leading to a porous layer structure. We obtained significant improvement of the layer density with higher process temperature (above 230°C).
We also studied the boron contamination of the amorphous silicon layer during the deposition of a solar cell in a one-chamber process. For the deposition of a solar cell p-i-n structure, we use trimethylboron (TMB) for the p-doped layer. TMB is a strong contaminant for the i layer and induces bad qualities of solar cells. We have successfully optimised several procedures to remove the boron contamination during the deposition of the i-layer.

Raul BONADE: *"A study of the constitutive behaviour and fracture behaviour of tempered martensitic steels in relation to their microstructure"*
The general objective of this work is related to the development of the assessment methods of fracture toughness on small specimens applied to the tempered martensitic steels. The specific goals will be: i) gathering more data on standard specimens to better characterize the fracture toughness in the transition region where quasi-cleavage is the dominant mechanism, ii) modeling the constitutive behavior in relation to the microstructure and deformation conditions based on dislocation mechanics, iii) modeling the fracture toughness-temperature curve and developing a physically-based constraint loss correction method in order to properly take into account the specimen size/geometry effect on fracture. The main results obtained during the first six months of this PhD work were: i) develop the acquisition technique making use of a confocal scanning laser microscope to determine the topographic maps (3D profiles) of the fracture surfaces of a specimen. These profiles are then necessary to perform fracture reconstruction, technique that allows following the sequence of events leading to fracture. ii) model alloys, based on the 9Cr and 12Cr composition, have been defined and ordered to study the constitutive behaviour. Basically, two ferritic and two martensitic model alloys have been chosen. The idea is to investigate the effect of the microstructure and that of the Cr content on the constitutive behaviour and fracture properties.

Paolo BOSSHARD: *"Charge exchange spectroscopy measurements of ion temperature and impurity ion density"*
The Charge eXchange Recombination Spectroscopy and the Diagnostic Neutral Beam Injector of TCV have recently been upgraded to improve the diagnostic efficiency in terms of signal noise (S/N=2-->10) and active/passive signal ratio (A/P=12%-->20% at a density of n_e~$6{\cdot}10^{19}m^{-3}$). The actual configuration allows T_i measurements from the CVI(n=8-->7) line (5291Å) in plasmas with average densities up to $8.10^{19}m^{-3}$.
During the last year, the ion contribution to the power balance and the ion energy confinement have been measured in ohmic discharges where shape parameters (elongation, triangularity, and limited and diverted configurations) and plasma density have been modified. The deuterium contribution to the energy balance $W_D/(W_e+W_D)$ is in the range 15-40%, with measured $T_i(0)/T_e(0)$ ratios up to 80-90% at average plasma densities of $6.10^{19}m^{-3}$ and carbon (the main impurity of these plasmas) concentrations typically of 3-5%. The ion temperature behaviour has been studied as a function of the plasma shape, showing in particular a strong decrease of the ion confinement when the triangularity varies from negative to positive values, as previously measured for the electron confinement. Furthermore, the ion contribution to thermal conduction, the main energy loss channel, is often negligible because of the low ion temperature gradients at the plasma edge ($\nabla T_e/\nabla T_i \geq 2$). The ion behaviour in ECH-X2 heated discharges has been measured for the first time on TCV, showing no clear influence of the additional heating on the ion temperature profiles because of the low electron-ion coupling due to the low plasma density in these operational regimes (X2 density cut-off ~$4.2{\cdot}10^{19}m^{-3}$).

Alberto BOTTINO: *"Modelling of magnetically confined plasmas"*
In the framework of a collaboration with the ASDEX Upgrade team, we performed a linear stability analysis for electrostatic microinstabilities in high confinement conditions by using the global electrostatic linear PIC LORB5 code. This code can directly simulate the effect of the ExB drift, induced by an imposed radial electric field, on Ion Temperature Gradient (ITG) modes and Trapped Electron Modes (TEM). In addition to the plasma rotation, we concluded that at least two other physical mechanisms contribute to the formation of an Internal Transport Barrier (ITB): the reversed shear profile and, to a lesser degree, the local value of the ratio between the ion and electron temperatures.
In addition to this, we worked on the non-linear tokamak electrostatic PIC code ORB5. In PIC non-linear simulations, energy conservation is usually lost in the saturation phase even though the underlying equations are energy conserving. We implemented an optimised tracer loading method, originally developed in theta-pinch geometry, in order to reduce the statistical noise due to the non-uniform sampling of the distribution function. Preliminary results show remarkable improvement to the conservation of the particle number and of the total energy.

Yann CAMENEN: *"Confinement studies in shaped and extremely shaped plasmas heated by electron cyclotron waves"*
In TCV, the shaping system and the flexible ECW system allow the study of the dependence of confinement with the plasma shape (κ, δ) in the presence of strong EC heating. During this year, the use of far off-axis EC power deposition to broaden the temperature profile, and hence the current profile, has been optimised and is now a powerful tool used to reduce the vertical instability of high q, high κ discharges. Routine operation at high κ will require feedback on the EC launcher mirrors to control the EC power deposition location in real time during the elongation process. These high q high κ discharges extend the stable operational

TCV domain, will enable us to decouple I_p and κ in the TCV τ_E experimental scaling law, and also, in combination with X3 central heating, will allow approaching the β limits at high κ and intermediate I_N. Significant X3 heating in discharges with $2<\kappa<2.5$ and $q\sim8$ has been recently achieved. More X3 power should allow to further increase β. New experiments, including transport and energy balance studies, will also be undertaken to determine the confinement trends with basic plasma parameters (κ, δ, P_{EC}, n_e) in EC dominated discharges. The improvement of the soft X-ray wire chamber (MPX) will provide temperature profiles using the absorber method, also valid in plasmas which are centrally overdense to X2 and hence information about the electron transport using EC modulation techniques. Simulations of the soft X-ray diagnostic response to modulation using different transport models will lead to better understanding of the relationship between the temperature and current profiles in far off-axis heated discharges.

Emiliano CAMPITELLI: *"Effect of neutron irradiation on microstructure and mechanical propertiesof Zr alloys"*
We are studying the effect of neutron irradiation on the microstructure and mechanical properties of Zr alloys. The following points describe the work carried out during the past year.
The selection of a suitable sample geometry for measuring the tensile properties in the transversal direction of a highly irradiated cladding tube has been studied. The selected sample is a smooth ring with the smallest possible volume for testing in a shielded facility and requiring considerable reduced machining operations.
These tests have been validated using steel and aluminium alloys to compare with the ring tests. The apparent yield stress is lower and "rounded" when compared to uniaxial tests.
An analytical study of the elastic deformation in these tests and the elastic stress and strain fields for the given loading path were calculated.
Fracto-mechanical experiments were performed on non-standard tube samples. The production of pre-cracked notches by fatigue cycling was successful.
TEM analysis mainly addressed the problems of optimisation of sample preparation methods from highly active material, TEM training and the observation of the un-irradiated microstructure.

Thierry DELACHAUX: *"Study of carbiding and nitriding plasmas in a high current arc reactor, with application to zirconium coating"*
Experiments reported last year showed that an adequate pre-treatment of our zirconia samples could lead, after the nitriding process, to a layer three times thicker than a non pre-treated sample. This enhancement in the process was correlated to surface microstructures on the zirconia. After calculation, it seems that this effect can be explained by an increase of the effective surface of only 1%. Such a weak difference is difficult to measure, but is in good agreement with our observations made by scanning electron microscopy. Optical characterisation shows that the pre-treated samples are brighter and have a reflectivity closer to gold than the non pre-treated, indicating that this is a suitable way to obtain ceramics with gold-like appearance.
To gain a better understanding of what is happening in the plasma during the nitriding process, we have started to develop a numerical chemical model. The aim is to describe the balance of the neutral species in the discharge and their transport in the diffusion zone where the samples are located. This model takes into account the argon, nitrogen and hydrogen gases, the radicals created in the plasma such as atomic nitrogen and hydrogen, ammonia molecules and other species in the

electronically excited levels of interest. So far, a compilation of the rate constants and cross sections has been prepared and the first results should be available soon.

Antoine DESCOEUDRES: *"Application of plasma emission spectroscopy to the electrical discharge during EDM"* (Top Nano 21 project n° 5768.2)
Electrical discharge machining (EDM) allows the production of mirror surface finishing with nanometre roughness and high machining accuracy. However, to obtain new challenging performance of this technology, it is necessary to understand the electrical discharge in detail. In the present project, a collaboration with Charmilles Technologies SA, optical emission spectroscopy is applied to study the discharge produced by an industrial device. This non-intrusive plasma diagnostic allows the measurement of elementary plasma parameters such as temperature, density and pressure and to determine contamination of the discharge and its origin. The dependence of the obtained plasma parameters on process relevant parameters such as current, plasma on-time, dielectric and electrode material is investigated. The first time-integrated spectra show a low electron temperature (about 0.75eV) and a very high electron density (up to $10^{19}cm^{-3}$), especially at the beginning of the discharge. The plasma is contaminated with material removed from the electrode. Time-resolved spectroscopy measurements are planned for the future.

Jean-Yves FAVEZ: *"Application of modern control methods to a tokamak plasma"*
All present-day tokamaks routinely use PID controllers, designed on crude assumptions and tuned by experience. Thus, as a result, the control performance is rather limited. Recently, considerable attention has focused on optimal controllers with enhanced robustness like LQG and H∞. Although these linear controllers have shown valid results, they can fail to maintain control in the presence of large disturbances such as ELMs. This weakness is frequently due to the saturation of the actuators and might cause considerable damage to the device. Our future work aims at the investigation of non-linear methods, which could avoid this problem by keeping the tokamak in a stable and safe operational domain even if large disturbances occur. A further goal in tokamak control research is to find a way to reduce the power consumption and the AC-losses while maintaining a fast response time. This work is targeted at the TCV, JET and ITER tokamaks.
Work has so far concentrated on understanding the modelling of the tokamak and on studying the controllability regions of linear systems with only one saturated input. We have already considered planar systems with one stable and one unstable pole under saturated linear state feedback and analysed its region of attraction. We have shown that there is a topological bifurcation in the region of attraction, i.e. the region of attraction changes between being an unbounded hyperbolic type region and a region bounded by a limit cycle. The main contribution of our work so far is to provide an analytical condition under which bifurcation occurs. This condition is based on the characteristics and position of the stable and unstable manifolds. Furthermore, the exact shape of the region of attraction has been provided.
Work has been carried out on a separate issue, namely the simulation of the full feedback control on TCV in the presence of ECH, using the DINA free-boundary simulation code, developed in collaboration with the Kurchatov and TRINITI institutes.
This project is carried out in collaboration with the Laboratoire d'Automatique of the EPFL.

Sergi FERRANDO: *"Bootstrap Current and Stability in the Asymptotic Regime in Quasi-Symmetric Configurations"*

The bootstrap Current arises from the difference of frictional and viscous forces between circulating and trapped particles. Trapping of particles is due to the inhomogeneity of the magnetic field strength B. In stellarators the inhomogeneity comes from the toroidicity and the helicity of the system. Equilibria with a consistent bootstrap current have been calculated in the collisionless regime for several reactor-size configurations. Results show the relationship between the magnetic field strength distribution and the trapping of particles. In a quasi-axisymmetric configuration particles with pitch-angles unable to overcome a certain magnetic field strength become trapped, performing a long excursion between reflections. Their interaction with passing particles gives a negative BC and increases the rotational transformThis increase is shown to destabilise the m/n=2/1 external kink mode. In quasi-helical geometry, particles become trapped in helical wells following a short trajectory before being reflected. The rotational transform is decreased and the BC flows in the opposite direction. The decrease weakly destabilises the m/n=9/8 internal kink for the relatively low beta cases studied.
Calculations of bootstrap current have also been performed for a W7 X-like reactor-size configuration, specially designed to combine toroidicity and helicity in order to neutralize the bootstrap current, obtaining accordingly small values for it.

Malko GINDRAT: *"Experimental study of the behaviour of a DC plasma spraying torch operated at low pressure"*
Low Pressure Plasma Spraying (LPPS) processes, which use DC plasma jets expanding at low pressure, are used for fast deposition of thin, thermally sprayed coatings on large surfaces. During the second year of this thesis the aim was to develop advanced diagnostic techniques to characterise the plasma jet flow in the lowest pressure range. Measurement of key plasma jet properties, such as the Mach number, electron density and temperature were performed using double electrostatic probes and Mach probes. An extensive mapping of these measurements was carried out for different chamber pressures between 2 and 80mbar and various plasma parameters such as torch currents (400 to 600A) and Argon gas flow (40 to 60slpm). Mach number profiles measured at different axial positions corresponding to successive expansion/compression zones show that the Mach number follows the pattern of these different zones: high Mach numbers in the expansion zones, low Mach numbers in the compression zones. Electron density and temperature radial profiles measured at the same axial positions as the Mach number measurements reveal that the electrons are also compressed and heated up as the flow slows down in the compression zones. Optical emission spectroscopy techniques have been developed and used to allow a comparison with the double probe measurements at different operating conditions. Plasma densities were measured by Doppler broadening and heavy particle temperatures were measured by Stark broadening. These techniques do not rely on the LTE assumption but they are not applicable simultaneously over the whole pressure range. Doppler broadening can only be used at low pressures because at higher pressures Stark broadening dominates. In parallel, further enthalpy probe measurements were also made on the installation belonging to the industrial partner of the project (Sulzer Metco) under LPPS process conditions, to allow a comparison with powder temperature and velocity measurements

Jan HORACEK: *"Measurement of edge electron temperature and turbulence in the tokamak plasma boundary"*
Activities covered the continuation and closure of the work on the overestimation of T_e by Langmuir probes operating under high recycling and detached conditions and preparations for the edge turbulence experiments expected to begin in earnest in

2003. Concerning the problem of Langmuir probe interpretation, combined analytical/numerical analysis has continued. In TCV, fast electrons arriving at the divertor targets due to strong T_e gradients parallel to the magnetic field in the scrape-off layer cannot account for the high apparent T_e which was consistently measured by the TCV probes.
Concerning the study of edge turbulence, good progress has been made in preparation for experiments in 2003. Measurements will be made using the TCV fast reciprocating Langmuir probe, a 5-pin system, the head of which has now been modified to more closely match the poloidal contour of the separatrix for the principle magnetic equilibrium that will be used. The new head has been successfully tested in plasma. DSP based electronics are being developed for real time analysis of the plasma sheath harmonic response to a fast sinusoidal sweep (100-400kHz) on a single probe tip. A new data acquisition unit with 2 16-channel, 14-bit resolution cards has been successfully implemented, permitting 8 channels of acquisition at 6 MSPS. Dedicated preparatory experiments have been performed to test some aspects of the turbulence diagnostic and the first results have been obtained for the turbulent particle flux and potential fluctuations during ELMs.
Effort was spent on the routine operation of TCV edge diagnostics in addition to analysis of results from helium discharges, the presence of parallel thermoelectric currents in the TCV edge plasma.

Igor KLIMANOV: *"Study of the electron distribution function during Electron Cyclotron Current Drive (ECCD)"*
The study requires the development of new diagnostic and analysis tools. A new 24-channel Low Field Side (LFS) radiometer is under construction. The RF-part that basically defines the sensitivity of the whole radiometer is being constructed at the CRPP. The IF part is being built in collaboration with the Scientific Research Institute in Kiev, Ukraine and the diagnostics will be ready for measurements in December 2002. It will allow LFS and High Field Side (HFS) measurements simultaneously. Vertical and Oblique Electron Cyclotron Emission (ECE) measurements will also be possible. In order to extract the information on the electron distribution function from the ECE measurements, a comparison with the results of numerical calculations, which may be based on a Fokker-Plank model, is needed. A numerical module to simulate the ECE emission spectra for any distribution function, for all modes and all angles of propagation is under development. At present, this code is combined with cold plasma ray-tracing to simulate ECE emission of any plasma, though some improvements can still be done. The code has been applied to X2 ECCD regimes for perpendicular viewing, corresponding to the existing experimental setup. This technique can also be applied X3 Electron Cyclotron Heating regimes.

Andrei MARTYNOV: *"MHD activity of tokamak plasmas"*
The stability of the ideal internal kink mode in tokamak plasmas was studied using the numerical codes CHEASE and KINX. The influence of the aspect ratio, current profile and plasma geometry was examined and compared with theoretical predictions. The stabilising effect of triangularity was demonstrated for TCV and MAST experimental conditions. For TCV, the scaling of the critical poloidal beta dependence on plasma geometry has been obtained. The scaling of the dependence of the ideal internal kink growth rate was obtained, including the role of both plasma aspect ratio and geometrical factors. In addition, the critical value of beta-Bussac was shown to depend strongly on aspect ratio as well as the dependence of the growth rate on beta.

Stefan MUELLER: *"Basic investigation of turbulence and transport in toroidal plasmas"*
The construction of the TORPEX experimental device will be finished by the end of 2002. The present work consisted of writing an interactive program for calculating, optimising and viewing the time-dependent electromagnetic fields for the TORPEX coil system, the dynamical magnetic force loads and the effects of current redistribution due to inductive coupling in macroscopic (5 mm x 50 mm) conductors.
This was followed by the installation and maintenance of a Linux-based computer system for instrument-control and data-acquisition for TORPEX. The major part of the work was to make our acquisition unit work together with the TORPEX mother clock and to guarantee data-flow from the probes to the screen.
The third element of this work concerns plasma theory (kinetic, gyrokinetic), mostly to estimate important parameters for drift-waves in the TORPEX machine. A program was written to semi-automatically solve complex dispersion relations.

Petri NIKKOLA: *"Simulations of electron cyclotron wave propagation in TCV"*
The CQL3D Fokker-Planck code has been used to model electron cyclotron current drive (ECCD) experiments in the TCV. As was found earlier, radial transport is needed in the calculations in order to simulate the ECCD efficiency observed experimentally. Lately, the main interest has been in modeling TCV plasmas with an electron internal transport barrier (eITB) present. These plasmas rely on off-axis ECCD. It has been found that due to the transport, the simulated ECCD current density is flat or centrally peaked. With the simulated current density profile, taking also into account the bootstrap current, we can calculate the q-profile in these plasmas. A specific diffusion model has been introduced in the presence of the barrier: divide the electrons into two groups according to their energy and assign a small diffusion coefficient for the lower energy group, in accordance with a small transport coefficient in the barrier region.

Mario PODESTA: *"Experimental studies of transport properties in toroidal plasmas"*
One of the goals of the TORPEX project is to increase our knowledge of anomalous transport properties in toroidal plasmas, starting from the measurements of basic plasma physics phenomena (wave-particle interactions, influence of radial electric fields on transport, and so on). Many diagnostics will be installed on TORPEX. Electrical and magnetic probes, as well as more sophisticated techniques like LiF and EC modulation, are conceived to give a good temporal and spatial resolution, as required for tracing the global plasma behaviour back to its microscopic dynamics.
The initial phase of this work included the development of the ECRH system, required both for plasma production and for EC modulation, as well as the design and construction of different diagnostics that will be installed on TORPEX, in particular low-frequency Langmuir probes.

Francesca Maria POLI: *"Study of fluctuations and turbulence in toroidal plasma"*
Up to now the work has focused on the development of diagnostics with good spatial and temporal resolution to be installed and tested on TORPEX. This thesis will concentrate on the electrostatic Langmuir probes and, in particular, in the project of a multi-tip array devoted to the study of the dynamics of the propagation of drift waves, which are expected to be the dominant modes in the TORPEX plasma. Three such arrays, each containing 11 probe pairs, will be mounted on the same poloidal cross section of the vacuum vessel. The geometry of the probe, together with the high acquisition frequency up to 10MHz will allow the reconstruction of the spectrum of fluctuations both in frequency and wave-number, as well as a mapping of turbulence structures, including their size and position.

Pavel POPOVITCH: *"Electromagnetic wave propagation in 3D plasma configurations"*
Low-frequency electromagnetic wave propagation in two- and three-dimensional plasma configurations is studied using a recently developed full wave code. The full wave problem is solved applying Fourier decomposition in the poloidal and toroidal angles and finite elements in the radial direction. A new version of the code has been developed that solves the equation in a general 3D geometry, using the metric provided by the VMEC and TERPSICHORE codes. The construction of the variational form in 3D geometry is numerically very demanding. In order to accelerate the code, we first apply a transformation of the equilibrium into Fourier space and then these Fourier components are used in the construction of the matrix. The code has been optimised to run on a vector processor platform. Several 3D plasma configurations have already been analysed, and characteristic 3D eigenmodes and gaps have been found in mirror-like and helical geometries.

Andrea SCARABOSIO: *"Studies on MHD activity as a function of plasma shape in standard TCV scenarios and MHD phenomena in advanced scenarios"*
In highly elongated discharges with far off-axis second harmonic EC heating and high core density, sawtooth activity is replaced by a continuous rotating mode with dominant (n,m)=(1,1), (2,2) and (3,3) components of small amplitude and slowly decreasing toroidal mode spectrum. Using numerical simulations, this behaviour is no longer consistent with the ideal kink model of the internal disruption previously found as the relevant model for high elongation κ plasmas in ohmic and centrally heated regimes. More work is needed to address the issue of pressure and current profile dependency of the internal disruption in particular with the addition of central X3 heating at high density.
MHD activity, limiting the plasma performance, has been observed during the ICEC scenario in TCV. A (2,1) tearing mode appears in the region of the steepest pressure profile and causes crashes in the emissivity of the soft X-ray in the core region. Often a (1,1) mode is seen to precede and then to lock to the (2,1) mode after slowing down in frequency. The tearing mode amplitude has showed clear β_p dependency, as expected for plasma regime with significant bootstrap current. When the plasma current is lowered and $q_0>1.2$, the tearing mode is no longer observed and the plasma pressure is limited by fast MHD events with (3/1) post-cursors.

Hannes SCHMIDT: *"Characterisation of a high density, large-area VHF Plasma Source"*
The objective of this project is a feasibility study of a novel, large-area plasma-based thin film production technique. A cylindrical reactor has been designed and constructed to show the "proof of principle" of a novel electrode design. The reactor parameters are 100cm electrode diameter at an excitation frequency of 100MHz. It has been shown that uniform electrode voltages can be obtained at these high excitation frequencies, a necessary condition for homogeneous etching and deposition. The corresponding experiments to obtain uniform plasma are underway. In addition it will be used to show that at this high excitation frequency high electron densities can be obtained compared to the one obtained in conventional 13.56MHz plasma.
During the past 18 months the project has been advanced to a stage where the scientific investigation of the plasma source is possible. The proof of principle for uniform electric field has been established in vacuum. The second phase comprises the development of the new high density industrial plasma reactor for PECVD application in collaboration with UNAXIS France SA.

Lukas STINGELIN: *"Beam Cavity Interactions in High Power Cyclotrons"*
Measurements on the main cavities of the PSI 590MeV ring cyclotron revealed a higher-order mode excitation at 1.8mA operation that coincides with the 10th beam harmonic. This suggests that beam-cavity interactions could have an important effect in future high current cyclotrons, planned for use in Accelerator Driven Systems - so that more detailed studies are warranted. We performed initial calculations on the ring cyclotron cavities using the E (eigensolver), T3 (wakefield solver), and TS3 (particle-in-cell) modules in the MAFIA code. In order to model the geometric deformation due to air pressure and wall heating calculated by ANSYS, SLAC's eigensolver (Omega3P) is used to take advantage of its unstructured grid and parallel computing features.
An attempt was made to explain the measured beam harmonic in the Omega3P calculations: The eigenmode of the deformed cavity geometry with a resonance frequency close to the 10th beam harmonic was found, and the total gap voltage over all 220 beam locations was calculated. Unfortunately, it did not explain the high signal levels measured, and both simulations and measurements still have to be refined. A vertical asymmetry of the electrodes, or the presence of an other mode which has not yet been found, could explain the discrepancies.
Particle In Cell (PIC) simulations were performed to investigate the influence of the excited fields back on the beam distributions. The eigensolver found a mode with longitudinal electric fields in the beam plane and resonance frequency close to the 10th beam harmonic. The corresponding fields were imported - with field amplitudes scaled to 10% of fundamental mode - as initial field distributions to the PIC-solver and led to a strong perturbation of the phase space.
Calculations with the MAFIA T3 module for 220 bunches, crossing the cavity at the same time with different energies, indicated a slight wakefield. Only small perturbations of the phase space were found in the subsequent PIC calculation.

Raluca STOENESCU: *"Irradiation effects on the microstructure, mechanical properties and residual stresses in the heat affected zone (HAZ) of stainless steel welds"*
The objective of this study is to correlate the residual stress state induced by welding in the HAZ of stainless steel welds with the microstructure and mechanical properties after neutron irradiation. During the first year, the unirradiated materials were characterized by means of Vickers microhardness measurements, tensile mechanical testing, optical and transmission electron microscopy observations. A very small variation of the grain size near the fusion line was evidenced; in the HAZ the grain size is about 600μm. The HAZ presents an increase in the yield strength as compared to the base material (BM). The deformation takes place via thermally activated mechanisms, and no significant strain rate sensitivity of the stress was evidenced. The dislocation and carbides densities were found higher in the HAZ than in the BM. Characterization of the low dose irradiated material will start in 2003

Alban SUBLET: *"Study of RF Atmospheric and Near Atmospheric Pressure Glow Discharges"*
Atmospheric Pressure Glow Discharges have many applications as an alternative to classical PECVD. Our study concerns silicon dioxide film deposition, in a capacitive discharge, using organo-silicon compounds. There are specific problems related with the plasma process by RF plasmas at atmospheric pressure: the applied RF voltage must be in the kiloVolt range which implies careful design of the power supply and of the reactor. Electrode gap, frequency and gas composition are also critical points to be considered in order to obtain the glow discharge.
The aim of this work consists of

- the electrical characterisation of the discharge in order to understand the influence of the electrical source, electrode configuration and gas composition;
- the study of the physico-chemistry of the discharge as the above parameters are varied;
- the study of the different chemical mechanisms as a function of pressure.

The first step of the thesis work was the design and construction of the electric circuit, the power supply and the reactor, carried out during the past year following a literature survey.

Marco WISCHMEIER: *"Divertor Detachment in the TCV and JET Tokamaks"*
Simulation of detachment in JET pure helium discharges in the MarkIIGB divertor constituted the main element of research effort in 2002. This was performed using the coupled fluid Monte Carlo code package SOLPS5.0, the principle tool adopted for this thesis. During the year, two periods of two weeks secondment at JET allowed strong interaction with SOLPS5.0 code support staff and a further two week period on EURATOM mobility at IPP-Garching concentrated on a detailed investigation of code internal power balance issues. The latter initially appeared to have been responsible for the inability of the code simulations to match experimental divertor target data for T_e and n_e, especially near the separatrix, obtained during plasma density ramps designed to investigate helium divertor detachment. Although the energy balance study has led to the discovery and correction of errors in certain coefficients governing the rate of energy transport, this does not, ultimately, appear to be the origin of the discrepancy between simulation and experiment. Efforts are continuing in order to understand this phenomenon, by which separatrix T_e values collapse to unphysically low values in the code at medium to high upstream densities when the power input to the scrape-off layer is low. Despite the disagreement, the global features of helium detachment are reproduced by the simulations which show the mechanism to be caused by the loss of He neutrals from target vicinity, radiating along the separatrix and in the X-point region, starving regions downstream from power. Such behaviour is in contrast to the general picture in D whereby ion-neutral frictional processes at low divertor T_e and eventually recombination reduce the target ion flux. The modeling has shown directly that recombination processes cannot play a role in He owing to the low residence times for He^+ in the divertor region, itself due to the lack of sufficient momentum removal by ion-neutral in comparison with D plasmas. During a second secondment at JET, new experiments were performed, designed to study detachment in deuterium in the MarkIISRP divetor (without septum). These will be studied using the SOLPS5.0 package.
Concerning simulation of TCV detachment, efforts are now underway to include molecular reactions into the Eirene code. The B2.5 plasma grid has been extended to a discretisation of the entire TCV vacuum vessel volume outside the separatrix (using a finite element mesh generator) and the inclusion of proper accounting for the toroidal curvature of the vessel (in place of the usual cylindrical assumption). This will be the starting point for a study of the potential for dissociative attachment and ion conversion reaction chains as the driving mechanisms behind the anomalous detachment observed in TCV.

Zhongwen YAO: *"Mechanical properties and microstructure of irradiated metals"*
In order to determine the saturation value in the defect accumulation in Ni single crystals, specimens were irradiated to 0.3dpa at room temperature in the PIREX facility. Complementary irradiations to 0.01dpa and 0.001dpa at room temperature were also performed. In order to understand Ni's behaviour relative to other fcc metals, Al and Ag samples were also irradiated to these low doses.

TEM work was continued for the 0.01dpa and 0.001dpa room temperature irradiation cases. The microstructure of the irradiated specimens consists of loops and stacking fault tetrahedra (SFTs). Defect densities measured by TEM using the weak beam technique are $1.3x10^{23}m^{-3}$, $1.5x10^{23}m^{-3}$ for 0.001dpa and 0.01dpa respectively. Results show the high density of defects is already accumulated at low dose at room temperature. It indicates that the SFTs to loops ratio is about 30%.
In-situ observations of the surface topography evolution of tensile samples were performed during the tensile test. In the irradiated case the deformation of the crystal is inhomogeneous and the surface presents sharp slip traces. After a shear strain of about 0.5, deformation tends to be more homogenous. In comparison the un-irradiated sample shows a homogenous evolution of the slip lines up to failure. Slip lines are less sharp, broader and wavy.
Mechanical tests at low temperatures were already performed for the un-irradiated Ni and Cu single crystals. In the range –196°C to room temperature, the flow stress increases and the elongation of the samples apparently increases with decreasing temperature. TEM observation of the deformed structures indicates that, in the case of copper tested at –196°C, deformation proceeds by twinning, while in the other cases the usual dislocation glide mechanisms operate.

Alexei ZABOLOTSKY: *"Particle transport in TCV"*
The electron density profiles in tokamaks are peaked, although the particle sources are usually situated at the wall. It is generally assumed that density peaking exists due to an inward particle pinch. However the nature of this pinch rests unknown. In a wide variety of TCV discharge conditions the electron density profile scales with the parameter $\langle j \rangle / j_0 q_0$ (inverse effective cylindrical safety factor). Moreover, scaling of the density peaking with additional ECH power is observed. Effort was devoted to interpreting such density profile behaviour in the framework of three potential turbulent particle transport mechanisms: Turbulent Equipartition (TEP), Turbulent Thermodiffusion (TTD) and the Ware pinch.
Analysis shows that only a combination of these models can predict all features of density profile behaviour observed in TCV. A good description of the profile behaviour in both Ohmic and ECH plasmas is provided by TEP with $\eta \approx 0.7$ (η defines the contribution of trapped and passed particles to the transport) together with Ware pinch with $D/\chi \approx 2/3$, where D and χ are the particle and effective heat diffusion coefficients respectively. However, the same degree of agreement between model predictions and experiment can also be obtained for a mixture of Ware pinch with $D/\chi \approx 2/3$ and some linear combination of TTD and TEP. Because of the strong correlation of the electron temperature and the parameter $\langle j \rangle / j_0 q_0$ in TCV it is very difficult to separate the influence of TTD and TEP on the density profile on the basis of available data. Several experiments aimed at resolving this uncertainty are planned next year in collaboration with JET.

6 PUBLIC RELATIONS ACTIVITIES IN 2002

2002 saw a number of public relations events, including two major meetings and many visits to the CRPP laboratories.

First major event: The European Physical Society annual divisional meeting on "Plasma Physics and Controlled Fusion" was held in Montreux, from the 17th to 21st June. This conference, uniting 700 scientists, triggered a press information campaign which involved written and spoken press, but not the TV!

During the opening ceremony, speeches were heard from several policy makers, from Switzerland and Europe. Notable extracts from these introductions are:

Secretary of State, Charles Kleiber:
"The threat of exhaustion of energy supplies is real. This creates the necessity for the authorities to take risks and, in name of the future of humanity, to work around sectorial interests to act on behalf of future generations.
But necessity alone will not work. You, scientists in the field of fusion energy must, through the strength of your conviction, but also by showing your capacity to listen to – and discuss with – society, you must build and develop the confidence in this long term endeavour.You are the agents of this confidence. In sporting terms, you are in the big leagues now."

European Commission, Umberto Finzi:
"In conclusion we have never been so close to a positive decision on the construction of ITER.
The situation is challenging and at the same time rather dangerous.
If this time, we don't succeed, fusion research in Europe will decay to a very modest level of basic research.
But I think that some optimism is justified …"

President of the EPFL, Prof. Patrick Aebischer:
"Controlled fusion constitutes a unique sustainable energy option not only for developed countries, but more importantly for emerging countries where the biggest

needs are. Being a long term quest, controlled fusion strongly benefits from being associated with academic institutions: the advancement of fusion requires a general frame which allows the development of ambitious projects, but also, the education of young generation of talented physicists."

During the opening ceremony, the annual Hannes Alfvén prize was awarded to Professor Marshall Rosenbluth, from UCSD.

The mini fusion expo was set up during this conference for which thanks are due to CEA Cadarache and Euratom. CEA Cadarache and CIEMAT-Madrid each presented their prospective ITER sites in Cadarache and in Vandellos. A live remote participation link was set up between Montreux and JET, to see what was going on on the JET project, ...a thousand km away!

Second major event: The Swiss Physical Society meeting was held at the EPFL, on February 28, and the CRPP was the main institution of the EPFL presented to about 60 delegates.

Programmed visits: A total of about 1000 people visited the CRPP during 2002. They ranged from from secondary schoolgroups to university researchers, coming from Switzerland and abroad. Among the visits were:

- The Leiden Students Association, "De Leidsche Flesch", organisation of all physics, astrophysics, mathematics and informatics students at the Leiden University: 50 students (16th May).
- Students from the Czech Technical University in Prague, 35 people (22nd August)
- Chinese TV (Shandong Dong Qi Film & TV Art Development Center) (July 1st)
- CERN Summer School, 50 participants, August 31st. Students from Italy, Germany, England, Belgian, Poland, Sweden, Holland, Spain, Israel, Greece, Bulgaria, Switzerland, France ...
- Kantonalen Mittelschule Stans, 2 visits of 18 pupils (16th & 30th April)
- ETML, about 30 apprentices in automatic control (19th April)
- Association AROPAC (Officiers protection atomique -chimique) 20 people (20th April)
- Ecole des Métiers, 2 visits in 2 groups of 20 people (8th May & 14th June)
- During the summer: Summer Science Passport, 40 pupils (13-17 year olds) came for half a day for 4 visits.

The movie **"The starmakers"** was translated into six languages, including: French, Spanish, Italian, Portuguese, Catalan and Korean. A DVD prototype was created by Hugues Desmedt (CEA-Cadarche).

The movie is now showing for two months (up to the end of February 2003) at the Palais de la Découverte, in Paris, as part of a 3D scientific festival of 7 movies.

"In Reach" meeting
One meeting (March) was dedicated to CRPP collaborators, in a so-called "in-reach" science information. As the CRPP is split into two sites (Lausanne and Villigen, near Zürich), the personnel from both sites warmly appreciated the meeting to learn bout our main research topics.

Outreach activities
Prof. M. Q. Tran gave general talks on fusion in Baden, Locarno, Thoune and Lausanne. Dr Ch. Hollenstein presented the activities of the industrial plasmas group. Various articles - or interviews - from CRPP staff appeared in Swiss newspapers or weekly magazines.

"**CRPP Clip**"
A short (1' to 2') film on CRPP, for the expo, was produced in the summer of 2002. A second, longer version for open days and school visits should be ready in 2003.

Visit by CORE: The Coordination group for Energy Research in Switzerland visited the TCV Tokamak in September 2002.

APPENDIX A Articles Published in Scientific Reviews During 2002

Alberti S., Goodman T.P., Henderson M.A., Manini A., Moret J.-M., Gomez P., Blanchard P., Coda S., Sauter O., Peysson Y., and the TCV Team, *"Full absorption of 3rd harmonic ECH in TCV tokamak plasmas in presence of 2nd harmonic EC-waves",* Nuclear Fusion **42**, 42 - 45 (2002)

Allfrey S.J., Bottino A., Sauter O., Villard L., *"The role of radial electric fields in linear and nonlinear gyrokinetic full radius simulations",* New Journal of Physics **4**, art. No. 29 (2002) (http://www.njp.org)

Angioni C., Pochelon A., Gorelenkov N.N., McClements K.G, Sauter O., Budny R.V., de Vries P.C., Howell D.F., Mantsinen M., Nave M.F.F., Sharapov S.E., & contributors to the EFDA-JET workprogramme, *"Neutral beam stabilization of sawtooth oscillations in JET",* Plasma Phys. & Contr. Fusion, **44**, 205-222 (2002)

Ariol M., Ambrosino G., Pironti A., Lister J.B., Vyas P., *"Design and experimental testing of a robust multivariable controller on a tokamak",* IEEE Trans. on Control Systems Technol., **10**(5), 646-653 (2002)

Blanchard P., Alberti S., Coda S., Weisen H., Klimanov I., *"High field side measurements of non-thermal electron cyclotron emission on TCV plasmas with ECH and ECCD",* Plasma Phys. & Contr. Fusion, **44**, 2231-1149 (2002)

Borba D., Berk H.L., Breizman B.N., Fasoli A., Nabais F., Pinches S.D., Sharapov S.E., Testa D., *"Modelling of Alfvén waves in JET plasmas with the CASTOR-K code"*, Nucl. Fusion **42**, 1029 (2002)

Bottura L., Marinucci C., Bruzzone P., *"Application of the code THEA to the CONDOPT experiment in SULTAN"*, IEEE Appl. Supercon. **12**, 1528-1531 (2002)

Bruzzone P., Fuchs A., Stepanov B., Vécsey G., *"Transient Stability Results for Nb3Sn Cable-in-Conduit Conductors"*, IEEE Appl. Supercon. **12**, 512-515 (2002)

Bruzzone P., Fuchs A., Stepanov B., Vécsey G., *"Performance Results of Nb3Sn Cable-in-Conduit Conductors under cyclic Load"*, IEEE Appl. Supercon **12**, 516-519 (2002)

Bruzzone P., Anghel A., Fuchs A., Pasztor G., Stepanov B., Vogel M., Vécsey G., *"Upgrade of Operating Range for SULTAN Test Facility"*, IEEE Appl. Supercon. **12**, 520-523 (2002)

Bruzzone P., *"Coupling currents loss in Nb3Sn cable-in-conduit conductors"*, IEEE Appl. Supercon. **12**, 524-527 (2002)

Buttery R.J., Sauter O., Akers R., et al., *"Neoclassical tearing physics in the sperical tokamak MAST",* Phys. Rev. Lett. **88**, 125005 (2002)

Cooper W.A. , Gruber R., Tran T.M., *"Benchmark Measurements on PCs"*, Supercomputing Review, EPFL, pp. 33-36, May 2002

Cooper W.A., Yamazaki K., Watanabe Y., Narushima Y., Yamada H., *"MHD stability analysis on helical system with bootstrap current including electric field effects"*, Proceedings of 11th Int. Toko Conference on Potential and Structure in Plasmas, Ceratopia Toki, Gifu, Japan, December 2000, Journal of Plasma Fusion Research, Vol **4**, ISBN4- 9900586-6-6, 418-421, 2001

Cooper W.A., Ferrando i Margalet S., Allfrey S.J., in collaboration with Kurchatov Institute, NIFS, Toki-shi, PPPL, IPP-Greifswald, UKAEA Dounreay, *"Bootstrap current destabilisation of ideal MHD modes in 3D reactor configurations"*, Special Issue: Invited paper at the 29th EPS Conference on Plasma Physics and Controlled Fusion, Montreux, Switzerland, June 17 - 21, 2002, Plasma Physics and Controlled Fusion, **44**, B357-B373 (2002)

deAlmeida P., Victoria M., *"Microstructure of ion-irradiated stoichiometric NiAl intermetallic: a comparative image simulation and transmission electron microscopy study"*, J. Phys. D: Appl. Phys. **35**, 2032 (2002)

Fasoli A., Testa D., Sharapov S., et al., and contributors to the EFDA-JET work programme, *"MHD spectroscopy"*, Invited paper at the 29th EPS Conference on Plasma Physics and Controlled Fusion, Montreux, Switzerland, June 17 - 21, 2002, Plasma Physics and Controlled Fusion, **44**, 1 (2002)

Favez J.-Y., Khayrutdinov R.R., Lister J.B., Lukash V.E., *"Comparing TCV experimental VDE responses with DINA code simulations"*, Plasma Phys. & Contr. Fusion, **44**, (2002), 171-193

Fikar J., Schaller R., Guilbaud N., Baluc N., *"Mechanical spectroscopy of icosahedral Al-Cu-Fe quasicrystals metal-based composites"*, Defect and Diffusion Forum, Vols **203-205**, 289 (2002)

Fischer O., Cooper W.A., Isaev M.Yu, Villard L., *"Neoclassical transport and alpha-particle confinement in novel 3D reactor systems"*, Nucl. Fusion **42**(7), 817-826 (2002)

Fuchs A.M., Wesche R., Anghel A., Roth F., Heller R., Tasca M., *"Test Results of a 10 kA Current Lead using Ag/Au cladded Bi-2212 Tubes"*, IEEE Appl. Supercon. **12**, 1281-1284 (2002)

Gallagher A., Howling A.A., Hollenstein Ch., *"Anion reactions in Silane plasmas"*, J. Appl. Phys. **91**(9), 5571 (2002)

Giacometti E., Fikar J., Baluc N., Bonneville J., *"Mechanical behaviour versus structure of Al63.6Cu24.0Fe12.4"*, Philosophical Magazine Letters, Vol. **82**, 183 (2002)

Graves J.P., Dendy R.O., Hopcraft K.I., Jakeman E., *"The role of clustering effects in interpreting nondiffusive transport measurements in tokamaks"*, Phys. Plasmas **9**(5), 1596-1605 (2002)

Harvey R.W., Sauter O., Prater R., Nikkola P., *"Radial transport and electron cyclotron current drive in the TCV and DIII-D tokamaks"*, Phys. Rev. Lett. **88**, 205001 (2002)

Hatzky R., Könies A., Kleiber R., Allfrey S.J., *"Energy conservation in a non-linear gyrokinetic particle-in-cell code for ion-temperature-gradient-driven (ITG) modes in theta-pinch geometry"*, Phys. of Plasmas **9**(3), 898-912 (2002)

Heller R., Friesinger G., Fuchs A.M., Wesche R., *"Development of High Temperature Superconductor Current Leads for 70 kA"*, IEEE Appl. Supercon. **12**, 1285-1288 (2002)

Hender T., Hennequin P., Alper B., et al., Pochelon A., *"MHD with strongly reverse shear in JET"*, Plasma Phys. & Contr. Fusion, **44**, 1143-1154 (2002)

Hofmann F., Coda S., Lavanchy P., Llobet X., Marmillod Ph., Martin Y., Martynov A., Mlynar J., Moret J.-M., Pochelon A., Sauter O., *"Extension of the TCV operating space towards higher elongation and higher normalized current"*, Nucl. Fusion **42**, 743-749 (2002)

Hofmann F., Furno I., Gersasimov S., Martin Y., Milani F., Nave M.F.F., Reimerdes H., Sartori F., Sauter O., *"Effect of ELMs on the measurement of vertical plasma position in TCV and JET"*, Nucl. Fusion **42**, 59-65 (2002)

Ilyin Yu, Nijhuis A., ten Kate H.H.J., Bruzzone P., *"Self Field Measurements by Hall Sensors on the SeCRETS Long Sample CICCs in SULTAN",* IEEE Appl. Supercon. **12**, 1667-1671 (2002)

Khraishi T.A., Zibib H.M., Diaz de la Rubia T., Victoria M., *"Localised deformation and hardening inirradiated metals: three-dimensional discrete dislocation dynamics"*, Metall. & Mater. Trans. **33B**, 285 (2002)

Lazzaro E. et al., Sauter O., *"Error field locked modes thresholds in rotating plasmas, anomalous braking and spin-up"*, Phys. Plasmas **9**, 3906 (2002)

Letsch A., Zohm H., Ryter F., Suttrop W., Gude A., Procelli F., Angioni C., Furno I., *"Incomplete reconnection in sawtooth crashes in ASDEX Upgrade"*, Nucl. Fusion **42**, 1055-1059 (2002)

Lister J.B., Sharma A., Limebeer D.J.N., Nakamura Y., Wainwright J.P., Yoshino R., *"Plasma equilibrium response modelling and validation on JT-60U"*, Nuclear Fusion **42**, 708 - 724 (2002)

Llobet X., Duval B.P., *"128 Channel PCI-based data acquisition system for MDSplus"*, Fusion Engineering and Design **60**, 285-289 (2002)

Maddison G.P. et al., Sauter O., *"ELM moderation in high density H-modes on JET and Alcator C-Mod"*, Plasma Phys. & Contr. Fusion **44**, 1937 (2002)

Manini A., Moret J.-M., Alberti S., Goodman T.P., Henderson M.A., "Modulated ECH power absorption measurements using a diamagnetic loop in the TCV tokamak", Plasma Phys. & Contr. Fusion **44**, 139-157 (2002)

Mantsinen M.J., Angioni C., et al., Sauter O., *"Analysis of ion cyclotron heating and current drive at w~2wch for sawtooth control in JET plasmas"*, Plasma Phys. & Contr. Fusion **44**, 1521-1542 (2002)

Marinucci C., Bottura L., Bruzzone P., *"Transient stability analysis of the SeCRETS experiment in SULTAN"*, IEEE Appl. Supercon. **12**, 1524-1527 (2002)

Martin Y.R., Degeling A.W., Lister J.B., *"Search for determinism in ELM time series in TCV"*, Special issue: Papers from the 8th IAEA Technical Committee Meeting on H-mode Physics and Transport Barriers, 5-7 September 2001, Toki, Japan, Plasma Physics and Controlled Fusion **44**, Supplement 5A (A373-A382), May 2002 (ISSN 0741-3335)

Martin Y.R., TCV team, *"H-mode threshold power in TCV ohmic plasmas"*, Special issue: Papers from the 8th IAEA Technical Committee Meeting on H-mode Physics and Transport Barriers, 5-7 September 2001, Toki, Japan, Plasma Physics and Controlled Fusion **44**, Supplement 5A (A143-A150), May 2002 (ISSN 0741-3335)

Mikhailov M.I., Shafranov V.D., Subbotin A.A., Isaev M.Yu, Nührenberg J., Zille R., Cooper W.A., *"Improved alpha-particle confinement in stellarators with poloidally closed contours of the magnetic field strength"*, Nucl. Fusion **42**, L23-L26 (2002) (Letter)

Moret J.-M., Ahmed S.M., Alberti S., and TCV Team, *"ECH physics and new operational regimes on TCV"*, Special Issue: Invited paper at the 29th EPS Conference on Plasma Physics and Controlled Fusion, Montreux, Switzerland, June 17 - 21, 2002, Plasma Physics and Controlled Fusion, **44**, B85-B97 (2002)

Pamela J., et al., Sauter O., *"Overview of results and possibilities for fast particle research on JET"*, Nucl. Fusion **42**, 1014 (2002)

Redi M.H., Johnson L., Klasky S., Canik J., Dewar R.L., Cooper W.A., *"Anderson localization of ballooning modes, quantum chaos and the stability of compact quasiaxially symmetric stellarators"*, Phys. of Plasmas, **9**(5), 1990-1995 (2002),

Reimerdes H., Sauter O., Goodman T., Pochelon A., *"From current driven to neoclassically driven tearing modes"*, Phys.Rev.Lett., Vol. **88**, No.10,105005-1-105005-4, (2002)

Ryter F., and the H-Mode Threshold Database Group, Martin Y., *"Progress of the international H-mode power threshold database activity"*, Special issue: Papers from the 8th IAEA Technical Committee Meeting on H-mode Physics and Transport Barriers, 5-7 September 2001, Toki, Japan
Plasma Physics and Controlled Fusion **44**, Supplement 5A (A415-A421), May 2002 (ISSN 0741-3335)

Samaras M., Derlet P.M., Van Swygenhoven H., Victoria M., *"Computer simulation of displacement cascades in nanocrystalline Ni"*, Phys. Rev. Lett. **88**, 125501 (2002)

Sansonnens L., Schmitt J., *"Shaped electrode and lens for a uniform radio-frequency capacitive plasma",* Appl. Phys. Lett. **82**(2), 182 - 184 (2003)

Sauter O., and members of, Task Force M, Fask Force H, and contributors to the EFDA-JET Workprogramme, *"Control of neoclassical tearing modes by sawtooth control"*, Physical Review Letters, Vol **88**, No 10, 105001-1-105001-5 (2002)

Sauter O., Buttery R.J., Felton R., Hender T.C., Howell D.F., and contributors to the EFDA-JET Workprogramme, *"Marginal beta limit for neoclassical tearing modes in JET H-Mode dischrages"*, Plasma Physics and Controlled Fusion **44**, 1999-2019 (2002)

Sauter O., Angioni C., Lin-Liu Y.R., *"Erratum: Neoclassical conductivity and bootstrap current formulas for general axisymmetric equilibria and arbitrary collisionality regime",* [Phys. Plasmas 6, 2834 (1999)],Physics of Plasmas **9**(12), 5140 (2002)

Schmitt J., Elyaakoubi M., Sansonnens L., *"Glow discharge processing in the liquid crystal display industry",* 25th Int. Conf. On Phenomena in Ionized Gases, Nagoya, Japan, 17-22 July 2001, Plasma Sources Sci. Technol. **11**, A2006-A210 (2002)

Scharer J., Degeling A., Borg G., Boswell R., *"Measurements of Helicon wave propagation and ArII emission"*, Phys. Plasmas **9**, 3734-3742 (2002)

Sharapov et al., Fasoli A., *"Alfvén cascades in tokamaks"*, Phys. Plasmas **9**, 2027 (2002)

Suttrop W.A., et al., Sauter O., *"High density high performance ELMy H-mode plasmas in JET"*, 43rd Annual Meeting, APS Division of Plasma Physics, Long Beach, CA, USA, October-November 2001 (Invited talk), Phys. Plasmas **9**, 2103 (2002)

Testa D., Giroud C., Fasoli A., et al., *"On the measurement of toroidal rotation for the impurity and the main ion species on the Joint European Torus",* Phys. Plasmas **9**, 243 (2002)

Thomsen K., Cordey J.G., The H-Mode Database Working Group, Martin Y., *"The Pedestal Database Working Development of a two-term model for the confinement in ELMy H-modes using the global confinement and pedestal databases"*, Special issue: Papers from the 8th IAEA Technical Committee Meeting on H-mode Physics and Transport Barriers, 5-7 September 2001, Toki, Japan, Plasma Physics and Controlled Fusion **44**, Supplement 5A (A429-A435), May 2002 (ISSN 0741-3335)

Tran M.Q., "Fusion energy research: The central role of the European Union", The Parliament Magazine **139**, 30 (2002)

Valovic M. et al., Sauter O., *"Long time-scale density peaking in JET"*, Plamsa Phys. & Contr. Fusion **44**, 1911 (2002)

Villard L., Bottino A., Sauter O., Vaclavik J., *"Radial electric fields and global electrostatic microinstabilities in tokamaks and stellarators"*, Phys. Plasmas **9**, 2684-2691 (2002)

Weisen H., Furno I., Alberti S. and the TCV Team, *"Shape dependence of sawtooth inversion radii and profile peaking factors in TCV L-mode plasmas"*, Nucl. Fusion **42**, 136 (2002)

Weisen H., Martin Y., Moret J.-M., and TCV Team, *"On the dependence of energy confinement on elongation in single null divertor plasmas"*, Nucl. Fusion (Letter) Vol. **42**, L5 - L7, (2002)

Westerhof E., Sauter O., Mayoral M.L., et al., Angioni C., and contributors to the EFDA JET Workprogramme, *"Control of sawteeth and triggering of neoclassical tearing modes with ion cyclotron resonance frequency waves in JET"*, Nucl. Fusion **42** (2002) 1324-1334

Zuev A.A., Ivanov A.A., Karpushov A.N., Kolesnikov E.Yu., Marakhtin S.V., Strogalova S.L., *"Dynamics of ion heating in a gas-dynamic trap during neutral beam injection"*, Plasma Physics Reports, Vol. **28**(4), 268 - 273 (2002)

APPENDIX B Conferences and Seminars

B.1 Conference proceedings published in 2002

Alberti S., Porte L., Arnoux G., Goodman T.P., Henderson M.A., Hogge J.-P., Nelson-Melby E., *"Top Launch 3rd Harmonic X-mode Electron Cyclotron Heating in the TCV Tokamak",* Proc. 29th EPS Conference on Plasma Physics and Controlled Fusion, Montreux, Switzerland, June 2002, ECA Vol. 26B (2002) (P-2.073)

Allfrey S.J., Hatzky R., Bottino A., Villard L., *"Global Gyrokinetic Simulations of Nonlinear Interaction of Zonal Flows with ITG Modes"*, Proc. 29th EPS Conference on Plasma Physics and Controlled Fusion, Montreux, Switzerland, June 2002, ECA Vol. 26B (2002) (P-4.059)

Allfrey S.J., Hatzky R., Bottino A., Villard L., *"Role of self-generated and externally applied radial electric fields in the development of ITG driven modes"*, Proc. Joint Varenna-Lausanne International Workshop on "Theory of Fusion Plasmas", Varenna, Italy, August 2002, edited by J.W. Connor, O. Sauter and E. Sindoni, ISPP-20 (Editrice Compositori, Bologna, 2002)

Angelino P., Falchetto G.L., Vaclavik J., Villard L., *"Ion and electron temperature ratio and magnetic shear effects on electromagnetic instabilities"*, Proc. Joint Varenna-Lausanne International Workshop on "Theory of Fusion Plasmas", Varenna, Italy, August 2002, edited by J.W. Connor, O. Sauter and E. Sindoni, ISPP-20 (Editrice Compositori, Bologna, 2002)

Anghel A., Marchand P., Pedrozzi M., Bredy P., *"The cryogenic system for the third harmonic superconductivity cavity at SLS and Electra"*, Proc. 19th Int. Cryogenic Engineering Conference and Industrial Exhibition (ICEC-19), Grenoble, France, July 2002

Anghel A., *"A simple model for the prediction of quenelle point in cable-in-conduit conductors"*, Proc. Of CHATS-2002, Karlsruhe, Germany, 16-18 September 2002

Angioni C., Goodman T.P., Henderson M.A., Mantsinen M.J., Sauter O., *"Understanding Sawtooth Period Behaviour with Electron and Ion Cyclotron Resonance Heating and Current Drive"*, Proc. 29th EPS Conference on Plasma Physics and Controlled Fusion, Montreux, Switzerland, June 2002, ECA Vol. 26B (2002) (P-1.118)

Arnoux G., Manini A., Moret J.-M., Alberti S., *"Modulated ECH Power Absorption Measurement with a Diamagnetic Loop in TCV Tokamak",* Proc. 29th EPS Conference on Plasma Physics and Controlled Fusion, Montreux, Switzerland, June 2002, ECA Vol. 26B (2002) (P-2.076)

Ballutaud J., Howling A.A., Sansonnens L., Hollenstein Ch., Kroll U., Schönbachler I., Bucher C., Poppeller M., Weichart J., Buechel A., Jomard F., *"Plasma Deposition of p-i-n Devices using a Single PECVD Chamber: Study of the Boron Contamination"*, Proc. 29th EPS Conference on Plasma Physics and Controlled Fusion, Montreux, Switzerland, June 2002, ECA Vol. 26B (2002) (P-2.029)

Baluc N., Schäublin R., Spätig P. Victoria M., *"Hardening mechanisms in ferritic/martensitic steels"*, 21st ASTM Sympositum on Effects of Radiation on Materials, Tucson, USA, June 2002

Baluc N., *"Structural materials for fusion reactors"*, 2nd Int. Conf. on Advanced Materials and Structures, Politehnica Univ. of Timisoara, Timisoare, Romania, September 2002

Baluc N.L., Schäublin R., Spätig P., Victoria M., *"On the potentiality of using ferritic/martensitic steels as structural materials for fusion reactors"*, 19th IAEA Fusion Energy Conference, Lyon, France, October 2002, IAEA-CN-94/FT/1-1Rb

Blanchard P., Alberti S., Coda S., Weisen H., *"Analysis of the Electron Cyclotron Emission from the Non-Thermal Electron Population Generated by ECRH and ECCD"*, Proc. 29th EPS Conference on Plasma Physics and Controlled Fusion, Montreux, Switzerland, June 2002, ECA Vol. 26B (2002) (P-2.074)

Bosshard P., Duval B.P., Karpushov A., Mlynar M., *"Ion Temperature Behaviour and Ion Contribution to the Power Balance Measured by CXRS in Ohmic and ECR Heated Plasmas on TCV"*, Proc. 29th EPS Conference on Plasma Physics and Controlled Fusion, Montreux, Switzerland, June 2002, ECA Vol. 26B (2002)(P-4.120)

Bottino A., Allfrey S.J., Peeters A.G., Sauter O., Villard L., and ASDEX Upgrade Team, *"E x B Flow Effects on ITG Modes in Reverse Shear ASDEX Upgrade Discharges"*, Proc. 29th EPS Conference on Plasma Physics and Controlled Fusion, Montreux, Switzerland, June 2002, ECA Vol. 26B (2002) (P-1.040)

Bottino A., Hatzky R., Allfrey S.J., Sauter O., Villard L., *"Global nonlinear gyrokinetic simulations of ITG modes using particles in tokamak geometry"*, Proc. Joint Varenna-Lausanne International Workshop on "Theory of Fusion Plasmas", Varenna, Italy, August 2002, edited by J.W. Connor, O. Sauter and E. Sindoni, ISPP-20 (Editrice Compositori, Bologna, 2002)

Bottura L., Marinucci C., Bruzzone P., *"Analysis of current redistribution in a cable-in-conduit"*, Proc. CHATS-2002, Karlsruhe, Germany, 16-18 September 2002

Brunetti M., Grandgirard V., Allfrey S., Bottino A., Bertrand P., Ghendrih P., Sauter O., Vaclavik J., Villard L., *"Comparisons between Semi-Lagrangian Drift-Kinetic Code and PIC Code Simulations for ITG Studies"*, Proc. 29th EPS Conference on Plasma Physics and Controlled Fusion, Montreux, Switzerland, June 2002, ECA Vol. 26B (2002) (P-4.102)

Bruzzone P., Wesche R., Stepanov B., Vogel M., *"Recent results from Superconductor R&D at CRPP"*, 19th IAEA Fusion Energy Conference, Lyon, France, October 2002, IAEA-CN-94/CT/P-16

Bruzzone P., Stepanov B., Vogel M., Gloor T., Wesche R., *"Parametric studies of subsize NbTi calbe-in-conduit superconductors for ITER FEAT"*, Proc. of ASC-2002

Bruzzone P., Wesche R., Stepanov B., *"The voltage/current characteristic (n index) of the cable-in-conduit conductors for fusion"*, Proc. of ASC-2002

Bruzzone P., *"Learning about hydraulics and stability through an AC loss test"*, Proc. CHATS-2002, Karlsruhe, Germany, 16-18 September 2002

Buttery R.J., Akers R., Arends E., et al., Sauter O., *"Stability at high performance in the MAST spherical tokamak"*, Proc. 19th IAEA Fusion Energy Conference, Lyon, France, October 2002, IAEA-CN-94/EX/S1-6

Camenen Y., Pochelon A., Hofmann F., Angioni C., Goodman T.P., Henderson M.A., Nikkola P., Porte L., Sauter O., *"Current profile tailoring with far off-axis ECH power deposition in TCV elongation experiments"*, to be published in Proc. 12th Joint Workshop in Electron Cyclotron Emission and ElectronCyclotron Resonance Heating (EC-12), Aix-en-Provence, May 2002

Chel S., Bosland P., Bredy P., Anghel A., *"Super 3HC cryomodule general layout and first tests"*, Proc. Of EPAC 2002

Coda S., Alberti S., Blanchard P., Goodman T.P., Henderson M.A., Nikkola P., Peysson Y., Sauter O., *"Electron cyclotron current drive and suprathermal electron dynamics in the TCV tokamak"*, Proc. 19th IAEA Fusion Energy Conference, Lyon, France, October 2002, IAEA-CN-94/EX/W-5

Coda S., Alberti S., Blanchard P., Goodman T.P., Henderson M.A., Nikkola P., Peysson Y., Sauter O., *"Unfolding the dynamics of Suprathermal Electrons: Experimental and Numerical Tools on the TCV Tokamak"*, Proc. 29th EPS Conference on Plasma Physics and Controlled Fusion, Montreux, Switzerland, June 2002, ECA Vol. 26B (2002) (O-4.03)

Condrea I., Pitts R.A., Duval B.P., Ahmed S.M., Zabolotsky A., Wischmeier M., Karpushov A., Horacek J., Martin Y.R., Mlynar J., *"Helium Discharge Operation in TCV"*, Proc. 29th EPS Conference on Plasma Physics and Controlled Fusion, Montreux, Switzerland, June 2002, ECA Vol. 26B (2002) (P-2.079)

Cooper W.A., Nührenberg J., Drozdov V.V., Ivanov A.A., Martynov A.A., Medvedev S.Yu., Poshekhonov Yu.Yu., Isaev M.Yu., Mikhailov M.I., *"3D Equilibrium Averaged Description and Consistency Check",* Proc. 29th EPS Conference on Plasma Physics and Controlled Fusion, Montreux, Switzerland, June 2002, ECA Vol. 26B (2002) (P-2.113)

Crisanti F., Albanese R., Ambrosino G., Ariola M., Lister J., Mattei M., Milani F., Pironti A., Sartori F., Villone F., *"Upgrade of the Present JET Shape and Vertical Stability Controller"*, Book of Abstracts, 22nd Symposium on Fusion Technology, Helsinki, Finland, September 2002, 371 (2002)

Cunningham G., Lister J.B., Akers R., McArdle G., Qin J., Wilson H., *"High Elongation in teh MAST Spherical Tokamak"*, Proc. 29th EPS Conference on Plasma Physics and Controlled Fusion, Montreux, Switzerland, June 2002, ECA Vol. 26B (2002) (P-5.092)

Dammertz G., Alberti S., Arnold A., et al., Hogge J.-P., Tran M.Q., *"140 GHz, 1 MW, CW gyrotron for fusion plasma heating*", Proc. 3rd IEEE Int. Vacuum Electronics Conf. (IVEC), Monterey, California, April 2002, 330-331

Dammertz G., Alberti S., Fasel D., et al., Tran M.Q., *"Power modulation capabilities of the 140 GHz / 1 MW gyrotron for the Stellarator W7-X"*, Book of

Abstracts, 22nd Symposium on Fusion Technology, Helsinki, Finland, September 2002, 183 (2002)

Darbos. C, et al., Alberti S., Tran M.Q., *"Very Long Pulse Operation of the TORE Supra ECRH System"*, Book of Abstracts, 22nd Symposium on Fusion Technology, Helsinki, Finland, September 2002, 191 (2002)

Degeling A.W., Martin Y.R., Lister J.B., Llobet X., *"Active Modification of the ELM Frequency in TCV"*, Proc. 29th EPS Conference on Plasma Physics and Controlled Fusion, Montreux, Switzerland, June 2002, ECA Vol. 26B (2002) (P-2.078)

Descoeudres A., Sansonnens L., Hollenstein Ch., *"Negative Ions Dynamics and Attachment-induced Ionization Instability in O2, CF4 and SF6 Low-pressure Modulated Capacitive RF Plasmas"*, Proc. 29th EPS Conference on Plasma Physics and Controlled Fusion, Montreux, Switzerland, June 2002, ECA Vol. 26B (2002) (P-4.027)

Elzendoorn B.S.Q., and ECH Team, inclduding, Henderson M., *"Design of an ECRH launcher for JET"*, Book of Abstracts, 22nd Symposium on Fusion Technology, Helsinki, Finland, September 2002, 201 (2002)

Falchetto G., Vaclavik J., *"Global Gyrokinetic Study of Finite beta Effects on Linear Microinstabilities"*, Proc. 29th EPS Conference on Plasma Physics and Controlled Fusion, Montreux, Switzerland, June 2002, ECA Vol. 26B (2002) (P-5.061)

Fasel D., Alberti S., Bonicelli T., Cleasen R., Goodman T.P., Hogge J.P., Perez A., Santinelli M., Sterk A., Tran M.Q., **Verhoeven A.G.A..,** *"Design study of a test stand for ITER gyrotron"*, Book of Abstracts, 22nd Symposium on Fusion Technology, Helsinki, Finland, September 2002, 199, (2002)

Ferrando i Margalet S., Cooper W.A., Allfrey S., Focketyn M., *"Bootstrap Current for 3D Reactor-Size Configurations"*, Proc. 29th EPS Conference on Plasma Physics and Controlled Fusion, Montreux, Switzerland, June 2002, ECA Vol. 26B (2002) (P-2.088)

Ganesh R., Vaclavik J., Villard L., *"Effect of parallel magnetic field fluctuations (finite beta) in linear gyro-kinetic stability analysis of drift waves"*, Proc. Joint Varenna-Lausanne International Workshop on "Theory of Fusion Plasmas", Varenna, Italy, August 2002, edited by J.W. Connor, O. Sauter and E. Sindoni, ISPP-20 (Editrice Compositori, Bologna, 2002)

Gindrat M., Dorier J.-L., Hollenstein Ch., Loch A., Refke A., Salito A., Barbezat G., *"Effect of specific operating conditions on the properties of LPPS plasma jets expanding at low pressure"*, Proc. Inte. Thermal Spray Conf. 2002, Essen Germany, 4-6 March 2002, published in ITSC 2002 proceedings, Ed. E. Lugscheider, Pub. DVS, Düsseldorf, Germany 2002, p. 459

Giunchi G., Ceresara S., Ripamonti G., et al., Wesche R., Bruzzone P., *"High performance new MgB2 superconducting hallow wires"*, Proc. of BOROMAG Symposium 2002, Genova, Italy, June 17-19, 2002

Goodman T.P., and TCV Team, IPP-Garching, LANL, USA, DRFC-CEA Cadarache, IPR, Bhat, India, GA, San Diego, RRC Kurchatov, Moscow, *"An*

overview of recent results from the TCV tokamak", 19th IAEA Fusion Energy Conference, Lyon, France, October 2002, IAEA-CN-94/OV/4-2

Goodman T.P., Behn R., Coda S., Condrea I., Henderson M.A., Nikkola P., Sauter O., *"ECCD and Bootstrap Current Profiles in Advanced Scenario Plasmas in TCV"*, Proc. 29th EPS Conference on Plasma Physics and Controlled Fusion, Montreux, Switzerland, June 2002, ECA Vol. 26B (2002) (P-2.081)

Goodman T.P., Mück A., Angioni C., Henderson M.A., Sauter O., Ryter F., Westerhof E., Zohm H., and ASDEX Upgrade Team, *"Control of the sawtooth instability by electron cyclotron heating and current drive in the TCV and ASDEX upgrade tokamaks"*, 19th IAEA Fusion Energy Conference, Lyon, France, October 2002, IAEA-CN-94/EX/P5-11

Goodman T.P., *"Summary on electron cyclotron heating and current drive experiment"*, to be published in Proc. 12th Joint Workshop in Electron Cyclotron Emission and Electron Cyclotron Resonance Heating (EC-12), Aix-en-Provence, May 2002, p. 235

Grandgirard V., Brunetti M., Allfrey S., Bottino A., Bertrand P., Ghendrih P., Garbet X., Ghizzo A., Manfredi G., Ottaviani M., Sarazin Y., Sauter O., J., Villard L., *"Semi-Lagrangian Drift-Kinetic Code for Slab-ITG Turbulence"*, Proc. 29th EPS Conference on Plasma Physics and Controlled Fusion, Montreux, Switzerland, June 2002, ECA Vol. 26B (2002) (P-4.095)

Graves J.P., Gorelenkov N.N., Sauter O., *"Critical Behaviour of Fast Particles Induced by NBI in Sawtooth Stability Modelling"*, Proc. 29th EPS Conference on Plasma Physics and Controlled Fusion, Montreux, Switzerland, June 2002, ECA Vol. 26B (2002) (P-5.065)

Graves J.P., Dendy R.O., Hopcraft K.I., Jakeman E., *"The Rôle of Clustering Effects in Interpreting Non-diffusive Transport Measurements in Tokamaks"*, Proc. Joint Varenna-Lausanne International Workshop on "Theory of Fusion Plasmas", Varenna, Italy, August 2002, edited by J.W. Connor, O. Sauter and E. Sindoni, ISPP-20 (Editrice Compositori, Bologna, 2002)

Graves J.P., Sauter O., Gorelenkov N.N., *"The effects of anisotropy and plasma rotation on the stabilisation of the internal kink mode by NBI"*, Proc. Joint Varenna-Lausanne International Workshop on "Theory of Fusion Plasmas", Varenna, Italy, August 2002, edited by J.W. Connor, O. Sauter and E. Sindoni, ISPP-20 (Editrice Compositori, Bologna, 2002)

Günter S., Gantenbein G., Gude A., et al., Sauter O., *"Neoclassical tearing modes on ASDEX Upgrade: Improved scaling laws, high confinement at high betaN and new stabilization experiments"*, Proc. 19th IAEA Fusion Energy Conference, Lyon, France, October 2002, IAEA-CN-94/EX/S1-4

Harvey R.W., Sauter O., Prater R., Nikkola P., O'Connel R., Forest C.B., *"Radial transporteffects on ECCD in the TCV and DIII-D tokamaks and on ohmic discharges in the MST RFP"*, to be published in Proc. 12th Joint Workshop in Electron Cyclotron Emission and ElectronCyclotron Resonance Heating (EC-12), Aix-en-Provence, May 2002

Hender T.C., Sauter O., Alper B., et al., Angioni C., Pochelon A., Testa D., and EFDA-JET contributors, *"Sawtooth,neo-classical tearing mode and error field studies in JET"*, Proc. 19th IAEA Fusion Energy Conference, Lyon, France, October 2002, IAEA-CN-94/EX/S1-2

Henderson M.A., Alberti S., Bird J., Elzendoorn B.S.Q., Goodman T.P., Hoekzema J.A., MacMillan G., Piosczyk B., Porte L., Verhoeven A.G.A., *"Design of the evacuated waveguide transmission lines for JET-EP"*, to be published in Proc. 12th Joint Workshop in Electron Cyclotron Emission and ElectronCyclotron Resonance Heating (EC-12), Aix-en-Provence, May 2002

Hogge J.-P., Alberti S., Porte L., Arnoux G., *"Preliminary results of top launch 3rd harminic X-mode electron cyclotron heating in the TCV tokamak"*, to be published in Proc. 12th Joint Workshop in Electron Cyclotron Emission and ElectronCyclotron Resonance Heating (EC-12), Aix-en-Provence (EC-12), May 2002

Hole M.J., Appel C., Buttery R.J., et al., Sauter O., Martynov A., and the MAST Team, *"Stability at high performance in the MAST Spherical Tokamak"*, Proc. 29th EPS Conference on Plasma Physics and Controlled Fusion, Montreux, Switzerland, June 2002, ECA Vol. 26B (2002) (O-2.02)

Ilyin Yu, Nijhuis A., TenKate H.H.J., Bruzzone P., *"Self field measurements fy Hall sensors on the SeCRETS short sample CICC's subjected to cyclic load"*, Proc. of ASC-2002

Jodoin B., Gindrat M., Dorier J.-L., Hollenstein Ch., Loch M., Barbezat G., *"Modelling and diagnostics of a supersonic DC plasma jet expanding at low pressure"*, Proc. Inte. Thermal Spray Conf. 2002, Essen Germany, 4-6 March 2002, published in ITSC 2002 proceedings, Ed. E. Lugscheider, Pub. DVS, Düsseldorf, Germany 2002, p. 716

Karpushov A., Bosshard P., Condrea I., Duval B., Mlynar J., Perez A., Weisen H., and collaborators of the, Budker INP, Novosibirsk, *"Upgrade of the diagnostic neutral beam injector for the TCV tokamak"*, Book of Abstracts, 22nd Symposium on Fusion Technology, Helsinki, Finland, September 2002, 250 (2002)

Karpushov A.N., Bosshard P., Duval B.P., Mlynar J., *"Relaxation of the DNBI Deposited Particles in the TCV Plasmas"*, Proc. 29th EPS Conference on Plasma Physics and Controlled Fusion, Montreux, Switzerland, June 2002, ECA Vol. 26B (2002) (P-4.119)

Leuterer F., Dux R., Gantenbein G., Goodman T.P. et al., *"Recent ECRH results in ASDEX Upgrade"*, to be published in Proc. 12th Joint Workshop in Electron Cyclotron Emission and Electron Cyclotron Resonance Heating (EC-12), Aix-en-Provence, May 2002, p. 267 (Invited paper)

Liévin C., Alberti S., Arnold A., et al., Hogge J.-P., Tran M.Q., *"Status of the 1 MW, 140 GHz, CW gyrotron for W7-X"*, Book of Abstracts, 22nd Symposium on Fusion Technology, Helsinki, Finland, September 2002, 196 (2002)

Lloyd B. et al., Sauter O., *"Overview of recent experimental results on MAST"*, Proc. 19th IAEA Fusion Energy Conference, Lyon, France, October 2002, IAEA-CN-94/EX/OV2-3

Lukash V., Favez J.-Y., Khayrutdinov R., Lister J.B., Daniel R., *"DINA simulations of TCV discharges"*, Book of Abstracts, 22nd Symposium on Fusion Technology, Helsinki, Finland, September 2002, 364 (2002)

Madeira T.I., Amorim P., Duval B.P., Varandas C.A.F., *"Pulse Height Analysis X-ray Spectroscopy in the Tokamak TCV"*, Proc. 29th EPS Conference on Plasma Physics and Controlled Fusion, Montreux, Switzerland, June 2002, ECA Vol. 26B (2002) (P-4.122)

Madeira T.I., Amorim P., Duval B.P., Varandas C.A.F., *"Real time signal treatment with TCV PHA diagnostic"*, Proc. 14th Topical Conf. on High Temperature Plasma Diagnostics, 8-11 July 2002, Madison, Wisconsin, USA (2002)

Magne R., Darbos C., Bouquey F. et al., Alberti S., Hogge J.-P., *"Status of the ECRH system of Tore Supra"*, Proc. 29th IEEE Int. Conf. on Plasma Science ICOPS (2002)

Manini A., Moret J.-M., Alberti S., Goodman T.P., Henderson M.A., *"Exploitation of a diamagnetic loop for modulated ECH power absorption measurements in TCV"*, to be published in Proc. 12th Joint Workshop in Electron Cyclotron Emission and ElectronCyclotron Resonance Heating (EC-12), Aix-en-Provence (EC-12), May 2002

Manini A., Moret J.-M., Ryter F., Sushkov A., and the ASDEX Upgrade Team, *"Interpretation of Plasma Dynamic Response to Additional Heating Power in ASDEX Upgrade and TCV"*, Proc. 29th EPS Conference on Plasma Physics and Controlled Fusion, Montreux, Switzerland, June 2002, ECA Vol. 26B (2002) (P-2.050)

Mao S., Luongo C., Marinucci C., *"Quench simulation in superconducting cables using optimzed DRP scheme"*, Proc. of ASC-2002

Marchand P., Gloor W., Pedrozzi M., Anghel A., Bredy P., *"Cryogenic system for the SLS third harmonic RF cavity"*, Proc. of EPAC 2002

Marinucci C., Bottura L., Bruzzone P., *"Analysis of the Measurement of the Current Sharing Temperature in the ITER TF Model Coil"*, Book of Abstracts, 22nd Symposium on Fusion Technology (SOFT), Helsinki, Finland, September 2002, 264 (2002)

Martynov An., Sauter O., *"Shape Effects on the Stability Limit of the Ideal Internal Kink Mode"*, Proc. 29th EPS Conference on Plasma Physics and Controlled Fusion, Montreux, Switzerland, June 2002, ECA Vol. 26B (2002) (P-1.098)

Martynov A., Sauter O., *"Shape and aspect ratio effects on the ideal internal kink mode"*, Proc. Joint Varenna-Lausanne International Workshop on "Theory of Fusion Plasmas", Varenna, Italy, August 2002, edited by J.W. Connor, O. Sauter and E. Sindoni, ISPP-20 (Editrice Compositori, Bologna, 2002)

Mayoral M.L., Westerhof E., Sauter O., et al., and contributors to EFDA-JET work programme, *"Neo-Classical Tearing Mode Control through Sawtooth Destabilisation in JET"*, Proc. 29th EPS Conference on Plasma Physics and Controlled Fusion, Montreux, Switzerland, June 2002, ECA Vol. 26B (2002) (P-1.026)

Medvedev S. Yu., Martin Y., Sauter O., Villard L., "Edge Kink/Ballooning Mode Stability in Tokamaks with a Separatrix", Proc. 29th EPS Conference on Plasma Physics and Controlled Fusion, Montreux, Switzerland, June 2002, ECA Vol. 26B (2002) (P-1.116)

Mlynar J., Duval B., Horajek J., Lister J.B., *"Present and perspective roles of soft X-ray tomography in tokamak plasma position measurements"*, Book of aAbstracts, 22nd Symposium on Fusion Technology, Helsinki, Finland, September 2002, 251 (2002)

Mück A., Goodman T.P., Koslowski H.R., Ryter F., Westerhof E., Zohm H., and ASDEX Upgrade Team, *"Sawtooth Tailoring Experiments with ECRH in ASDEX Upgrade"*, Proc. 29th EPS Conference on Plasma Physics and Controlled Fusion, Montreux, Switzerland, June 2002, ECA Vol. 26B (2002) (P-1.037)

Narushima Y., Watanabe K.Y., Sakakibara S., et al., Cooper W.A., *"Study of Ideal External Mode in LHD"*, Proc. 29th EPS Conference on Plasma Physics and Controlled Fusion, Montreux, Switzerland, June 2002, ECA Vol. 26B (2002) (P-1.080)

Nikkola P., Sauter O., Behn R., Coda S., Condrea I., Goodman T.P., Henderson M.A., Harvey R.W., Peysson Y., and the TCV Team, *"Fully off-axis ECCD driven plasmas in TCV"* (Invited paper) to be published in Proc. 12th Joint Workshop in Electron Cyclotron Emission and ElectronCyclotron Resonance Heating (EC-12), Aix-en-Provence, May 2002, p. 257

Nikkola P., Coda S., Harvey R.W., Sauter O., *"Simulation of hard X-ray spectra of TCV EDRH/ECCD experiments"*, Proc. Joint Varenna-Lausanne International Workshop on "Theory of Fusion Plasmas", Varenna, Italy, August 2002, edited by J.W. Connor, O. Sauter and E. Sindoni, ISPP-20 (Editrice Compositori, Bologna, 2002)

Noterdaeme J.-M. et al., Sauter O., *"Heating, current drive and energetic particles studies on Jet in preparation of ITER operation"*, Proc. 19th IAEA Fusion Energy Conference, Lyon, France, October 2002, IAEA-CN-94/EX/W-1

Okamura S. et al., NIFS, Toki, Japan, Wakatani M. et al, Graduate School of Energy Science, Kyoto, Japan, Cooper W.A., *"Physics design of quasi-axisymmetric stellarator CHS-qa"*, 19th IAEA Fusion Energy Conference, Lyon, France, October 2002, IAEA-CN-94/IC/P-07

Ongena J., Monier-Garbet P., Suttrop W., et al., Sauter O., & EFDA-JET workprogramme contributors, *"Towards the realization on JET of an integrated H-mode scenario for ITER"*, Proc. 19th IAEA Fusion Energy Conference, Lyon, France, October 2002, IAEA-CN-94/EX/C2-4

Pamela J. et al., Alberti S., Alffrey S. et al., Blanchard P., Coda S., Duval B.P., Fasel D., Fasoli A., Henderson M., Lister J.B., Marmillod Ph., Martin Y., Mlynar J., Pitts R.A., Pochelon A., Sauter O., Scarabosio A., Siegrist M.R., Tran M.Q., Wischmeier M., *"Overview of JET results"*, Proc. 19th IAEA Fusion Energy Conference, Lyon, France, October 2002, IAEA-CN-94/EX/OV1-4

Piosczyk B., Alberti S., Arnold A., et al., Goodman T.P., Hogge J.-P., Tran M.Q., *"A 2 MW, CW, 170 GHz gyrotron for ITER"*, 19th IAEA Fusion Energy Conference, Lyon, France, October 2002, IAEA-CN-94/CT-7Rb

Pochelon A., Arnoux G., Camenen Y., Scarabosio A., Alberti S., Hofmann F., Manini A., Behn R., Bosshard P., Blanchard P., Coda S., Goodman T.P., Hnederson M.A., Hogge J.P., Karpushov A., Moret J.-M.,, Nelson-Melby E., Porte L., Sauter O., Sushkov A., Tran M.Q., *"Optimisation of current profile using far off-axis ECH power deposition to extend high elongation operation in TCV",* 19th IAEA Fusion Energy Conference, Lyon, France, October 2002, IAEA-CN-94/EX/P5-14

Pochelon A., Camenen Y., Hofmann F., Alberti S., Angioni C., Goodman T.P., Henderson M.A., Nikkola P., Porte L., Sauter O., Scarabosio A., *"Optimisation of the Current Profile with far off-axis ECH Power Deposition in high Elongation TCV Plasmas"*, Proc. 29th EPS Conference on Plasma Physics and Controlled Fusion, Montreux, Switzerland, June 2002, ECA Vol. 26B (2002) (P-2.075)

Popovich P., Cooper W.A., Villard L., *"A Low-Frequency Electromagnetic Wave Propagation Code in 2D and 3D"*, Proc. 29th EPS Conference on Plasma Physics and Controlled Fusion, Montreux, Switzerland, June 2002, ECA Vol. 26B (2002) (P-5.072)

Popovich P., Cooper W.A., Villard L., *"Full wave propagation code, 2D and 3D for a cold plasma"*, Proc. Joint Varenna-Lausanne International Workshop on "Theory of Fusion Plasmas", Varenna, Italy, August 2002, edited by J.W. Connor, O. Sauter and E. Sindoni, ISPP-20 (Editrice Compositori, Bologna, 2002)

Porte L., Alberti S., Arnoux G., Martin Y., Hogge J.-P., Goodman T.P., Henderson M.A., Nelson-Melby E., Pochelon A., Tran M.Q., *"3rd Harmonic X-mode electron cyclotron resonance heating on TCV using top and low field side launch",* 19th IAEA Fusion Energy Conference, Lyon, France, October 2002, IAEA-CN-94/EX/P5-15

Raju D., Dokouka V.N., Favez J.-Y., Kharutdinov R.R., Lister J.B., Lukash V.E., *"DINA Simulations of TCV Electron Cyclotron Current Drive and Heating"*, Proc. 29th EPS Conference on Plasma Physics and Controlled Fusion, Montreux, Switzerland, June 2002, ECA Vol. 26B (2002) (P-2.082)

Sauter O., Angioni C., Behn R., Coda S., Condrea I., Goodman T.P., Henderson M.A., Martynov A., Nikkola P., Pochelon A., Scarabosio A., *"Steady-state fully non-inductive reverse shear scenarios with electron ITB and dominant bootstrap current"*, Proc. 19th IAEA Fusion Energy Conference, Lyon, France, October 2002, IAEA-CN-94/EX/P5-06

Sauter O., Behn R., Coda S., Condrea I., Goodman T.P., Henderson M.A., Nikkola P., *"Electron ITB in Fully Non-Inductive Reverse Shear Scenarios"*, Proc. 29th EPS Conference on Plasma Physics and Controlled Fusion, Montreux, Switzerland, June 2002, ECA Vol. 26B (2002) (P-2.087)

Scarabosio A., Pochelon A., Martin Y., *"MHD Instabilities during Current Ramp Up as a Function of Plasma Shape in the TCV Tokamak"*, Proc. 29th EPS Conference on Plasma Physics and Controlled Fusion, Montreux, Switzerland, June 2002, ECA Vol. 26B (2002) (P-2.080)

Scavino E., Bakos J.S., Duval B.P., Weisen H., *"Investigation of Impurity Transport in TCV"*, Proc. 29th EPS Conference on Plasma Physics and Controlled Fusion, Montreux, Switzerland, June 2002, ECA Vol. 26B (2002) (P-4.121)

Scharer J., White B., Tysk S., Akhtar K., Degeling A., Borg G., Boswell R., *"Measurement of Helicon Wave propagation and Ar II emission"*, Proc. 29th EPS Conference on Plasma Physics and Controlled Fusion, Montreux, Switzerland, June 2002, ECA Vol. 26B (2002) (P-4.030)

Sterk A.B., and ECRH Team, including, Henderson M., *"Design and R & D for an ECRH power supply and power modulation system on JET"*, Book of Abstracts, 22nd Symposium on Fusion Technology, Helsinki, Finland, September 2002, 178 (2002)

Subbotin A.A., Cooper W.A., Isaev M. Yu., et al., *"Quasi-Isodynamical Configurations without Transitional Particle Orbits"*, Proc. 29th EPS Conference on Plasma Physics and Controlled Fusion, Montreux, Switzerland, June 2002, ECA Vol. 26B (2002) (P-5.086)

Sushkov A., Camenen Y., Coda S., Klimanov I., Pochelon A., Weisen H., *"TCV High Resolution X-ray Imaging Diagnostic"*, Proc. 29th EPS Conference on Plasma Physics and Controlled Fusion, Montreux, Switzerland, June 2002, ECA Vol. 26B (2002) (P-4.118)

Testa D., Fasoli A., Borba D.N., Fu G.Y., Jaun A., Mantsinen M., deVries P., and contributors to the EFDA-JET work programme, *"Measurement of Alfvén Waves on the JET Tokamak",* Proc. 29th EPS Conference on Plasma Physics and Controlled Fusion, Montreux, Switzerland, June 2002, ECA Vol. 26B (2002) (P-1.121)

Testa D., Fasoli A., Fu G., Jaun A., Borba D., de Vries P. and JET-EFDA contributors, *"Experimental study of the stability of Alfvén eigenmodes on JET"*, 19th IAEA Fusion Energy Conference, Lyon, France, October 2002, IAEA-CN-94/EX/P1-17

Verhoeven A.G.A., and ECRH Team, including, Alberti S., Goodman T., Henderson M., *"Design and R & D of an ECRH system on JET"*, Book of Abstracts, 22nd Symposium on Fusion Technology, Helsinki, Finland, September 2002, 221 (2002)

Verhoeven A.G.A., Bongers W.A., Elzendoorn B.S.Q., et al., Alberti S., Goodman T., Henderson M., *"The 113 GHz ECRH system for JET"*, to be published in Proc. 12th Joint Workshop in Electron Cyclotron Emission and ElectronCyclotron Resonance Heating (EC-12), Aix-en-Provence, May 2002

Villard L., Allfrey S.J., Bottino A., Brunetti M., Falchetto G.L., Grandgirard V., Hatzky R., Nührenberg J., Peeters A.G., Sauter O., Sorge S., Vaclavik J., *"Full radius linear and nonlinear gyrokinetic simulations for tokamaks and stellarators: zonal flows, applied ExB flows, trapped electrons and finite beta"*, 19th IAEA Fusion Energy Conference, Lyon, France, October 2002, IAEA-CN-94/TH/1-3

Villard L., Bottino A., Allfrey S., Sauter O., "Stabilization of ITG Modes and Destabilization of Trapped Particle Modes with ExB Flows", Proc. 29th EPS Conference on Plasma Physics and Controlled Fusion, Montreux, Switzerland, June 2002, ECA Vol. 26B (2002) (P-4.069)

Weng P.D., Bruzzone P., Chen Z.M., Stepanov B., Chen J.L., Wang F.T., Fang J., Yao D.M., Xiao B.J., Bi Y.F., Li Z.B., *"Test results and preliminary analysis of HT-7U short samples"*, Proc. of CHATS-2002, Karlsruhe, Germany, 16-18 September 2002

Wesche R., Stepanov B., Vogel M., Gloor T., Bruzzone P., *"DC Behaviour of NbTi CICC for ITER-FEAT"*, Book of Abstracts, 22nd Symposium on Fusion Technology, Helsinki, Finland, September 2002, 288 (2002)

Zabolotsky A., Weisen H., and TCV Team, *"Particle Transport and Density Profile Behaviour in TCV"*, Proc. 29th EPS Conference on Plasma Physics and Controlled Fusion, Montreux, Switzerland, June 2002, ECA Vol. 26B (2002) (P-2.077)

American Physical Society (APS)

Condrea I., Sauter O., Behn R., Coda S., Goodman T., Henderson M.A., Nikkola P., *"Electron transport properties of steady-state eITB scenarios in TCV"*, 44th Annual Meeting, APS Division of Plasma Physics, Orlando, Florida, USA, November 2002

Henderson M., *"Recent results from the EC heated plasmas in the TCV tokamak"*, 44th Annual Meeting, APS Division of Plasma Physics, Orlando, Florida, USA, November 2002 (Invited Talk)

Pamela et al., Alberti S., Alffrey S. et al., Blanchard P., Coda S., Duval B.P., Fasel D., Fasoli A., Henderson M., Lister J.B., Marmillod Ph., Martin Y., Mlynar J., Pitts R.A., Pochelon A., Sauter O., Scarabosio A., Siegrist M.R., Tran M.Q., Wischmeier M., *"Overview of JET results"*, DPP02 Meeting of the Amerian Physical Society

Watkins M.L., Pamela et al., Alberti S., Alffrey S. et al., Blanchard P., Coda S., Duval B.P., Fasel D., Fasoli A., Henderson M., Lister J.B., Marmillod Ph., Martin Y., Mlynar J., Pitts R.A., Pochelon A., Sauter O., Scarabosio A., Siegrist M.R., Tran M.Q., Wischmeier M., *"Studying ITER physics issues at JET"*, DPP02 Meeting of the Amerian Physical Society

Société Suisse de Physique (SSP)

Arnoux G., Alberti S., Hogge J.-P., Porte L., *"Current profile tailoring with far off-axis ECH power deposition in the TCV-Tokamak"*, Société Suisse de Physique, Réunion Annuelle 2002, Lausanne, Bull. SPG/SSP 19, 243, 64 (2002)

Camenen Y., Hofmann F., Pochelon A., Angioni C., Goodman T.P., Henderson M.A., Nikkola P., Sauter O., **"Current profile tailoring with far off-axis ECH power deposition in the TCV-Tokamak"**, Société Suisse de Physique, Réunion Annuelle 2002, Lausanne, Bull. SPG/SSP 19, 242, 64 (2002)

Scarabosio A., Pochelon A., Martin Y., *"Dynamics of MHD instabilities during current ramp up as a function of plasma shape in the TCV tokamak"*, Société Suisse de Physique, Réunion Annuelle 2002, Lausanne, Bull. SPG/SSP 19, 241, 63 (2002)

Tran M.Q., **"Fusion Energy; Scientific and technical challenges"**, Société Suisse de Physique, Réunion Annuelle 2002, Lausanne, Bull. SPG/SSP 19, 901, 119 (2002

B.2 Participation in other conferences in 2002

Bottino A., Allfrey S., Peeters A.G., Sauter O., Villard L., *"E x B flow effects on ITG in reverse shear ASDEX Upgrade discharges"*, IAEA Technical Meeting on Theory of Plasma Instabilities, Kloster Seeon, Germany, April 2002

Cooper W.A., Ferrando i Margalet S., Allfrey S.J., and members from, Kurchatov Institute, NIFS, Toki-shi, PPPL, IPP-Greifswald, UKAEA Dounreay, *"Bootstrap current destabilisation of ideal MHD modes in 3D reactor configurations"*, Invited paper at the 29th EPS Conference on Plasma Physics and Controlled Fusion, Montreux, Switzerland, June 17 - 21, 2002,

Dammertz G., Alberti S., Arnold A., et al., Hogge J.-P., Tran M.Q., *"Status of the 1 MW 140 GHz, CW gyrotron for W7-X"*, 5th Int. Workshop on Strong Microwaves in Plasmas, Nizhny Novogord, Russia, August 2002

Dammertz G., Alberti S., Arnold A., et al., Hogge J.-P., Tran M.Q., *"Progress of the 1 MW 140 GHz, CW gyrotron for W7-X"*, 27th Int. Conf. on Infrared and Millimeter Waves, San Diego, CA, September 2002

Degeling A., Martin Y.R., Lister J.B., Llobet X., Bak P.E., "*ELM Dynamics in TCV H-modes",* 11th Int. Congress on Plasma Physics, Sydney, Australia, July 2002

Dorier J.-L., Gindrat M., Hollenstein Ch., Loch M., Refke A., Salito A., Barbezat G., *"Effect of specific operating conditions on the properties of LPPS plasma jets expanding at low pressure"*, International Thermal Spray Conference and Exposition, Essen, Germany, March 2002

Falchetto G.L., Vaclavik J., Villard L., *"Global gyrokinetic study of electromagnetic microinstabilities"*, IAEA Technical Meeting on Theory of Plasma Instabilities, Kloster Seeon, Germany, April 2002

Hollenstein Ch., *"The physics of plasma-enhanced CVD for large area coating"*, Symposium : Plasmaoberflächentechnik - Beschichten, Aetzen und Modifizieren, DPG-Frühjahrstagung, Regungsbuerg, Germany, March 2002

Hollenstein Ch., *"WE-Heraeus-Course on Low Temperature Plasma Physics and Applications - Dusty Plasmas"*, Bad Honnef, Hanau, Germany, September 2002

Klinger L., Vos J.B., Appert K., Barbezat G., *"Numerical simulation of a stationary 3D direct current plasma torch"*, 29th IEEE Int. Conference on Plasma Science, Banff, Alberta, Canada, May 2002

Lister J.B., Participation in Fusion Energy Sciences Summer Study, Snowmass Village, Colorado, USA, July 2002

Marmy P., Luppo M., *"Effect of hydrogen on the fracture toughness of the Titanium alloys TI6AL4V and TI5AL2.5SN before and after neutron irradiation"*, 7th Int. Conference EPTR 2002, Engineering Problems of Thermonuclear Reactors, St Petersbourg, Russia, October 2002

Sansonnens L., Bondkowski J., Schmitt J., *"Development of a numerical simulation tol for improvement of large area PECVD film processing"*, E-MRS 2002 Spring Meeting, Strasbourg, France, June 2002

Victoria M., *"The plastic deformation of irradiated metals and alloys"*, The plasticity of irradiated pure metals and alloys, Plasticity 2002, Aruba, Netherlands Antilles, January 2002 (invited talk)

Victoria M., *"Uses of spallation sources in fusion materials studies"*, IEA meeting during the 6th Int. Symposium on Fusion Nuclear Technology (ISFTN), San Diego, U.S.A., April 2002

Victoria M., *"The plastic deformation of irradited metals"*, The Z.S. Basinski Memorial Int. Symposium on Advances in Material Plasticity, Cracow, Poland, 10-12 June 2002 (invited talk)

Victoria M., *"Helium effects in ferritic-martensitic steels"*, 7th China-Japan Symposium on Materials for Advanced Energy Systems and Fusion Engineering (Lanzhou) (Invited keynote lecture)

B.3 Seminars presented at the CRPP in 2002

P. Bünzli, ETHZ, *"High-temperature Series Expansion for Frustrated Spin System"*

Dr. T.S. Hahm, PPPL, Princeton, N.J. U.S.A., *"GyrokineticSstudies of Turbulent Transport Scaling in Tokamak"*

Dr. M.I.Mikhailov, Russian Research Centre "Kurchatov Institute", Moscow, Russia, *"Improved Alpha-particle Confinement in Stellarators with Poloidally Closed Contours of the Magnetic Field Strength"*

Dr. W.A., Cooper, CRPP-EPFL, *"MHD Stability of 3D Plasma Confinement System with Finite Plasma Current*

Dr. R. Ganesh, CRPP-EPFL, *"Vortex-Hole Pattern Formation in Nonneutral Electromagnetic Microinstabilities in Tokamak Plasmas"*

Dr. G. Falchetto, CRPP-EPFL, *"Global Kinetic Simulations of electro-magnetic Microinstabilities in Tokamak Plasmas"*

Dr. Bharat Doshi, Institute for Plasma Research, Bhat, Gandhinagar, Gujarat, India, *"An Overview of SST-1 Tokamak : Assembly, Integration and the Present Status"*

Dr. R.A. Pitts, CRPP-EPFL, *"The Impact of ELM on the TCV Divertor Targets"*

Dr. C. Angioni, CRPP-EPFL, *"Electron Transport in TCV and Sawtooth Stabilisation with NBI in JET: Two Applications for a Transport Code"*

Dr. J. Pamela, EFDA, Associate Leader for JET, JET, Abingdon, U.K., *"JET's Recent Results and Future Programme / A Major Contribution to the Preparation of ITER"*

Dr. H. Reimerdes, Columbia University, New York, U.S.A., *"Stabilisation of Resistive Wall Modes in DIII-D"*

Dr. J.A. Jimenez, on behalf of the TJ-II Team, CIEMAT, Madrid, Spain, *"Overview of TJ-II Flexible HELIAC Experiment"*

Dr. M.A. McGrath, UKAEA, Culham and University College, Dublin, *"Using Charge Exchange Doppler Spectroscopy to Investigate Ion Behaviour in the MAST Tokamak"*

Dr. R. Gruber, STI, EPFL, *"Some Ideas on How to Tailor PC Clusters to MHD Codes"*

Dr. M. Töwe, Institute of Physics, University of Basle, *"Photoelectron Spectroscopy Studies of Carbon Based Fusion Reactor Material and what they have to do with TCV"*

Dr. Y. Idomura, Department of Fusion Plasma Research, Naka Fusion Research Establishment, JAERI, Japan, *"Gyrokinetic Global Analysis of Ion Temperature Gradient Driven Mode in Reversed Shear Tokamaks"*

Prof. D. Reiter, KFA-Jülich, Germany, *"Plasma chemistry effects in fusion edge plasmas"*

Dr. L. Bottura, CERN, AT Division, *"Accelerator Magnets"*

Dr. S.L. Dudarev, EURATOM/UKAEA Fusion Association, Culham Science Centre, U.K., *"Evanescent Solutions in Diffraction and Diffusion: Application to Surfaces and Grain Boundaries"*

Dr. R. Hatzky, Max-Planck-Institut für Plasmaphysik, Greifswald, Germany, *"Energy Conservation in a Nonlinear Gyrokinetic Particle-in-cell Code for Ion-temperature-gradient-driven (ITG) Modes Using the δf Method"*

Dr. J. Doane, General Atomics, San Diego, U.S.A., *"Recent EC Results on DIII-D and High Power Microwave Components"*

Dr. R.A. Pitts, CRPP-EPFL, *"Comparing Scrape-off Layer and Divertor Physics in JET Pure He and D Discharges"*

Dr. R. Granier, Laboratoire des Plasmas et des Couches Minces, institut des Matériaux jean Rouxel UMR 6502 Nantes, France, *"Mechanisms Involved in the PECVD of Thin Films in Low Pressure Organosilicon Plasmas"*

Dr. I. Pavlov, All Russian Electrotechnical Institute, Moscow, Russia, *"Laser Probing of Imploding Plasma of Fast Z-pinch"*

Dr. L. Berry, Oak Ridge National Laboratory, Oak Ridge, U.S.A. *"Recent Development in All Orders, Full-wave Radio Frequency Plasma Analysis"*

Dr. N. Fisch, PPPL, Princeton, U.S.A., *"Phase Space Engineering in Tokamaks: Perspectives on RF Heating, Current Drive and Alpha Channeling"*

Prof. M. Porkolab, PSFC, MIT, Cambridge U.S.A., *"The MIT Plasma Science and Fusion Center: A Paradigm of How to Operate a Major Fusion Laboratory in a University Environment"*

Dr. A. Pankin, Department of Physics, Lehigh University, Bethlehem, U.S.A., *"The NTCC Modular Approsach and its Application to the BALDUR and TRANSP Codes"*

Dr. A. Ram, MIT, Cambridge, U.S.A., *"Electron Cyclotron Resonance Heating of Overdense Plasmas"*

Dr. F. Ryter, Max-Planck-Institut für Plasmaphysik, Garching, Germany, *"A Selection of Experiments with ECH in ASDEX Upgrade"*

Dr. A. Manini, CRPP-EPFL, *"Analysis and interpretation of the plasma dynamic response to modulated ECH using ECE and soft X-ray diagnostics"*

Dr. B. Labit, DRFC, CEA-Cadarache, France, *"Numerical study of fluid electron temperature gradient-driven turbulence and transport scaling"*

Dr. G. Hagelaar, Centre de Physique des Plasmas et Applications de Toulouse, CPAT, France, *"Modelling of stationary plasma thrusters"*

Dr. M. Ferrara, Electrical Engineering Dept., University of l'Aquila, Italy, *"Scanning Probe Microscopy: A Story of Nanoworld Exploration"*

Dr. L. Klinger, CRPP-EPFL, *"3D Numerical Simulation of a Plasma Torch Using a Finite Volumes Method"*

R. Sobbia, Univ. Manchester, Inst. Of Science and Technology, UMIST, Manchester, UK, *"Computational modelling of UMIST magnetron"*

Dr. D. Mazon, DRFC, CEA-Cadarache, France, *"Derniers résultats (obtenus au JET) de contrôle de pression et du profil de densité de courant en temps réel"*

B.4 Other external presentations in 2002

Alberti S., *"ECRH on the TCV Tokamak"*, Forschungszentrum Karlsruhe GmbH, Karlsruhe, Germany, April 2002

Baluc N., *"On the use of the hot labor at the PSI by the CRPP-EPFL group"*, Paul Scherrer Institute, Villigen, Switzerland, August 2002

Behn R., *"Untersuchungen zum Energietransport im TCV bei dominierender Elektronenheizung"*, Institut für Plasmaforschung Stuttgart, Germany, January 2002

Bottino A., Max-Planck-Institut für Plasmaphysik, Garching, Allemagne, December 2002, "Global linear stability of electrostatic microinstabilities in ASDEX Upgrade discharges and recent advantages in global nonlinear simulations"

Hollenstein Ch., Dusty plasmas course on Low Temperature Plasma Physics and Applications (CCTPP-6) International WE-Heraeus, Summer School Bad Honnef (D), 8-13 September 2002

Hollenstein Ch., *"La technique du vide"*, Course with Swiss Vacuum Society, 28-29 November 2002, Le Locle, Switzerland

Hollenstein Ch., *"Industrial plasmas at CRPP"*, Colloque des matériaux, EPFL, 12 novembre 2002

Hollenstein Ch., "The physics of plasma enhanced CVD for large area coating", DPG Tagung Regenburg, 11-15 March 2002

Marmy P., CRISM "Prometey" Institute, St Petersburg, Russia,, November 2002, and, ENTEK Institute, ENES, Engineering Centre of Nuclear Equipment, Strength, Reliability and Lifetime, Moscow, Russia, "High strain fatigue properties of the F82H ferritic martensitic steel under proton irradiation"

Marmy P., Luppo M., CRISM "Prometey" Institute, St Petersburg, Russia,, November 2002, and, ENTEK Institute, ENES, Engineering Centre of Nuclear Equipment, Strength, Reliability and Lifetime, Moscow, Russia, "Effect of hydrogen on the fracture toughness of the titanium alloys T16AL4V and TI5AL2.5SN before and after neutron irradiation"

Nikkola P., *"Fully off-axis ECCD driven plasmas in TCV"*, Helsinki University of Technology, Espoo, Finlande, May 2002

Pitts R.A., *"Divertor target response to Type III ELMs in TCV"*, Univ. Innsbruck, Dept. of Theoretical Physic, Innsbruck, Austria, February 2002

Schäublin R., *"Approche intégrée du comportement mécanique d'échantillons sous-dimensionnés: Application au cas des aciers ferritiques/martensitiques irradiés"*, Institut des Matériaux, EPF-Lausanne, Colloque de Sciences des Maériaux et de la SVMT, Février 2002

Tran M.Q., *"Fusion: A sustainable energy option",* Groupe d'Etude des Perspectives Energétiques, Baden, Suisse, September 2002

Tran M.Q., *"La fusione controllata: un'opzione energetica per il futuro dell'umanità"*, Alta Scuola Pedagogica, Rep. e Cantone Ticino, Locarno, Svizzera, October 2002

Tran M.Q., Politique de la Science: Enjeux Généraux (Module 1), EPF-Lausanne, Novembre 2002, "La fusion et le CRPP dans le cadre de la politique de la science"

Victoria M., "Radiation damage in pure metls and alloys", University of Science and Technology, Beijing, PRC, July 2002

Victoria M., *"Ferritic-martensitic steels as structural materials for fusion reactors"*, China Institute of Atomic Energy, Beijing, PRC, July 2002

Victoria M., *"Ferritic and oside dispersion steel for fusion applications"*, Southwest Institute of Physics, Chengdu, PRC, July 2002

Victoria M., *"The mechanical properties of nanocrystalline Ni",* Northwest Polytechnical Institute, Xian, PRC, July 2002

B.5 Other external activities organised by the CRPP in 2002

29th European Physical Society Plasma Physics Divisional Conference on Plasma Physics and Controlled Fusion

This annual conference was held in Montreux from 17-21 June 2002 and was organised by a Local Organising Committee from the CRPP. Over 630 delegates, mostly from Europe, USA and Japan attended this meeting. 2 year's of preparatory work were rewarded by a high quality meeting and an excellent atmosphere. A reception was held on the steamer "Lausanne" and a Gala Dinner was held in the Château d'Aigle. Delegates were able to explore the Pays d'Enhaut on the Wednesday afternoon with activities ranging from cheese making to white water rafting.

The conference itself was opened on the Monday morning in the presence of Prof. Charles Kleiber, Swiss Secretary of State for Science and Research and Prof. Patrick Aebischer, President of the EPFL. During the opening ceremony, the Hannes Alfven Prize was awarded to Prof. Marshall Rosenbluth from the USA.

The electronic submission of abstracts and 4-page contributions was once again organised using the ELISE software, developed for our EPS division by staff members of the CRPP.

The proceedings of the conference are available at:
Contributed papers: http://epsppd.epfl.ch (2002 and previous years)
Invited papers: http://www.iop.org/journals/ppcf (Volume 44 No. 12B)

Theory of Fusion Plasmas, Joint Varenna-Lausanne International Workshop, Villa Monastero, Varenna, Italy, August 27 - 30, 2002

This biennial meeting is organised by the CRPP, for the scientific part, in collaboration with the Istituto di Fisica del Plasma del CNR, Milano and the "Piero Caldirola" International Centre for the Promotion of Science and International School of Plasma Physics for the logistics and local organisation. This year, 53 participants attended the meeting, mainly from Europe, USA and Japan. There were 21 invited talks and 30 poster presentations, most of which will be published in the book series issued in December 2002: Theory of Fusion Plasmas (Proc. Joint Varenna-Lausanne Int. Workshop) (Varenna 2002), edited by J.W. Connor, O. Sauter and E. Sindoni, ISPP-20, ISBN 88-7438-005-4 (Bologna, Editrice Compositori) (2002).
The meeting was very productive, with the help also of the meeting place and surroundings, which encourage lively informal discussions.

Second IEA Fusion Materials Agreement Workshop on Modelling and Experimental Validation, Les Diablerets, Switzerland, September 30 – October 04, 2002

This 5-day workshop brought together 67 scientists from 12 different countries widely representing Europe, America, Russia and Asia. It consisted of oral presentations and poster and discussion sessions about the modelling of radiation damage in metals and alloys and its experimental validation. Primary damage, microstructure evolution, interaction of irradiation-induced defects with mobile dislocations, and effects of helium and other impurities on phase stability and mechanical properties, have been successively reviewed. Modelling tools included mainly ab initio calculations, molecular dynamics and kinetic Monte-Carlo simulations, while experimental tools referred to macroscopic mechanical testing and transmission electron microscopy observations. The results presented gave an excellent picture of the current worldwide knowledge in the field of the effects of radiation damage on materials.

2nd International Tokamak Physics Activity: Scrape-off layer and Divertor topical group meeting, October 21-23.

This was the first occasion on which the CRPP has welcomed the edge physics group, having previously organised MHD and H-mode Expert group workshops and is a sign of the growing importance of TCV's contribution to this important area of tokamak research. The October meeting was a great success, with 24 participants representing the four ITPA partners (Japan (3), Europe(13), USA(6) and the Russian Federation(2)). A total of 27 technical contributions were presented including a talk from TCV with four lengthy and lively discussion periods during which the major issues addressed by the meeting and the group's high priority research areas for 2003 were agreed.

APPENDIX C External activities of CRPP Staff during 2002

C.1 National and international committees and ad-hoc groups

MEMBERSHIP

P. Bruzzone	International Magnet Technology Conference Organising Committee EFDA, Magnet Expert Group
A. Fasoli	Scientific and Technical Advisory Committee, Euratom ASDEX Programme Committee, Germany Science Center Review for the United States Civilian Research and Development Foundation for the Independent States of the Former Soviet Union Programme Committee of the Turin Easter Plasma Conference
Ch. Hollenstein	"Conseil scientifique du Département Science pour l'Ingénieur du CNRS" Scientific council of the Institute of Surface Modifications at Leibzig (Wissenschaftsgemeinschaft Gottfried Wilhlem Leibniz) Expert for a "Sonderforschungsbereich-Projekt" of the Deutschen Forschungsgemeinschaft.
J.B. Lister	International Tokamak Physics Activity: MHD, Disruption and Control Topical Group 29th EPS Conference Programme Committee
C. Marinucci	CHATS, Scientific Programme Committee
R.A. Pitts	International Tokamak Physics Activity: Diagnostics Topical Group 30th EPS Conference Programme Committee
R. Schäublin	Member of the board of the Swiss Society for optics and microscopy
M.Q. Tran	Electron Cyclotron Wave Task Area Leader Chairman of the Electron cyclotron Wave-Coordinating Committee Consultative Committee for the Euratom Specific Research and Training Programme in the field of Nuclear Energy, Fusion (CCE-FU) CCE-FU Special Working Group on "Possible joint implementation of ITER" CCE-FU Fusion Physics Committee EFDA* Steering Committee Fusion Technology Committee, Euratom Accelerator Driven System Working Group set-up by the Secretary of Science and Research Scientific and Technical Advisory Committee, Euratom Chairman of the Review Panel on Fusion, Helmolz Gemeinschaft, Germany Standing Committee of the International Symposium on Fusion Nuclear Technology Scientific Committee of the IAEA Technical Meeting on ECRH Physics and Technology for ITER Selection Committee of the IAEA 3rd TCM on Steady State Operation of magnetic fusion devices
G. Vecsey	SOFT Organising Committee

* EFDA: European Fusion Development Agreement

	International Magnet Technology Conference, Organising Committee Chairman, executive committee of the IEA Agreement on Fusion Materials Coordinator, EU Fusion Materials Program: Modelling and experimental verifiction Tasks
M. Victoria	Chairman, Executive Committee IEA Fusion Material Agreements Chairman, IEA Modeling and Experimental Validation Collaboration International Advisory Committee fo the Int. Conf. On Fusion Reactor Materials EFDA Task Coordinator on Modelling
L. Villard	CCE-FU Fusion Physics Committee "Conseil Scientifique du Département de Recherche sur la Fusion Contrôlée" – CEA - France
H. Weisen	International Advisory Board of the IPP Prague, Czech Republic

PARTICIPATION

B. Duval	Remote Participation Users Group, EFDA-JET
C. Marinucci	ITER TFMC Test and Analysis Group
Y.R. Martin	International Tokamak Physics Activity: Confinement Database and Modelling Topical Group
R.A. Pitts	International Tokamak Physics Activity: SOL and Divertor Topical Group
O. Sauter	International Tokamak Physics Activity: MHD, Disruption and Control Topical Group

C.2 Editorial and society boards

S. Alberti	Committee of the Swiss Physical Society, Responsible for Applied Physics
Ch. Hollenstein	Vice President of the Swiss Vacuum Society Committee "Union Radio-Scientifique Internationale" Editorial Board of Plasma Chemistry and Plasma Processing
J.B. Lister	Vice President of the European Physical Society Plasma Physics Division Editorial Board of Plasma Physics and Controlled Fusion
Y.R. Martin	Chairman of the Association Vaudoise des Chercheurs en Physique
P.J. Paris	Fusion Expo Consortium Committee EFDA Information Network "Fédération Romande de l'Energie" Committee Chairman of the "International Association of Specialists in Energy" (AISEN) Council of the "Chambre Franco-Suisse du Commerce et de l'Industrie"
M.Q. Tran	Board of Editors of Nuclear Fusion
M. Victoria	Invited Editor, J. Nucl. Materials

C.3 EPFL committees and commissions

J-L. Dorier	Commission des Doctorants de la Section de Physique, FSB-EPFL
A. Fasoli	Commission d'Enseignement de la Section de Physique, FSB-EPFL
J-Ph. Hogge	Commission des Doctorants de la Section de Physique, FSB-EPFL
Ch Hollenstein	Commission de Recherche de la Section de Physique, FSB-EPFL
A. Pochelon	Commission de Recherche de la Section de Physique, FSB-EPFL
O. Sauter	Commission d'Informatique, FSB-EPFL
M.Q. Tran	Président de l'Assemblée d'Ecole Commission de Recherche de la Section de Physique, FSB-EPFL
L. Villard	Commission d'Enseignement de la Section de Physique, FSB-EPFL Délégué à la "Commission Scientifique du 3ème Cycle de la Physique en Suisse Romande"

APPENDIX D

D.1 Lausanne Reports (LRP)

Blanchard P., *"Etudes du rayonnement suprathermique émis lors du chauffage cyclotronique électronique du plasma du tokamak TCV",* (Thèse EPFL No. 2606(2002))
LRP 730/02

Blanchard P., Alberti S., Coda S., Weisen H., Klimanov I., *"High field side measurements of non-thermal electron cyclotron emission on TCV plasmas with ECH and ECCD"*
LRP 729/02

Coda S., Alberti S., Blanchard P., Goodman T.P., Henderson M.A., Nikkola P., Peysson Y., Sauter O., *"Electron cyclotron current drive and suprathermal electron dynamics in the TCV tokamak",* Proc. 19th IAEA Fusion Energy Conference, Lyon, France, October 2002, IAEA-CN-94/EX/W-5
LRP 742/02

Delachaux T., Hollenstein Ch., Lévy F., Verdon C., *"Nitriding of tetragonal zirconia in a high current dc plasma source"*
LRP 740/02

Deschenaux C., "*Etude de l'origine et de la croissance de particules sub-micrométriques dans des plasmas radiofréquence réactifs",* (Thèse EPFL No. 2590(2002))
LRP 725/02

EC12 Workshop Participants, Papers presented at the, 12th Joint Workshop in Electron Cyclotron Emission and Electron Cyclotron Resonance Heating (EC-12), Aix-en-Provence, May 2002
LRP 726/02

EPS Participants, Papers presented at the 29th EPS on Plasma Physics and Controlled Fusion, Montreux, Switzerland, June 2002
LRP 728/02

Falchetto G.L., *"Electromagnetic microinstabilities in tokamak plasmas using a global spectral approach"* (Thèse EPFL No. 2524 (2002))
LRP 722/02

Henderson M., Alberti S., Bird J., Doane J., Elendoern B., Flemming C., Goodman T.P., Hoekzena F., Hogge J.-P., MacMillan G., Magnin J.-C., Pioscyk B., Porte L., Tran M.Q., Verhoeven A.G.A., *"General description of the evacuated wave-guide transmission line for the JET-EP ECRH project"*
LRP 735/02

Henderson M., Alberti S., Bird J., Doane J., Elendoern B., Flemming C., Goodman T.P., Hoekzena F., Hogge J.-P., MacMillan G., Magnin J.-C., Pioscyk

B., Porte L., Tran M.Q., Verhoeven A.G.A., *"An ITER relevant evacuated waveguide transmission system for the JET-EP ECRH project"*
LRP 736/02

Henderson M., Alberti S., Goodman T.P., Hogge J.-P., Porte L., Tran M.Q., *"CRPP's evacuated waveguide proposal for JET-EP ECRH transmission line"*
LRP 719/02

Henderson M.A., Alberti S., Angioni C., Arnoux G., Behn R., Blanchard P., Bosshard P., Yamenen Y., Coda S., Condrea I, Goodman T.P., Hofmann F., Hogge J.-Ph., Karpushov A., Manini A., Martynov An., Moret J.-M., Nikkola P.,Nelson-Melby E., Pochelon A., Porte L., Sauter O., Ahmed S.M., Andrèbe Y., Appert K., Chavan R., Degeling A., Duval B.P., Etienne P., Fasel D., Fasoli A., , Favez J.-Y., Furno I., Horacek J., Isoz P., Joye B., Klimanov I., Lavanchy P., Lister J.B., Llobet X., Magnin J.-C., Marlétaz B., Marmillod P., Martin Y., Mayor J.-M., Mlynar J., Paris P.J., Perez A., Peysson Y., Pitts R.A., Raju D., Reimerdes H., Scarabosio A., Scavino E., Seo s.H., Siravo U., Sushkov A., Tonetti G., Tran M.Q., Weisen H., Wischmeier M. Zabolotsky A., Yhuang G., *"Recent results from the EC heated plasmas in the TCV"*, 44th Annual Meeting, APS Division of Plasma Physics, Orlando, Florida, USA, November 2002 (Invited talk)
LRP 747/03

Hofmann F., Coda S., Lavanchy P., Llobet X., Marmillod Ph., Martin Y., Martynov A., Mlynar J., Moret J.-M., Pochelon A., Sauter O., *"Extension of the TCV operating space towards higher elongation and higher normalized current, accepted for publication in Nuclear Fusion"*
LRP 717/02

IAEA Participants, Papers presented at the, 19th IAEA Fusion Energy Conference, Lyon, France, October 14 - 19, 2002
LRP 738/02

Klinger L., *"Simulation numérique 3D d'une torche à plasma par une méthode de volumes finis"*(Thèse EPFL No. 2678 (2002))
LRP 739/02

Lister J.B., Bruzzone P.L., Favez J.Y., Schaerz B., Bugnion L., Zapretilina E., *"Plasma Current, Position and Shape Control, Contract FU05-CT2001-00018 (EFDA/00-551)"*
LRP 741/02

Manini A., *"Analysis and interpretation of the plasma dynamic response to additional heating power using different diagnostics"* (Thèse EPFL No. 2599(2002))
LRP 724/02 (Thèse EPFL No. 2599 (2002))

Mlynar J., Coda S., Degeling A., Duval B.P., Hofmann F., Goodman T., Lister J.B. , Weisen H., *"Investigation of the consistency of magnetic and soft X-ray plasma position measurements on TCV by means of a rapid tomographic inversion algorithm"*
LRP 732/02

PSI15 Participants, Paper presented by J.Horacek at the, 15th Int. Conference on Plasma Surface Interactions in Controlled Fusion Devices, Gifu, Japan, May 2002
LRP 734/02

PSI15 Participants, Papers presented by R. Pitts and M. Wischmeier at the, 15th Int. Conference on Plasma Surface Interactions in Controlled Fusion Devices, Gifu, Japan, May 2002
LRP 727/02

Sauter O., Buttery R.J., Felton R., Hender T.C., Howell D.F., and contributors to the EFDA-JET, Workprogramme, *"Marginal beta limit for neoclassical tearing modes in JET H-Mode dischrages"*
LRP 731/02

Sauter O., Westerhof E., Mayoral M.L., et al., Task Force M, Task Force H and contributors to the EFDA-JET workprogramme, *"Control of Neoclassical Tearing modes by sawtooth control"*
LRP 718/02

SOFT 2002 Participants, Papers presented at the, 22nd Symposium on Fusion Technology, Helsinki, Finland, September 2002
LRP 733/02

SULTAN Team, *"User specifications for conductor samples to be tested in the SULTAN facility"*
LRP 723/02

Varenna Participants, Papers presented at the Joint Varenna-Lausanne International Workshop on "Theory of Fusion Plasmas", Varenna, Italy, August 27–30, 2002
LRP 737/02

Weisen H., Martin Y., Moret J.-M., and TCV team, *"On the dependence of energy confinement on elongation in single null divertor plasmas"*
LRP 721/02

Wesche R., *"Thermodynamic optimisation of 70kA bimary current lead"*
LRP 720/02

D.2 Internal Reports (INT)

Kalvin S., Zoletnik S., *"Tomographic reconstruction of radiation intensity profiles from bolometric measurements on the TCV tokamak"*
INT 204/02

Schlatter Ch., Mlynar J., *"TCV diagnostics – Documentation: Fast-algorithm bolometric computer aided tomography (FABCAT)"*
INT 205/02

Howling A.A., *"Power transfer efficiency to a RF plasma reactor via a transmission line (balanced, shielded stripline) of length comparable to the RF wavelength"*
INT 206/02

Graves J.P., *"Comment on deployment of analytical expressions for flux surface shaping and toroidal effects on the ideal MHD m = n = 1 instability"*
INT 207/02

Schlatter Ch., *"Study of magnetic flux shaped base functions for tomography TCV Diagnostics - Semestrial report"*
INT 208/02

APPENDIX E The basis of controlled fusion

E.1 Fusion as a sustainable energy source

Research into controlled fusion aims to demonstrate that it is a valid option for generating power in the long term future in an environmentally, politically and economically acceptable way. Controlled fusion is a process in which light nuclei fuse together to form heavier ones: during this process a very large amount of energy is released. For a fusion reactor it is planned to use the two isotopes of hydrogen: deuterium (D) and tritium (T), which fuse together much more readily than any other combination of light nuclei according to the following reaction:

$$D^2 + T^3 \rightarrow He^4 + n + 17.6MeV$$

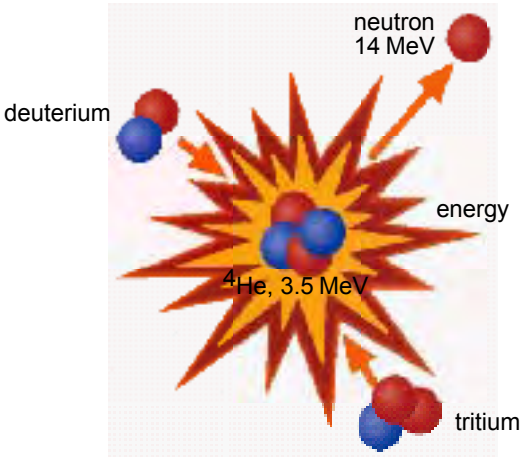

Fig. E.1 *Schematic of a fusion reaction between deuterium and tritium nuclei. The products are 3.5MeV ^4He, the common isotope of helium, and a 14MeV free neutron.*

The end products are helium and neutrons (n). The total energy liberated by fusing one gram of a 50:50% mixture of deuterium and tritium is 94000kWh, which is 10 million times more than from the same mass of oil. 80% of this energy is carried by the neutrons with an energy of 14MeV while the remaining 20% is carried by the helium nucleus. All this energy eventually becomes heat to be stored or converted by conventional means into electricity.

The temperature at which fusion reactions start to become significant are above a few tens of millions of degrees. For the D-T reaction, the optimal temperature is of the order of 70-200 million degrees. At such temperatures the D-T fuel is in the plasma state.

Deuterium is very abundant on the earth and can be extracted from water (0.034g/l). Tritium does not occur naturally, since its half-life is only 12.3 years, but it can be regenerated from lithium using the neutrons produced by the D-T fusion reactions. The two isotopes of natural lithium contribute to this breeding of tritium according to the reactions:

$$Li^6 + n \rightarrow He^4 + T^3 + 4.8MeV$$

$$Li^7 + n \rightarrow He^4 + T^3 + n - 2.5MeV$$

The relative abundance of the two lithium isotopes Li^6 and Li^7 are 7.4% and 92.6%, respectively. The known geological resources of lithium both in the earth and in the sea water are large enough to provide energy in an unlimited time.

E.2 Attractiveness of fusion as an energy source

The inherent advantages of fusion as an energy source are:

- The fuels are plentiful and their costs are negligible because of the enormous energy yield of the reaction;
- The end product of the reaction is helium, an inert gas;
- No chain reaction is possible; at any time only a very small amount of fuel is in the reacting chamber and any malfunction would cause an immediate drop of temperature and the reaction would stop;
- No after-heat problem can lead to thermal runaway;
- None of the materials required by a fusion power plant are subject to the provisions of the non-proliferation treaties.

Its further potential advantages are:

- Radioactivity of the reactor structure, caused by neutrons, can be minimised by careful selection of low-activation materials resulting in a manageable quantity of long lived radioactive waste;
- The release of tritium in normal operation can be kept to a very low level. The inventory of tritium in the breeding section of the reactor and on the site can be sufficiently small so that the worst possible accident could not lead to a harmful release to the environment requiring evacuation of the nearby population.

APPENDIX F Glossary

A general purpose glossary for the field of controlled fusion and plasma physics is provided in the CRPP Annual Report every two years. This report is an even year and the glossary is therefore not provided.

APPENDIX G Sources of Financial Support

The work carried out at the CRPP and presented in this annual report was financed from several sources. The major long-term financial support is derived from the Ecole Polytechnique Fédérale de Lausanne (EPFL), EURATOM, the Paul Scherrer Institute (PSI), which hosts the supraconductivity and materials science activities, and the Swiss National Science Foundation. Other public and private organisations which contributed funding for our research in 2001 include, in alphabetical order: Balzers Tribology, Charmilles SA, the Swiss Commission pour la Technologie et l'Innovation (CTI), Dow Corning, Rolex, Sulzer Metco AG, Tetra Pak SA and Unaxis.

The CRPP is the Host of a Marie Curie Fellowship, Dr. M. McGrath, *"Nonlinear structures in turbulent transport plasmas and methods of control".*

The Fonds National Suisse de la Recherche Scientifique provides a grant during this period for *"Basic plasma physics for fusion energy research",* which partly finances TORPEX and the CRPP-JET collaboration on Alfven waves and fast particles. Prof. A. Fasoli is supported by this grant as “Professeur Boursier du Fonds National”.